RUHR-UNIVERSITÄT BOCHUM

Muhammad Ibrar Khan

# Hydraulic Conductivity of Moderate and Highly Dense Expansive Clays

Bochum 2012

Heft 48

Schriftenreihe des Lehrstuhls für
Grundbau, Boden- und Felsmechanik

Herausgeber: Tom Schanz

ISSN 2190-3255

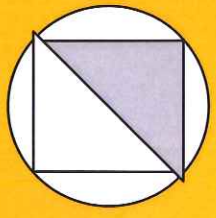

# Hydraulic Conductivity of Moderate and Highly Dense Expansive Clays

Dissertation
as a requirement for the degree of

Doktor - Ingenieur

at the Faculty of Civil and Environmental Engineering
Ruhr-Universität Bochum

submitted by

**Muhammad Ibrar Khan**
from Bannu / Pakistan

Reviewers:

Prof. Dr. –Ing. habil. Tom Schanz
Dr. Snehasis Tripathy
Prof. Dr. –Ing. habil. Achim Hettler

May 2012
Bochum

*This work is dedicated to my father and brother*

# ABSTRACT

Compacted clays are often used to line landfills and waste impoundment, to cap the waste disposal units, and to close the old disposal facilities. Bentonite has attracted considerable attention in such applications on account of its high swelling capacity, low hydraulic conductivity, and high radionuclide adsorption capacity. Among several attributes of bentonites, the hydraulic conductivity is expected to play a crucial role in both retarding movement of radionuclide to the geosphere and delaying the corrosion of the metal waste canisters.

A detailed study to determine the hydraulic conductivity of moderate and highly dense expansive clays is presented. The proposed investigation is comprised of both experimental and theoretical studies. In experimental investigation, clay samples of various bentonites are prepared by compaction of clay water mixtures to a range of predetermined dry density and water content simulating the actual placement conditions commonly prevailed for the barrier and back-filling materials in waste disposal repository. The initial water content is varied to examine the effects on hydro-mechanical characteristic of the clays. Swelling pressure tests followed by the hydraulic conductivity tests are carried out in the newly fabricated high pressure constant volume cells. Two types of permeant (i.e., distilled water ($10^{-4}$M) and high concentration solution ($10^{-2}$M)) are chosen for the swelling pressure and hydraulic conductivity tests.

The experimentally determined hydraulic conductivities of the bentonite in this study are compared with the predictions of existing models like: Kozeny-Carman model, cluster model, and laminar flow model. Different approaches have been considered in models to estimate the hydraulic conductivity. Similarly, experimental swelling pressures of bentonites are compared with the calculated swelling pressure using Gouy-Chapman diffuse double layer theory. The relationship between the theoretical void ratio from diffuse double layer theory and as prepared total void ratio was established and new modified void ratios were suggested. Two new equations were proposed for estimating swelling pressure that has theoretical support and the equations were verified with six other reported bentonites. At the end, conclusions regarding the hydro-mechanical characteristics of the materials are drawn and suggestions for future studies are made.

# ZUSAMMENFASSUNG

Verdichtete Tone werden häufig zur Abdichtung von Deponien und unterirdischen Ablagerungen für toxischen und radioaktiven Abfall verwendet, zum einen, um direkt die Abfallbehälter abzudecken und zum anderen, um den Ablagerungsbereich mit Hilfe eines horizontalen Abdichtungsbauwerks zu versiegeln. Bentonit erfährt in diesem Zusammenhang durch sein hohes Quellpotential, seine geringe hydraulische Durchlässigkeit und seine hohe Adsorptionsfähigkeit von Radionukleiden besondere Aufmerksamkeit. Von den unterschiedlichen Eigenschaften des Bentonits wird der hydraulischen Durchlässigkeit sowohl hinsichtlich der Verzögerung des Transports der Radionukleide in die Geosphäre als auch hinsichtlich der Verzögerung der Korrosion der metallischen Behälter die größte Bedeutung beigemessen.

Es wird eine detaillierte Untersuchung zur Bestimmung der hydraulischen Durchlässigkeit von mitteldichten bis sehr dichten, quellfähigen Tonen vorgestellt. Die Untersuchung beinhaltet experimentelle und theoretische Methoden. In der experimentellen Untersuchung wurden Tonproben verschiedener Bentonite mittels Verdichtung von Ton-Wasser-Mischungen in einem festgelegten Spektrum von Trockendichten und Wassergehalten vorbereitet, um die Lagerungsbedingungen zu simulieren, die in den Abdichtungs- und Verfüllmaterialien in den Ablagerungsbereichen typischerweise vorherrschen. Der initiale Wassergehalt wurde variiert, um dessen Einfluss auf die hydro-mechanischen Eigenschaften der Tone zu studieren. Quelldruckversuche, gefolgt von Versuchen zur Bestimmung der hydraulischen Durchlässigkeit, wurden in den neu hergestellten Hochdruckzellen unter konstantem Volumen durchgeführt. Für die Versuche wurden zwei Arten von Fluiden ausgewählt, destilliertes Wasser ($10^{-4}$M) und eine hochkonzentrierte Lösung ($10^{-2}$M).

Die experimentell ermittelten hydraulischen Durchlässigkeiten der verwendeten Bentonite wurden mit theoretischen Modellen wie dem Kozeny-Carman-Modell, dem Cluster-Modell und dem laminaren Modell verglichen. In den Modellen werden unterschiedliche Ansätze verfolgt, um die hydraulische Durchlässigkeit abzuschätzen. In Analogie dazu sind die experimentell ermittelten Quelldrücke der Bentonite mit Quelldrücken verglichen worden, die mit der DDL-Theorie nach Gouy-Chapman berechnet wurden. Es wurde eine

Beziehung zwischen der in der DDL-Theorie definierten theoretischen Porenzahl und der experimentell erreichten, totalen Porenzahl aufgestellt und darüber hinaus wurden modifizierte Definitionen für Porenzahlen vorgeschlagen. Außerdem wurden zwei neue, theoretisch fundierte Gleichungen zur Abschätzung des Quelldrucks vorgeschlagen und anhand von sechs Bentoniten aus der Literatur verifiziert. Abschließend werden Schlussfolgerungen hinsichtlich der hydro-mechanischen Eigenschaften der Materialien gezogen und Vorschläge für zukünftige Untersuchungen gegeben.

# Vorwort des Herausgebers

Die Arbeit von Herrn Dr. Khan erfolgte in Fortführung unserer langjährigen Untersuchungen zur Eignung von Geomaterialien als Dichtelemente im Rahmen der unterirdischen Lagerung hochtoxischer Abfälle. Besonders Bentonite sind der Baustoff der Stunde für derartige Aufgabenstellungen. Bentonite bzw. Mischungen von Bentoniten mit Sand werden hochverdichtet, wodurch Eigenschaften erzielt werden, die sich in hohen Quelldrücken, geringen Permeabilitäten, hohen Steifigkeiten und Festigkeitenäußern. Besonders der Quantifizierung der Permeabilität derartiger Materialien ist in der Literatur noch zu wenig Beachtung geschenkt worden. Zwar existieren umfangreiche Arbeiten zum Thema Permeabilität von Tonen, dies betrifft jedoch ausschließlich Tone bei normaler Verdichtung.

Herr Khan beschäftigt sich in seiner Arbeit das erste Mal systematisch mit der Untersuchung der Permeabilität von hochverdichteten Bentoniten unter Berücksichtigung der Tonzusammensetzung und der Chemie des Porenfluids. Daneben wird dem Einfluss des initialen Zustandes (Porenzahl und Wassergehalt, initiale Saugspannung), d.h. nach Verdichtung der Bentonite, besondere Aufmerksamkeit geschenkt.

Die Arbeit ist in acht Kapitel gegliedert und enthält des Weiteren einen umfangreichen Literaturteil und einen Anhang mit detaillierten Versuchsergebnissen.

*Kapitel 1* gibt den Hintergrund und die Motivation der Promotionsarbeit wieder. Klar werden die Fragen der Arbeit formuliert, die im Mittelpunkt der Betrachtungen stehen und es wird der Weg aufgezeigt, wie sich diesen Fragen genähert werden soll. *Kapitel 2* beschäftigt sich mit einem Überblick der aktuellen Literatur zur behandelten Forschungsaufgabe. Eine besondere Bedeutung kommt der Beschreibung des Ton-Porenfluid-Systems zu. Das Verständnis dieses Ton-Porenfluid-Systems auf der Mikroskala ist Voraussetzung für das Verständnis der phänomenologischen Eigenschaften auf der Makroskala. Korrekterweise wird sowohl auf existierende Erkenntnisse zum Quelldruck, als auch zu der eigentlich im Vordergrund stehenden Frage der Permeabilität verwiesen. Dem Quelldruck kommt eine besondere Bedeutung zu, weil bei der Sättigung der Proben in einem ersten Versuchsschritt zwangsläufig Quellerscheinungen der Bentonite auftreten. Da die Versuche unter volumenkonstanten Bedingungen durchgeführt wurden, resultiert die Unterdrückung dieses Quellpotentials direkt in einem Quelldruck. In einer zweiten Phase wird dann die eigentliche Permeabilitätsuntersuchung an den nunmehr gesättigten Proben durchgeführt.

In *Kapitel 3* werden die existierenden Methoden zur Bestimmung der hydraulischen Permeabilität gesättigter Materialien eingeführt und ihre Anwendungsgrenzen in Bezug auf

hochverdichtete Bentonite diskutiert. Von besonderer Bedeutung in Kapitel 3 ist Unterabschnitt 3.5, der sich ausführlich mit drei theoretischen Modellen zur Beschreibung der gesättigten hydraulischen Permeabilität beschäftigt. Diese für „normale“ Böden entwickelten Modelle werden in Folge der Arbeit von Herrn Khan modifiziert um sie den speziellen Randbedingungen der von ihm untersuchten Materialien anzupassen. In *Kapitel 4* wird das in der Promotion untersuchte Material in Form von drei verschiedenen Tonen mit seinen physikalischen Eigenschaften, den Verdichtungseigenschaften und den physikochemischen Eigenschaften detailliert beschrieben. *Kapitel 5* beschäftigt sich mit den von Herrn Khan speziell für seine Studie entwickelten Versuchsgeräten. In Anbetracht der speziellen Eigenschaften der untersuchten Materialien mussten sowohl die Versuchszellen, als auch die Beaufschlagung mit Porenfluid geändert und neue Versuchsgeräte entwickelt werden. Die unterschiedlichen Komponenten werden ausführlich kalibriert und validiert. *Kapitel 6* beschäftigt sich mit den experimentellen Resultaten von Herrn Khan. Im ersten Abschnitt werden die Quelldrücke für die drei verschiedenen Bentonite in Abhängigkeit der initialen Bedingungen und des verwendeten Porenfluids dargestellt und mit Ergebnissen aus der Literatur validiert. Der zweite Abschnitt beschäftigt sich mit den ermittelten hydraulischen Permeabilitäten, wiederum in Funktion des Initialzustands und der Eigenschaften des Porenfluids. Hier liegt es in der Natur der Sache, dass die Vergleichsmöglichkeiten sehr beschränkt sind. In *Kapitel 7* werden die von Herrn Khan verwendeten klassischen Permeabilitätsmodelle und Lösungen für den Quelldruck mit seinen experimentellen Ergebnissen verglichen. Basierend auf einer genauen Kenntniss der physikochemischen Kräfte in der Mikrostruktur gelingt es Herrn Khan, sowohl die Gleichungen für den Quelldruck als auch für die hydraulische Permeabilität so zu modifizieren, dass ihm eine sehr gute Anpassung an seine ermittelten experimentellen Resultate möglich ist.

Die Arbeit von Herrn Khan beinhaltet sowohl theoretische als auch experimentelle Komponenten. Auf allen Gebieten gelingt es Herrn Khan, an den aktuellen Stand der Wissenschaft aufzuschließen bzw. besonders im Bereich der experimentellen Untersuchungen einen entscheidenden Schritt weiter zu gehen.

Wir danken dem BMBF und dem BMWi für die kontinuierliche Förderung unserer Arbeiten in den vergangenen Jahren.

Bochum, Juni 2012 Tom Schanz

# ACKNOWLEDGEMENTS

Firstly, all praises and thanks be to God for giving me strength and courage to achieve one of the challenging tasks of my life. This PhD thesis is a result of four years of research work carried out at Laboratory of Soil Mechanics, Bauhaus-Universität Weimar and Laboratory of Foundation Engineering, Soil and Rock Mechanics, Ruhr-Universität Bochum. I hereby express my special thanks to my promoter Prof. Dr.-Ing. habil. Tom Schanz who gave me the opportunity to start my PhD research and has provided his continues support over all these years. His encouragement and supervision all the way are highly appreciated.

My sincere gratitude goes to Dr. Snehasis Tripathy from Cardiff University, who helped me during my research and the discussion with him throughout these years and for his comments and suggestions.

I would also like to acknowledge the financial support provided by BMBF (Bundesministerium fur Bildung und Forschung) through project grant No. 02E10437 and the DAAD (German Academic Exchange Service).

My gratitude also extended to my former colleagues from Laboratory of Soil Mechanics at Bauhaus-Universität Weimar. Special thanks to Dipl.-Ing. (FH) Gabriele Tscheschlok and Frank Hoppe for their assistance in the laboratory.

I would like to thank my office mate Dr.-Ing. Yasir Al-Badran for his assistance during the laboratory work and useful discussions. I am privileged to know colleagues like Qasim Al-Obaidi, Usama Al-Anbaki, Long Nguyen Tuan, Houman Soleimani Fard, Alborz Pourzargar and new comers who are worth mentioning here. Indeed their friendship and company have enriched my academic experience. I wish them all the best for their future endeavors.

I am thankful to Dr.-Ing. Lars Röchter who translated my dissertation's abstract into German and for his kind behaviour during my stay here. In particular, I wish to thanks Dipl.-Ing. Wiebke Baille, Dr.-Ing. Yvonne Lins and Dr.-Ing. Diethard König for their assistance wherever I needed.

My thanks are also for Prof. Dr.-Ing. habil. Achim Hettler, Dr. Snehasis Tripathy and Prof. Dr.-Ing. Rüdiger Höffer for their agreement to be external reviewers of this dissertation. I would like pass my gratefulness to all parties who indirectly assisted me during my period of stay in Bochum.

Most importantly, has been the encouragement of my family. Especially important has been the unwavering love, support, and patience of my wife Marium who has never ceased to provide encouragement and my son Musa has also provided a constant source of love. My mother prayers were always there with me during the hardest times. Also many thanks are due to my brother and sister for their support and care. Finally, we have made it together as a family.

*Muhammad Ibrar Khan*

Bochum, 2012

# LIST OF CONTENTS

Abstract …….....i
Zusammenfassung…….....ii
Vorwort des Herausgebers …….v
Acknowledgements…….....vii
List of Contents .....…….....ix
List of Figures .....…….....xv
List of Tables...…….....xxi
List of Symbols.....xxiii

**Chapter 1 Introduction.....1**

1.1 Background and motivations .....1
1.2 Research objectives and scope .....3
1.3 Thesis overview .....4

**Chapter 2 Review of literature .....7**

2.1 Introduction.....7
2.2 Structural unit and charge on clay minerals.....7
2.3 Forces in clay system and modes of particle association .....14
2.3.1 Interparticle forces in clay.....17
2.3.2 Modes of particle association in clay.....20
2.4 Water in compacted clay.....23
2.5 Hydration process in compacted clays.....25
2.6 Clay-water interaction and relation.....27
2.6.1 Diffuse double layer model for clay-water system.....30
2.7 Swelling and non swelling clays.....35
2.7.1 Swelling mechanism in clays.....36
2.7.1.1 Crystalline swelling .....36
2.7.1.2 Diffuse double layer swelling .....37

2.8 Swelling pressure testing .....38
2.8.1 Laboratory testing of swelling clays .....38
2.8.2 Theoretical prediction of swelling pressure .....42
2.9 Mechanisms governing hydraulic flow through soils .....44
2.10 Factor influencing the hydraulic conductivity of clays .....45
2.10.1 Influence of type of bentonite on HC .....45
2.10.2 Influence of compaction density on HC .....47
2.10.3 Influence of water content on HC .....49
2.10.4 Influence of type of pore fluid on HC .....52
2.10.5 Influence of temperature on HC .....56
2.11 Summary .....58

**Chapter 3 Methods available to assess hydraulic conductivity .....59**

3.1 Introduction .....59
3.2 Hydraulic properties of soils and flow law .....59
3.2.1 Darcy Law .....60
3.2.2 Steady state and unsteady state flow .....62
3.2.3 Effect of magnitude of hydraulic gradient .....63
3.3 Empirical relationships for saturated coefficient of hydraulic conductivity .....66
3.3.1 Introduction .....66
3.3.2 Relation between saturated hydraulic conductivity, void ratio and grain size distribution .....67
3.4 Measurements of saturated hydraulic conductivity .....69
3.4.1 Introduction .....69
3.4.2 Laboratory measurement of hydraulic conductivity .....70
3.4.2.1 Constant head method .....70
3.4.2.2 Falling head method .....70
3.4.2.3 Oscillatory hydraulic method .....72
3.5 Theoretical models for saturated hydraulic conductivity .....74
3.5.1 Poiseuille model for saturated hydraulic conductivity .....74
3.5.2 Kozeny Carman model for saturated hydraulic conductivity .....76
3.5.3 Cluster model for saturated hydraulic conductivity .....78
3.6 Summary .....82

**Chapter 4 Material used and experimental program.....83**

4.1 Introduction .....83
4.2 Materials .....83
4.2.1 Calcigel bentonite .....83
4.2.2 MX-80 bentonite.....84
4.2.3 Kunigel bentonite .....84
4.3 Physical properties.....84
4.3.1 Natural water content.....84
4.3.2 Specific gravity .....85
4.3.3 Particle size distribution .....86
4.3.4 Liquid limit .....88
4.3.5 Plastic limit .....88
4.3.6 Plasticity Index .....89
4.3.7 Activity.....89
4.4 Compaction characteristics .....90
4.5 Physico-chemical characteristics .....92
4.5.1 Specific surface area .....92
4.5.2 Cation exchange capacity.....93
4.5.3 Mineralogy and chemical composition.....96
4.6 Summary of the material.....99
4.7 Experimental program.....100
4.8 Summary.....102

**Chapter 5 Experimental equipments, design and methodology.....103**

5.1 Introduction.....103
5.2 Available devices and their limitations.....103
5.3 Need for the new experimental device.....108
5.4 Design criteria of the devices.....109
5.5 Description of the devices.....110
5.5.1 Constant volume high pressure cell .....110
5.5.2 Volume pressure controller.....113
5.6 Calibration of the devices .....114
5.6.1 Constant volume high pressure cell .....114

5.6.2 Volume pressure controller .....116
5.7 Methodology developed .....117
5.7.1 Sample preparation .....117
5.7.2 Method to achieve specimen saturation .....118
5.7.3 Swelling pressure measurement.....119
5.7.4 Hydraulic conductivity measurement .....120
5.8 Summary.....122

**Chapter 6 Experimental results and Discussions .....123**

6.1 Introduction.....123
6.2 Swelling pressure results.....123
6.2.1 Calcigel bentonite .....124
6.2.1.1 Swelling pressure and water uptake with time .....124
6.2.1.2 Swelling pressure at low and high water content .....126
6.2.1.3 Swelling pressure at distilled water and high concentration solution128
6.2.2 MX-80 bentonite.....129
6.2.2.1 Swelling pressure and water uptake with time .....129
6.2.2.2 Swelling pressure at low and high water content.....131
6.2.2.3 Swelling pressure at distilled water and high concentration solution133
6.2.3 Kunigel bentonite.....134
6.2.3.1 Swelling pressure and water uptake with time .....134
6.2.3.2 Swelling pressure at low and high water content .....136
6.2.3.3 Swelling pressure at distilled water and high concentration solution138
6.3 Overall discussion on swelling pressure results.....139
6.4 Hydraulic conductivity results .....145
6.4.1 Calcigel bentonite .....145
6.4.1.1 Hydraulic conductivity at low and high water content .....146
6.4.1.2 HC at distilled water and high concentration solution .....148
6.4.2 MX-80 bentonite .....148
6.4.2.1 Hydraulic conductivity at low and high water content .....149
6.4.2.2 HC at distilled water and high concentration solution.....150
6.4.3 Kunigel bentonite.....151
6.4.3.1 Hydraulic conductivity at low and high water content .....151
6.4.3.2 HC at distilled water and high concentration solution.....152

6.5 Overall discussion on hydraulic conductivity results .....153
6.6 Summary .....159

**Chapter 7 Assessment of hydraulic conductivity and swelling pressure .....161**

7.1 Introduction .....161
7.2 Comparison of experimental results with existing model .....162
7.2.1 Kozeny Carman model .....162
7.2.2 Cluster model .....165
7.2.3 Laminar flow model .....170
7.3 New modifications in existing models.....172
7.3.1 Kozeny Carman model .....172
7.3.1.1 KC model (effective porosity) .....173
7.3.1.1.1 Verification and application.....175
7.3.1.2 KC model (DDL with reduce SSA).....177
7.3.2 Cluster model .....179
7.3.2.1 Verification and application .....182
7.3.3 Laminar flow model .....186
7.4 Estimation of swelling pressure.....188
7.4.1 Experimental and theoretical swelling pressure .....189
7.4.2 Proposed equations for void ratio .....192
7.4.3 Verification of the new swelling pressure equations .....196
7.5 Summary.....201

**Chapter 8 Conclusion and recommendation .....203**

8.1 Introduction .....203
8.2 Conclusions .....204
8.2.1 Experimental results.....204
8.2.2 Theoretical results .....205
8.3 Recommendations.....206

**References .....209**

**Appendix A1.....237**

# LIST OF FIGURES

Figure 2.1 Schematic of silica tetrahedral unit .....9
Figure 2.2 Schematic of Octahedral units .....9
Figure 2.3 Sketch of microstructure of compacted clay (Arifin 2008).....10
Figure 2.4 General Structural arrangements of clay minerals.....11
Figure 2.5 Typical X-Ray diffraction patterns for clay minerals.....12
Figure 2.6 Diffuse double layer.....14
Figure 2.7 Dipole character of water.....14
Figure 2.8 Interparticle forces at particle level.....16
Figure 2.9 Microscopic water-soil interaction in soils .....20
Figure 2.10 Modes of particles association in clay suspension.....21
Figure 2.11 Arrangement of domain, cluster, peds and macropores.....22
Figure 2.12 Representation of interlayer water, double later water and free water in compacted bentonites (Bradbury and Baeyens 2002) .....24
Figure 2.13 Potential ion arrangements at the particle water interface (Yong et al. 1992) .....32
Figure 2.14 Distribution of ions at charged surface (Guven 1992a), a) model for multilayer configuration at clay-water interface, b) Decay of surface potential ($\psi_o$) in interface region .....34
Figure 2.15 Swelling pressure measurement using different methods (Agus 2005) .39
Figure 2.16 Experimental and calculated swelling pressure result .....43
Figure 2.17 Effect of three types of clays on HC (Mesri and Olson 1970) .....46
Figure 2.18 Effect of compaction and water content on structure of clay soils (Lambe 1958).....48
Figure 2.19 Typical dry density-moisture content-hydraulic conductivity relationships for compacted clay (Murray et al. 1997) .....51
Figure 2.20 Effect of pore fluid on smectite (Mesri and Olson).....53
Figure 2.21 Hydraulic conductivity versus dry density of Febex bentonite using three types of pore fluids (Villar et al.2003).....55
Figure 3.1 Steady state and unsteady state flows.....62

Figure 3.2 Typical relationships between flow velocity and hydraulic gradient (modified from Daniel 1994) .....63
Figure 3.3 Plot of log flux versus log hydraulic gradient (Dixon 1995).....65
Figure 3.4 Principle of Hydraulic conductivity test (a) Constant head method (b) Variable head method (Agus 2001) .....71
Figure 3.5 Standard experimental set up for oscillatory pore pressure testing.....73
Figure 3.6 Assumed relationship between total, cluster (or intra-cluster or micro) and inter-cluster (or macro) void ratio (Olsen, 1962).....80
Figure 4.1 Particle size distribution curve for Calcigel bentonite by hydrometer method.....86
Figure 4.2 Particle size distribution curve for MX-80 bentonite by hydrometer method.....87
Figure 4.3 Particle size distribution curve for Kunigel bentonite by hydrometer method .....87
Figure 4.4 Compaction curve for Calcigel bentonite via standard Proctor method91
Figure 4.5 Compaction curve for MX80 bentonite via standard Proctor method...91
Figure 4.6 Compaction curve for Kunigel bentonite via standard Proctor method.92
Figure 4.7 XRD results for a) Calcigel b) MX-80 and c) Kunigel bentonites.....98
Figure 5.1 Rigid wall constant volume fixed flow rate design .....105
Figure 5.2 Basic design of flexible walled design .....107
Figure 5.3 New constant volume high pressure device .....112
Figure 5.4 Individual components of constant volume device .....112
Figure 5.5 Volume pressure controller for water injection pressure .....113
Figure 5.6 Calibration of the cell with volume pressure controller .....114
Figure 5.7 Calibration of the load cell with volume pressure controller.....115
Figure 5.8 Calibration of load cell with high pressure loading machine.....116
Figure 5.9 Calibration of load cell with manometer device.....117
Figure 5.10 Schematic of the test setup for measuring hydraulic conductivity.....121
Figure 6.1 Development of constant volume swelling pressure of Calcigel bentonite (a) swelling pressure and (b) water uptake versus time.....125
Figure 6.2 Swelling pressure as function of dry density for low and high initial water contents for Calcigel bentonite.....127
Figure 6.3 Comparison of swelling pressure versus dry density

for Calcigel bentonite .....127
Figure 6.4 Swelling pressure as function of dry density for distilled water and high concentration solution for Calcigel bentonite .....128
Figure 6.5 Development of constant volume swelling pressure of MX-80 bentonite (a) swelling pressure and (b) water uptake versus time.....130
Figure 6.6 Swelling pressure as function of dry density for low and high initial water contents for MX-80 bentonite.....132
Figure 6.7 Comparison of swelling pressure versus dry density for MX80 and Volclay bentonites .....132
Figure 6. 8 Swelling pressure as function of dry density for distilled water and high concentration solution for MX-80 bentonite .....133
Figure 6.9 Development of constant volume swelling pressure of Kunigel bentonite (a) swelling pressure and (b) water uptake versus time .....135
Figure 6.10 Swelling pressure as function of dry density for low and high initial water contents for Kunigel bentonite.....137
Figure 6.11 Comparison of swelling pressure versus dry density for Kunigel bentonite .....137
Figure 6.12 Swelling pressure as function of dry density for distilled water and high concentration solution for Kunigel bentonite .....138
Figure 6.13 Influence of initial water content on the swelling pressure (modified from Villar and Lloret 2008).....142
Figure 6.14 Swelling pressure values for different concentration and solutions (Lloret et al. 2007) .....143
Figure 6.15 Swelling pressure as function of initial dry density for distilled water and artificial seawater (Komine et al. 2009).....144
Figure 6.16 Inflow and outflow for Calcigel bentonite .....146
Figure 6.17 Hydraulic conductivity as function of dry density for low and high initial water content for Calcigel bentonite .....147
Figure 6.18 Hydraulic conductivity as function of dry density for distilled water and high concentration solution for Calcigel bentonite .....148
Figure 6.19 Hydraulic conductivity as function of dry density for low and high initial water content for MX-80 bentonite .....149
Figure 6.20 Hydraulic conductivity as function of dry density for distilled water and high concentration solution for MX-80 bentonite.....150

Figure 6.21 Hydraulic conductivity as function of dry density for low and high initial water content for Kunigel bentonite .....152
Figure 6.22 Hydraulic conductivity as function of dry density for distilled water and high concentration solution for Kunigel bentonite .....153
Figure 6.23 Influence of initial degree of saturation on the hydraulic conductivity of bentonite specimens (Dixon 1999) .....155
Figure 6.24 Influence of pore fluid on the hydraulic conductivity of bentonite specimens (Dixon 1999) .....157
Figure 6.25 Hydraulic conductivity of bentonite with distilled water and different strength chloride salt solution (Studds et al. 1998).....158
Figure 7.1 Measured and calculated hydraulic conductivity Kozeny-Carman model for Calcigel bentonite .....163
Figure 7.2 Measured and calculated hydraulic conductivity Kozeny-Carman model for MX-80 bentonite .....163
Figure 7.3 Measured and calculated hydraulic conductivity Kozeny-Carman model for Kunigel bentonite .....164
Figure 7.4 Flow chart showing the determination of hydraulic conductivity using cluster model .....166
Figure 7.5 Measured and calculated hydraulic conductivity from cluster model for Calcigel bentonite .....167
Figure 7.6 Measured and calculated hydraulic conductivity from cluster model for MX-80 bentonite .....167
Figure 7.7 Measured and calculated hydraulic conductivity from cluster model for Kunigel bentonite .....168
Figure 7.8 Relationship between the total $e_T$, and micro void ratio, $e_c$, from diffuse double layer for Calcigel, MX80 and Kunigel bentonites .....169
Figure 7.9 Measured and calculated hydraulic conductivity from laminar flow model for Calcigel bentonite .....170
Figure 7.10 Measured and calculated hydraulic conductivity from laminar flow model for MX-80 bentonite .....171
Figure 7.11 Measured and calculated hydraulic conductivity from laminar flow model for Kunigel bentonite .....171
Figure 7.12 Effective void ratios versus dry density relationship for the Calcigel and MX-80 bentonites .....174

Figure 7.13 Calculated versus measured hydraulic conductivity for the Bentonites .....176
Figure 7.14 Calculated versus measured hydraulic conductivity for Bentonites.....178
Figure 7.15 Relationship between the $e_T$, $e_c$, and $e_{c\_bk}$ from cluster model for MX80 and Calcigel bentonites .....180
Figure 7.16 Algorithm of proposed method .....180
Figure 7.17 Experimental and calculated hydraulic conductivity from suggested equation for MX80 bentonite .....181
Figure 7.18 Experimental and calculated hydraulic conductivity from suggested equation for Calcigel bentonite .....182
Figure 7.19 Experimental and calculated hydraulic conductivity from suggested equation for MX80 bentonite (Data from Pusch, 1980).....183
Figure 7.20 Experimental and calculated hydraulic conductivity from suggested equation for Kunigel bentonite (Present study) .....183
Figure 7.21 Experimental and calculated hydraulic conductivity from suggested equation for Calcigel bentonite (Data from Baille et al. 2010) .....184
Figure 7.22 Experimental and calculated hydraulic conductivity from suggested equation for Febex bentonite (Data from ENRESA 2000) .....184
Figure 7.23 Experimental and calculated hydraulic conductivity of bentonites from the suggested equations …….....185
Figure 7.24 Calculated versus measured hydraulic conductivity for bentonites.....187
Figure 7.25 Theoretical *u-Kd* relationship of MX 80 bentonite ($v$ = 1.27) .....189
Figure 7.26 Theoretical *u-Kd* relationship of Calcigel bentonite ($v$ = 1.95) .....190
Figure 7.27 Experimental and theoretical swelling pressures of MX80 bentonite .191
Figure 7.28 Experimental and theoretical swelling pressures of Calcigel bentonite192
Figure 7.29 Relationship between the total void ratios, $e_T$ and void ratio from diffuse double layer, $e_d$ for MX80 bentonite .....193
Figure 7.30 Relationship between the total void ratios, $e_T$ and void ratio from diffuse double layer, $e_d$ for Calcigel bentonite .....194
Figure 7.31 Experimental swelling pressure and swelling pressure from suggested equation for MX80 bentonite .....195
Figure 7.32 Experimental swelling pressure and swelling pressure from suggested equation for Calcigel bentonite .....196

Figure 7.33 Experimental swelling pressure and swelling pressure from suggested equation for MX80 bentonite (Data from Bucher and Muller-Vonmoos 1989) .....198
Figure 7.34 Experimental swelling pressure and swelling pressure from suggested equation for Volclay (Data from Komine et al. 2009) .....198
Figure 7.35 Experimental swelling pressure and swelling pressure from suggested equation for MX80 bentonite (Data from Komine et al. 2009) .....199
Figure 7.36 Experimental swelling pressure and swelling pressure from suggested equation for S-2 bentonite (Data from ENRESA 2000) .....199
Figure 7.37 Experimental swelling pressure and swelling pressure from suggested equation for Calcigel bentonite (Data from Schanz and Tripathy 2009) .....200
Figure 7.38 Experimental swelling pressure and swelling pressure from suggested equation for Febex bentonite (Data from ENRESA 2000) .....200
Figure 7.39 Experimental and calculated swelling pressures from suggested equations .....201

# LIST OF TABLES

Table 2.1 Mineral groups and physico-chemical properties (Yong et al. 1992) .....13

Table 2.2 Thickness in Å and complete hydrate layers for different exchangeable cation (Pusch et al. 1990) .....23

Table 2.3 Temperature effects on physical properties of water .....56

Table 3.1 Basic assumptions for application of Darcy Law.....…61

Table 4.1 Summary of properties of the clays studied .....……...99

Table 4.2 Chemical composition of the clays studied (BGR Hannover) .....99

Table 4.3 Initial condition of specimens and summary of the experimental Program .....101

Table 7.1 Properties of bentonites used for verification.....177

Table 7.2 Properties of bentonites used for verification of swelling pressure equations .....197

# LIST OF SYMBOLS

| | |
|---|---|
| $d_{001}$ | unit layer thickness of crystal |
| $S_b$ | specific basal surface area |
| $dt$ | thickness of monolayer |
| $\rho_w$ | density of liquid water |
| $\rho_c$ | density of mineral |
| $m_w$ | mass of water component |
| $m_c$ | mass of clay component |
| $j$ | number of monolayers of water |
| $n$ | number of silicate crystal |
| $p$ | swelling pressure |
| $n_0$ | ionic concentration of bulk fluid |
| $u$ | nondimensional midplane potential |
| $k.$ | Boltzmann constant |
| $T$ | absolute temperature |
| $\xi$ | distance function |
| $y$ | nondimensional potential at $x$ |
| $z$ | nondimensional potential at surface |
| $B$ | cations exchange capacity |
| $S$ | specific surface area |
| $\varepsilon_0$ | permittivity of vacuum |
| $D$ | dielectric constant |
| $K$ | diffuse double layer parameter |
| $v$ | cations valency |
| $e$ | void ratio |
| $G$ | specific gravity of soil solid |
| $d$ | half distance between clay platelets |
| $\alpha$ | inner Helmholtz plane |
| $\beta$ | $1^{st}$ layer of hydrated ions |

| | |
|---|---|
| D-plane | beginning of diffuse double layer |
| (1/k) | plane located in diffuse region |
| $e'$ | elementary charge |
| ξ-plane | slip shear plane |
| $h$ | hydraulic head loss |
| $\Delta u_w$ | pore-water pressure differential |
| $\gamma_w$ | uni weight of water |
| $i_a$ | pneumatic gradient |
| $\Delta u_a$ | pore air pressure differential |
| $q$ | flow rate |
| $A$ | cross-sectional area of specimen |
| $Q$ | quantity of flow |
| $\mu$ | fluid viscosity |
| $K$ | intrinsic permeability |
| $D$ | effective diameter of pores |
| $f(n_s)$ | porosity function |
| $de$ | effective grain diameter |
| $k$ | hydraulic conductivity |
| $g$ | acceleration due to gravity |
| $U$ | coefficient of grain uniformity |
| $L$ | length of drainage path in the soil |
| $h_1$ | head of water at $t_1$ |
| $h_2$ | head of water at $t_2$ |
| $v_{avg}$ | average fluid velocity |
| $R$ | tube radius |
| $v$ | flow velocity |
| $i$ | hydraulic gradient |
| $R_h$ | hydraulic radius of tube |
| $C_s$ | shape factor |
| $S$ | degree of saturation |
| $S_o$ | specific surface area of soil particle |
| $k_o$ | pore shape factor |
| $T$ | tortuosity factor |

| | |
|---|---|
| $\rho_{aw}$ | density of interlayer water between two parallel plate layers |
| $\mu_{aw}$ | viscosity of interlayer water between two parallel plate layers |
| $e_c$ | intracluster (micro) void ratio |
| $e_p$ | intercluster (macro) void ratio |
| $e_T$ | total void ratio |
| $k_{CM}$ | measured flow rate of water (Cluster model) |
| $k_{KC}$ | predicted flow rate using the Kozeny-Carman model |
| $N$ | average number clay particles per cluster |
| σ* | true effective stress |
| $\sigma$ | total effective stress |
| (σ - $U$) | pore water pressure |
| $B$ | Hamakar's constant ($10^{-19}$ J) |
| $\delta$ | thickness of the unit layer of clay platelets (0.66 nm) |
| $LL$ | liquid limit |
| $PL$ | plastic limit |
| $PI$ | plasticity index |
| $CEC$ | cation exchange capacity |
| $\lambda$ | wavelength |
| $XRD$ | x-ray diffraction |
| $\theta$ | angle at crystal lattice plane |
| $P_{\text{in}}$ | water-pressure at bottom of specimen |
| $P_{\text{out}}$ | water pressure at top of the specimen |
| $P_{LWC}$ | swelling pressure in low initial water content |
| $P_{HWC}$ | swelling pressure in high initial water content |
| $P_{DW}$ | swelling pressure in distilled water |
| $P_{HC}$ | swelling pressure in high concentration solution |
| $e_{eff}$ | effective void ratio |
| $\rho_d$ | dry density |

# Chapter 1

# INTRODUCTION

## 1.1 Background and motivations

Clay based barriers against the movement of water and contaminates have seen increasing use during the past decade. They are required to perform reliably and predictably for decades, and for some proposed applications for centuries. Such barriers are expected to limit the flow in such a way that contaminant movement is controlled. In designing a barrier system the engineer is required to understand mineralogy, chemistry, physics and hydraulics. When dealing with very low flow rates and mass transport, it is necessary to examine the accepted models for flow and mass transport, where simple models for flow through porous media are often adequate for the coarse grained natural soil and they may be inadequate for use in engineered material for fine grained soils under the hydraulic gradients that exists in most applications (Dixon 1995).

The need for the impermeable barriers to water and contaminant movement are particularly crucial in the conceptual design being developed for high level waste (HLW) (spent nuclear fuel waste) disposal. The concept being examined by many nuclear waste management programs includes the use of clay based material to act as barriers to contaminant migration. These barriers are needed to prevent or delay any escape of radioactive materials or decay products from a disposal vault. A sufficiently long isolation time to allow the natural decay of the radioactive waste materials is central to this disposal concept.

The spent nuclear fuel disposal involves emplacement of waste containers in boreholes drilled at depth of 500 – 1000m in the rocks. It includes the use of compacted clay based buffer materials to fill the annulus between the waste container and the surrounding rock mass. The buffer must support the waste container, conduct heat away from the heat generating waste containers, and provide ability for the system to self seal while maintaining the low hydraulic conductivity and to limit the movement of radionuclides.

The range of candidate clays has been examined to establish their potential for use in the buffer material. The montmorillonite clays of the smectite family of layer silicates have shown the greatest potential for successful application. Much work has been done from past many years on the behaviours of these clays. However most of this work has been on slurry or low density material. One of the primary reasons for the lack of data on the hydraulic behaviour of dense smectites has been the technical difficulty in actually measuring flow through them. These materials commonly exhibit hydraulic conductivities in order of $10^{-12}$ m/s to $10^{-14}$ m/s.

Bentonite is the name used both as a label for montmorillonite type smectite clays sold commercially as sealants, and for a specific variety of swelling clay. The term bentonite will be used throughout this thesis when discussing montmorillonite type clay (smectites) minerals.

Migration of fluid and gas through compacted clays depend upon the ability of the material to imbibe such phases under a given boundary conditions and the flux associated to trigger such flows. The placement conditions (water content, dry density) of the chosen materials suggest a very low porosity, high expansiveness, and very high initial negative pore water pressure. It is agreeable that compacted clays posses various pore system at different scales. Upon swelling, the intracluster pores affect the intercluster pores that in turn are responsible for the hydraulic conductivity. The possible interactions of the clay platelets during the saturation process includes both physico-chemical and physical interferences that occur at various level of clay platelet spacing. Some of the key aspects associated with the compacted clays that have been considered thoroughly by different researchers are: swelling pressure, swell potential, water absorption and desorption behaviour, behaviour of the material under isothermal and non-isothermal conditions, swelling behaviour under high injection fluid pressure, behaviour of the material while interacting with actual fluid prevailed at a particular location, and so on (Müller-Vonmoos and Kahr 1982, Pusch 1982, Swedish Nuclear Fuel and Waste Management Company 1983, Gray et al. 1984, Dixon and Gray 1985, National Cooperative for the Storage of Radioactive Waste 1985, Kanno and Wakamatsu 1992, Komine and Ogata 1996, Japan Nuclear Cycle Development Institute 1999, ENRESA 2000, Herbert and Moog 2002*a*, Agus 2005, Arifin 2008). Some of the detailed studies also include: variation in the fluid content, negative pore water pressure, porosity, dry density, and temperature (Dixon et al. 2002, Villar et al. 2005).

Much of the literature describes attempts to apply classical models for fluid flow in granular media to the fluid flow through dense saturated clays. Little data is available on water movement through moderate to dense bentonite based materials exposed to very slow regional ground water gradients (Dixon 1995). However, such condition is of particular interest in nuclear fuel waste management program. The lack of data is the result of technological limitation and the demanding time required for such tests. For most researchers one to two years duration for each test is an impractical application of laboratory resources and too expensive to undertake. Due to particular sensitivity of high level nuclear waste management program the resources needed to conduct such tests.

## 1.2 Research objectives and scope

The proposed research comprises of both experimental and theoretical research studies. The experimental study involves laboratory measurements of saturated hydraulic conductivity in several compacted clays. The saturated hydraulic conductivity is measured at constant head method after the measurement of swelling process at constrained conditions. The main objectives of the research may be summarised as:

1. Provide a state-of-the-art review of development of theories and experimental work related to moisture movement in saturated clays from the beginning of 19th century to date. The literature review covers background on clay structure and mineralogy, and clay-water interaction.

2. Design and build new test apparatus to facilitate a large number of combinations of hydro-mechanical and hydraulic gradient experiments. Create new laboratory facilities to provide operational support for the new cells. Conduct a preliminary experimental programme to demonstrate the working capacity and functionality of the new apparatuses.

3. Establish a basic experimental methodology for sample preparation to obtain uniform homogenous samples and for subsequent testing procedure. Determine basic geotechnical properties that include physical and chemical properties and hydraulic parameter of tested clays.

4. Perform hydro-mechanical tests to investigate the water uptake, swelling behaviour, moisture movement in clays with different initial water contents and dry density.

5. Develop different approaches in the existing hydraulic models to calculate the hydraulic conductivity of swelling clays. Verify and validate the new approaches against the results obtained from the experiments performed in this study as well as against hydraulic conductivity data from the literature.

## 1.3 Thesis overview

The thesis consists of eight chapters. A brief description of each chapter is presented below:

The first chapter describes the background and motivation, research objectives and scope, and thesis overview.

Chapter 2 presents the conceptual description of the clay mineral composition, water and clay interactions, and gives brief introduction to diffuse double layer theory. The chapter explains non-swelling and swelling clay types, swelling pressure measurements, laboratory and theoretical predictions of swelling pressure. Further sections deals with flow mechanisms in soils and clays, and factor affecting the hydraulic behaviour of clays. The review provides a background for the motivation of the research reported in this thesis.

Chapter 3 details the hydraulic properties of soil and the determinations of saturated coefficient of hydraulic conductivity are described. Laboratory measurements of the hydraulic conductivity performed by other researchers are elaborated. In addition the empirical equations for estimating hydraulic conductivity and theoretical models used for hydraulic conductivity are discussed.

Chapter 4 describes the testing materials used for experimental investigation and details their physical, chemical and geotechnical properties and the determination technique used to obtain them. Physical properties including natural water content, specific gravity, particle size distribution, Atterberg limits are covered. The compaction characteristic of the materials, which includes the development of compaction methodology to achieve the targeted uniform density and uniform water content, is presented. Physico-chemical

properties including specific surface area, cation exchange capacity and mineralogy and chemical composition of clays are then considered. Subsequently, determination of specific surface area using ethylene glycol monoethyl ether (EGME) adsorption method is described. Finally, the chapter follows the detailed description of the experimental program including initial placement condition and permeant used for the tests.

Chapter 5 presents the design and construction stages of the new devices that are needed to facilitate swelling and hydraulic conductivity tests. In this chapter it is firstly discussed the design, the applicability and the limitation of different devices available for measurement of hydraulic conductivity. Necessity of new experimental devices to be built to carry out the experimental tests is emphasized. The design criteria to be met for the construction of new devices are discussed. Furthermore, the chapter gives description of new devices, and its various components. The calibration of the new devices and its working limits are covered. Experimental methodology developed to carry out the tests is discussed.

In chapter 6 the experimental results of the laboratory test program are presented. Results of the swelling pressure and water uptake for the bentonites via the newly designed constant volume device for the bentonites are shown. Effect of distilled water and high concentrated solution on swelling behaviour are drawn and discussed in detail. Similarly, after achieving the constant swelling pressure, the hydraulic conductivity tests results for distilled water as well as for high concentration solution are shown. The aim of the test results to be used for a qualitative analysis of hydraulic behaviour of selected bentonites.

Chapter 7 presents the outcome of the experimental results and aim to study the existing models for hydraulic conductivity and the application of developed new modifications employing the existing models to estimate the hydraulic conductivity for compacted clays. The experimental hydraulic conductivities of the bentonite are compared with the existing models like: Kozeny-Carman model, cluster model, and laminar flow model. Furthermore, the swelling pressure was estimated using the new approach based on diffuse double layer theory.

Chapter 8 presents the conclusions that can be drawn from this work, and suggestions are made for further research.

# Chapter 2

# LITERATURE REVIEW

## 2.1 Introduction

This chapter summarizes a review of the relevant literature to provide a background on clay structure and mineralogy, clay-water interaction, diffuse double layer theory, swelling soil behaviour (i.e., crystalline and diffuse double layer swelling), swelling pressure testing (laboratory swelling pressure and swelling pressure prediction). Further sections deals with flow mechanisms in soils, and factors affecting the hydraulic behaviour of clays. The review provides a background for the motivation of the research reported in this thesis.

## 2.2 Structural unit and charge on clay minerals

The most important parameter in determining the hydraulic performance of a barrier material is the minerals present in the soil. The mineral size, shape, orientation, and electro-chemical properties all combined to determine the manner in which water, other permeant, or solvated ions will be transported through the soil.

The mineral composition of the materials investigated as part of this thesis includes quartz, and smectites. Feldspar, calcite, chlorite minerals, as well as cristobalite and clinoptilolite have been identified as minor components in some of the mineralogical analyses. A detailed presentation of the results of mineralogical analysis of the materials investigated here is presented in Chapter 4.

Quartz is a silicon dioxide ($SiO_2$) which is linked in a framework of $SiO_4$ tetrahedra (Mason and Berry 1968). The feldspar group of minerals is continuous three-dimensional networks of $SiO_4$ and $AlO_4$ tetrahedra with positively charged sodium, potassium, calcium, or barium in the interstices of the negatively charged tetrahedra (Mason and Berry 1968).

As these minerals are generally electrically neutral internally they carry only weak surface charges which are readily satisfied by water molecules. Quartz and feldspar are primary minerals and so they are typically larger in dimension than the secondary clay minerals such as illite, kaolinite or smectite. As a result they have a much lower specific surface area ($m^2/g$) than clay minerals.

Carbonates and sulphates can be present either as individual particles or as coatings on other particles (Yong et at. 1992). Carbonates such as calcite ($CaCO_3$), magnesite ($MgCO_3$), or dolomite ($Ca,Mg(CO_3)_2$), and sulphates (gypsum ($CaSO_4 2H_2O$) have been identified as minor components in the bentonite deposits (Dixon and Woodcock 1986, Oscarson and Dixon 1989). Gypsic and carbonate minerals are most commonly found in arid or semi-arid regions as they are relatively soluble in water or acidic environments. They are therefore much more susceptible to dissolution when placed in an environment where there is a considerable volume of fluid which is not calcium or magnesium saturated. This means that hydraulic conductivity testing of calcareous or sulphate containing soils must have either very little pore fluid exchange or must involve so much flow that all the readily soluble material is removed.

***Soil Structure and microstructure of clays***

Smectite clay is very highly plastic clay which contains large quantity of montmorillonite (bentonite) and expands when it is in contact with water in liquid form or in vapor form. This is related to the mineralogical composition of the elementary layer or structural unit of the minerals. According to Mitchell (1993), the structure of mineral is a unit made of an alumina octahedral sheet sandwiched between two silica tetrahedral sheets. The silica tetrahedral is composed of a silicon atom and four oxygen atoms in a tetrahedral coordination (Figure 2.1) where as, the alumina octahedral structure is composed of an aluminium atom and six hydroxyls in an octahedral coordination (Figure 2.2).

The elementary layers stacked together to form particle (platelet or crystal). In dry condition, bonding between the elementary layers is provided by van der Waals and by exchangeable cations. These types of bonding are weak and broken when water or polar liquid inserts between them (Mitchell 1993).

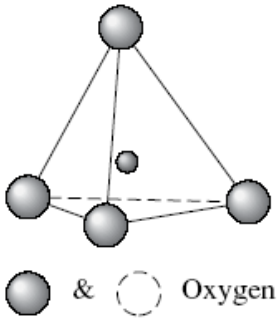


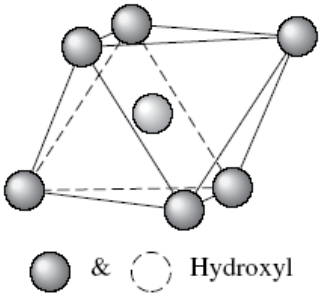


Figure 2.1 Schematic of silica tetrahedral unit

Figure 2.2 Schematic of Octahedral unit

A particle is made of several to hundred elementary layers depending on the moisture conditions (Pusch et al. 1990). Using transmission electron microscope (TEM), Tessier et al. (1998) found that the microstructure of the Fourges clay (i.e., clay which contains calcium type montmorillonite and kaolinite minerals) consists of aggregates of particle with 2-4 elementary layers on average. Inside each particle unit, it was found the interlayer distance is approximately 12Å. Moreover, the type of exchangeable cation also influences the number of elementary layer in a particle (Pusch et al.1990, Mitchell 1993, Saiyouri et al. 2004). In suspension, a particle is made of 3-5 elementary layers and 10-20 elementary layers for sodium-type bentonite and calcium-type bentonite, respectively (Pusch et al., 1990). Saiyouri et al. (2004) reported that the compaction also affected the number of elementary layers in a particle and the numbers were different for sodium and calcium type bentonites for suction higher than 3000 kPa. For suction less than 3000 kPa, they found that the number of elementary layers in a particle is almost the same for both bentonite types. The particles aggregated together to make an aggregate. These features are very important in order to investigate the behavior of clays especially on the microstructure of the bentonite (Delage 2007).

The presence of structural units (i.e., elementary layer), particles, and aggregates results in presence of different type of pores in the clays. In general, compacted soil has two types of pores (i.e., micro-pores and macro-pores) (Gens and Alonso 1992, Yong 1999). The micro-pores are defined as pores within the aggregates (i.e., pores between the elementary layers and between the particles) or called as intra-aggregate pores.

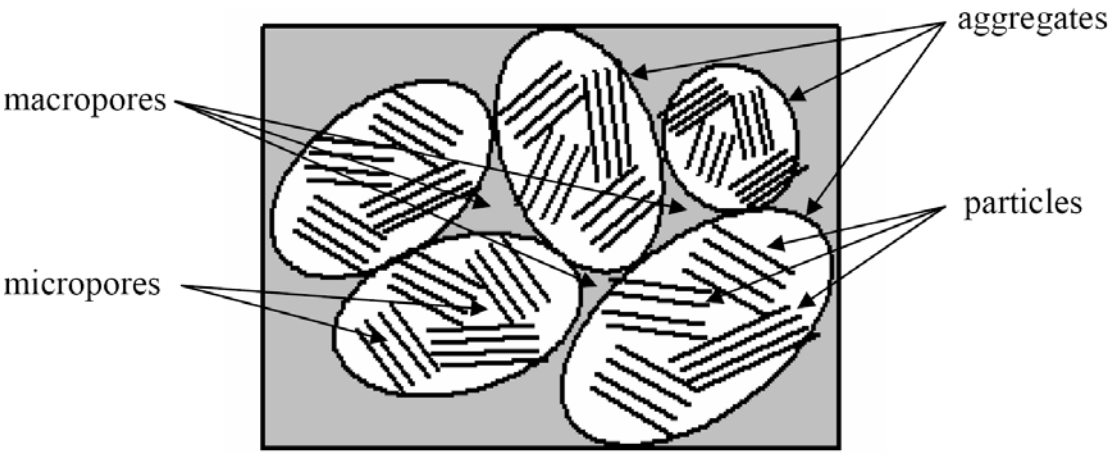


Figure 2.3 Sketch of microstructure of compacted clay (Arifin 2008)

The macro-pores are defined as pores existed between the aggregates or called as interaggregates pores. The sketch of the microstructure of compacted clay is shown in Figure 2.3. The microstructure of clay is discussed in more detail in section 2.3. The presence of macro pores, the larger voids corresponding to secondary structure such as clod interfaces and all defects, defines the macro hydraulic conductivity of the soil. Elsbury et al. (1988) observed a very permeable soil morphologically and found that the macro-pores were typically 0.001 to 0.003 μm in size. Acar and Olivieri (1989) observed that macro pores were of the same scale as clay particles with effective diameters of 0.1 to 0.3 μm.

***Clay minerals***

The manner in which octahedral sheets are arranged and bonded controls the specific clay mineral formed. As a result of isomorphous substitution within the octahedral layer, a charge imbalance is generated. The resulting negative charge expresses itself on the surface of the clay particle as a negative face charge (Yong and Warkentin 1975). The layer silicates (phyllosilicates) are among the most highly charged mineral particles present in a soil. The magnitude of the charge depends on the structure of the layer silicates, the specific cations in the crystal lattice and the size of the particles. The building blocks for the creation of clay minerals, namely the tetrahedral silica sheets and the octahedral aluminum sheets are found in three basic layer combinations. The clay types are defined by

the number of each layer type present in the basic unit of the clay. The specific clay mineral families are presented in Figure 2.4 and in Table 2.1.

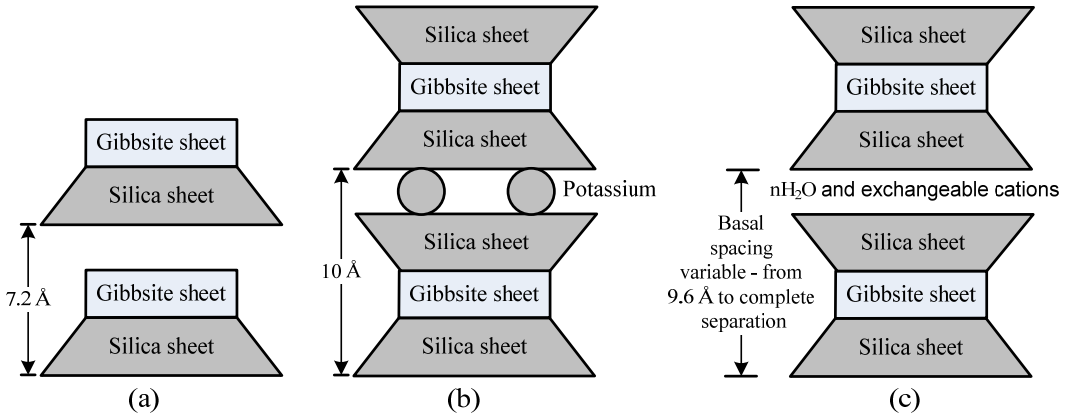


Figure 2.4 General structural arrangements of (a) kaolinite, (b) illite and (c) montmorillonite clay minerals

***Kaolinite***

Kaolinite is composed of alternating silica and alumina sheets, each sheet sharing a plane of oxygen atoms, making this a 1:1 layer clay, between these layers the tetrahedral and octahedral sheets in adjoining layers are strongly hydrogen bonded (Yong and Warkentin 1975). The strong hydrogen bonds prevent the kaolinite crystal from hydrating and expanding under most conditions. Multiple layers tend to accumulate, leading to formation of relatively large particles (70 to 100 layers thick) (Yong and Warkentin 1975). Kaolinite particles have low specific surfaces and cation exchange capacities relative to most other clay minerals (Table 2.1). The kaolinite unit layer is 0.713 nm in thickness. As it is relatively stable, it will not show changes in unit cell dimension as the result of hydration or glycolation. This produces a strong and permanent X-ray diffraction pattern of peaks at 7.13Å (0.713nm), 3.56Å (0.356nm) and 2.37Å (0.237nm) (Yong and Warkentin 1975). A typical X-ray diffraction pattern generated by kaolinite is presented in Figure 2.5.

***Illite***

Illite is composed of an octahedral alumina sheet sandwiched between two silica sheets. The octahedral and tetrahedral sheets share oxygen atoms, resulting in the formation of a

four oxygen thick layer between these sheets. The unit cells are 9.98Å (10 Å) thick and are bonded together by potassium ions. Potassium ions fit into the ditrigonal spaces present in the silica sheet neutralizing the negative charges caused by aluminum substitution or empty sites within the octahedral layer (Yong and Warkentin 1975). Under ideal conditions these potassium ions co-ordinates with 12 oxygen atoms, six from each unit layer of illite. This is a relatively stable bond and hence illite does not readily expand when it is chemically pure.

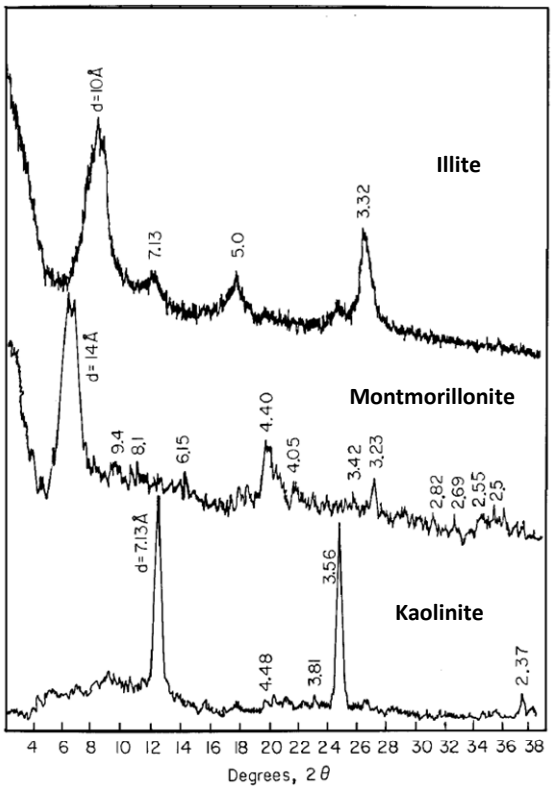


Figure 2.5 Typical X-Ray diffraction patterns for clay minerals (Yong et al. 1992)

Illites found in soil tend to be less strongly ordered or structured, and have fewer potassium ions present in the interlayer than their structural equivalent in rock (muscovite or biotite). This leads to weaker bonding between the layers and the presence of other ions such as calcium, magnesium or sodium to balance the surface charge requirements. The result is a mineral which can expand to some degree given the right environmental circumstances. Illite therefore shows properties such as specific surface, and cation exchange capacity (CEC) which are intermediate between low activity kaolinite and high activity bentonite

clays (Table 2.1). Illites being relatively stable tend to exhibit a stable X-ray diffraction pattern and are little affected by hydration or glycolation. A typical X-ray diffraction pattern presented in Figure 2.5 shows strong peaks at 10 Å (1.0nm), 5 Å (0.5nm) and 3.3 Å (0.33nm).

Table 2.1 Mineral groups and physico-chemical properties (Yong et al. 1992)

| Clay Mineral | Lattice Description | Isomorphous Substitution | CEC (cmol/kg) | Specific Surface | Source of Charge | Charge Type |
|---|---|---|---|---|---|---|
| Kaolinite | 1:1 Strong H – Bonds | 1/3 of Dioctrahedral Site are not Al | 5-15 | 10-20 | Edge broken bonds | Variable & permanent |
| Illite | 2:1 Strong K – Bonds | Al for Si Al for Mg | 25 | 70-150 | Isomorphous substitution Edge bonds | Mostly permanent |
| Chlorites | 2:2 Strong | Al for Si | 10-40 | 80 | Isomorphous substitution | Mostly permanent |
| Montmorillonite | 2:1 Very weak Bonds | Mg for Al Al for Si Fe for Al | 80 - 100 | 600 – 800 | Isomorphous substitution Edge bonds | Mostly permanent |
| Vermicullite | 2:1 Weak Mg - Bonds | Al for Si | 100 – 150 | 700 | Isomorphous substitution | Mostly permanent |

***Montmorillonite***

Montmorillonitic clays are similar in general composition to illite, having an alumina sheet located between two tetrahedral silica sheets. In montmorillonite, isomorphous substitution, typically magnesium for iron within the octahedral layer, leads to high surface charges. The specific ions substituted dictate the exact mineral type generated the intensity of surface charge and associated cation exchange capacity, and specific surface. The main difference between illite and montmorillonite is the lack of potassium ions to bond the unit cells together. Water can easily enter between the layers, leading to disaggregation and expansion of the clay in an attempt to decrease the intensity of the repulsive forces between the adjacent negatively charged clay faces. This tendency to dissociate provides a simple means for identifying the montmorillonite family of clays. Oven-dried clay will show a first-order diffraction peak at 1.0nm, an air-dry clay will have a first-order diffraction peak at approximately 1.4nm, representing 1.0nm of mineral and 0.4nm of

surface-bound water. By replacing this surface water with various organic liquids the amount by which the clay platelets will expand can be controlled. Glycerol is among the most commonly used fluids. It results in 1.77nm spacing, 1.0nm of clay and 0.77nm of glycerol, (Yong and Warkentin 1975), In general, as is shown in Table 2.1, smectite clays such as montmorillonite and vermiculite have the ability to dissociate, exchange cations, and change volume, and so are classified as high activity clays. They have a correspondingly higher CEC and specific surface than illite or kaolinite.

## 2.3 Forces in clay system and modes of particle association

As discussed in preceding section, the clay particles carry a net negative charge on their surfaces. This is the result of both of isomorphous substitution and of a break in continuity of the structure at its edges. Larger negative charges are derived from larger specific surfaces. Some positively charged sites also occur at the edges of the particles. In dry clay, the negative charge is balanced by exchangeable cations like $Ca^{2+}$, $Mg^{2+}$, $Na^{+}$, and $K^{+}$ surrounding the particles being held by electrostatic attraction. When water is added to clay, these cations and a few anions float around the clay particles. This configuration is referred to as a diffuse double layer (Figure 2.6). Diffuse double layer is discussed in more detail in section 2.6.1. The cation concentration decreases with the distance from the surface of the particle.

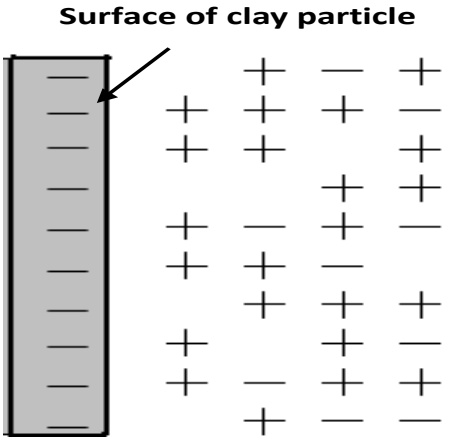


Figure 2.6 Diffuse double layer

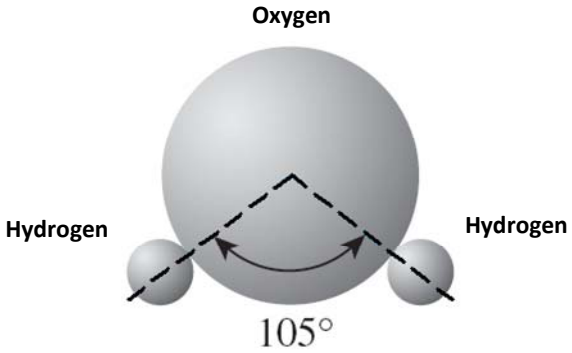


Figure 2.7 Dipolar character of water

Water molecules are polar. Hydrogen atoms are not axisymmetric around an oxygen atom; instead, they occur at a bonded angle of $105^{o}$ (Figure 2.7). As a result, a water molecule has a positive charge at one side and a negative charge at the other side. It is known as a dipole. Dipolar water is attracted both by the negatively charged surface of the clay particles and by the cations in the double layer. The cations, in turn, are attracted to the soil particles. A third mechanism by which water is attracted to clay particles is hydrogen bonding, where hydrogen atoms in the water molecules are shared with oxygen atoms on the surface of the clay. Some partially hydrated cations in the pore water are also attracted to the surface of clay particles. These cations attract dipolar water molecules. The force of attraction between water and clay decreases with distance from the surface of the particles. All the water held to clay particles by force of attraction is known as double-layer water. The innermost layer of double-layer water, which is held very strongly by clay, is known as adsorbed water. This water is more viscous than free water.

According to Santamarina (2003), interparticle forces at the micro-scale can be separated into the following three categories:

1. *Skeletal Forces Due to External Loading*: These forces are transmitted through particles from the forces applied externally e.g., foundation loading (Figure 2.8a).

2. *Particle Level Forces*: These include particle weight force, buoyancy force when a particle is submerged under fluid, and hydrodynamic forces or seepage forces due to pore fluid moving through the interconnected pore network (Figure 2.8b).

3. *Contact Level Forces*: These include electrical forces, capillary forces when the soil becomes unsaturated, and cementation-reactive forces (Figure 2.8c).

When external forces are applied, both normal and tangential forces develop at particle contacts. All particles do not share the forces or stresses applied at the boundaries in equal manner. Each particle has different skeletal forces depending on the position relative to the neighboring particles in contact. Strong particle force chains form in the direction of major principal stress. The evolution and distribution of interparticle skeletal forces in soils govern the macroscopic stress–strain behavior, volume change, and strength. As the soil approaches failure, buckling of particle force chains occurs and shear bands develop due to localization of deformation.

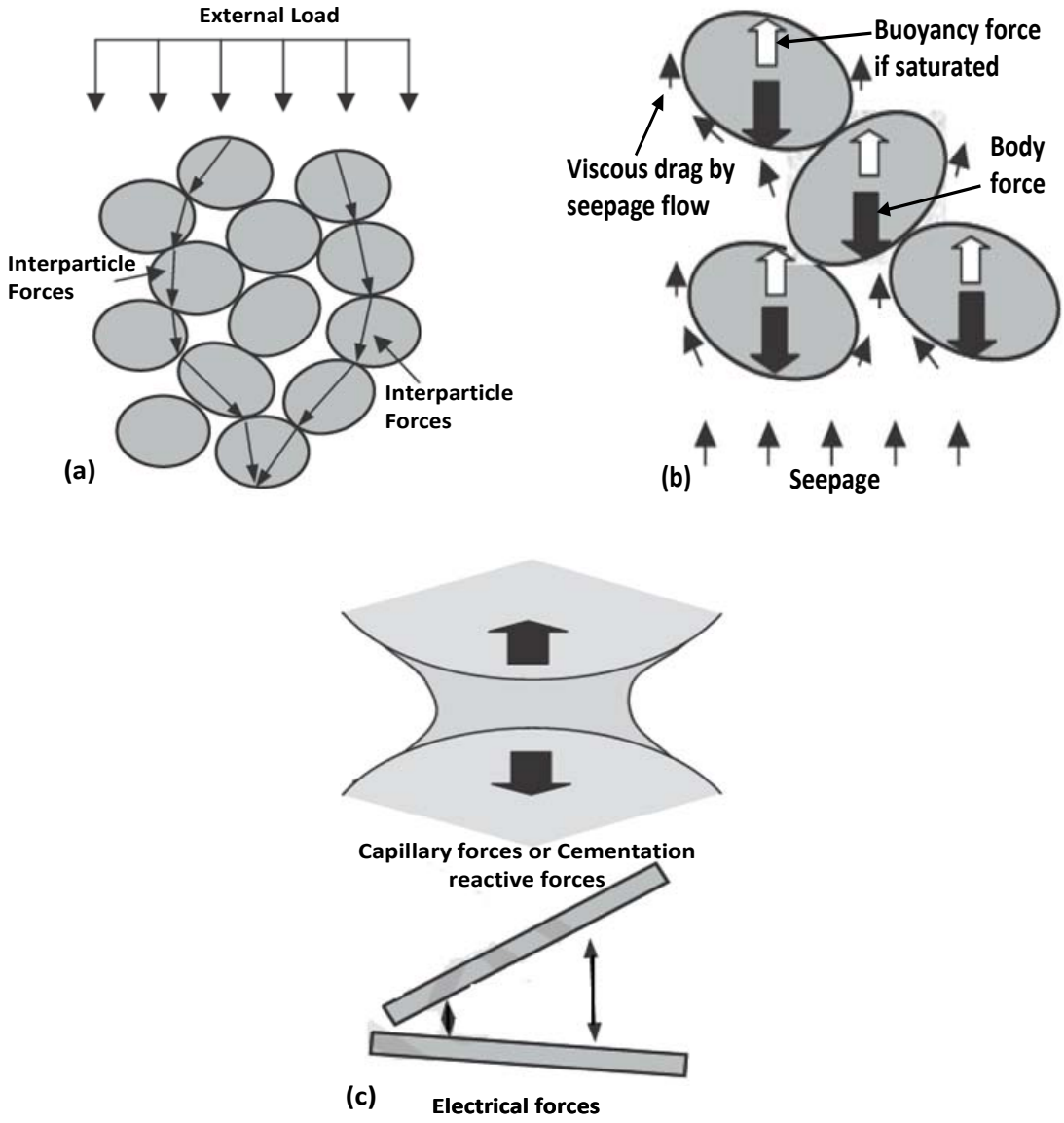


Figure 2.8 Interparticle forces at particle level: (a) skeletal forces by external loading (b) particle level forces, and (c) contact level forces (from Santamarina 2003)

Particle weights act as body forces in dry soil and contribute to skeletal forces. When the pores are filled with fluids, the weight of the fluids adds to the body force of the soil fluids mixture. However, hydrostatic pressure results from the fluid weight, and the uplift force due to buoyancy reduces the effective weight of a fluid-filled soil. This leads to smaller skeletal forces for submerged soil compared to dry soil. Seepage forces that result from

additional fluid pressures applied externally produce hydrodynamic forces on particles and alter the skeletal forces.

### 2.3.1 Interparticle forces in clay

Interparticle forces control the flocculation–deflocculation behavior of clay particles in suspension, and they are important in swelling soils that contain expanding lattice clay minerals. In denser soil masses, other forces of interaction become important as well since they may influence the intergranular stresses and control the strength at interparticle contacts, which in turn controls resistance to compression and strength. In a soil mass at equilibrium, there must be a balance among all interparticle forces, the pressure in the water, and the applied boundary stresses.

***Interparticle repulsive forces***

**Electrostatic Forces:** Very high repulsion, the Born repulsion, develops at contact points between particles. It results from the overlap between electron clouds, and it is sufficiently great to prevent the interpenetration of matter. At separation distances beyond the region of direct physical interference between adsorbed ions and hydration water molecules, double-layer interactions provide the major source of interparticle repulsion. This repulsion is very sensitive to cation valence, electrolyte concentration, and the dielectric properties of the pore fluid.

**Surface and Ion Hydration:** The hydration energy of particle surfaces and interlayer cations causes large repulsive forces at small separation distances between unit layers (clear distance between surfaces up to about 2 nm). The net energy required to remove the last few layers of water when the clay plates are pressed together. The corresponding pressure required to squeeze out one molecular layer of water may be as much as 400 MPa (van Olphen 1977). Thus, pressure alone is not likely to be sufficient to squeeze out all the water between parallel particle surfaces in naturally occurring clays. Heat and/or high vacuum are needed to remove all the water from a fine grained soil. Hydration repulsions decay rapidly with separation distance, varying inversely as the square of the distance.

### *Interparticle Attractive Forces*

**Electrostatic Attractions:** When particle edges and surfaces are oppositely charged, there is attraction due to interactions between double layers of opposite sign. Fine soil particles are often observed to adhere when dry. Electrostatic attraction between surfaces at different potentials has been suggested as a cause. When the gap between parallel particle surfaces separated by distance at different potentials, there is an attractive force per unit area, or tensile strength (Ingles 1962).

**Electromagnetic Attractions:** Electromagnetic attractions caused by frequency-dependent dipole interactions also called van der Waals forces. Permanent dipole bonds such as the hydrogen bond are directional. Fluctuating dipole bonds, commonly termed van der Waals bonds, also exist because at any one time there may be more electrons on one side of the atomic nucleus than on the other. This creates weak instantaneous dipoles whose oppositely charged ends attract each other. Although individual van der Waals bonds are weak, typically an order of magnitude weaker than a hydrogen bond, they are non-directional and additive between atoms. Consequently, they decrease less rapidly with distance than primary valence and hydrogen bonds when there are large groups of atoms. They are strong enough to determine the final arrangements of groups of atoms in some solids (e.g., many polymers), and they may be responsible for small cohesions in fine grained soils.

**Primary Valence Bonding:** Chemical interactions between particles and between the particles and adjacent liquid phase can only develop at short range. Covalent and ionic bonds occur at spacings less than 0.3 nm. In covalent bond, one or more bonding electrons are shared by two atomic nuclei to complete the outer shell for each atom, whereas, ionic bonds form between positively and negatively charged free ions that acquire their charge through gain or loss of electrons. Cementation involves chemical bonding and can be considered as a short-range attraction. Whether primary valence bonds, or possibly hydrogen bonds, can develop at interparticle contacts without the presence of cementing agents. Very high contact stresses between particles could squeeze out adsorbed water and cations and cause mineral surfaces to come close together, perhaps providing opportunity for cold welding.

**Cementation:** Cementation may develop naturally from precipitation of calcite, silica, alumina, iron oxides, and possibly other inorganic or organic compounds. The addition of stabilizers such as cement and lime to a soil also leads to interparticle cementation. If two particles are not cemented, the interparticle force cannot become tensile; they loose contact. However, if a particle contact is cemented, it is possible for some interparticle forces to become negative due to the tensile resistance (or strength) of the cemented bonds. There is also an increase in resistance to tangential force at particle contacts. However, when the bond breaks, the shear capacity at a contact reduces to that of the uncemented contacts. An analysis of the strength of cemented bonds should consider three cases: (i) failure in the cement, (ii) failure in the particle and (iii) failure at the cement-particle interface. Cementation allows interparticle normal forces to become negative, and, therefore, the distribution and evolution of skeletal forces may be different than in uncemented soils, even though the applied external stresses are the same. Thus, the stiffness and strength properties of a soil are likely to differ according to when and how cementation was developed.

**Capillary Stresses** As water is attracted to soil particles and water can develop surface tension, suction develops inside the pore fluid when a saturated soil mass begins to dry. This suction acts like a vacuum and will directly contribute to the effective stress or skeletal forces. The negative pore pressure is usually considered responsible for apparent and temporary cohesion in soils, whereas the other attractive forces produce true cohesion. When the soil continues to dry, air starts to invade into the pores. If the water surrounding the soil particles remains continuous term as “funicular” regime Bear (1972), the interparticle force acting on a particle with radius can be estimated from the size of the pore into which the air has entered. Since the fluid acts like a membrane with negative pressure, this force contributes directly to the skeletal forces like the water pressure as shown in Figure 2.9a.

As the soil continues to dry, the water phase becomes disconnected and remains in the form of menisci or liquid bridges at the interparticle contacts, term as “pendular” regime Bear (1972). The curved air-water interface produces a pore water tension, which, in turn, generates interparticle compressive forces. The force only acts at particle contacts in contrast to the funicular regime, as shown in Figure 2.9b. The interparticle force generally depends on the separation between the two particles, the radius of the liquid bridge,

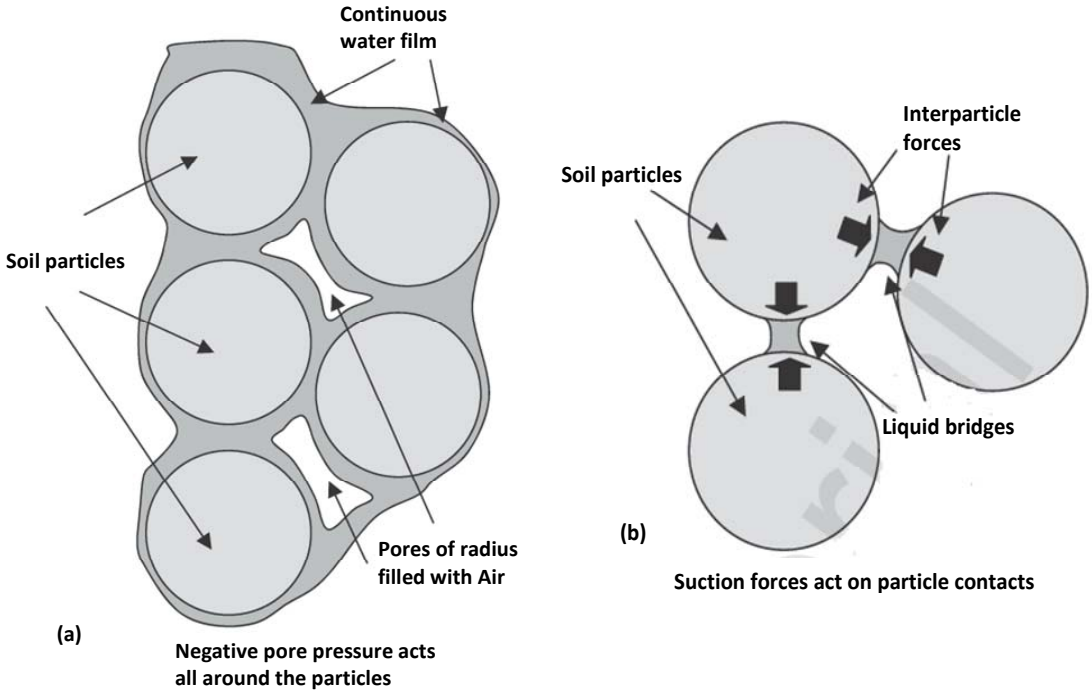


Figure 2.9 Microscopic water-soil interaction in soils: (a) funicular regime and (b) pendular regime

interfacial tension, and contact angle (Lian et al. 1993). Once the water phase becomes discontinuous, evaporation and condensation are the primary mechanisms of water transfer. Hence, the humidity of the gas phase and the temperature affect the water vapor pressure at the surface of water menisci.

### 2.3.2 Modes of particle association in clay

The knowledge of particle associations in suspensions is a good starting point for understanding how soil fabrics are formed and changed throughout the history of a soil. The term fabric refers to the arrangement of particles, particle groups, and pore spaces in a soil. The term structure is sometimes used interchangeably with fabric. It is preferable, however, to use structure to refer to the combined effects of fabric, composition, and interparticle forces. Particle associations in clay suspensions may be more complex and can be classified into following categories (van Olphen 1977).

1. Dispersed: No face to face association of clay particles
2. Aggregated: Face to face (FF) association of several clay particles
3. Flocculated: Edge to edge (EE) or edge to face (EF) association of aggregates
4. Deflocculated: No associated between aggregate

The terms flocculated and aggregated are used to refer to multi-particle assemblages, and the terms deflocculated and dispersed are used to refer to single particles or particle groups acting independently.

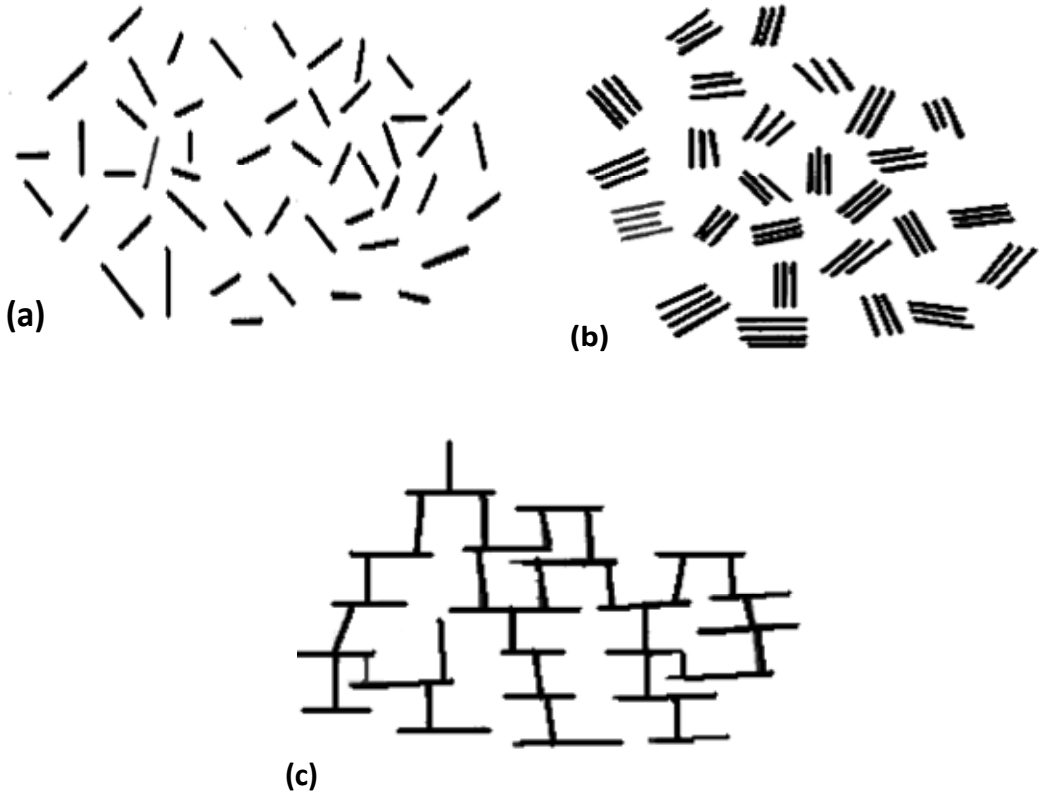


Figure 2.10 Modes of particles association in clay suspension (a) Dispersed and deflocculated (b) aggregated but deflocculated (face to face association) (c) flocculated but dispersed (edge to face or face to edge association)

Figure 2.10 shows three different modes of particle association in clay suspension, however, particle associations compacted clays assume a variety of forms; most of them

are related to combinations of the configurations shown in Figure 2.10. Compacted clays are almost composed of multi-particle aggregates. Overall, three main groupings of fabric elements may be identified (Collins and McGown 1974): Elementary particle arrangements: Single forms of particle interaction at the level of individual clay. Particle Assemblages: Units of particle organization having definable physical boundaries and a specific mechanical function, and which consist of one or more forms of the elementary particle arrangements and Pore Spaces: Fluid and/or gas filled voids within the soil fabric.

***Fabric scale***

When a soil has 50% or more particles with sizes of 0.002 mm or less, it is generally termed clay. Studies with scanning electron microscopes (Yong and Sheeran 1973, Collins and McGown 1974) have shown that individual clay particles tend to be aggregated or flocculated in submicroscopic units as discussed above. These units are referred to as domains. The domains then group together, and these groups are called clusters. Clusters can be seen under a light microscope. This grouping to form clusters is caused primarily by interparticle forces. The clusters, in turn, group to form peds. Peds can be seen without a microscope. Groups of peds are macrostructural features along with joints and fissures. Figure 2.11 shows the arrangement of domains and clusters with particles size and the arrangement of the peds and macropore spaces.

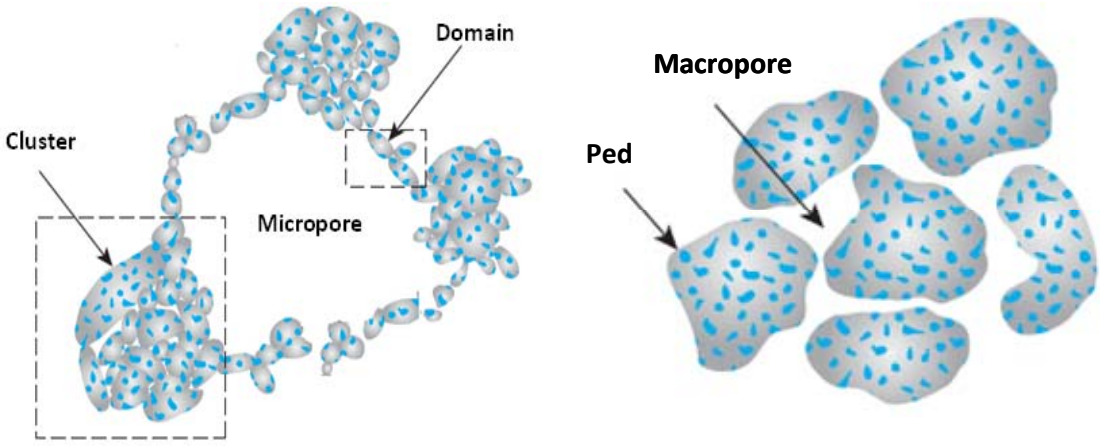


Figure 2.11 Arrangement of domain, clusters, peds and macropore

Soil mechanical and flow properties depend on details of these levels of fabric scale to varying degrees. For example, the hydraulic conductivity of a fine grained soil is almost dominated by the macropores.

## 2.4 Water in compacted clays

Mitchell (1993) summarized the possible mechanisms for clay-water interaction. The mechanisms are hydrogen bonding, hydration of exchangeable cations, attraction by osmosis, charged surface-dipole attraction, and attraction by London dispersion forces. For clays, at dry or low water content the hydration of exchangeable cations is the main mechanism. In dry condition, the exchangeable cations are located on the surface of the layers or tetrahedral sheet to balance the negative charge of the clay surface. In the hydration process, the water molecules are absorbed in between the elementary clay layers to develop water layers. The thickness of dehydrated montmorillonite crystals and of complete hydrate layers depend on the exchangeable cation. Pusch et al. (1990) has reported the thickness and the complete hydrate layers of water molecules for different exchangeable cations as summarized in Table 2.2. From the table, it is shown that there are 3 layers of water molecules for $Mg^{2+}$ and $Na^{+}$ bentonite and 2 layers of water molecules for $Ca^{2+}$ and $Na^{+}$ bentonite developed on the clay surface in order to fulfill the hydration force. The total water thicknesses of the bentonites are 9.08, 5.64, 9.74, and 6.15 Å for Mg, Ca, Na, and K bentonite, respectively.

Table 2.2 Thickness in Å and complete hydrate layers for different exchangeable cation (Pusch et al. 1990)

| | | 0 hydrate | 1st | 2nd | 3rd |
|---|---|---|---|---|---|
| **Montmorillonite** | $Mg^{2+}$ | 9.52 | 12.52 | 15.55 | 18.6 |
| | $Ca^{2+}$ | 9.61 | 12.5 | 15.25 | ..... |
| | $Na^{+}$ | 9.62 | 12.65 | 15.88 | 19.36 |
| | $K^{+}$ | 10.08 | 12.5 | 16.23 | ..... |

Water content of bentonite at the end of the hydration process can be calculated roughly from data presented in Table 2.2 by calculating the weight of water per gram soil from

multiplication of the total water thickness, specific surface area of the bentonite, and the volumetric weight of water. The water content is equal to the weight of water per gram soil multiplied by 100 percent divided by 2. For bentonite with 500 $m^2/g$ and the volumetric weight of water of 1 $Mg/m^3$, the water content of the bentonites are 22.7, 14.1, 23.9, and 15.4% for the $Mg^{2+}$, $Ca^{2+}$, $Na^+$, and $K^+$ type bentonite, respectively. It seems that sodium type bentonite absorbs more water in hydration process compared to other bentonites. Since volumetric weight of water is more than 1 $Mg/m^3$ for less than 3 layers of water molecules on the clay surfaces (Mitchell, 1993), the water content can be higher than those values. In addition, Saiyouri et al. (2004) reported that four water layers were developed on the clay surface of the bentonites used in their study (i.e., MX 80 and FoCa7).

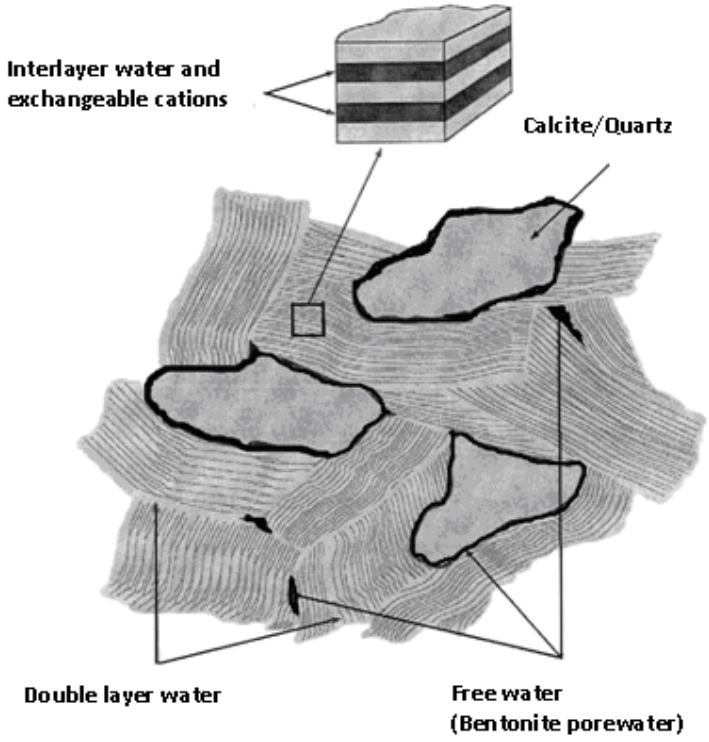


Figure 2.12 Representation of interlayer water, double layer water and "free water" in compacted bentonite (Bradbury and Baeyens 2002)

According to Mitchell (1993), for fully expanding, sodium type bentonite having specific surface area with 800 $m^2/g$ would reach water content of 400% to fulfill the hydration of the exchangeable cation. After about three to four monolayers of water molecules in between the elementary layers, surface hydration becomes less important. Water molecules

tend to diffuse toward the surface in an attempt to equalize ion concentrations. This occurs in between the external surface of particle or crystal (Pusch et al. 1990, Bradbury and Baeyens 2002, Pusch and Yong 2003, Saiyouri et al. 2004). Since for Sodium bentonite, the particles break up to be elementary layers due to hydration (Pusch 2001), the diffuse double layer can be developed in between elementary layers. The remaining fraction of water can be regarded as "free water" which exists as inter connected thin film on the outside of the clay particle and also as films surrounding the other component mineral grains in bentonite. The amount of "free water" and concentration of dissolve salt in the "free water" in the compacted bentonite depend on the initial dry density of the specimen (Bradbury and Baeyens 2002). A schematic picture of water in compacted bentonite is presented in Figure 2.12.

## 2.5 Hydration processes in compacted clays

Pusch and Yong (2003) distinguished three boundary conditions that are believed to cause different hydration rates in expansive clays. The three boundary conditions are the clay exposed to water vapor, the clay exposed to non-pressurized liquid water, and the clay exposed to pressurized water. For the clay contacted with water vapor, the water molecules migrate into the open channels and adsorbed on exposed mineral surface. The water molecules then migrate into the elementary sheets that have higher hydration potential. The entire migration process of the water molecules is diffusion-like process. The saturation process is sufficiently slow to let entrapped air be dissolved and diffuse out from the clay without delaying saturation, which will, however, probably never be complete.

For the clay exposed to non-pressurized liquid water, water is absorbed by capillary forces in the open channels. Then the water migrates into finer void and further into the elementary sheets. Since water molecules entering the elementary sheets result in expanding clay particles and/or aggregates, the large channels become closed and hydration is then controlled by diffusion. In this case, the hydration rate is somewhat higher than the first condition (i.e., the clay exposed to water vapor) since the larger channels are filled quickly.

For the clay exposed to pressurized water, water is pressed into the large channels and move quickly. The penetrating water displaces air and compresses the unsaturated matrix.

The hydration rate is faster than those of first and second conditions (i.e., water exposed to vapor and non pressurized water). However, when the large channels become closed by the expansion of the clay aggregates, the hydration process follows the same procedure as the second procedure. This occurs in case of the heavily compacted bentonite.

Pusch (1980) investigated the hydration process of highly compacted MX-80 bentonite with initial water content of 10% and bulk density range 2 – 2.1 $Mg/m^3$. Water is absorbed and transported inward due to suction potential which is very high at low water content i.e. at small interlamellar distance. In particular, the rate of water migration from the surface should therefore be governed by the potential gradient produced by different average interlamellar distances at the water front and at outer water saturated parts. This can be interpreted as a diffusion process, where the concentration gradient is equivalent to the water content gradient.

Tessier et al. (1998) showed experimentally the hydration process of Fourges clay, FoCa, having initial water content 10%, specific area 300 $m^2/g$, with dry density of 1.95 $Mg/m^3$. They found that the microstructure of the Fourges clay (i.e., clay which contains calcium type montmorillonite and kaolinite minerals) consists of aggregates of particle with 2-4 elementary layers on average. Microstructure changes appeared when the clay was hydrated in the oedometric cell. Changes occurred in the texture of the clay since the particle thicknesses and their dimensions in the plane can be multiplied by 10 and more. Inside the particles, the inter crystal unit spaces between the kaolinite and/or smectites have practically disappeared so that these spaces have become similar to the interlayer distances.

Saiyouri et al. (2004) investigated the hydration mechanism by controlling suction to the compacted bentonites. Two types of bentonites (i.e., FoCa7 and MX-80 which are calcium and sodium bentonites, respectively) were used in the study. Three methods were used in controlling suction (i.e., applying air pressure in Plexiglas tube equipped with pore filter for controlling suction from 1-100 kPa, a high-pressure membrane cell for applying suction at 1000 kPa, and vapor equilibrium technique for controlling suction from 3000-100000 kPa). Using XRD method, they found that the placement of water molecules is a function of suction, with 1 layer above 50000 kPa, 2 layers at suction from 50000 to 7000 kPa, 3 layers at suction from 7000 to 60 kPa, and 4 layers below 60 kPa. Both bentonite types

showed similar phenomena. At the same time, the number of elementary layers in the particle decreases with suction.

The hydration of expansive clays and the corresponding changes in microstructure at the level of clay layers and clay particles inside the aggregates have been described by Delage et al. (2006). Delage et al. (2006) stated that for the MX-80 specimen hydrated in confined condition, by considering the permeability and microstructure, the immediate stress release modifies mainly the macro-pores (i.e., inter-aggregate pores) due to decrease in inter-aggregate stresses and hence allowing global volume expansion. They stated that no change in the micro-pores occurs due to the very small pore size, slow water transfer phenomena, and strong attraction between water and minerals. Delage et al. (2006) also investigated the density effects on the compacted MX-80. It was found that, at the same water content, the change in porosity of specimen compacted with higher dry density was due to the change in the large pores. These large pores correspond to the pore located between clay aggregates or inter-aggregate pores. They confirmed that hydration was governed by the progressive placement of layers of water molecules along the surface of the elementary clay layer, inside the clay particles, starting from one layer in dry conditions and ending up with a maximum number of four layers. Simultaneously, the number of stacked layers per particle was observed to decrease, from various hundreds down to 10.

## 2.6 Clay-water interaction and relation

Accounting for the influence of a surface charge on the mineral faces is just the first step in understanding the very complex interactions in a clay-water system. According to (Guven 1992), a proportion of the water in a clay–water mixture is structurally bonded to the surface of highly charged clay platelets. The presence of surface charges and exchangeable cations, especially in active clays such as bentonite, can significantly affect the distribution of ions and the water structure (Yong et al. 1992). “Bound” water is different in its physical structure, density, thermal expansivity, and viscosity compared with the normal values for “unbound” water (Dixon et al. 1993). The boundary between bound and unbound water defines the “effective porosity” in which water can move in the normal way under hydraulic gradients. Pashley and Israelachvili (1984a) suggest that

hydration forces can affect the pore fluid at distances up to 2.5 nm, 10 layers of water molecules in layered silicates such as Illites. In loose clays and slurries with large pore sizes, much of the water is beyond this distance from the mineral surface. It is in its normal (unbound) state and can move in the usual way under the influence of hydraulic gradients. However, in the densely compacted bentonite, the average pore size corresponds to only two to four molecular thicknesses of water. Much of the water is therefore bonded to the mineral surfaces and can be expected to exhibit different flow behaviour. Compacted clays consist of aggregates (or peds) of closely spaced mineral particles as shown in Figure 2.11. The spaces (micropores) between particles inside the aggregates are small. The water content at the time of hydration controls the size of these spaces and is generally insufficient for the clay to be fully hydrated (Wan et al. 1995). The separation of mineral particles forming the micropores contributes to the net unit repulsive force between the particles when saturated (Graham et al. 1992), and to both osmotic and matric suctions when unsaturated (Wan et al. 1995). The microstructures of the aggregates ultimately control the strength of the material. The aggregates are not stiff like mineral particles but distort under external loading. Spaces between the aggregates (macropores) depend on the energy used for compaction. They control hydraulic property of the material, but have a lesser effect on strength. Clearly, to support external loads, the contact area between neighbouring aggregates must be appreciable. This leads to an understanding that macropores may not be continuous and that some of the "throats" between neighbouring macropores may restrict water flow. Restricted flow should be more noticeable when densities are high, external pressures are high.

A number of models have been proposed to describe the interaction between the water and mineral components in clay-water systems. The role of mineral charge and structure on the water associated with smectite minerals has been discussed in considerable detail by Guven (1992a). In fine-grained materials such as smectites (bentonites), a general relationship was developed to provide an approximation of the number of layers of adsorbed water and the density of the water present on the surface of smectite minerals (Guven 1992a). The relationships developed in Equations 2.1 to 2.5 take into account possible variations in the number of individual crystals present in each quasicrystal (package of unseparated basic mineral platelets), as well as the number of layers of water present:

$$m_w = S_b dt \rho_w \tag{2.1}$$

$$m_c = S_b d_{001} \rho_c / 2 \tag{2.2}$$

where: $d_{001}$ is the unit layer thickness of the individual crystals (0.96 nm), $S_b$ is the exposed specific basal surface area per gram of clay, $dt$ is the thickness of a monolayer of water (assuming normal density of liquid water a single water layer is approximately 0.25nm thick), $\rho_w$ is the density of liquid water, $\rho_c$ is the density of the mineral, $m_w$ is the mass of the water component and $m_c$ is the mass of the clay component (Guven 1992a).

For a single (mono) layer of water on the surface of a specimen consisting of fully dispersed clay, Equations 2.1 and 2.2 can be simplified.

$$m_w / m_c \approx 0.2 j \tag{2.3}$$

where $j$ is the number of monolayer's of water present on the surface of the particle. Under conditions where the clay is not entirely dispersed, Equation 2.3 can be altered to give a more general solution where the number of silicate layers ($n$) in the quasicrystal is taken into account.

$$m_w / m_c \approx 0.1\left(\left(n+1\right)/n\right) j \rho_w \tag{2.4}$$

In a system where the number of silicate layers is significant (>10), then the relationship in Equation 2.4 can be simplified to provide a general equation for estimating the quantity of water which will be present:

$$m_w / m_c \approx 0.1 j \tag{2.5}$$

The literature indicates that water associated with charged surfaces of clay particles is more highly structured and of a different density than that of free water. Anderson and Low (1958) reported that the density of water associated with bentonite clays is much less than that of free water. However, a number of other researchers including Mitchell (1976) have suggested that the density of water associated with bentonites is higher than that of free

water. The density decrease reported by Anderson and Low (1958) was reported to extend as far as 6 nm from the particle surface. Although no mention of water density changes was reported. Lutz and Kemper (1959) reported structured water to exist to more than 10 nm from the mineral surface in sodium bentonite, whereas structured water seemed to exist only to 1 nm in calcium bentonite. The density of this water was reported to decrease as the surface of the clay particle was approached. A decrease of 2% to 3% in the density was reported at a distance of approximately 1 nm from the clay surface. Lutz and Kemper (1958) described the water in clay-water systems as having a "broken down ice structure" in which there is a tendency for each water molecule to bond itself tetrahedrally to four neighbouring water molecules. The bonds are continually breaking and reforming so that, on the average, each molecule is bonded to less than four neighbours and has other neighbours at longer distances.

### 2.6.1 Diffuse double layer model for clay-water system

The negative surface charges associated with the clay particles present an electrified interface. Since clay-water contains dissolved solutes with positive charges, e.g. cations, the interaction between a negatively charged soil particle surface and the cations in the clay-water will generate diffuse double layer as shown in Figure 2.6. The best known of the models developed to predict ionic concentration at various distances from the surface of a charged surface is the Diffuse Double Layer (DDL) model. The model known as the Gouy-Chapman model provides a means of accounting for ionic mobility in solution (Mitchell 1976, Sridharan et al. 1986, Tripathy et al. 2004, Schanz and Tripathy 2009). The following equations present the basic formulation of the model.

$$p = 2n_0 kT(\cosh u - 1) \tag{2.6}$$

$$\begin{aligned} &-\left(\frac{dy}{d\xi}\right)_{x=0} = \sqrt{(2\cosh z - 2\cosh u)} \\ &= \left(\frac{B}{S}\right)\sqrt{\left(\frac{1}{2\varepsilon_0 D n_0 kT}\right)}, x = 0, y = z \end{aligned} \tag{2.7}$$

$$\int_z^u \frac{1}{\sqrt{(2\cosh y - 2\cosh u)}}\, dy = \int_0^d d\xi = -Kd \tag{2.8}$$

$$K = \left( \frac{2n_0 e'^2 v^2}{\varepsilon_0 DkT} \right)^{1/2} \tag{2.9}$$

$$e = G\rho_w Sd \times 10^6 \tag{2.10}$$

where $p$ is swelling pressure in (N/m$^2$), $n_0$ is the ionic concentration of the bulk fluid in (ions/m$^3$), $u$ is the nondimensional midplane potential, $k$ is the Boltzmann's constant (1.38 $\times$ 10$^{-23}$ J/K), $T$ is the absolute temperature in Kelvin, $\xi$ is the distance function, $y$ is the nondimensional potential at a distance $x$ from the clay surface, $z$ is the nondimensional potential function at the surface ($x$ = 0), $B$ is the cation exchange capacity (meq/100g), $S$ is the specific surface area (m$^2$/g), $\varepsilon_0$ is the permittivity of vacuum (8.8542 $\times$ 10$^{-12}$ C$^2$J$^{-1}$m$^{-1}$), $D$ is the dielectric constant of bulk fluid (80.4 for water), $K$ (1/m) is the diffuse double layer parameter, $e$' is the elementary electric charge (1.602 $\times$ 10$^{-19}$ C), $v$ is the valency of exchangeable cations, $e$ is the void ratio of the clay specimen, $G$ is the specific gravity of soil solids, $d$ is the half the distance between clay platelets in meters, and $\rho_w$ is the unit weight of water.

It is recognized that the Gouy Chapman model does not truly represent the conditions actually present in a clay-water system. The model does provide a means of estimating the thickness of the diffuse layer and the influences of surface potential pore solution and temperature on the diffuse double layer thickness (Mitchell 1976). The theory has been found to be inadequate to allow accurate prediction of ion distributions in most systems. The factors that may arise while applying the theory (Schanz and Tripathy 2009) are:

(*a*) Poorly developed or partially developed diffuse double layers.

(*b*) Reduced specific surface area due to formation of clay particles.

(*c*) Surface and ion hydration at close platelet spacing are ignored.

(d) The clay plates are not of uniform size and arranged parallel with a uniform separation distance, as assumed.

(*e*) In the theory, electrical attraction is not taken into consideration.

(*f*) Presence of various types of exchangeable cation.

(*g*) Presence of minerals other than montmorillonite in the clay.

(*h*) Ions are approximated as point charges in the theory.

(*i*) The void ratio/separation distance 2d is not a unique function of stress, and fabric and structure are important.

Extensive discussions on the surface charge sources, magnitudes and locations in clay-water systems have been presented by Yong et al. (1992) and Guven (1992a). The counterions (ions which balance the surface charges of the clay minerals), were visualized as forming three types of complexes with the reactive sites on particle surfaces (Figures 2.13 and 2.14).

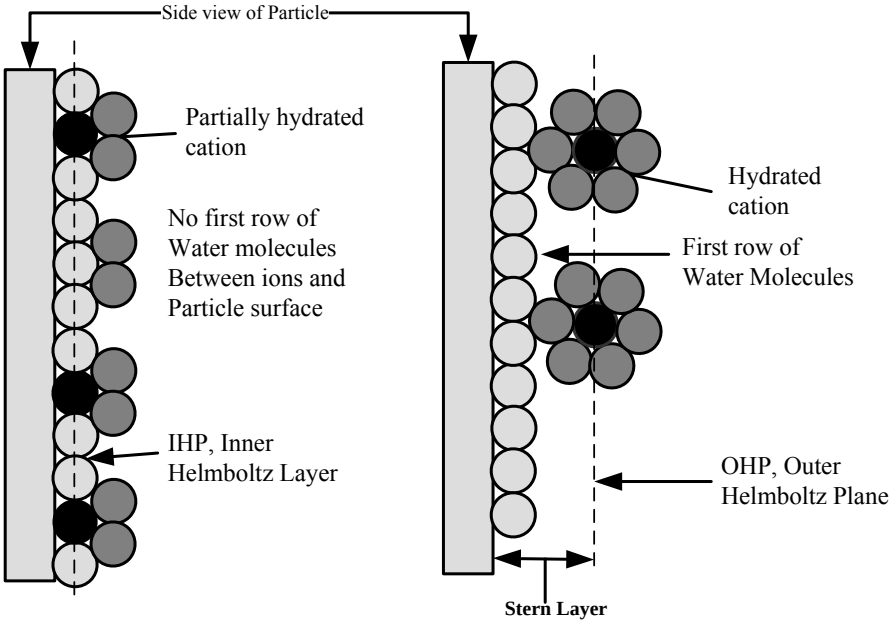


Figure 2.13 Potential ion arrangements at the particle water interface (Yong et al. 1992)

These complexes were as follows:

(*a*) Inner-sphere complexes in which the counter ions are directly bound to the surface without a solvent molecule linking them (Figure 2.13A),

(*b*) Outer-sphere complexes which contain at least one solvent molecule between the counterions and the surface (Figure 2.13B),

(*c*) The diffuse ion swarm consisting of hydrated ion clusters that move (diffuse) parallel to the surface (Figure 2.14).

Sposito (1992) discussed the Gouy-Chapman theory; he presented the argument for the presence of quasicrystals which are generally perceived to form in solutions where divalent cations are present. These quasicrystals are composed of stacks of cations four to seven layers in thickness which has been solvated by six water molecules in an outer-sphere surface complex structure. These hydrated cations (also referred to as counterions) provide an electrostatic binding mechanism to hold the clay layers together. The quasicrystal concept also provides a means by which a portion of the total porosity of the clay can be defined as being unable to conduct water in a normal Newtonian manner. Newtonian flow is the condition where a constant, linear relationship exists between rate of fluid-shear (velocity) and the shear stress (pressure difference across fluid).

The model for a multilayer clay-water interface presented in Figure 2.14 consists of several regions (Yong et al. 1992, Guven 1992a), and these include:

1. The $\alpha$, (inner Helmholtz) plane is mainly oriented water dipoles on the clay surfaces. De-hydrated counterions may also exist between this plane and the surface. These molecules and ions represent the inner-sphere or bonded layer of the clay particle. This is also known as the Stern water layer.

2. The $\beta$-plane represents the first layer of hydrated ions.

3. The D-plane is the beginning of the diffuse double layer, and may coincide with the outer-Helmholtz plane.

4. The (1/k) plane is located somewhere in the diffuse region, where the potential ($\psi$) drops to a value of ($\psi$/e). 1/k is the thickness of the double layer and *e*' is the electron charge ($1.602 \times 10^{-19}$ C).

5. The $\xi$-plane is the slip (shear) plane which separates the section of the double layer that moves with the clay particle, or alternatively the portion of the double

layer which does not take part in normal flow. This plane is located somewhere in the diffuse layer, probably close to the (1/k) plane.

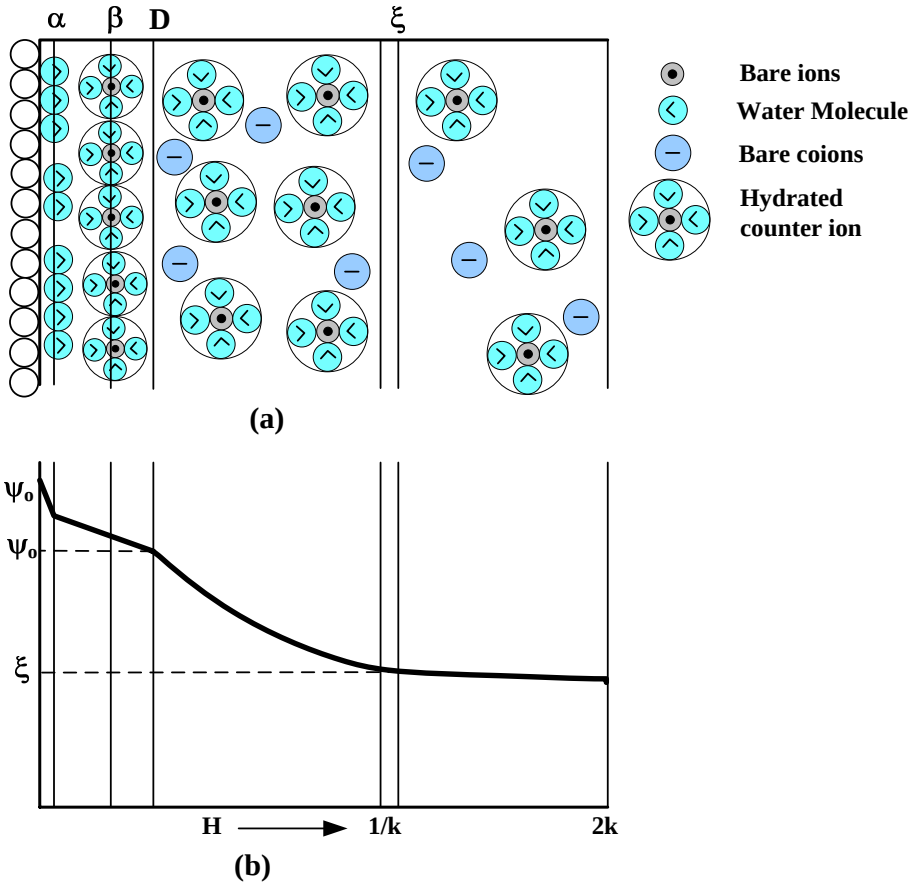


Figure 2.14 Distribution of ions at charged surface (Guven 1992a), a) model for multilayer configuration at clay-water interface, b) Decay of surface potential ($\psi_o$) in interface region

The diffuse double layer model presented in Figure 2.14 calls for the counterions of the inner-sphere to be immobile and located on the α, (inner Helmholtz) plane. The distance they extend outwards is determined by the radii of the dehydrated ions. This model provides for the existence of an ordered layer between the particle surface and the diffuse double layer (Guven 1992a). Figure 2.14 presents a conceptual diagram of the nature of the DDL distribution of pore fluid ions. The fluid-solid interface consists of an electrical double layer (EDL), composed of a row of negative charges on the particle and the first row of positive charged ions (cations) in solution. Neighbouring particles possess similar

charges and therefore net unit repulsive forces are developed between them. These forces are related to particle spacings, pore fluid chemistry, temperature and external loading. Any change in these parameters can result in changes in the EDL and any structured water associated with it.

The highly structured region of the double layer is normally defined as including the α- and β-planes and is believed to extend approximately 0.5 nm (2 water layers thickness), (Guven 1992a). Other researchers have found evidence that the hydration forces can have effects on the pore fluid at distances as great as 2.5 nm (10 water layers thickness), from the surface (Pashley and Israelachivili 1984a, 1984b). This would quantify the diffuse layer as existing between 0.5 nm and 2.5 nm (some 2 to 10 water layers out from the mineral surface).

An extensive region of structured water can have a significant impact on the behaviour of dense clay materials. In dense systems where the clay platelets or quasicrystals are present in a homogeneous structure there may only be a limited amount of water in the system which is other than Stern or β-plane water. In addition to the influence of the space available between clay platelets, there is a significant influence from the type of hydrated cations present in solution. Hydrated cation can occupy very significant portion of the pore space available, and may exhibit a range of field strengths. Likewise, changing the pore fluid chemistry can increase the ease of water movement if a small size hydrated cation is available to replace a larger complex that was previously associated with the particle surfaces. An example of such an ionic replacement would be potassium ($K^+$) replacing sodium ($Na^+$).

## 2.7 Swelling and non swelling clays

McKeen (1992) proposed a classification system for swelling (expansive) clays. According to his classification, clays that swell less than 2.8 % on wetting are considered as non-swelling (non-expansive) clays, those which swell 2.8 to 5.3 % are moderately swelling clays, those which swell more than 5.3 to 10% are highly swelling clays and finally soils which swell more than 10 % are considered as special case of highly swelling clays. It is, however, a tentative classification because the amount of swelling of a soil is a

function of the stress and suction histories of the soil (Sharma 1998). The amount of swelling in the soil depends upon the active clay mineral present. In these soils important physico-chemical interactions occur in the vicinity of the active clay minerals. Proper understanding of these interactions can explain some of the salient features of clay behaviour. This helps in constructing a conceptual picture of the swelling or non swelling processes in clays. However, in this thesis swelling (expansive) clays are discussed.

### 2.7.1 Swelling mechanism in clays

Swelling clays are found throughout the world and have both positive and negative effects associated with their swelling properties. Destructive effects to infrastructure have been reported on the order of billions of dollars per year (Jones and Holtz 1973). On the positive side, the self-healing abilities of swelling soils are exploited in the development and design of waste repositories. Compacted swelling clay materials are often used in these applications. As water attempts to transport waste materials into the biosphere the soil swells in response to increasing water content and reduces its conductivity. Currently, nuclear waste repository concepts are being developed throughout the world and are using compacted swelling clay-based materials. These materials are compacted in an unsaturated state and subjected to conditions over a long-range of time, including extremely high heat followed by groundwater infiltration while the repositories cool.

Swelling of expansive clay occurs when the clay is dispersed in a solvent, or when the clay is in contact with an atmosphere having a high vapor pressure of the solvent. Laird (2006) mentioned six separate processes controlling swelling of smectites in aqueous systems (i.e., crystalline swelling, double-layer swelling, the breakup of quasicrystals (or crystals), cation demixing, co-volume swelling, and Brownian swelling). He stated that crystalline swelling, double-layer swelling, and the breakup of clay particles (or crystals) control dominantly the swelling processes of expansive clays.

#### 2.7.1.1 Crystalline swelling

Many studies have focused on crystalline swelling. Madsen and Müller-Vonmoos (1989) and Slade and Quirk (1991) reported that the development of crystalline swelling takes place due to absorption of three to four mono-layers of water molecules in the inter-laminar pores of the expansive clays. The absorption of three to four water layers occurs in steps which signify that crystalline swelling is also a stepwise process. Madsen and Müller-

Vonmoos (1989) further added that in unconfined condition, the volume of smectite (or montmorillonite) might increase two times larger than its initial volume due to crystalline swelling, whereas, in constant volume condition, the swelling pressure as a result of crystalline swelling can reach more than 100000 kPa. In heavily compacted condition, the crystalline swelling is of major importance pertaining to its use as a containment barrier for the nuclear waste repository (Bucher and Müller- Vonmoos 1989).

Iwata et al. (1995) further added that in the case when the swelling is restrained, there is a development of swelling pressure and in the case of crystalline swelling; the swelling pressure developed is very high, reaching several thousands of kPa. However, Yong (1999) explained that this type of swelling pressure acts at a short range (up to about 10 Å separation distance). Laird (2006) suggested that the various potential energies presence in between the elementary layers, the crystalline swelling is balanced by the Columbic and van der Waals attraction and Born repulsion. However, the macroscopic swelling proceeds beyond crystalline swelling, simultaneously, it was admitted that it is difficult to expatiate this kind of phenomenon when the double valence ion with more hydration energy cannot expand into one larger than single valence ion. In order to extricate from the difficult position, researchers reported that there may exist the osmotic repulsion force of diffuse double layer. Up to the recent literature, the view that crystal expansion is caused by cation hydration and inter-particle swelling is caused by osmotic pressure of double layer and so on, is still considered as the basis for the swelling mechanism of expansive clays.

#### 2.7.1.2 Diffuse double layer swelling

Beyond the crystalline swelling, the double layer swelling becomes significant in the swelling mechanism. Double-layer swelling occurs due to overlapping diffuse double layer in between particles (or crystals) (Pusch et al. 1990, Bradbury and Baeyens 2003, Laird 2006) and also in between elementary layer (Mitchell 1993, Delage et al. 2006). The diffuse double layer swelling depends on the mineralogical and chemical properties of soil (i.e., specific surface area and cation, cation concentration in the bulk water, dielectric constant, and valance of the cation), and the distance between the elementary layers (Sridharan and Jayadeva 1982). Attempts have been done to calculate the swelling pressure of expansive clay or bentonite using diffuse double layer theory (Bolt 1956, van Olpen 1963, Mitchell 1993, Tripathy et al. 2004). Diffuse double layer theory has been discussed in detail in previous section 2.6.1. Tripathy et al. (2004) reported that there is good

agreement between swelling pressure predicted using modified diffuse double layer theory and the experiment at low dry densities (i.e., below 1.6 $Mg/m^3$). The method used by Tripathy et al. (2004) is described in more detail in following section 2.8.2.

The phenomenon reported by Pusch (2001) using TEM image for the sodium type bentonite (i.e., MX-80). However, this is largely true for sodium type bentonite. Insertion of water molecules between elementary clay sheets occurs on a large scale for sodium bentonite. For calcium type bentonite, insertion of water molecules between elementary clay sheets is limited. Repulsion between the clay particles and aggregates surfaces plays important role in swelling mechanism after crystalline swelling for calcium type bentonite (Saiyouri et al. 2004). Using high resolution transmission electron microscope (TEM) image, Laird (2006) investigated the microstructure of bentonite from the particles orientation to the elementary layers. The TEM image showed that, first, the smectite microstructure was formed by individual particles (or crystals) which are curved and flexible. Second, the particles are joined together forming a smectite fabric. Third, the join between particles are both face-to face and edge-to-face as shown in Figure 2.10c. These particles break up to be elementary layers due to hydration.

## 2.8 Swelling pressure testing

### 2.8.1 Laboratory testing of swelling clays

Several methods for measuring swelling pressure of clays have been adopted by a number of researchers (Sridharan et al.1986, Komine and Ogata 1994, Dixon et al. 1996, Tripathy et al. 2004, Agus 2005 and Baille et al. 2010). The methods are broadly classified into three main categories; namely swell under load, swell load and constant volume methods (Sridharan et al. 1986). Different methods measure different values of swelling pressure. One method includes measuring the increase in height of specimens under either a nominal pressure or in situ stress, followed by compaction down to original height and further, such test is known as swell under load test. The first phase measures volume increase during wetting while the second phase measures the stress to counteract the swelling potential. The stress required to bring the specimen to original height is interpreted as the swelling pressure. The second method known as swell load test which involve first loading specimens to the in situ stress level and then inundating them with

water while load is added to keep the specimen at constant volume. The final load applied is interpreted to be the swelling pressure. Third method considers determination of swelling pressure keeping the volume of specimen constant. Figure 2.15 shows the swelling pressure measurement using different methods.

Many researchers have used these procedures to obtain measurements of swelling volume potential as well as swelling pressure (Komine and Ogata 1994, Sridharan and Gurtug 2004). Komine and Ogata (1994) performed tests on Na-Kunigel bentonite using the first procedure described above with a range of vertical stresses as well as constant volume oedometer tests. They reported that the time-dependent swelling was a function of initial dry density, vertical pressure, and initial water content. Maximum swell volume and swelling pressure were only a function of initial dry density and vertical pressure, and was independent of initial water content. Similar tests were also performed while varying bentonite and sand contents as well as pore fluid chemistry (Komine and Ogata 2004).

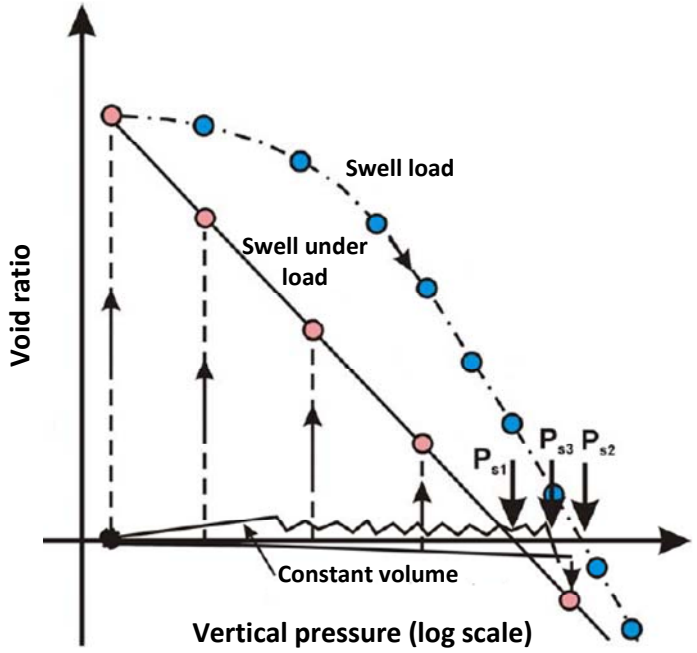


Figure 2.15 Swelling pressure measurement using different methods (Agus 2005)

Komornik et al. (1980) investigated the influence of suction and confining pressure on the swelling behaviour of expansive clays having high liquid limit and initial water content.

They used hollow test specimens with osmotic suction applied at the center through a semi-permeable membrane and cell pressure applied from the exterior. Changes in suction were applied under constant cell pressures. Results showed either expansion or compression with application of suction. Their results indicated that over a range of 0-1000 kPa suction there is a linear relationship between swelling pressure and suction. Swelling pressure was shown to decrease with increasing suction values. Also, higher suctions resulted in lower swell volume changes. Swelling soil behaviour has been investigated using suction control through vapour equilibrium techniques (Delage et al. 1998, Blatz and Graham 2000, Likos 2004, Agus and Schanz 2005). Vapour equilibrium applies water vapour at specified relative humidity values to specimens to control suction.

Al-Shamrani and Al-Mhaidib (2000) recognized swelling as a three dimensional phenomenon and performed both oedometer and triaxial swelling tests. The bentonite having predominant clay minerals were kaolinite and illite, having liquid limit 65%, specific gravity 2.78 and dry density equal to 1.8 $Mg/m^3$. The average moisture content was about 19%. The triaxial swelling tests consisted of infiltrating triaxial bentonite specimens and measuring axial and total volume using a stress path cell. They compared volume swell changes in the oedometer and triaxial tests and also reported swell ratios of vertical swell to volumetric swell in the triaxial tests. Swell ratio was found to be directly related to confining pressure and also increased with time during tests.

Katti and Shanmugsundaram (2001) performed one dimensional swelling test in the oedometer apparatus for Wyoming bentonite with initial void ratio 2.14 with specific gravity of 2.67, and correlated their results to micro structural changes in the clay fabric. Their procedure used, allowed zero stress expansion up to 0, 50%, or 75% of the original height followed by measurement of the remaining vertical swell pressure. In their apparatus the top cap moved upwards to the desired height and remained stationary for the remainder of the test. Scanning electron microscope (SEM) photos taken after testing revealed that during swelling the clay peds break down into smaller particles.

Agus (2005) also investigated the swelling pressure and constant volume wetting behavior of heavily compacted bentonite-sand mixture specimen. Two different methods were used (i.e., vapor equilibrium technique, VET and axis translation technique, ATT) depending upon the suction range. In the swelling pressure development at constant volume condition, it was found that very small development of swelling pressure occurs upon wetting from

suction range 22700 kPa to about 2000 kPa. A rapid development of swelling pressure occurred afterward. Very small development in swelling pressure at suction higher than 2000 kPa is related to the method how to apply suction to the specimen (i.e., vapor equilibrium technique, VET. For the specimen exposed to water vapor, the water molecules migrate into the open channels (i.e., macro-pores) and absorbed on exposed mineral surface. An internal redistribution of water occurs in order to balance the water potential gradient exist between macro-pores and micro-pores. Agus (2005) stated that the insignificant swelling pressure development during wetting up to 2000 kPa suction might be due to a delayed true equilibrium in the specimen and the true equilibrium might be attained after long test duration.

Agus and Schanz (2005a) investigated the rate of swelling pressure of compacted bentonite-sand mixtures using plot of time versus pressure divided by maximum pressure (or swelling pressure). It was found that the rate of swelling pressure development is a function of initial total suction of the specimen. This is not true for low bentonite content (i.e., less than 50%) resulting low bentonite dry density and for heavily compacted 50/50 bentonite-sand mixture (i.e., dry density of 2 $Mg/m^3$). The effect of density plays a role in the low bentonite dry density and heavily compacted bentonite-sand mixture.

The evolution of swelling pressure with time during the saturation process has been shown to be influenced by the initial water content and dry density of clays (Schanz & Tripathy 2009, Baille et al. 2010). Schanz and Tripathy (2009) measured the swelling pressures of several compacted bentonite specimens employing constant volume for a range of dry density from 1.10 to 1.73 $Mg/m^3$. The clay used was a divalent-rich Ca-Mg-bentonite. Their results also indicated that the swelling pressure development is the function of saturation process and the dry density. Baille et al. (2010) investigated the swelling behaviour of Ca-bentonite with initial water content of 9.0 %. They reported that initial compaction conditions affected the swelling pressure of the bentonite. At the same water content, the swelling pressure increased with an increase in the dry density, whereas, at the same dry density, the swelling pressure was found to decrease with an increase in the water content. Sridharan et al. (1986a) stated that molding water content influences the fabric that may have some influence on the swelling pressure. Gens & Alonso (1992) stated that at the same compaction dry density, clay specimens having very high initial water contents

or very low initial suctions tend to exhibit lower swelling pressures than that of specimens with lower water contents or higher suctions.

### 2.8.2 Theoretical prediction of swelling pressure

Several approaches have been adopted to predict the swelling behaviour of clays. One of the method based on diffuse double layer (DDL) theory for predictions of swelling pressure, because the molecular activity of the clay particles can be directly related to the stresses induced under zero volume change conditions. In these calculations, assumptions must be made as to the orientation of the clay particles. However two approaches have been adopted to use the DDL theory in describing the behaviour of clay soils. The first approach given by Komine and Ogata (2003) and Xie et al. (2004) considers a single DDL without interaction between one DDL and another whereas the second approach proposed by Sridharan and Jayadeva (1982) and Tripathy et al. (2004) considers interacting DDL. The former approach may be applicable in the case of clay suspension while the later approach appears to be more applicable for compacted clays.

Sridharan and Choudhury (2002) proposed simple equation for predicting the swelling pressure of montmorillonitic clays. The proposed equation is based on the diffuse double layer theory. The equation can be used to obtain the swelling pressure of several sodium bentonite clay water electrolyte systems for any void ratio and pore fluid properties.

Tripathy et al. (2004) reported on swelling pressures of three compacted bentonites (MX-80, Febex and Montigel). They summarized previous work which suggested that at low dry densities, theoretical predictions overestimate swelling pressures compared with experimental measurements. At high dry densities the opposite was observed to be the case. Their work consisted of making corrections to the relationship between a midplane potential function and nondimensional distance function relationship. The corrections involved back calculating the midplane potential function from the experimentally measured values, calculating the error between the original midplane potential function and nondimensional distance function, followed by subtracting the error from the original theoretical prediction to gain new functions. The calibration process resulted in good predictions for those materials over various ranges of average valence. For verification, the corrected equations were used to calculate swelling pressures for materials using their average valence. Figure 2.16 shows experimental and calculated swelling pressure results

and three semi-empirical equations proposed by Tripathy et al. (2004) with average valence ranges of 1.14 – 1.50, 1.66 – 1.73 and 1.97.

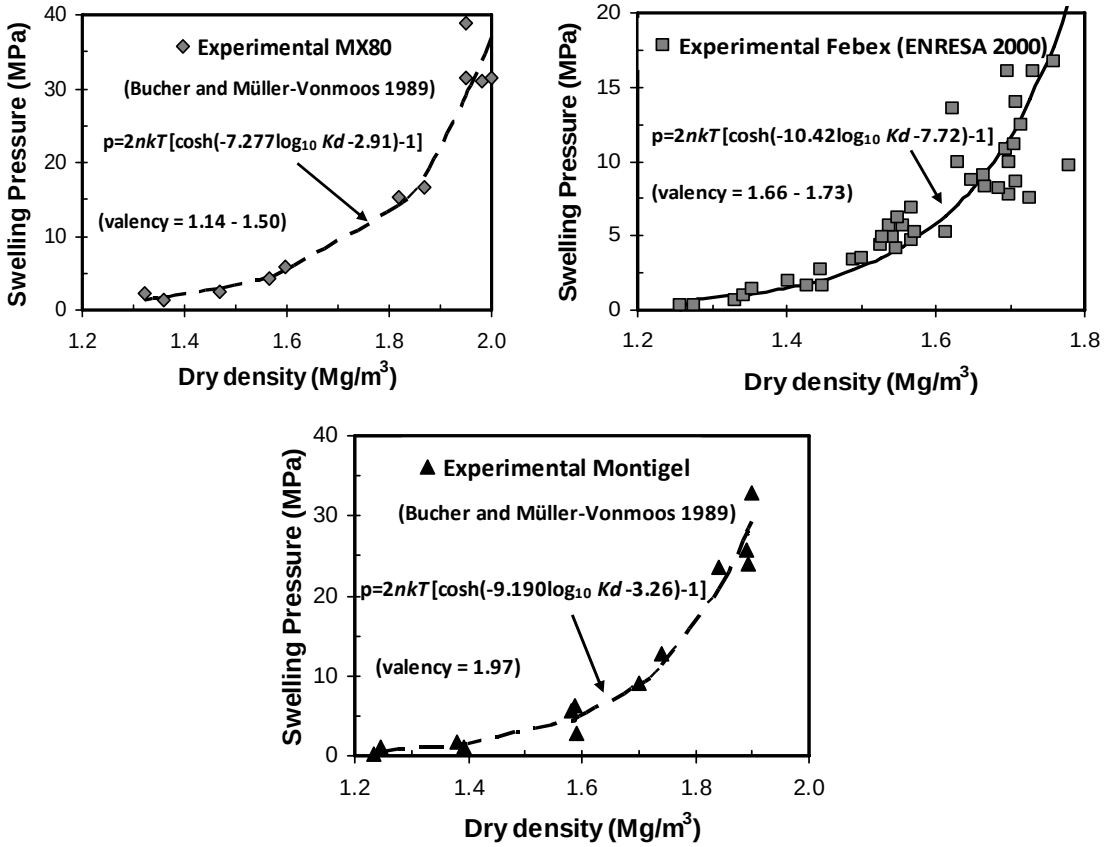


Figure 2.16 Experimental and calculated swelling pressure results (Tripathy et al. 2004)

Agus and Schanz (2008) proposed an approach for predicting swelling pressure of bentonites based on thermodynamic relationships between swelling pressure and suction. A series of swelling pressure tests were performed on compacted specimens of bentonite-sand mixtures with different bentonite contents, water contents, and dry densities. The sorption curve of the bentonite was found to follow a straight line on the semi-logarithmic plot of water content versus suction for a quite wide range of suction indicating that the water content of the bentonite is logarithmically related to suction. A step wise procedures are suggested for predicting the swelling pressure of compacted bentonites.

## 2.9 Mechanisms governing hydraulic flow through soils

The word soil generally refers to the layers of materials overlying solid rock, called bedrock Brady N.C (1974). These soil materials consist of four major components: minerals, organic matter, water, and gases. The various combinations of minerals and organic matter produce different soil types, ranging from dense, impermeable clays to loose, gravelly sands. Soils are formed from the decomposition of both bedrock and organic materials. Bedrock decomposes slowly over decades or centuries, gradually weathering into minerals such as quartz, calcite, or dolomite (soil minerals and structure has been discussed in the beginning of this chapter). Soil material in any one location may have been derived from the underlying bedrock or may have been carried there by glaciers, streams, or wind. Whatever their origin, the mineral particles combine with organic matter from decomposition of plant and animal tissue to form soils. Most organic matter is found in the topsoil, with gradually increasing percentages of minerals in the underlying layers of subsoil.

Soil water generally flows downward to deeper depths and from wetter areas to drier ones. This movement of water through soil occurs in response to two types of forces:

1. The downward pull of gravity.

2. The forces of attraction between water molecules and soil particles.

Just as gravity pulls all objects toward the center of the earth, it pulls water molecules downward through the soil profile. In sandy soils this is the primary cause of water draining downward through soil to groundwater. In clay soils forces of attraction between soil and water molecules also play a key role in determining movement of soil water.

Hillel. D. (1980) further explained that the intermolecular forces of attraction between soil and water are called matric or capillary forces. They are determined by soil properties and moisture content and are most significant in small pores. These intermolecular forces usually act in opposition to gravity, producing the net effect of holding water in soil pores. However, these forces also cause water movement from wet soil zones to dry ones in any direction because of the strong attraction between water molecules and dry soil surfaces. When evaporation dries surface soils, water moves upward through the soil profile to rewet the dry pores. Similarly, water moves horizontally to moisten soils along the edges of

drainage ditches, furrows, and impoundments. The narrower the tube, the higher the water will rise because of the larger surface area relative to water volume. In capillary action in soils, the most common molecule in soil minerals is silicate, similar to the silicate molecules in the glass capillary tubes. Because of these same capillary forces, small pore spaces in soils hold water more tightly than the larger pores. Water drains more rapidly from the larger pores, causing them to be mostly air-filled, whereas smaller pores still contain water. The mixture of pore sizes in most soils, therefore, helps to provide plants with both a reservoir of water and areas for gaseous exchange. However, the water cycle to and through the ground varies considerably from humid regions to more arid regions. The amounts following these various pathways depend on the local climate, topography, and soil conditions. In general, the northeastern states have far less evapo-transpiration and more water percolating to groundwater more than arid regions. Recharge does not remain constant over the course of the year, especially in the northeast where soils become frozen in the winter, which result in a periodic rise and fall in the depth to groundwater. Spring and fall generally are the times of greatest recharge and, therefore, also of highest water table elevations. Groundwater levels tend to go down in summer when evaporation and plant uptake are high and in winter when recharge is hampered by frozen soils. Such fluctuations in recharge quantities can have consequences for recharge quality as well.

## 2.10 Factor influencing the hydraulic conductivity of clays

In most cases the maximum allowable hydraulic conductivity for a barrier material is specified. The task to provide a barrier material, which meets the criteria given at the lowest possible hydraulic conductivity, requires good knowledge of the different factors affecting the final hydraulic conductivity of the clay. The following section describes the several factors influencing the hydraulic behaviour of the clays.

### 2.10.1 Influence of type of bentonite on hydraulic conductivity

Bentonite is a brand name for fine grained swelling types of clay. Often clays with a high content of swelling clay minerals (smectites) are used. The minerals swell during uptake of water, which is absorbed into the crystalline lattice and bound through electrical charges. The electrical bindings are mediated by the cations, which are loosely connected to the crystalline lattice. The amount of cations and the ion strength of the liquid determine

the magnitude of the swelling. The most common cations are calcium and sodium, where sodium has the greater ability to swell and consequently gives better sealing i.e. lower hydraulic conductivity (Mitchell 1976, Lundgren 1981). Normally, the bentonite is pre-treated by drying and grinding, but sometimes the cation of the bentonite is changed. For example, the calcium cations are changed to the sodium cations in order to increase the swelling ability of the bentonite. Moreover, the bentonite can be treated with polymers, which makes it more resistant to saline liquids, liquids with low pH or other contaminated liquids. Depending on the pore fluid, different types of bentonite behave differently, and it is therefore important to consider the chemical state of both the bentonite and the fluid when, determining the components of the mixture (Kenney et al. 1992). The most common types of bentonite are sodium bentonite, calcium bentonite and sodium activated bentonite. These bentonites are usually available both in granular and powdered form. Beside the type of bentonite, the physical properties of the particles in clay also plays important role. It is generally accepted with justification that the finer particles have a disproportionate effect on hydraulic conductivity (Murray et al. 1997).

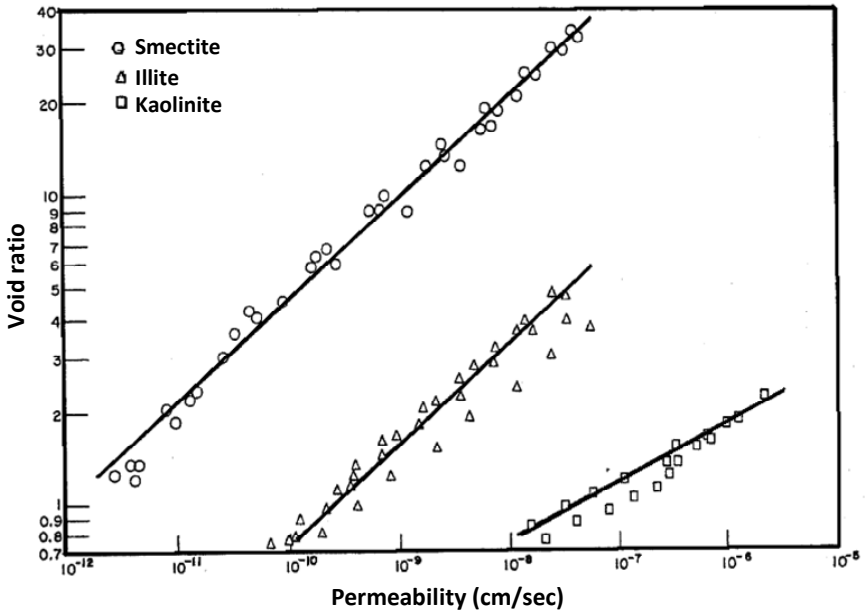


Figure 2.17 Effect of three types of clays on hydraulic conductivity
(Mesri and Olson 1971)

Clays are composed of very fine plate like particles which results in low transmission rate of fluid flow. The particle size is of great importance and clays composed of larger particle

types yield greater hydraulic conductivities than those with smaller size particles when the other factors being equal. Mesri and Olson (1971) discussed the role of the size of clay particles on the pore size and the resulting value of hydraulic conductivity that will be measured. The smallest particles, smectites, were observed to have the lowest hydraulic conductivity. Illite and kaolinite clays, composed of particles which are progressively larger than smectites, exhibited higher than smectites for the same density as shown in Figure 2.17. Differences in the measured hydraulic conductivity were attributed to the particle size.

Rao and Mathew (1995) conducted a laboratory study of the hydraulic conductivity of marine clay with monovalent, divalent and trivalent cations and revealed large differences in hydraulic conductivity. The exchangeable cations employed were $Na^{+}$, $K^{+}$, $NH_4$, $Mg^{2+}$, $Ca^{2+}$ and $Al^{3+}$ in order of increasing valency. An interpretation of the results derived from hydraulic conductivity tests suggests that hydraulic flow is significantly affected by the valency and size of the adsorbed cations. An increase in the valency of the adsorbed cations leads to quicker rate of flow, while, for a constant valency, increase in the hydrated radius of the adsorbed cations results in a lower rate of flow. The reduction in hydraulic conductivity was related to the dispersion and deflocculation of clay. Lower valency and higher hydrated radii of the exchangeable cations enable the double layer repulsive forces to predominate, thereby increase dispersion and deflocculation. Sodium saturated clay is approximately six times less permeable than potassium and ammonium clays. Saturation of marine clay with divalent cations increases its hydraulic conductivity nine times in comparison with the sodium clays. The trivalent clay in turn is more permeable than the divalent clay.

### 2.10.2 Influence of compaction density on hydraulic conductivity

The procedure on site for mixing, placing and compacting the bentonite plays an extremely important role for the final quality of the barrier. A thorough mix of the bentonite is important for reducing the scatter in the hydraulic conductivity. Equally important is to follow the procedure for placing and compaction. The most effective compaction is reached when the bentonite has water content close to optimum or just above (about 2%), (Haug and Wong 1992). The greater is the compaction, the lesser the pore volume and the lower be the hydraulic conductivity. However, the pores opening available for flow in any particular direction with be influence by the particle configuration

and shape. For example, the alignment of plate like particles in a horizontal direction will lead to less pore area available to transport the permeant and more tortuous flow path in a vertical direction than the horizontal direction. The vertical hydraulic conductivity will be less than the horizontal conductivity (Lambe 1958, Arch et al. 1993). An ordered soil structure of this kind can result from compaction operations, be a result of natural decomposition or a consequence of particles reorientation on deformation plane. Aggregation of the clay platelets also influences the distribution of the pore space and the flow of permeant (Mesri and Olson 1970). Though it is the distribution of the particles which controls the pore space and the anisotropy of fluid flow, nevertheless it is the pore space along which the permeant flows, and the distribution of the particles only gives a guide to the pore space characteristics.

Lambe (1958) studied the effect of compaction on the structure of clay soils, and the results of his study are illustrated in Figure 2.18. If clay is compacted with moisture content on the dry side of the optimum, it will possess a flocculent structure.

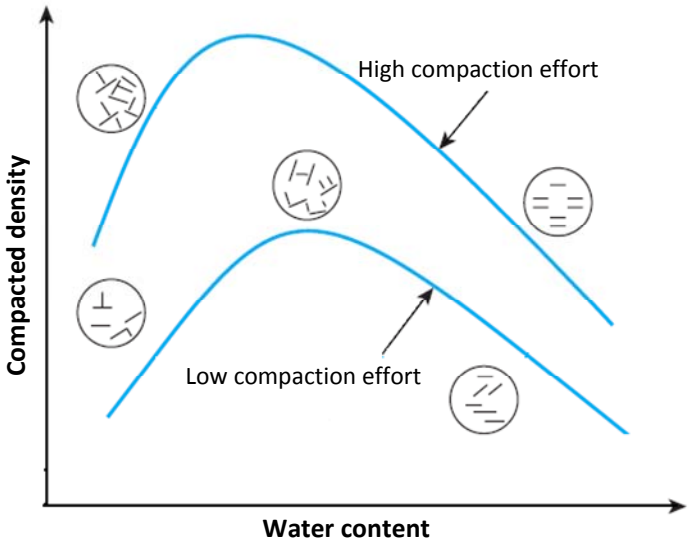


Figure 2.18 Effect of compaction and water content on structure of clay soils (Lambe 1958)

This type of structure results because, at low moisture content, the diffuse double layers of ions surrounding the clay particles cannot be fully developed; hence, the interparticle repulsion is reduced. This reduced repulsion results in a more random particle orientation and a lower dry unit weight. Such soils will be more likely to contain larger pores and

exhibit a wide range of pore size. When the moisture content or compaction is increased, the diffuse double layers around the particles expand, which increases the repulsion between the clay particles and gives a lower degree of flocculation and a higher dry unit weight. A continued increase in moisture content expands the double layers more. This expansion results in a continued increase of repulsion between the particles and thus a still greater degree of particle orientation and a more or less dispersed structure. Such soils will contain smaller average pore size and exhibit a narrow range of pore size. Such differences in soil structure will affect the manner in which water flows through soils.

Pusch (1983) reported that Ca-bentonite had a slight higher swelling pressure than Na-bentonite at a very high dry density. These results suggest that in contrast to the uncompacted Ca-bentonite with a lower dry density, compacted Ca-bentonite with a very high density when permeated with distilled water might have hydraulic conductivity ($<10^{-11}$ m/s) comparable to compacted Na-bentonite when permeated with distilled water if no volume change is allowed.

Chapuis (2002) mentioned different mixing methods which can also influence the hydraulic conductivity. The methods includes field and laboratory mixing which affect the quality in terms of homogeneity, as evaluated and discussed by Chapuis (1990b), and Chapuis and Pouliot (1996).

Ahn and Jo (2008) experimentally investigated two types of bentonite (calcium and sodium bentonites) with dry density range from 0.8 to 1.3 $Mg/m^3$. Their results show that the hydraulic conductivities decreased with increasing final dry density. The decrease in hydraulic conductivity was more significant for Calcium bentonite (CaB) than Sodium bentonite (NaB). In addition, at a given final dry density, the hydraulic conductivity of CaB was higher than that of NaB. The hydraulic conductivity of NaB decreased from $5.1 \times 10^{-11}$ m/s to $5.5 \times 10^{-12}$ m/s with increasing dry density from 1.11 to 1.31 $Mg/m^3$. However, the hydraulic conductivity of NaB decreased from $3.8 \times 10^{-9}$ m/s to $9.9 \times 10^{-10}$ m/s with increasing dry density from 0.84 to 1.05 $Mg/m^3$. The decrease of the difference in the hydraulic conductivity with increasing final dry density might be due to the absence of osmotic swelling as no volume change was allowed.

Baille et al. (2010) reported hydraulic conductivity tests for Ca-bentonite for wide range of void ratios. A rapid decrease in the hydraulic conductivity was observed at void ratio of

about 1.7. The hydraulic conductivity for the bentonite varied between $10^{-10}$ m/s and $10^{-14}$ m/s for the void ratios 4.0 to 0.6 respectively.

### 2.10.3 Influence of water content on hydraulic conductivity

Almost all compaction work, where density is an issue, is preceded by a laboratory compaction test. Hereby, the optimal water content is determined, which defines the water content for which the highest dry density is obtained. For clayey material, the hydraulic conductivity of the compacted material is greatly dependent on whether compaction is made on the wet side or the dry side of optimum. Compaction on the wet side leads to good kneading and a fairly homogeneous distribution of voids within the material. Compaction on the dry side often results in a large portion of much larger pores, due to aggregation of the clay matrix, and usually results in substantially larger hydraulic conductivity.

Terzaghi (1922) warned designers that the hydraulic conductivity value of compacted clay does not depend only on its void ratio or porosity, but also on the preparation and compaction modes. This was confirmed by many tests (Lambe 1958, Peirce et al. 1987, Wright et al. 1997) that documented the importance of the molding water content, and more especially the degree of saturation reached after compaction, on the hydraulic conductivity value of clay. Mitchell et al (1965) performed a detailed laboratory investigation of the hydraulic conductivity of compacted clays and found that the specimens compacted wet of optimum may have hydraulic conductivity values two to three orders of magnitude less than specimens compacted dry of optimum.

In clays the presence of fissures, laminations and other discontinuities making up the macro fabric present preferential flow paths which lead to enhanced hydraulic conductivity in the direction of the discontinuities. Such behaviour has been reported by (Leroueil et al. 1992, little et al. 1992 and Hossain 1992). The tortuosity of fluid flow along the discontinuities is likely to be significantly less than that of interparticle flow. Discontinuities may be viewed as representing large void spaces with an increased hydraulic conductivity above that of the surrounding intact soil. This is true for undisturbed as well as recompacted clays. In recompacted clays the identification of clod size as being a major contributor to the presence of discontinuities or fissures (Benson and Daniel 1990, Wright et al. 1996) goes a long way to explain why there are often large discrepancies

between in-situ hydraulic conductivity and lower values obtained on laboratory prepared samples. Nevertheless, dry of optimum moisture content a compacted soil exhibits a fissured structure.

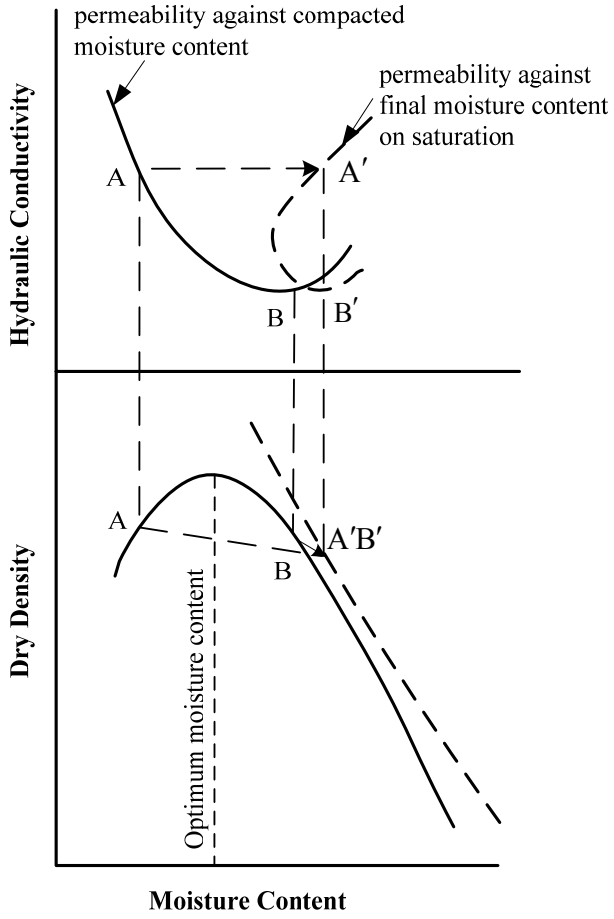


Figure 2.19 Typical dry density-moisture content-hydraulic conductivity relationships for compacted clay (Murray et al. 1997)

Figure 2.19 presents the typical dry density – moisture content - hydraulic conductivity relationships for the compacted clay soil (Day and Daniel 1985, Murray et al. 1997). It is usual to plot the hydraulic conductivity against the as compacted moisture content and dry density and the condition of a sample compacted dry of optimum with relatively high hydraulic conductivity is given by A. However, the quoted hydraulic conductivity is usually for a saturated or near saturated soil and in achieving this condition the sample can be expected to exhibit swelling. Thus the condition of the sample at the end of the

hydraulic conductivity test may be represented by A′. Points B and B′ represent the corresponding conditions of a sample compacted wet of optimum. Though in the final condition the two samples have the same dry density and moisture content given by the correspondence of A′ and B′, they have significant different hydraulic conductivities as the flow of the permeant through sample A is controlled largely by the fissured structure and the flow through the lower hydraulic conductivity sample B by inter-particle flow.

Watabe et al. (2000) have shown that compaction conditions strongly influence the fabric of compacted clays. Although compaction at degrees of saturation greater than the corresponding optimum value provide to the soil a homogeneous fabric, compaction at smaller degrees of saturation gives aggregates, macropores, and, consequently, higher hydraulic conductivity. For the specimens compacted at degrees of saturation greater than optimum, the hydraulic conductivity is about the same in all tests and equal to about $9\times10^{-7}$ m/s. For the specimens compacted at smaller degrees of saturation, the hydraulic conductivity varies between $3.3\times10^{-6}$ and $7.6\times10^{-6}$ m/s. Watabe et al. (2000) and Vanapalli et al. (1997) attributed this behaviour to the development of macroporosity when the soil is compacted at degree of saturation, $S$r values smaller than optimum $S\mathrm{r}_{\mathrm{opt}}$. The moisture content of the clay subjected to compaction also influences the micro and macro structure. Aggregation influences the porosity distribution and gives rise to the presence of many small flow channels within aggregations and a small number of large flow channels between aggregations. This gives relatively high hydraulic conductivity compared to a dispersed structure where pore spaces are of more uniform size.

### 2.10.4 Influence of type of pore fluid on hydraulic conductivity

In equating the forces resisting flow of the permeant to those causing flow it is necessary to take account of the unit weight and the dynamic viscosity of the permeant. Both these parameter are influence by the temperature and also likely to be influenced by physio-chemical interaction of the permeant with the soil particle system particularly close to the particle surface (Terzaghi 1925).

Macey (1942) measured hydraulic conductivity of clays in water and non polar fluids. He reported rate of flow for benzene is much higher than for water in the same clay. He considered that particle spacing, particle size as influence by aggregation or dispersion, particle rearrangement, adsorbed layers, interlamellar swelling all influenced the hydraulic

conductivity, but he considered the most important cause for the lower hydraulic conductivity in water to be the anomalous viscosity of the water near the clay surface. Other factors such as the thickness of the fluid film adsorbed to the particles (double layer), inter-lamellar swelling (Mesri and Olsen 1971) and the osmotic and other physio-chemical effects (Michaels and Lin 1954) have a potentially major influence on hydraulic conductivity and transportation of contaminant. Michaels and Lin (1954) suggested that the adsorbed liquid attached to the soil particles appeared in experiments to have little effect on the hydraulic conductivity and suggested the major influence of the permeant was in controlling the tendency of the clay particles to disperse or to form aggregation. Grace (1953) demonstrated that the improved dispersion is the main reason for the marked reduction of hydraulic conductivity caused by the use of certain electrolytes and he pointed out the importance of particle reorientation.

Michaels and Lin (1954) showed experimentally that the hydraulic conductivity of kaolinite decreased markedly as the polarity of the permeating fluid increased and that the most importance factor controlling the hydraulic conductivity was the degree of dispersion of the kaolinite in the original suspending fluid. They concluded that the electro-osmotic counter flow might be of some importance when the aqueous solution were used as permeant, but such colloidal effect as adsorbed liquid surface films appeared to have little effect on the hydraulic conductivity.

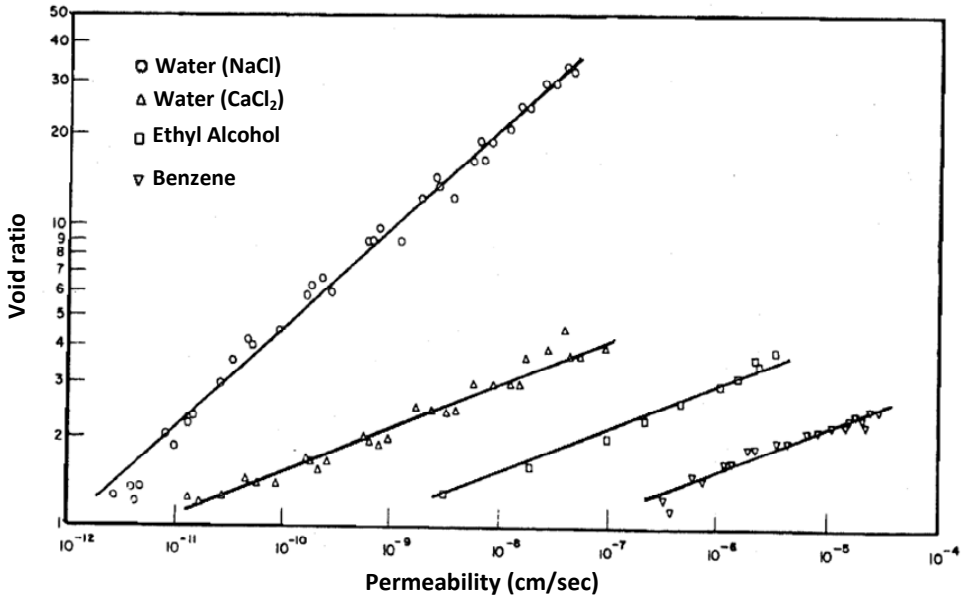


Figure 2.20 Effect of pore fluid on smectite (Mesri and Olson 1970)

Mesri and Olson (1970) used several types of fluids as permeant to measure the hydraulic conductivity of smectite which includes Volclay bentonite having liquid limit of 500 %, specific area of 700 $m^2/g$ and CEC of 100 meq/100g. They stated that the physico-chemical variables exert great influence on the hydraulic conductivity by controlling the tendency of the clay to disperse or to form aggregate. Aggregation leads to the existence of many tiny flow, and small numbers of relatively large channels through which the main flow occurs. Dispersion leads to channels that are all of nearly the same size, and tend to be non equidimensional and thus reduce the flow. Figure 2.20 shows the effect of different types of pore fluids on the hydraulic conductivity of smectite. It is clear from the Figure that as the concentration of pore fluid increases, conductivity also increases.

Achari et al. (1999) stated that the concentration of ions in the permeating fluid affects the hydraulic conductivity of clays. The concentration of the ions in solution affects the volume of water adsorbed on the clay platelets. The hydraulic conductivity of the clay is increased, when leachate with high concentration of ions are permeated, due to an increase in the edge-face and edge-edge association of particles leading to flocculation.

Cho et al. (2002) experimentally investigated the hydraulic conductivity of Ca-bentonite for the range of dry densities (i.e., 1.0 $Mg/m^3$ to 1.8 $Mg/m^3$). The permeant used in their tests were demineralized water, referred as freshwater, a 0.4M NaCl solution, and a 0.04M NaCl solution referred as mixture of freshwater and seawater. Their results show that the hydraulic conductivities increase with increasing salinity only when the dry density of bentonite is relatively low. The degree of increase becomes more remarkable at a lower dry density of bentonite. For bentonites with densities of 1.0 $Mg/m^3$ and 1.2 $Mg/m^3$, the hydraulic conductivities associated with the 0.4 M NaCl solution increase beyond those associated with the fresh water solution by factor of 7 and 3 times, respectively. However, for the bentonite with dry density higher than 1.4 $Mg/m^3$, the salinity has an insignificant effect on the hydraulic conductivities, and the hydraulic conductivity is nearly constant within the salinity range of 0 to 0.4 M NaCl. Cho et al. (2002) attributed such behaviour as, when saline water is intruded into bentonite, the cation concentration in pore water is increase, and it causes the diffuse double layer to contract. A reduction in the double layer thickness may result in changes in the net repulsive forces between the montmorillonite sheets, which in turn decreases the tendency to separate. If the individual clay particles are free to move, then microstructure changes may take place due to the opening of micro pore

(Fernandez and Quigley 1985, 1988) resulting in an increase in hydraulic conductivity. Also, when concentrated sea water permeates into clay, shrinkage due to osmotic consolidation occurs. The shrinkage may lead to an alternation of the macro and microstructure of the clay, causing a change in hydraulic conductivity. However, the experimental results obtained from their study show that changes in the hydraulic conductivity are not large, and the microstructural change of bentonite fabric might not occur in the NaCl concentration range of 0 to 0.4 M. Even without particle reorientation, changes in pore fluid chemistry may alter the thickness of the diffuse double layer. A reduction in double layer thickness may result in a new pathway available for flow, and consequently, an increase in hydraulic conductivity.

Villar et al. (2003) investigated three different types of pore fluids (i.e., granitic, saline, and distilled water) as permeant to measure the hydraulic conductivity of Febex bentonite with initial water content of 13.7 %. No clear trend was observed concerning the variation of the values obtained with granitic water with respect to those obtained with distilled water. The values obtained with saline water were, however, almost two times higher on average than those expected for a sample of the same density tested with distilled water, and in addition, they show greater dispersion.

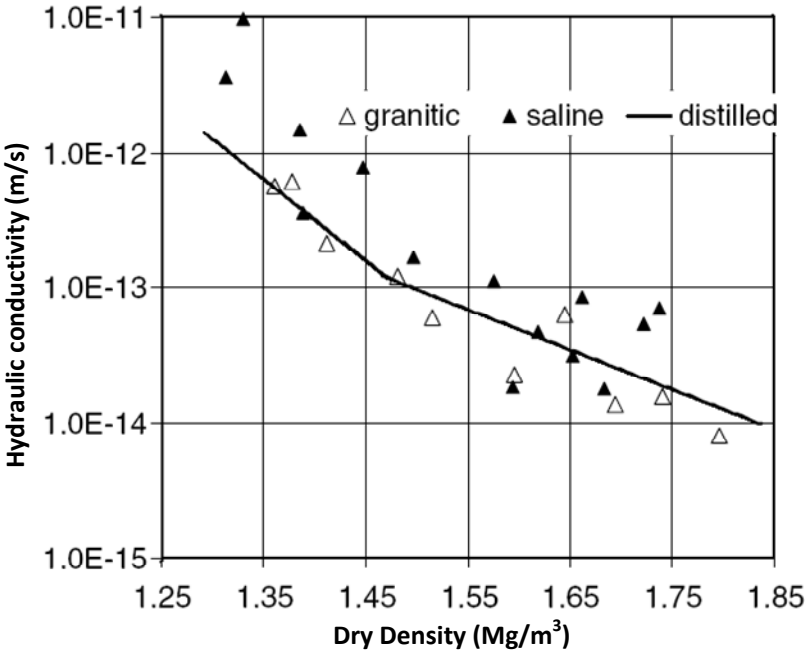


Figure 2.21 Hydraulic conductivity versus dry density of Febex bentonite using three types of pore fluids (Villar et al. 2003)

On the other hand, the shrinkage of clay aggregates due to an increment of the salinity of the permeant causes changes in the pore volume of the macrostructure that may increase the hydraulic conductivity. This higher hydraulic conductivity to saline water with respect to that expected for distilled water is more significant for low densities. The increase of water conductivity with the salinity of permeant water has been observed by Karnland et al. (1992) and Pusch (2001) in Friedland Ton clay, and Mata and Ledesma (2003) in a granite/Na bentonite mixture. Figure 2.21 shows the hydraulic conductivity of Febex bentonite with three different pore fluids.

### 2.10.5 Influence of temperature on hydraulic conductivity

Water is one of the components related to soil behavior that are influenced by temperature. Physical properties of water such as density, vapor pressure, viscosity, dielectric constant and surface tension changes by changing temperature. Table 2.3 summarizes the temperature effects on physical properties of water. The data presented in Table 2.3 was taken from CRC handbook of chemistry and physics (Lide 1995). As shown in Table 2.3, water density decreases by increasing temperature. Based on Table 2.3, water viscosity decreases by increasing temperature.

Table 2.3 Temperature effects on physical properties of water‡

| Temperature ($^oC$) | Density ($Mg/m^3$) | Vapor pressure (kPa) | Viscosity (μPa s) | Dielectric constant | Surface tension (mN/m) |
|---|---|---|---|---|---|
| 0 | 0.99984 | 0.6113 | 1793 | 87.90 | 75.64 |
| 10 | 0.99970 | 1.2281 | 1307 | 83.96 | 74.23 |
| 20 | 0.99821 | 3.3388 | 1002 | 80.20 | 72.75 |
| 30 | 0.99565 | 4.2455 | 797.7 | 76.60 | 71.20 |
| 40 | 0.99222 | 7.3814 | 653.2 | 73.17 | 69.60 |
| 50 | 0.98803 | 12.344 | 547.0 | 69.88 | 67.94 |
| 60 | 0.98320 | 19.932 | 466.5 | 66.73 | 66.24 |
| 70 | 0.97778 | 31.176 | 404.0 | 63.73 | 64.47 |
| 80 | 0.97182 | 47.373 | 354.4 | 60.86 | 62.67 |
| 90 | 0.96535 | 70.117 | 314.5 | 58.12 | 60.82 |
| 100 | 0.95840 | 101.325 | 281.8 | 55.51 | 58.91 |

‡CRC handbook of chemistry and physics, 75th edition (Lide 1995)

Viscosity is commonly perceived as 'thickness' or as resistance of a liquid to flow. Therefore, an increase in temperature results in the decrease in resistance of a liquid to flow. Decrease in water viscosity due to increase in temperature is believed to be the reason why hydraulic conductivity of compacted clay increases with the increase in temperature (Pusch et al. 1990 for calcium and sodium bentonites, Cho et al. (1999) for calcium bentonite, Romero et al. (2003) for Boom clay, Lloret and Villar (2004) for FEBEX bentonite).

Kharaka and Smalley (1976) reported hydraulic conductivity values of a Na-bentonite and Mingarro et al. (1991) of a granite/Ca-bentonite mixture, which increased with temperature (ranging from 20 to 100 °C) roughly according to estimates from the decreases in the kinematic viscosity of water. Likewise, Cho et al. (1999) found similar results for a Ca-bentonite, and Khemissa (1998), for a kaolinite. On the other hand, Towhata et al. (1993) found a higher hydraulic conductivity increase with temperature than that calculated by using the properties of free and pure water in a kaolinite and a bentonite. They consider that the degeneration of adsorbed water into bulk pure water at elevated temperatures (Derjaguin et al. 1986) may result in an increase in the dimension of flow channels and therefore of intrinsic permeability to liquid phase.

Moreover, the effect of temperature on hydration forces were studied and analyzed by Woessner (1980), Carlsson (1986) and Pusch et al. (1990). The technique proton nuclear magnetic resonance (NMR) was used for the above mentioned study. The NMR technique can be used to determine and distinguish the different states of water (i.e., free and bound states). The different states of water in bentonite were specified by measuring the water proton relaxation time (*T2*). Carlsson (1986) used parameter *T2* in order to investigate the internal water (i.e., water bound in between two elementary layers) and external water (i.e., water placed out of two elementary layers). The effects of water content and temperature on different types of bentonite were investigated in the study. It was concluded that the increase in water content from 20-60% resulted in increase of the relaxation time (*T2*) due to increase in external water in the bentonite. This is because the frequency of motion of water molecules is high in the external water. Thus, it takes longer time for protons to transfer their magnetic energy to lattice (clay surfaces).

Romero et al. (2001) analyzed the influence of temperature on the unsaturated water conductivity of Boom clay and concluded that, although it is more relevant at high degrees

of saturation, it is smaller than it could be expected from the thermal change in water viscosity. They consider that thermo-chemical effects altering clay fabric and porosity redistribution could be relevant processes that affect the change of hydraulic conductivity with temperature.

The increase of hydraulic conductivity with temperature has been attributed to the changes in water kinematic viscosity (Villar and Lloret 2004). This increase, resulting from the decrease in water viscosity with temperature, was calculated for Febex bentonite. Moreover, Villar and Lloret (2004) suggested that thermo-chemical effects altering clay fabric (flocculation or dispersion), porosity redistribution (creating preferential pathways or blocking macropores) and pore fluid chemistry (affecting viscosity) could be relevant issues regarding the effect of temperature on Hydraulic conductivity.

## 2.11 Summary

This chapter discusses the hydro-mechanical behavior of compacted expansive clay. The discussion is commenced by the brief description about the structural units of expansive clay, clay minerals, and different forces in clay system and modes of particle association. Interparticle forces, clay fabric, water in compacted clays, hydration processes have been discussed. The chapter gives overview of the literature referring to the basic physico-chemical interaction between clay and water. The development of the theory of clay-water interaction, which provide a means of estimating the thickness of the diffuse layer and the influences of surface potential pore solution on the diffuse double layer thickness. Classification system for swelling and non swelling clays is discussed. Experimental development in the area of swelling clays and three methods for evaluating the swelling pressure are presented. Different theoretical approaches for swelling pressure prediction given by past researcher are outlined. Furthermore, the flow mechanisms in soils are highlighted, and several factors affecting the hydraulic behaviour of clays are summarized based on the literature review.

# Chapter 3

# METHODS AVAILABLE TO ASSESS HYDRAULIC CONDUCTIVITY

## 3.1 Introduction

In this chapter the hydraulic properties of soil and the determinations of saturated coefficient of hydraulic conductivity are described. Laboratory measurements of the hydraulic conductivity performed by past researchers are elaborated. In addition to that the empirical equations for estimating hydraulic conductivity and theoretical models used for hydraulic conductivity are discussed.

## 3.2 Hydraulic properties of soil and flow law

In saturated soil mechanics, fluid flow refers to flow of water through soil voids. The understanding of flow mechanism in saturated soils needs knowledge of the driving potential. Soils have interconnected voids through which water can flow from point of high energy to point of low energy. The driving potentials for water phase that cause water to flow can be considered in term of water content gradient, hydraulic gradient (Fredlund and Rahardjo 1993). Hydraulic gradient can be considered as the driving potential of water in saturated soils. The hydraulic gradient is usually expressed in terms of hydraulic head.

$$h = z + \frac{\Delta u_w}{\gamma_w} \tag{3.1}$$

where: $h$ is hydraulic head or total head, $z$ is elevation at the observed point, $\Delta u_w$ is pore-water pressure differential, $\gamma_w$ is unit weight of water.

### 3.2.1 Darcy Law

The Darcy equation that gives the mathematical description of the Darcy law was developed in the 19th century by Darcy (1856). The equation is based on an empirical relationship found for the flow of water through sand and gravel. Darcy (1856) found that the mean effective flow velocity of water ($v$) is directly proportional to the flow rate ($q$) and the applied hydraulic gradient ($i$) (Equations 3.3 and 3.4). Hydraulic gradient ($i$) is defined as $\Delta h/l$ (change in hydraulic head divided by the flow distance through specimen). Hydraulic head is the difference between the water potential on the inflow and the outflow surfaces of the soil column. While Darcy's law is suitable for predicting flow through sands and gravels, it is recognized as inadequate to describe the flow of fluids through low permeable clays under low applied hydraulic conditions. The basic relationship developed by Darcy is well known and is the basis for most of the models for predicting water flow (Olsen 1965, Yong and Warkentin 1975, Mitchell 1976, Lambe and Whitman 1979, Olsen and Daniel 1981). While the symbols used by these authors vary, the relationships presented are the same. The basic equations which are used to describe Darcian flow are presented in Equations 3.3 through 3.6 (Yong and Warkentin 1975).

$$v = \frac{Q}{At} = ki = \frac{k\Delta h}{l} \tag{3.3}$$

and

$$q = kiA \tag{3.4}$$

where: $v$ is the flow velocity, $q$ is the flow rate, $A$ is the cross-sectional area of the specimen normal to the direction of flow and $Q$ is the quantity of flow measured over time increment, $t$. The hydraulic conductivity, $k$ is the flow velocity term normalized to a flux at a hydraulic gradient of 1.0.

Equations 3.3 and 3.4 can be more clearly expressed if the properties of the fluid flowing through the soil can be defined, leading to Equations 3.5 and 3.6.

$$v = \frac{K\rho g}{\mu} \tag{3.5}$$

or

$$K = \frac{k\mu}{\rho g} \tag{3.6}$$

where: $\rho$ is fluid specific weight, $\mu$ is fluid viscosity, $K$ is intrinsic permeability (expressed in units of length$^2$) which excludes the effect of permeant viscosity and the fluid unit weight on flow velocity, $g$ is the gravitational constant, $k$ is hydraulic conductivity.

Table 3.1 presents the basic assumptions for the application of the Darcy equation and compares these with the conditions believed to exist in three different soil materials. The table provides a good indication of the potential short comings of using the Darcy equation to estimate flow through clays, and in particular through soils containing clays with a high surface charge.

While Darcy's equation for flow through a porous medium was found to be adequate for describing the measurement of water flow through most granular soils, it was soon determined that Darcy law had some limitations. King (1898) was one of the first to report deviations from Darcian flow behaviour. He observed that for clayey materials there is a tendency for hydraulic conductivity to increase with increasing hydraulic gradient. A large number of researchers have also observed deviations from the Darcy equation for flow in soils other than sands and gravels. The apparent limitations of the Darcy equation has led to the development of a large number of flow models, some of these models are presented in section 3.5 in more detail.

Table 3.1 Basic assumptions for application of Darcy Law

| Darcy law assumptions | Sand | Illite | Bentonite |
|---|---|---|---|
| 1) Fluid viscosity is constant | Yes | No | No |
| 2) Fluid density is constant | Yes | No | No |
| 3) Soil fabric does not change | Yes | ? | ? |
| 4) Laminar flow occurs | Yes | ? | ? |
| 5) Isotropic soil structure exists | Yes | ? | No |

### 3.2.2 Steady state and unsteady state flow

It is shown in Equation 3.4 that the flow rate ($q$) is a constant at a certain hydraulic gradient. When this condition is achieved, the flow is considered as a steady-state flow. In other words, steady state flow is the condition when the flow rate is independent of time. In hydraulic conductivity measurements, steady-state flow is achieved when the inflow rate is

equal to the outflow rate. As the hydraulic gradient is applied, the inflow edge has a higher pressure than the outflow edge and water starts to flow from the inflow end to outflow end of the specimen. However, the outflow edge does not instantaneously experience water flow through it. After a certain elapsed time the water will reach the outflow end and measurement can be performed. During the period of time between the first applications of the hydraulic gradient to the time when the outflow is equal to the inflow, the soil specimen will experience unsteady-state flow or the flow will be under transient condition. As a result, the relationship between flow velocity, *v* and elapsed time, t, is non-linear and changes with time (Figure 3.1). Thus, during this period, steady-state hydraulic conductivity measurement cannot be performed since neither the inflow nor the outflow can be used.

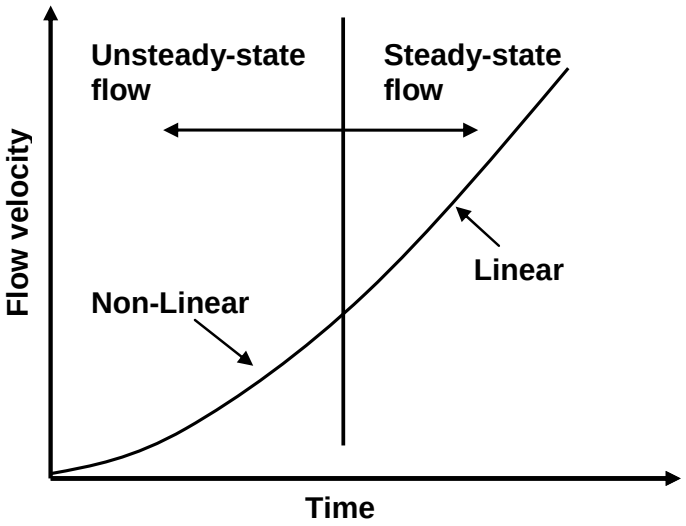


Figure 3.1 Steady state and unsteady state flows

It is sometimes very difficult to achieve the steady-state condition, unless a tolerance limit is accepted. ASTM D5084 states two criteria at which the steady state condition is assumed to be reached. The first criterion is the difference between inflow and outflow rates must be less than 25%. The second criterion is there should not be any upward or downward trend of the plot of the coefficient of hydraulic conductivity versus time.

### 3.2.3 Effect of magnitude of hydraulic gradient

Some factors should be taken into account when using Darcy's law as the governing equation to explain the flow of any liquid through pores. Darcy's experiment was based on laminar flow, where the movement of fluid is essentially in parallel lines when viewed on a macroscopic scale. The other type of flow is turbulent flow that is reached when the velocity of water exceeds the critical value (Figure 3.2). In 1883, Reynolds expanded the results of the experiments of Darcy and defined a critical velocity. The critical velocity is stated in terms of a dimensionless ratio called Reynolds number and defines the range of validity of Darcy's flow. The Reynolds number, $R_e$, is formulated as:

$$R_e = \frac{Dv\rho}{\mu} \tag{3.7}$$

where: $D$ is effective diameter of pores, $v$ is flow velocity, $\rho$ is density of liquid, $\mu$ is viscosity of liquid.

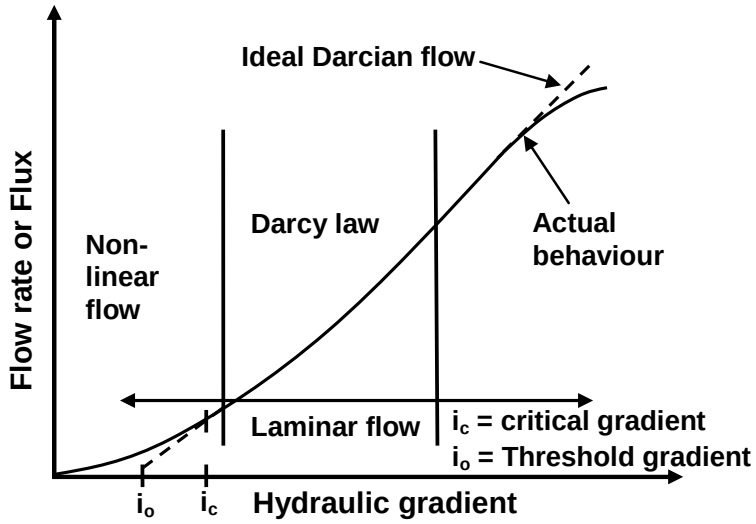


Figure 3.2 Typical relationships between flow velocity and hydraulic gradient (modified from Daniel 1994)

In order to work in the range of laminar flow, $R_e$ must be less than 2000 for flow through a pipe (Bear 1972). In a porous medium such as soil, $R_e$ <0.01 is suitable to ascertain that laminar flow occurs (Zaradny 1993) and the hydraulic gradient can be adjusted to give a certain water particle velocity. The maximum hydraulic gradient obtained using this

criterion may be very high. Zaradny (1993) found that for fine sand with a coefficient of permeability of $10^{-5}$ m/s, the maximum hydraulic gradient can be as high as 100.

An excessively high hydraulic gradient may cause a soft soil specimen to consolidate resulting in a lower hydraulic conductivity being measured. On the other hand, a very low hydraulic gradient is also not advisable since at this gradient the relationship between flow rate and hydraulic gradient becomes non-linear (Hansbo 1960) and Equation 3.3 is no longer valid (Figure 3.2). The magnitude of hydraulic gradient applied in the hydraulic conductivity tests depends on the compressibility of the soil specimens used. ASTM D5084 and DIN 18130 provides some guidelines in determining a suitable hydraulic gradient to be used in saturated hydraulic conductivity tests.

The ultimate test of the validity of the Darcy or any other model for fluid movement is the ability of the model to predict the hydraulic gradient versus flow velocity (flux) relationship for the specimen. Two widely used plotting methods to evaluate deviations from Darcian flow model are:

1) Flow velocity (flux) versus hydraulic gradient

2) Log flow velocity (flux) versus log hydraulic gradient

As shown in Figure 3.2, a plot of measured flow velocity versus hydraulic gradient such as presented by Daniel (1994) should provide a measure of any threshold or critical gradient. Changes in hydraulic conductivity are detected as changes in the slope of the plots. While significant changes in the slope of this line are readily detectable, it is possible that slight changes in the flux-gradient relationships may not be readily detected, particularly if a wide range of gradients or flow velocities (fluxes) are recorded (Dixon 1995).

Concave or convex flux-gradient relationships in a normal linear plot have been reported in the literature (Yong and Warkentin 1975). The reasons suggested are soil fabric effects, the presence of osmotic forces, equipment limitations, real changes in the structure and behaviour of water in clay-water system. The classical Darcy model for Newtonian water flow through a porous media calls for a straight line relationship passing through the origin of the plot (Figure 3.2). Observed deviations from this behaviour have been the cause for much of the past debate over the applicability of the Darcy relationship.

If the flux-hydraulic gradient plot is a straight line intersecting the gradient axis in a location other than the origin, this intersect is defined as the threshold gradient ($i_o$) required to initiate flow. The hydraulic gradient at which Darcian flow begins in a flux-gradient relationship which is not a straight line plot at low gradient, is defined as the critical gradient ($i_c$) for flow.

The second technique for presenting flow data is to plot the flow velocity (flux) versus hydraulic gradient in log-log scale. Plotting of the flux-gradient relationship in log-log plane has been done by Sri Ranjan and Gillham (1991), Sri Ranjan and Karthigesu (1992), Dixon et al. (1993a) and Karthigesu (1994). This technique presents data in a manner which facilitates the identification of changes in the flux-gradient relationship. The measure flow velocity (flux) versus applied hydraulic gradient should plot as straight line which has slope of 1.0 (Figure 3.3). Any change in the hydraulic conductivity will result in vertical shift in the location of this line.

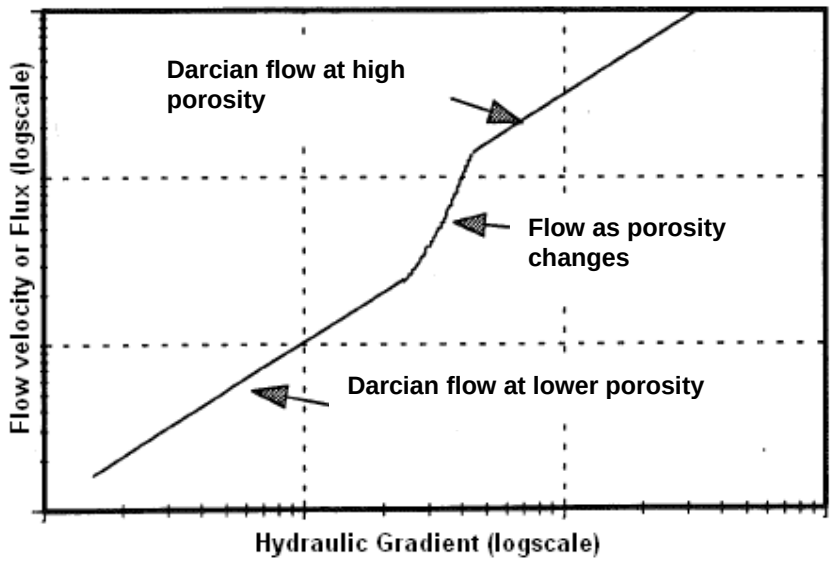


Figure 3.3 Plot of log flux versus log hydraulic gradient (Dixon 1995)

The technique provides the clearest display for examining hydraulic conductivity over wide range of gradients and emphasizes the location of any critical gradients for changes in flow behaviour. However, a log scale does not provide the visual means for detecting the threshold gradients defined by conventional means (zero flux occurs at a gradient equal to

zero). The plot is based on the validity of the Darcian flow model. A shift in the location of the line is interpreted as a change in the pore space available for flow. If such a shift occurs and provided that no further changes in the pore volume available for flow occurs, then the new flux-gradient relationship will again be a straight line with a slope of 1.0 which is offset from the initial line. The hydraulic conductivity, $k$ of the plot such as that shown in Figure 3.3 is calculated by either extending the plotted lines backwards or forward to the point at which it cuts the hydraulic gradient of 1.0. The flux at this gradient is defined as hydraulic conductivity. Alternatively, any value of the flux located along the regions showing Darcian flow behaviour can be divided by the hydraulic gradient applied to obtain this measured flow or flux.

In order to generate a good estimate of the potential changes in the hydraulic conductivity of a soil specimen both of these methods should be used. The linear plot provides a visual record of the presence of the threshold and or critical gradient. The log-log plot provides a sensitive means to detect subtle changes in the pore space available for flow.

## 3.3 Empirical relationships for saturated coefficient of hydraulic conductivity

### 3.3.1 Introduction

The saturated coefficient of hydraulic conductivity of a soil is a function of its void ratio. The relationship between saturated coefficient of hydraulic conductivity and void ratio is different for different soil types. Grain size distribution of the soils can account for some of the differences due to soil types. Therefore, the saturated coefficient of hydraulic conductivity is no longer a function of void ratio alone but a function of void ratio, grain size distribution and other soil parameters for different soil types. Several empirical equations for estimating hydraulic conductivity have been proposed in past, some of these are briefly discussed in following section.

### 3.3.2 Relation between saturated hydraulic conductivity, void ratio and grain size distribution

Researchers have attempted to develop empirical relationships for determination of the saturated hydraulic conductivity. The empirical formula is based on experimental data

obtained in the laboratory that relate the saturated coefficient of hydraulic conductivity with void ratio and grain size distribution characteristic.

**Hazen equation:**

Almost all of the empirical formulas are derived from one general relationship (Hazen 1892):

$$k = Cf(n_s)d_e^2 \tag{3.8}$$

where: $C$ is a constant, $f(n_s)$ is porosity function, $d_e$ is the effective grain diameter of soil particles.

Hazen (Vukovic and Soro, 1992) noted that $d_e$ can be taken as $d_{10}$ and the porosity function is expressed as:

$$f(n_s) = 1 + 10(n_s - 0.26) \tag{3.9}$$

Hazen's formula is valid only for soils with porosity greater than 0.16. For soils with porosity less than 0.16, Equation 3.8 will give negative values since $f(n_s)$ becomes less than zero. It was also noted that Hazen's formula is recommended for soils with $d_{10}$ ranging between 0.1 mm and 3 mm and/or with coefficient of uniformity, $U$ (i.e., $d_{60}/d_{10}$) smaller than 5 (Vukovic and Soro, 1992). However, Vukovic and Soro (1992) found that the Hazen's formula was also applicable for soils with characteristics that were not in the range in which the formula was derived. Hazen suggested that the constant $C$ is equal to 0.00583. Later it was also suggested that since the saturated coefficient of Hydraulic conductivity also depends on other factors that cannot be accounted for in the Hazen's formula (e.g., heterogeneity, fines content and pore size distribution), the constant $C$ is not necessarily a unique value.

**Terzaghi equation:**

Terzaghi (1925) formulated another empirical relationship in the same form as Equation 3.8 for large grained sands. The effective grain diameter, $d_e$ is taken as $d_{10}$ while the porosity function, $f(n_s)$ is defined as:

$$f(n_s) = \left[ \frac{n_s - 0.13}{\sqrt[3]{1 - n_s}} \right]^2 \tag{3.10}$$

The empirical constant C in Terzaghi's formula was found to be 6.63 to 7.50 for sea sand, 8 for dune sand, 4.60 to 6.96 for pure river sand and 2.03 for muddy river sand (Vukovic and Soro 1992). It indicates that the empirical constant C cannot be taken as a single value for all coarse-grained sands.

**Alyamani and Sen equation:**

Alyamani and Sen (1993) formulated empirical relationship using grain size distribution as follow:

$$k = 1300\left[ I_o + 0.025\left( d_{50} - d_{10} \right) \right]^2 \tag{3.11}$$

where: $k$, is the hydraulic conductivity (m/day), $I_o$ is the intercept (in mm) of the line formed by $d_{50}$ and $d_{10}$ with the grain-size axis, $d_{10}$ is the effective grain diameter (mm), and $d_{50}$ is the median grain diameter (mm). It should be noted that the terms in the formula above bear the stated units for consistency. This formula therefore, is exceptionally different from those that take the general form of Equation 3.8. It is however, one of the well known equations that also depend on grain-size analysis. The method considers both sediment grain sizes $d_{10}$ and $d_{50}$ as well as the sorting characteristics.

**Breyer and Slitcher equation:**

The Breyer equation does not employ porosity as part of its formula and is therefore applicable to samples with a heterogeneous porosity. The formula for Breyer equation is:

$$k = g\rho / \mu \times 6 \times 10^{-4} \log \frac{500}{U} d_{10}^2 \tag{3.12}$$

where: $g$ is the acceleration due to gravity, $\rho$ is the mass density of water, $\mu$ is water viscosity, and $U$ is the coefficient of grain uniformity equal to $d_{60}/ d_{10}$.

It is also the most appropriate equation to use for poorly sorted samples. The equation can be used for samples with uniformity values from 1 to 20 and effective grain sizes between 0.06 mm and 0.6 mm.

Slitcher formula is most applicable for grain-size between 0.01mm and 5mm and is given by:

$$k = g\rho / \mu \times 1 \times 10^{-2} n^{3.28} d_{10}^2 \tag{3.13}$$

**United State Bureau of Reclamation:**

U.S. Bureau of Reclamation (USBR) formula calculates hydraulic conductivity from the effective grain size ($d_{20}$), and does not depend on porosity; hence porosity function is a unity. The formula is most suitable for medium-grain sand with uniformity coefficient less than 5 (Cheng and Chen 2007).

$$k = g\rho / \mu \times 4.8 \times 10^{-4} d_{20}^{0.3} d_{20}^2 \tag{3.14}$$

## 3.4 Measurements of saturated hydraulic conductivity

### 3.4.1 Introduction

The saturated coefficient of hydraulic conductivity can be obtained either in the laboratory or in the field. There are different methods for determining saturated coefficient of hydraulic conductivity in the laboratory, namely constant head, variable or falling head and oscillatory pore pressure methods. The laboratory methods are described in following sections.

### 3.4.2 Laboratory measurement of hydraulic conductivity

#### 3.4.2.1 Constant head method

Measurement of coefficients of hydraulic conductivity of soils in the laboratory can be performed using the constant head and the variable head tests. The principle of these methods is described schematically in Figure 3.4. In the constant head method, the

coefficient of hydraulic conductivity is computed from the volume of water, $Q$ collected in time, $t$ and is given by:

$$k = \frac{QL}{Aht} \tag{3.15}$$

where: $A$ is cross sectional area of the soil specimen, $h$ is hydraulic head of water, $L$ is length of drainage path in the soil and $t$ is elapsed time.

In constant head hydraulic conductivity test the pressure gradient across the specimen is kept constant throughout the test. This constant gradient is commonly achieved by using over flowing inflow and outflow reservoirs. In this technique a supply of water is supplied to a reservoir at a rate slightly higher than the specimen will transmit the water. The surplus fluid will overflow the reservoir and be lost to the inflow reservoir. Likewise, the outflow reservoir is initially filled to the preset level and the outflow from the specimen will overflow this reservoir, thereby ensuring that the outflow pressure is kept constant. In this manner the applied hydraulic gradient is kept constant. There is a difficulty in using this technique when very high gradients, or back pressuring are used since the overflow systems must be maintained at elevated pressures. Alternatively a bladder-type system can be used to ensure that the hydraulic head is kept constant despite relatively large fluid movements.

### 3.4.2.2 Variable or falling head method

In the variable head method, the coefficient of hydraulic conductivity is computed using a general equation based on the continuity of flow, which defines that the input flow is equal to the output flow and thus:

$$k = \frac{aL}{At} In\left(\frac{h_1}{h_2}\right) \tag{3.16}$$

where: $a$, is area of water reservoir, $h_1$ is head of water at $t_1$, $h_2$ is head of water at $t_2$.

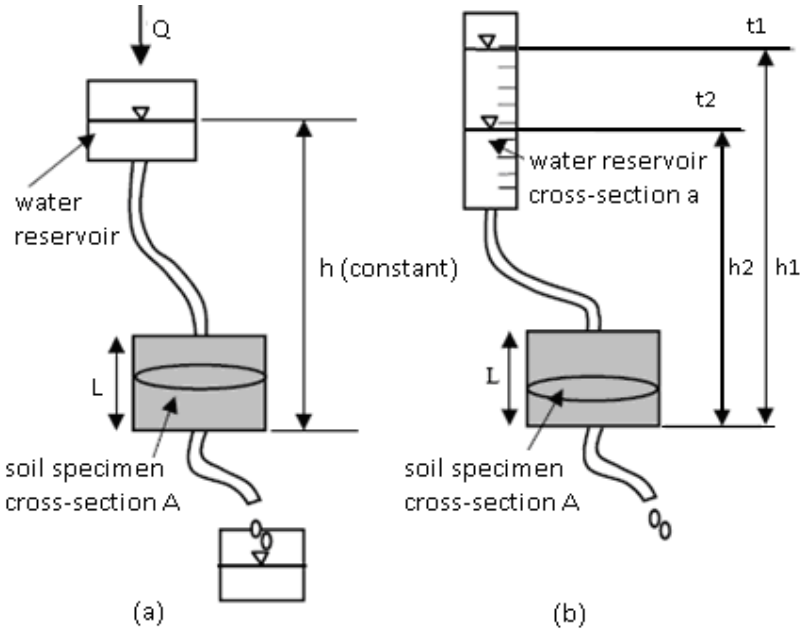


Figure 3.4 Principle of hydraulic conductivity test (a) constant head method (b) variable head method (Agus 2001)

Variable head hydraulic conductivity tests have a preset initial hydraulic potential (head) difference applied across the specimen. The hydraulic head difference is allowed to decrease as water flows from the inflow reservoir through the specimen and into the outflow reservoir. The hydraulic gradient applied is defined as the difference in the hydraulic potentials of the inflow and outflow reservoirs, divided by the specimen length. For each time period where displacement was measured, the hydraulic gradient is assumed to be the average of the potential at the beginning and the end of the increment, divided by the specimen length. The volume displaced during this time increment is used to calculate the hydraulic conductivity of the soil.

The variable head technique, while the simplest to conduct, has a number of limitations. It assumes that the flow through the specimen is Darcian in nature and so the average hydraulic head is representative of the flow occurring at both the maximum and minimum hydraulic gradients present during testing. Additionally, this technique only works effectively when the head change and volume displacements are large enough to be monitored accurately. Associated with the measurement of head and displacement is the need to ensure that evaporative volume losses from the reservoirs are minimized or

prevented. It is possible to use fluid reservoirs with large volumes (especially large diameters) and sensitive displacement gauges to minimize any head changes while monitoring small fluid displacements. In such a system, the hydraulic head will vary by only a few millimeters over the course of the entire test. This means that the hydraulic gradient is for all purposes a constant. This technique has been used by a variety of researchers to measure flow through low hydraulic conductivity clays (Dixon et al. 1986, 1987, 1993a, Sri Ranjan and Karthigesu 1992, Karthigesu 1994). Hydraulic conductivities as low as $10^{-14}$ m/s have been reported by Pusch (1980 a, b) and Bucher et al. (1986) for materials tested using this technique.

Both methods of laboratory hydraulic conductivity tests can be conducted using either a rigid-wall permeameter where the soil specimen is confined in a rigid ring or a flexible-wall permeameter where a confining pressure can be applied to the soil specimen. Various specimen sizes can be used in the laboratory hydraulic conductivity tests. Many researchers such as Olson and Daniel (1981), Daniel and Trautwein (1986), Elsbury et al. (1988) and Trautwein and Boutwell (1994) have questioned the reliability of laboratory tests using small specimens. It was concluded that laboratory tests may yield inaccurate determination of coefficients of hydraulic conductivity due to unrepresentative specimens being used.

Lahti et al. (1987) found that the reliability of the laboratory measurement of the coefficient of hydraulic conductivity of the soil depends on the technique employed and the quality control given to the sampling method and the test procedures. No matter how big the soil specimen is, the result is questionable if improper procedures are adopted in the tests. Benson et al. (1993) suggested that soil specimens should be at least 30 cm in diameter and 0.5 in height to diameter ratio for the determination of the saturated coefficient of hydraulic conductivity of compacted soil reliably.

#### 3.4.2.3 Oscillatory pore pressure method

The pore pressure oscillation method relies on characterizing sinusoidal pore pressure signals at two different locations in terms of differences in amplitude and of relative time lag (Turner 1958, 1959, Stewart et al. 1961, Bennion and Goss 1971, Kranz et al. 1990, Fischer 1992, Renner et al. (2000), Bernabé et al. 2006). The two observables,

attenuation and phase shift, can in principle be inverted to the two effective hydraulic characteristics of an isotropic sample, permeability and specific storage capacity.

Standard test arrangement consists of a pore fluid system (water), a confining fluid system (oil), and a personal computer-aided control device (Song and Renner 2007). In the pore fluid system, a saturated sample is located between two reservoirs, downstream and upstream, the latter comprises a hydraulic pressure intensifier (Figure 3.5). Porous metal discs (SIKAR S) of 3 mm thickness, a permeability of $>10^{-12}$ $m^2$, and a pore diameter in the range of 7 to 14 μm serves a dual purpose at the sample ends. Firstly, pore fluid is evenly distributed over the sample end faces, and secondly, the confining pressure is transmitted to the sample in axial direction. A rubber jacket encloses the sample and the end-plugs separating pore and confining fluid and imposing conditions approximating one-dimensional flow. The operation of the pore pressure and the confining pressure intensifier is conducted servo-hydraulically. Two displacement and three pressure transducers measure the position of the intensifier pistons and the fluid pressures of the reservoirs and the vessel, respectively. These signals are digitally recorded and are available as feedback signal for the control unit.

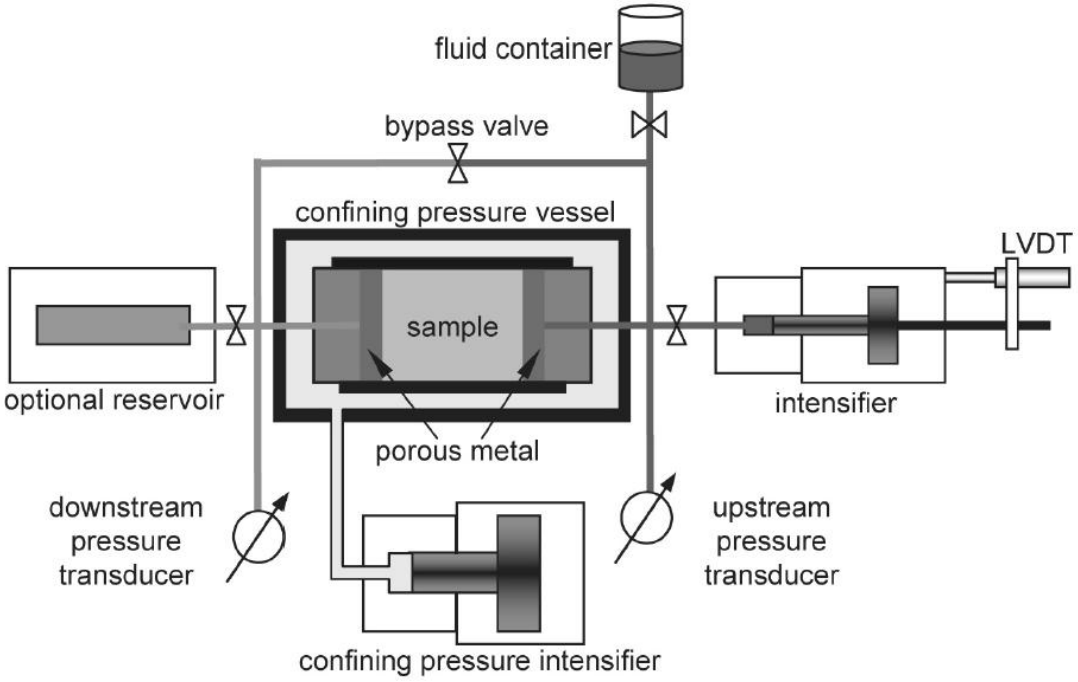


Figure 3.5 Standard experimental set-up for oscillatory pore pressure testing (Song and Renner 2007)

## 3.5 Theoretical models for saturated hydraulic conductivity

The transport of water in expansive soils may occur in two phases; namely in liquid phase (i.e., advection process) and in vapour phase (i.e., diffusion process). The transport property related to the liquid phase water transport is the coefficient of hydraulic conductivity whereas the coefficient of diffusivity can be used to describe the transport of water in the vapour phase. However, both the coefficient of hydraulic conductivity and the coefficient of diffusivity depend on the void ratio and other characteristics of the soils.

One of the commonly accepted relationships used in predicting advective flow is Darcy's law (section 3.2.1). Other models for predicting water flow through porous media include the Kozeny-Carman, cluster model and Poiseuille or laminar flow model. Despite the common usage of these models they all have practical limitations which limit their applicability to natural systems and materials. Much of the difficulty in using these relationships has been attributed to natural soil anisotropy, and the presence of non-hydraulic (chemical, thermal, electrical or other) gradients in soils. Such gradients have been repeatedly reported in the literature (Law and Lee 1981, Sri Ranjan and Gillham 1991, Karthigesu 1994, Dixon 1999). The following sections present the basic models for flow thorough a porous medium and discuss the strengths and weakness of these models, particularly when they are applied to clay soils.

### 3.5.1 Poiseuille model for saturated hydraulic conductivity

The Poiseuille equation provides the starting point for most attempts to describe water flow through soils (Yong and Warkentin 1975, Mitchell 1976, Lambe and Whitman 1979). This equation was developed to predict the average fluid flow through a tubular capillary with circular cross-section. In its simplest form it can be expressed:

$$v_{avg} = \rho_w R^2 i / 8\mu \tag{3.17}$$

where: $v_{avg}$ is the average fluid velocity, $R$ is the tube radius, $\rho_w$ is the mass density of the permeating water, $i$ is the hydraulic gradient and $\mu$ is the water viscosity. Modification of this basic equation begins with recognition that the size of the pores may vary, and so an average size must be used. The average pore size is accounted for using the hydraulic

radius ($R_h$), which for a circular tube flowing full is defined in Equation 3.18 (Mitchell 1976).

$$R_h = \pi R^2 / 2\pi R = R/2 \tag{3.18}$$

From this, the Poiseuille equation can be used to estimate flow rate ($q$) through a tube.

$$q = \rho_w R_h^2 ia / 2\mu \tag{3.19}$$

where: $a$ is the cross-sectional area of the tube. However since the pores in a soil are not ideal tubular capillaries, a shape coefficient ($C_s$) is used to modify the flow rate prediction (Mitchell 1976).

$$q = C_s \rho_w R_h^2 ia / \mu \tag{3.20}$$

Equation 3.20 can be further developed to account for parameters such as degree of saturation ($S$), specific surface of the soil particles ($S_o$), void ratio ($e$), total cross-sectional area ($A$) of the specimen and volume of particles ($V_s$). On completion of these substitutions Equation 3.20 can be expressed as:

$$q = C_s V_s^2 \rho_w e^3 S^3 iA / \left( \mu S_o^2 \left(1+e\right)\right) \tag{3.21}$$

Parameters such as degree of saturation ($S$), and Shape Factor ($C_s$), for fully saturated materials have established values (Mitchell 1976). Saturation is 1.0 in a fully saturated specimen, and $C_s = 1/k_o T^2$ (Mitchell 1976). The $k_o$ is the pore shape factor (approximately 2.5) and the tortuosity factor, $T$ is used to account for the fact that the pore paths are not straight. The tortuosity factor is defined as being the ratio of the effective flow path and the thickness of the test sample and is generally defined as being $\sqrt{2}$.

The Poiseuille equation is normally only taken as a starting point in the development of predictive equations. It is often combined with an assumption that the Darcy equation for flow is correct and then developed into relationships such as the Kozeny-Carman model presented in section 3.5.2, (Kozeny 1927, Carman 1937).

Komine (2008) proposed model for predicting hydraulic conductivity of compacted clays. He suggested streamline or laminar flow model between two parallel plate layers of the clay. In his model, it is assumed that water flow is two dimensional and that water is incompressible. This model is the equivalent of Poiseuille flow equation (Mitchell 1993), the hydraulic conductivity of a two parallel-plate layer can be calculated as:

$$k = \frac{\rho_{aw}}{12\mu_{aw}}\left(2d\right)^2 \tag{3.22}$$

where: $k$ is hydraulic conductivity between two parallel plate layers (m/s), $d$ is half the distance between two parallel plate layers (m), $\rho_{aw}$ is density of interlayer water between two parallel plate layers (Pa/m), and $\mu_{aw}$ is the coefficient of viscosity of interlayer water between two parallel plate layers (Pa.s).

In this thesis Equation 3.22 has been used to estimate the hydraulic conductivity using modified diffuse double layer equations (Tripathy et al. 2004), which will be discuss in detail in Chapter 7.

### 3.5.2 Kozeny-Carman model for saturated hydraulic conductivity

A widely used relationship between the saturated hydraulic conductivity and the physical properties of the fluid and the soil mass is based on the "hydraulic radius theory" and referred to as the Kozeny–Carman hydraulic model. The model was first proposed by Kozeny in 1927 and subsequently modified by Carman (1937). Kozeny and Carman developed a theory for a series of capillary tubes of equal length for predicting the saturated hydraulic conductivity for soils.

The derivation of Kozeny-Carman model is based on the combination of Darcy law (Equation 3.4) and Poiseuille equation (Equation 3.21).

For a fully saturated system, $\rho_w = 1$, $V_s = 1$, $S = 1$, tortuosity $T = V2$, and with a pore shape factor $k_o = 2.5$, the Poiseuille equation can be expressed (Lambe and Whitman 1979) as:

$$k = \rho_w e^3 / \left(k_o T^2 \mu S_o^2 \left(1+e\right)\right) = C_s \rho_w e^3 / \left(\mu S_o^2 \left(1+e\right)\right) \tag{3.23}$$

Carrier III (2003) found that the Kozeny-Carman model had the best theoretical basis as compared to the other models. This is due to the fact that the grain-size distribution of the soil is some how taken into account by using the specific surface area. Carrier III (2003) expressed Kozeny-Carman model as:

$$k = \left(\frac{\gamma}{\mu}\right)\frac{1}{k_o T^2 S_o^2}\left(\frac{e^3}{1+e}\right) \tag{3.24}$$

where: $\gamma$ is unit weight of permeant, $\mu$ is viscosity of permeant, $S_o$ is specific surface area per unit volume of particles (1/cm), $T$ is tortuosity factor, $k_o$ is pore shape factor and $e$ is void ratio.

In more general form, Kozeny-Carman model can be written as:

$$k = \left(\frac{\gamma}{\mu}\right)\left(\frac{1}{C_s}\right)\left(\frac{1}{S_o^2}\right)\left(\frac{e^3}{1+e}\right) \tag{3.25}$$

When the permeant is water at 20°, γ/μ is equal to 9.93 x $10^4$ 1/cm s. Carman (1956) reported the value of $C_s$ as being equal to 4.8±0.3 for uniform spheres, $C_s$ is usually taken to be equal to 5. Thus, Equation (3.25) becomes:

$$k = 1.99\times10^4\left(\frac{1}{S_o^2}\right)\left(\frac{e^3}{1+e}\right) \qquad \text{(for } 20^{\circ}\text{C)} \tag{3.26}$$

Even though the Kozeny-Carman model for flow is commonly recognized as one of the best model available for predicting the hydraulic conductivity of soils, its applicability is limited (Yong and Warkentin 1975, Mitchell 1976, Yong et al. 1992). Equation 3.23 to Equation 3.26 is recognized as being generally valid only for material where there is:

1. relatively uniform particle size
2. no soil structure or fissuring
3. laminar flow of liquid through pores

4. Darcian flow behaviour

5. absence of long and short range forces of interaction

These limitations to the application of this model means that it can only be applied for material such as gravel, fine sand, and silts. The structure and anisotropic fabric of most clay violate the basic requirements for the application of the Darcian, Poiseuille or Kozeny-Carman models.

### 3.5.3 Cluster model for saturated hydraulic conductivity

Olsen (1962) found discrepancies between the measured saturated hydraulic conductivity and that predicted using the Kozeny-Carman model (Equation 3.25) for clays. Factors that might influence the flow of water though clay soils are described in Olsen (1962) and included possible errors in Darcy's law, interaction between viscous and electric flows between water and clay particles (i.e., electrokinetic coupling), possible higher viscosity of water near the clay surfaces, non-constant tortuosity of the water flow paths as induced for instance by the anisotropic shapes and orientations of clay particles, and the existence of clusters that may induce unequal pore sizes in the soil. It was found that the deviation of Equation 3.25 from the measured data was attributed to the presence of clay clusters in the soil. Some other abovementioned factors that might induce the discrepancies were found to be insignificant (Olsen 1962). Based on the conclusion drawn regarding the factor that influences at most the deviation of the Kozeny-Carman model for predicting the water flow though clay soils, a saturated hydraulic conductivity model, called cluster model was proposed by Olsen in 1962.

The cluster model as suggested by Olsen (1962) divides the total void ratio $e_T$, into two components, the intracluster (micro) void ratio $e_c$ and the intercluster (macro) void ratio $e_p$. The micro void ratio that exists within a group of clay particle or within packets or clods, and the macro void ratio that remains in between the clay clusters or packets. The total void ratio $e_T$ is given as:

$$e_T = e_c + e_p \tag{3.27}$$

Assuming that flow only occurs through intercluster pores and that all clusters are spheres of the same size, Olsen (1962) derived the flowing equation for flow through clay:

$$\frac{k_{CM}}{k_{KC}} = N^{2/3}\frac{\left(1-e_c/e_T\right)^3}{\left(1+e_c\right)^{4/3}} \tag{3.28}$$

where: $k_{CM}$ is the measured flow rate of water, $k_{KC}$ is the predicted flow rate using the Kozeny-Carman model, $N$ is the average number clay particles per cluster, $e_c$ is the cluster void ratio (i.e., the intra-cluster or the intra-aggregate or the micro-pore void ratio), and $e_T$ is the total void ratio.

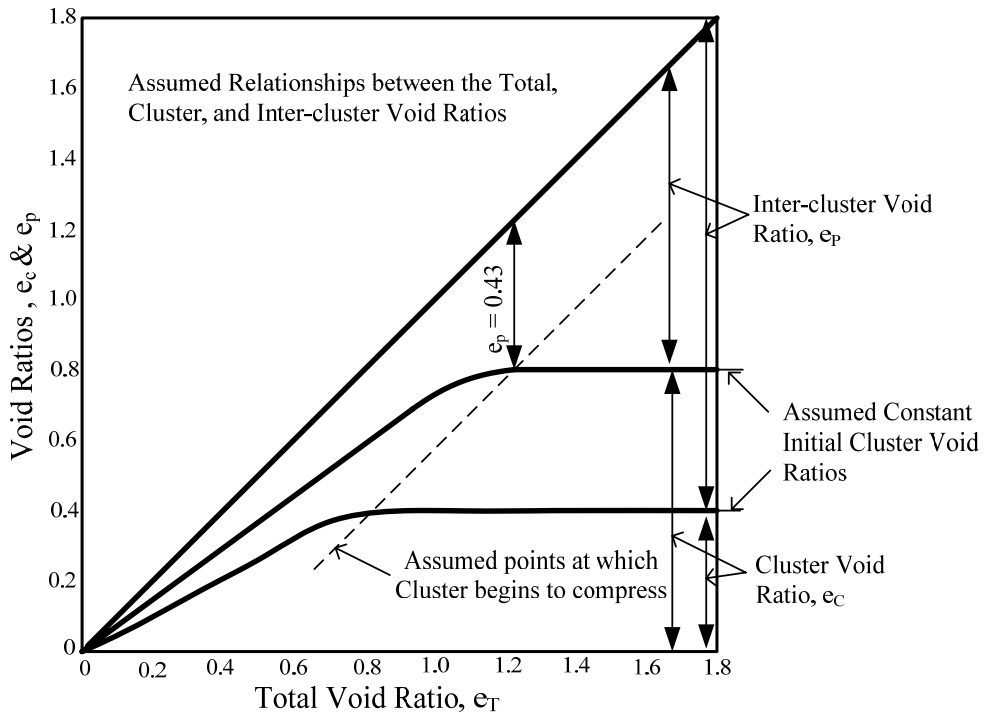


Figure 3.6 Assumed relationship between total, cluster (or intra-cluster or micro), and inter-cluster (or macro) void ratio (modified from Olsen, 1962)

For a particular soil, the ratio of flow rate as given in Equation 3.28 is equal to the ratio of the measured flow rate to the computed flow rate using the Kozeny-Carman model. Therefore, to compute the saturated hydraulic conductivity of a clay using Equation 3.28**,** the parameter N and the two void ratios (i.e., the cluster and the total void ratios) must be known. The number of clay particles per cluster (*N*) was assumed to be constant for a

specific soil permeant system. The clay-permeant dispersion systems were considered to affect the decrease in both cluster and initial cluster void ratios.

Olsen (1962) assumed relationships between the total void ratio, $e_T$, micro void ratio, $e_c$ and macro void ratio, $e_p$ for which at high total void ratios the micro void ratio, $e_c$ value is constant upon compression and then begins to reduce when $e_p$ ratio is equal to 0.43 (Figure 3.6). As compression continues, the $e_c$ has linear relationship with $e_T$ until both values (void ratios) reaches to zero.

Achari et al. (1999) used Olsen (1962)'s model to predict hydraulic conductivity of clays. Achari et al. (1999) used the modified diffused double layer (DDL) theory in conjunction with the true effective stress concept proposed by Lambe and Whitman (1969) for computing the cluster void ratio. The model presented by Achari et al. (1999) encompassed the following phenomena: (1) a compacted clay bed is a porous media, (2) clay exists as small clusters and not as individual particles, (3) the diffuse double layer around clay platelets affect the hydraulic flow, and (4) the clay cluster size is affected by consolidation pressure and the concentration of ions in the permeant. The true effective stress σ* is given by (Lambe and Whitman 1969) as:

$$\sigma^* = \left(\sigma - u_w\right) - \left(R - A\right) \tag{3.29}$$

where: $\sigma$ is the total stress, $u_w$ is the pore-water pressure, ($\sigma$ - $u_w$) is the effective pressure, $R$ is the repulsive pressure, $A$ is the attractive pressure. Equation 3.29 is a balance between the externally applied pressure and the internal physico-chemical stresses acting on the system. At equilibrium, the true effective stress approaches zero (Lambe and Whitman 1969). The total stress, $\sigma$ and the pore-water pressure, $U$ can be determined from the saturated unit weight of the soil and the unit weight of water.

The repulsive pressure $R$ in Equation 3.29 is the difference between the osmotic pressure in the central plane between clay particles and that in the bulk solution, and can be calculated using diffuse double layer equations (Equation 2.6). In Equation 2.6 swelling pressure $p$, has same meaning as that of repulsive pressure $R$.

The attractive pressure $A$ in Equation 3.29 is the van der Waal's attractive pressure, which can be written as (Sridharan and Jayadeva 1982).

$$A = \frac{B}{48\pi}\left[\frac{1}{d^3} + \frac{1}{\left(d+\delta\right)^3} - \frac{2}{\left(d+0.5\delta\right)^3}\right] \tag{3.30}$$

where: $B$ is Hamakar's constant, $2d$ is the separation distance between the clay platelets, and $\delta$ is the thickness of the unit layer of clay platelets measured between the planes of the centre of the oxygen atoms of the tetrahedral sheet. For montmorillonite, $B = 10^{-19}$ J and $\delta = 0.66$ nm (van Olphen 1991).

To compute the attractive pressure $A$, the value of $d$ is required. In the evaluation procedure, the value of $d$ is considered to be directly related to the intracluster void ratio $e_c$ through Equation 2.10 (Bolt 1956). In Equation 3.28, to compute the value of $N$, as function of effective stress and concentration of permeant, the following empirical relationship was proposed by Achari et al. (1999).

$$N = \frac{2.43\times10^{11}}{\left(\sigma - u_w\right)^2\sqrt{C_o}} \tag{3.31}$$

where: $(\sigma - u_w)$ is the effective stress in kPa and $C_o$ is the bulk concentration of permeant in g.equivalent/m$^3$.

An iterative procedure was set up by Achari et al. (1999) to solve the DDL equation and to compute the saturated hydraulic conductivity. The combination of DDL theory, true effective stress concept, and cluster model proposed by Achari et al. (1999) to compute saturated hydraulic conductivity is limited to homoionic clay and ionic solutions.

## 3.6 Summary

Testing the hydraulic properties of the clays is challenging. Many parameters have to be considered during the testing such as steady state condition, effect of hydraulic gradient. This chapter covered the hydraulic properties of soils and different methods for the determinations of hydraulic conductivity. The different methods include, namely constant head, variable or falling head and oscillatory pore pressure.

Moreover there are empirical equations for estimating hydraulic conductivity proposed by past researcher but most of these equations are for granular material with low plasticity soils. Similarly there are theoretical models used to predict hydraulic conductivity of soils, among them three models is discussed.

# Chapter 4

# MATERIAL CHARACTERIZATION AND EXPERIMENTAL PROGRAM

## 4.1 Introduction

This chapter discusses basic characterization of the materials that are used in this research. Several basic properties of the materials used are obtained through experiments and others are collected from literatures. The aim of the chapter is to characterize the materials accurately because their properties would be later used in subsequent chapters for analysis and validation. Where possible the determined material properties are compared with past work of other researchers. The chapter also follows the detailed description of the experimental program including initial placement condition and permeant used for the tests.

## 4.2 Materials

The investigation has been carried out on three different highly plastic montmorillonitic clays, namely, calcium bentonite named as Calcigel, MX-80 and Kunigel bentonites. The clays used in this study are 100% pure bentonites. The following sections discuss about each of these materials.

### 4.2.1 Calcigel bentonite

Bentonite is an industrial name for an ore which contains mainly smectite, the most common form in geological terms being montmorillonite-like, with particular properties of swelling and water absorption. Indeed bentonite presents strong colloidal properties and its volume increases several times when coming into contact with water, creating a gelatinous and viscous substance.

Calcium bentonite (Calcigel) is highly swelling clay and mined from Southern part (Bavaria) of Germany. The clay contains predominantly bivalent cations (i.e., $Ca^{2+}$ and $Mg^{2+}$). Among several attributes of bentonites, Calcigel bentonites have been proposed as a barrier and backfilling materials for the underground storage of high level radioactive waste.

### 4.2.2 MX-80 bentonite

Sodium bentonite (MX-80) was first found in Benton formation of Eastern Wyoming, USA. This bentonite typically consists of a large fraction of the 2:1 montmorillonite mineral. MX-80 bentonite has been selected for this investigation and has been subjected to a number of studies in the context of being a suitable engineering barrier material for a multi barrier high level nuclear waste disposal repository. MX-80 is mined in Wyoming USA. Its various physico-chemical properties are presented in the following sections.

### 4.2.3 Kunigel bentonite

Kunigel is a sodium type bentonite containing nearly 48% montmorillonite. It is produced at Tsukinuno mine in Japan. The bentonite consists of predominantly monovalent cations. Kunigel bentonite was been chosen as a test material because it has been extensively used in research and many published data are available on its properties (Komine and Ogata 1994, 1999, Komine 2001). Its physical and chemical properties are described in length in this chapter.

## 4.3 Physical properties

Physical characteristics like specific gravity, particle size distribution, Atterberg's limits (liquid limit and plastic limit) are important properties of any soil. The following sections discuss their determination techniques.

### 4.3.1 Natural water content

It is the ratio expressed as a percent of the mass of "pore" or "free" water in a given mass of material to the mass of the solid material. The natural water content was

determined by oven drying method. The specimens were dried in oven at 110 °C as per method described in ASTM D2216 (ASTM, 1998). The loss of mass due to drying is considered to be water. The water content is calculated using the mass of water and the mass of the dry specimen. The water content of materials containing extraneous matter (such as cement, and the like) may require special treatment or a qualified definition of water content. In addition, some organic materials may be decomposed by oven drying at the standard drying temperature for this method (110°C). Materials containing gypsum may present a special problem as this material slowly dehydrates at the standard drying temperature (110°C). In order to reduce decomposition in highly organic soils, it may be desirable to dry these materials at 60°C.

Calcigel bentonite was found to have natural water content from 8.5 % to 9.5 %; this is consistent with the result presented by Baille et al. (2010).

The MX-80 bentonite was found to have variable water content from 10 % to 12 %; this is consistent with the data presented by Müller-Vonmoos and Kahr (1982).

The natural water content of Kunigel bentonite at laboratory environment was found to be 6.0 % to 6.5 %; this is consistent with the result presented by Komine and Ogata (1996).

### 4.3.2 Specific gravity

The specific gravity or particle density of solid particles is defined as the ratio of the mass of a given volume of solids to the mass of an equal volume of water at 4 °C, in simple words; it is the ratio of the density of soil solids to the density of water (Arora 1997). For specific gravity determination, method proposed in DIN 18124 KP (DIN, 1997) was adopted in this study. The method proposed in ASTM D 854 (ASTM, 1987) for high plastic clay was performed for comparison. In order to release entrapped air in the specimen, the picnometer with the saturated specimen was placed on sand bath and stirred carefully. The test was performed in 5-7 days to ensure that there is no entrapped air in the specimen. This is longer than time proposed by DIN and ASTM standard (i.e., only 2 hours).

The specific gravity of Calcigel bentonite was found to be 2.72. Baille et al. (2010) reported the value for specific gravity equal to 2.8.

MX-80 bentonite exhibits gel like characteristic when mixed with water because the water is a polar liquid. Therefore, non-polar liquid kerosene was used to determine the specific gravity of the MX-80 bentonite. The specific gravity of MX-80 was found to be 2.80. In comparison Bradbury and Baeyens (2002) and Müller-Vonmoos and Kahr (1982) reported 2.76 specific gravity of MX-80 bentonite.

The specific gravity of the Kunigel bentonite using ASTM D854 method was found to be 2.75. Komine and Ogata (1996) reported 2.79 specific gravity of Kunigel bentonite.

### 4.3.3 Particle size distribution

The particle size distribution can be determined by two methods first, by using a hydrometer or sedimentation method (i.e., DIN 18123-7) (DIN, 1987) and second by using a laser diffractometer. In this study particle size distribution of bentonites was investigated using sedimentation method. In the sedimentation method, the sample was dispersed using a dispersing solution (i.e., sodium pyrophosphate) during experiment. Figures 4.1 to 4.3 show the particle size distribution found by the hydrometer method for Calcigel, MX-80 and Kunigel bentonites respectively. The data from literature is also shown for comparison. The amount of clay particle size fraction for Calcigel, MX-80 and Kunigel bentonites are 13 %, 80 % and 65 % respectively.

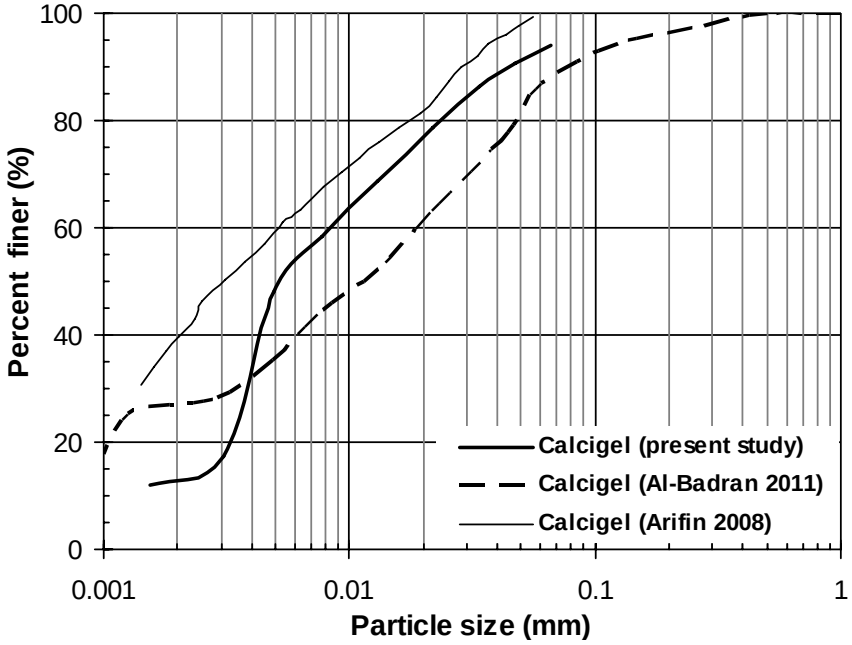


Figure 4.1 Particle size distribution curve for Calcigel bentonite by hydrometer method

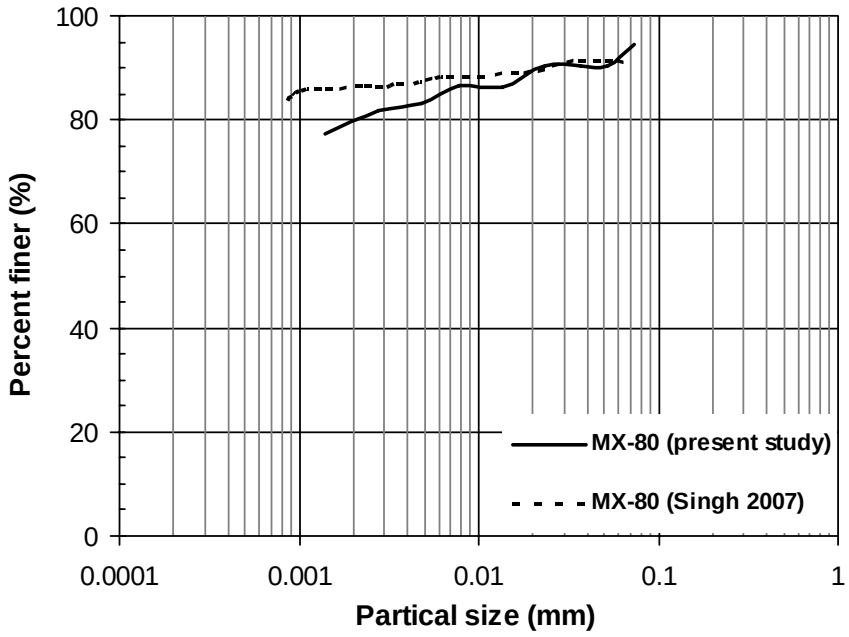


Figure 4.2 Particle size distribution curve for MX-80 bentonite by hydrometer method

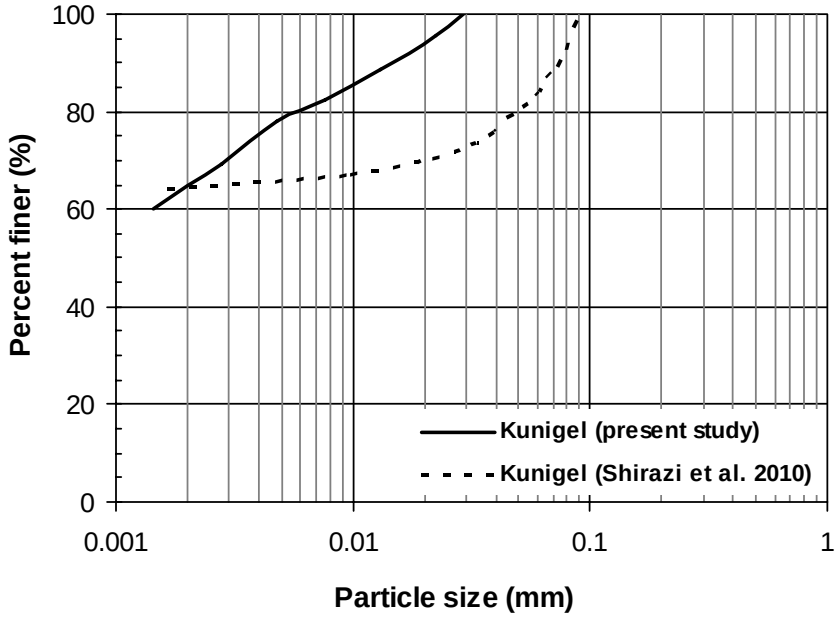


Figure 4.3 Particle size distribution curve for Kunigel bentonite by hydrometer method

### 4.3.4 Liquid limit

The liquid limit is the water content at which a soil changes from the liquid state to the plastic state. In other words liquid limit is the capability of soil to retain the water. Two types of tests are suggested to determine the soil liquid limit, namely cone penetrometer and the Casagrande method. The cone penetrometer method is a static test that depends on the shear strength of the soil (Head 1980). Alternatively, the Casagrande method is a dynamic test. Casagrande method has been used in this study to measure the liquid limit (ASTM D 4318) (ASTM 1997). The samples were mixed with distilled water to reach different values of water content and remixed everyday for minimum one week before investigation. In order to place definite, reproducible values, it is proposed that the liquid limit defined as that water content at which a pat of soil placed in the cup, cut with standard groove, and then dropped from the height of 10mm with undergo a groove closer when dropped 25 times. Several variables affect the LL test including size of soil sample in cup, rate of blow, length of time soil in the cup, accuracy of height of fall, type of grooving tool. All these variables are technician controllable and to reduce the test variables, test equipment should be standardized. It is believed that cone penetration method is more reproducible than that obtained using the Casagrande method, but the principal item requiring attention is that the point of the cone may blunted from excess use, in which case new cone must be obtained.

The liquid limit values for three bentonites used in this study are listed in Table 4.1.

### 4.3.5 Plastic limit

The plastic limit is the water content below which a soil stops behaving as a plastic material. The plastic limit of the selected clays has been determined by standard thread rolling method based on ASTM D 4318 (ASTM, 1997). The standard thread-rolling method requires that a ball of soil be moulded in the palms of the hands until the heat of the palms has dried the soil sufficiently for slight cracks to appear on its surface. The sample is the rolled into a thread of 3 mm diameter by forward and backward movement of the hand. The procedure is repeated until the thread has developed shear cracks longitudinally and transversely. This water content of the thread is defined as the plastic limit of the soil. It is also expressed as a percentage and reported to the nearest whole

number. It is an operator dependent method and depends upon the judgment of the operator.

The plastic limit of Calcigel bentonite has been determined as 39 % and that of MX-80 bentonite as 48 % and for Kunigel bentonite it was 35 % by this method.

### 4.3.6 Plasticity index

The plasticity index is defined as water content range over which a soil exhibits plastic behaviour. It is equal to the difference between the liquid limit and the plastic limit. Thus

$$PI = LL - PL \tag{4.1}$$

where: *PI* is the plasticity index, *LL* is the liquid limit and *PL* is the plastic limit.

Hence, the plasticity index for Calcigel bentonite found to be 71 %, MX-80 bentonite determined to have a plasticity index of 442 %, whereas, Kunigel bentonite has plasticity index 370 %.

### 4.3.7 Activity

Activity is a measure of the water holding capacity of clayey soil (Arora 1997). The changes in the volume of clayey soil during swelling or shrinkage depend upon the activity. The activity (A) of soil is defined as:

$$A = \frac{PI}{C} \tag{4.2}$$

where: *PI* is the plasticity index and *C* is the percentage of clay fraction finer than 0.002 mm in the soil.

Therefore the activity for the three studied bentonites i.e., Calcigel, MX-80 and Kunigel were found to be 5.46, 5.52 and 5.69 respectively.

## 4.4 Compaction characteristics

The compaction curves of the bentonites were obtained using standard proctor method with compaction energy of 600 kN-m/m$^3$ in accordance to DIN (DIN, 1987) and ASTM standards (ASTM, 1997). The compaction curves of Calcigel and Kunigel bentonites as obtained for specimens at water contents range between 6% and 55% are shown in Figures 4.4 to 4.6. The optimum water content and the maximum dry density for the Calcigel bentonite are 36 % and 1.23 Mg/m$^3$ respectively. For MX-80 bentonite, the optimum water content and maximum dry density is found to be 37 % and 1.08 Mg/m$^3$, whereas, for Kunigel bentonite the optimum water content is 31 % and maximum dry density 1.26 Mg/m$^3$. As can be seen in Figure 4.5, MX-80 bentonite shows double peaks, where the compaction curve has initially decreasing then increasing dry density as water content increases. Thus the compaction curve identifies two maximum dry densities and two optimum water contents (Benson et al. 1997, Sun et al. 2007, Razouki et al. 2008, Al-Badran 2011). Razouki et al. (1980) referred to the maximum dry density at lower water content. The bell, S, and M shaped nature of the compaction curve; some soils may be compacted to equal density at two, three or four different water contents. The dry side peak in compaction curve does not appear in most cases because the compaction curve starts with the water content higher than the dry optimum water content regarding for the applied compaction effort (Al-Badran 2011). If more than one curve exists for the same soil then the following scenarios are possible: (i) the dry peak compaction points do not appear for both low and high compaction efforts, (ii) the dry peak compaction points for both low and high compaction efforts appear, and (iii) the dry peak compaction point for either low or high compaction effort appears. Case (i) happens when compaction curve initially starts with water content more than the dry of optimum water content. Case (ii) occurs when the initial moulding water content is less than the dry optimum water content. Case (iii) occurs when the initial moulding water content falls between the two dry optimum water contents.

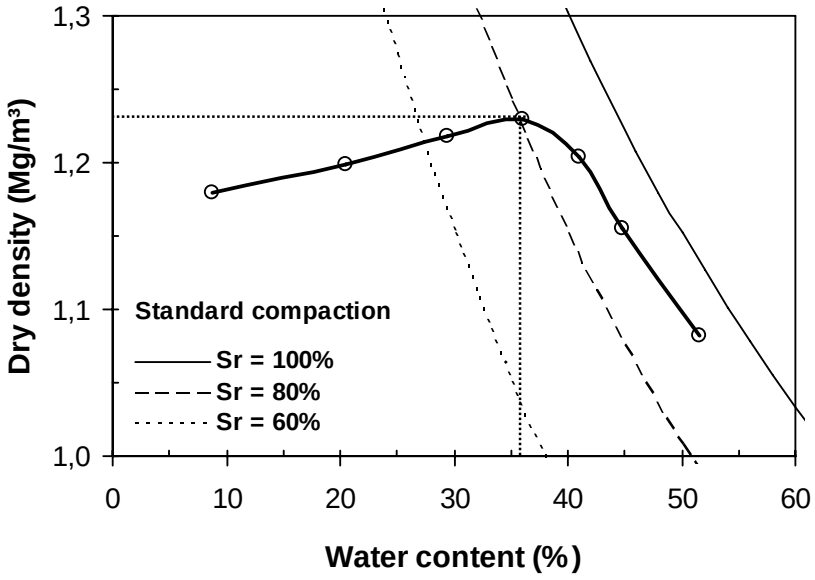


Figure 4.4 Compaction curve for Calcigel bentonite via standard Proctor method

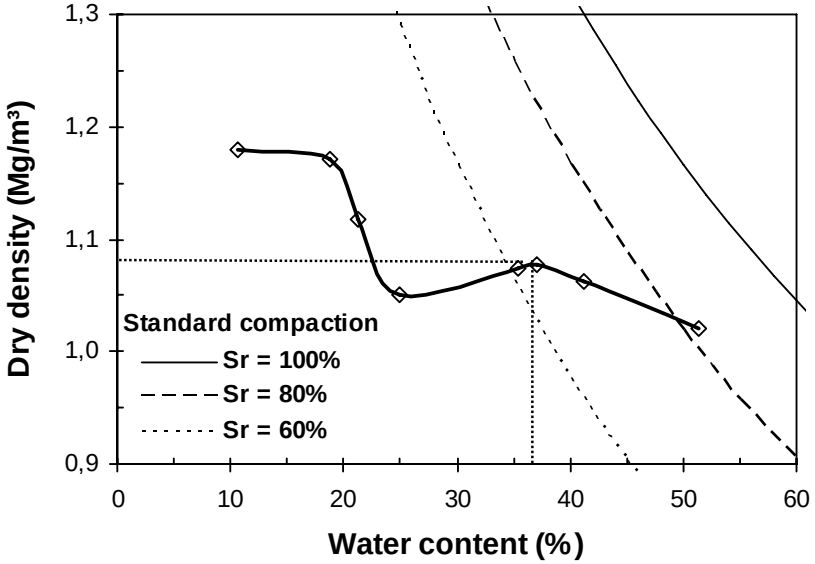


Figure 4.5 Compaction curve for MX-80 bentonite via standard Proctor method

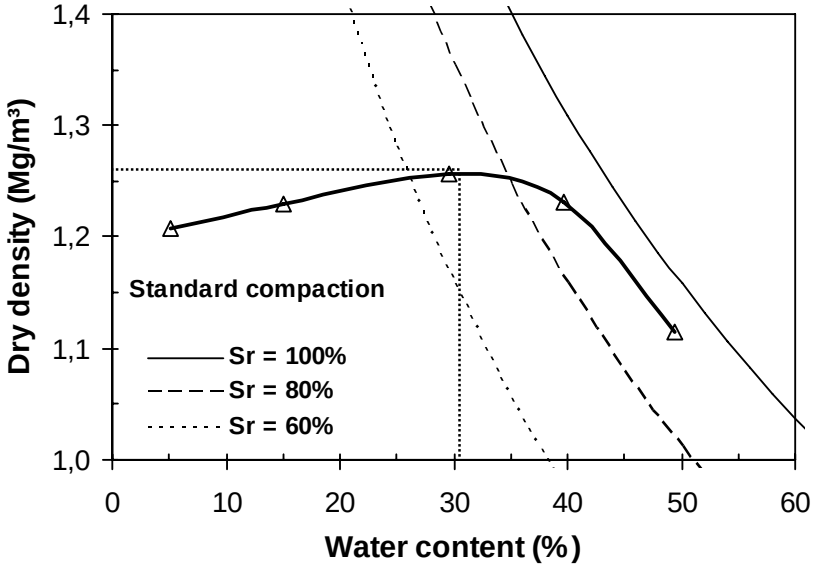


Figure 4.6 Compaction curve for Kunigel bentonite via standard Proctor method

## 4.5 Physico-chemical characteristics

The physical chemical and mineralogical characteristics of the bentonite are of concern since it has been known that the bentonite behavior such as compressibility, swelling behavior, hydraulic conductivity, etc are controlled by its physical chemical and mineralogical properties. The physical chemical and mineralogical determinations of bentonite used in this study included determination of specific surface area (SSA), cation exchange capacity (CEC), and mineralogical and chemical compositions.

### 4.5.1 Specific surface area

The specific surface area (SSA) is the surface area of the soil particles measured in $m^2/g$. It is also a strong indicator of the retention and sorption capacity of clays. The SSA was determined using the ethylene glycol monoethyl ether (EGME) adsorption method (Eltantawy and Arnold 1973, Carter et al. 1986, Hashm 1999, Cerato and Lutenegger 2002, Yukselen and Kaya 2006). EGME is a harmful substance and could be absorbed by body, so the SSA experiment is conducted in the closed cupboard. Following EGME method is used to determine the specific surface area:

1- 1 g of an oven dried soil sample was weighed and placed in an aluminum tare. The sample was then placed in a sealed vacuum desiccator over silica gel in order to dry the sample to a constant mass. The weighing of the soil sample was repeated every hour until a constant mass was attained. The mass of soil was measured using an electronic analytical balance with an accuracy of 0.0001 g.

2- Approximately 3 ml EGME was added to the soil sample until all the soil particles were completely covered and the mixture was allowed to equilibrate in the desiccator for 1 hour in the fume cupboard.

3- Afterwards the silica gel was removed from the desiccator and replaced with a solvate of about 120 g of calcium chloride ($CaCl_2$) and EGME. This solvate was prepared by 100 g of hot anhydrous $CaCl_2$ oven dried (100 $^oC$) for 1 hour and mixed with 20 ml EGME thoroughly in a cupboard. The solvate was allowed to cool and then placed in the base of the desiccator.

4- The aluminum tare containing soil plus EGME slurry was again placed in the desiccator. The aluminum tare was covered with another aluminum tare with some gap between them to prevent disturbance caused by the application of a vacuum. The desiccator was evacuated with a vacuum pump for 1 hour and the slurry allowed equilibrating for another hour. The slurry was again weighed using electronic analytical balance. This is repeated until a constant mass was achieved.

5- The amount of EGME to cover 1 $m^2$ of surface of clay particles with a monolayer is 2.86 x $10^{-4}$ g. Therefore, the SSA of the soil can be calculated by the following equation:

$$SSA\left(m^2/g\right)=\frac{\text{Mass of EGME retained}\left(g\right)}{\text{Mass of dry soil}\left(g\right)\times 2.86\times 10^{-4}} \tag{4.3}$$

The SSA of the Calcigel, MX-80 and Kunigel bentonites are shown in Table 4.1.

### 4.5.2 Cations exchange capacity

In order to investigate the chemical composition of the studied bentonites, the samples were tested in Federal Institute for Geosciences and Natural Resources (BRG) Hannover. Cation Exchange Capacity (CEC) is the quantity of exchangeable cations held

by the soil which is a measure of the positively charged ions that could be held on the negatively charged sites on soil minerals (Yong et al. 2001). It is generally equal to the amount of negative charge and expressed as milliequivalent per 100 g of soil (meq/100g). Cations can be classified as either acidic (acid- forming) or basic. The common acidic cations are hydrogen and aluminium and the basic ones are calcium, magnesium, potassium and sodium. The relative proportion of the acidic cation and the base cation on the exchange sites determines a soil's pH. CEC is sometimes also termed as the Base Exchange capacity when the basic cations are measured only. The ammonium acetate exchange method (Hesse 1971, Lavkulich 1981, Hashm 1999) was used to measure the four basic cations sodium, potassium, calcium and magnesium and the procedure can be summarized as follows:

**Extractable cations**

Ammonium acetate reagent is used to extract cations because ammonium ion replaces all the cations present in the soil. The following procedure is carried out to determine extractable cations.

1- 40 ml of ammonium acetate ($CH_3C00NH_4$) reagent was taken into a 50 ml polypropylene centrifuge tube. The reagent is prepared by adding 57 ml of concentrated acetic acid ($CH_3C00H$) to 700 ml of deionised water in a cupboard. Then 68 ml of concentrated ammonium hydroxide ($NH_4OH$) is added to the solution and finally made up to 1 liter. The pH value of the solution was required to be 7 which are achieved by adding acetic acid when the pH is higher than this value and ammonium acetate when it was lower.

2- A 2 g sample of dry soil was accurately weighed and added slowly into the ammonium acetate reagent in the polypropylene centrifuge tube.

3- The centrifuge tubes were placed on an end over end (tumbling) rotating agitator at 30 rpm for 23 hours.

4- The sample was then centrifuged at 3000 rpm for 5 minutes. The solid part precipitated and the clear supernatant decanted into another 50 ml.

5- The supernatant in centrifuge tube filter was then again centrifuged. The samples were centrifuged at 3000 rpm for 5 minutes and most of the supernatant filtered through and collected at the bottom of filtered centrifuge tube.

6- 1 ml filtered solution from the filtered centrifuge tube was then transferred into conical tubes. 1 ml of 10 % $HNO_3$ (10 ml $HNO_3$ and 90 ml deionised water) and 8 ml of deionised water was added into conical tubes and gave the solution of ratio 1:10. Preservation of the samples for longer time (up to180 days) requires that sample should be acidified to pH < 1.5 with $HNO_3$.

7- The samples in conical tubes were then analyzed by induced coupled plasma mass spectrometer (ICP-MS) for basic cations sodium ($Na^{+}$), potassium ($K^{+}$), calcium ($Ca^{+2}$) and magnesium ($Mg^{+2}$).

8- The ICP-MS gives the amount of extractable cations in mg/l which is converted into meq/l00g using the equation below:

$$\text{Ex.cation}\left(\text{meq}/100\text{g}\right)=\frac{\text{Cation}\left(\text{mg/l}\right)\times\text{Amonium acetate}\left(\text{l}\right)\times 100}{\text{Equivalent weight of cation}\times\text{Mass of soil}\left(\text{g}\right)} \qquad (4.4)$$

Here, the mass of soil is 2 g and the volume of ammonium acetate is 0.04 l (40 ml).

**Soluble cations**

The soluble amount of cations was found by adopting similar procedure mentioned above for extractable cations but deionised water was used instead of ammonium acetate reagent.

**Exchangeable cation**

The amount of exchangeable cations was calculated by subtracting the amount of soluble cations from the amount of extractable cations. The amount of exchangeable cations represents the CEC.

The total cation exchange capacity and basic exchangeable cation results are tabulated in Tables 4.1 for the three studied bentonites with the comparison from data from literature.

### 4.5.3 Mineralogy and chemical composition

The mineralogy of studied clays was investigated using X-ray diffraction (XRD) method. X-ray diffraction (XRD) is a non-destructive analytical technique to identify and quantify minerals in crystalline compounds within in a mixture or a pure phase. The results obtained from the XRD test are compound or mineral name opposed to element name determined by other analytical methods. The samples analyzed with the XRD are solid and crystalline with a regular 3D distribution of atoms occupying a space with a particular arrangement to form a series of parallel planes or lattices which are separated from each other by distances *d* or d-spacings. The XRD identifies minerals by relating the angle of incidence of the X-rays to the d-spacings according to Bragg's law. The Bragg's law states, when a monochromatic X-ray beam with a known wavelength (λ) is incident on the lattice plane in a crystal at an angle (θ) causes diffraction when the distance (d) travelled by the rays reflected from successive planes differs by a complete number (n) of wavelengths. It can be written in an equation form as:

$$n\lambda = 2d\sin\theta \tag{4.5}$$

By varying the angle (θ) the condition for Bragg's law is satisfied by different d-spacings within the crystalline structure. The different angular positions and intensities are then plotted and the plot is called diffractogram which is a fingerprint to identify the unknown mineral phase.

The XRD results for the three bentonites are shown in Figure 4.7. The predominant clay minerals of Calcigel bentonite are nontronite which is smectite family. Muscovite which is known as common mica is present. Quartz mineral which is a continuous framework of silicon oxygen tetrahedra with each oxygen being shared between two tetrahedra. Albite which is one of the plagioclase feldspars is present. The XRD result for MX-80 bentonite shows montmorillonite, quartz and cristobalite minerals. The mineral cristobalite is a high temperature polymorph of silica, meaning that it is composed of the same chemistry, $SiO_2$, but has a different structure. Both quartz and cristobalite are polymorphs with all the members of the quartz group. The Kunigel bentonite consists of clay minerals i.e., beidellite, which is smectite group, and quartz mineral. Calcite is a carbonate mineral and the most stable polymorph of calcium carbonate ($CaCO_3$). The other polymorphs are the minerals aragonite which changes to calcite at high temperature. Clinoptilolite mineral

present in Kunigel bentonite is a natural zeolite comprising a micro porous arrangement of silica and alumina tetrahedra.

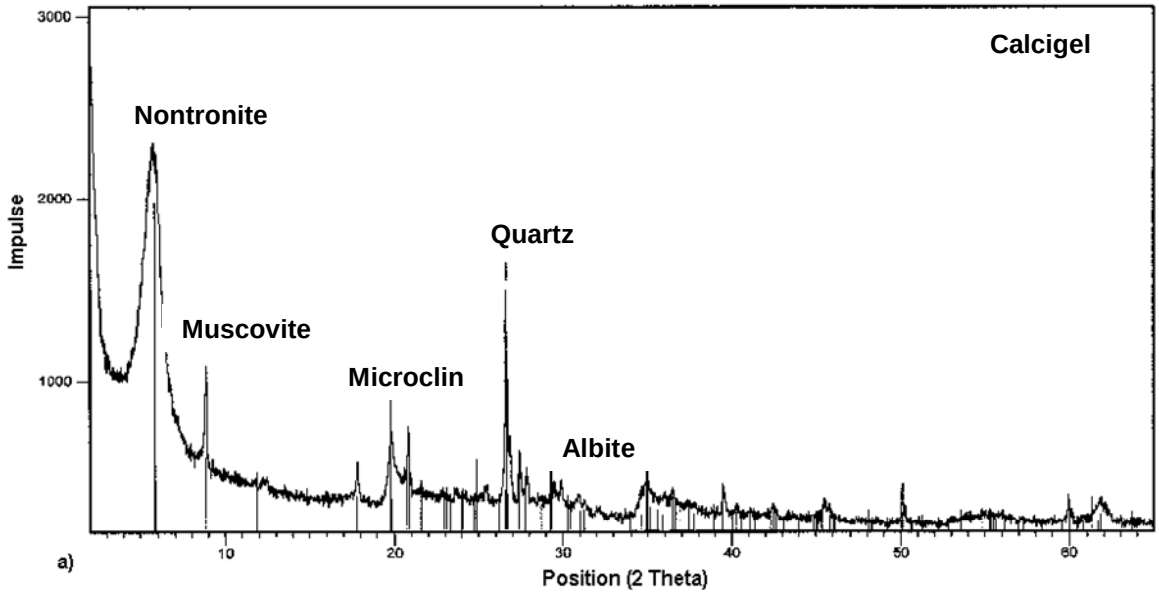


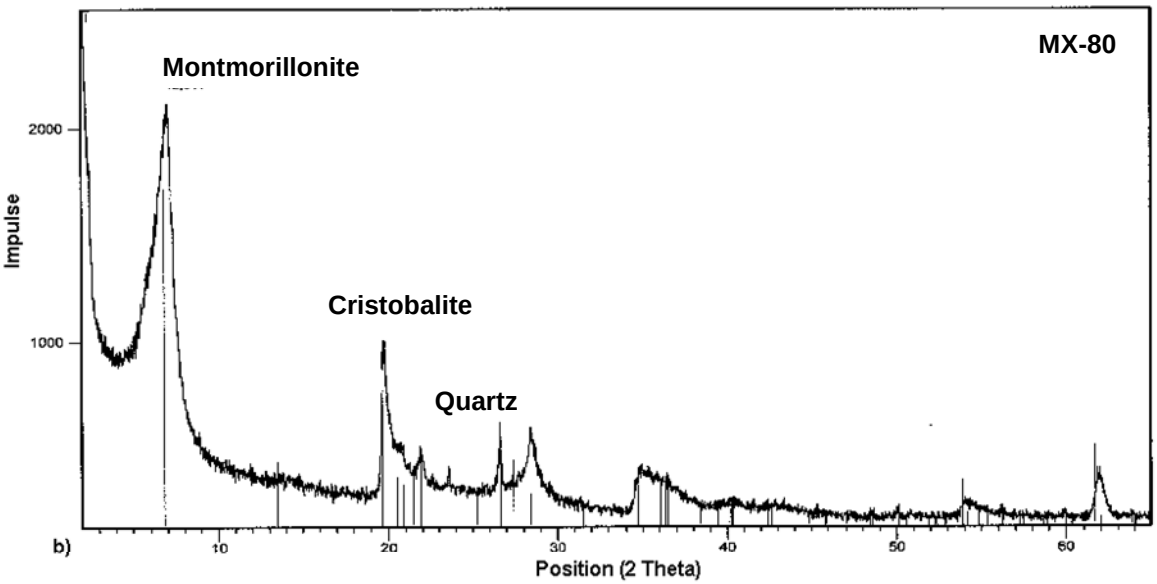

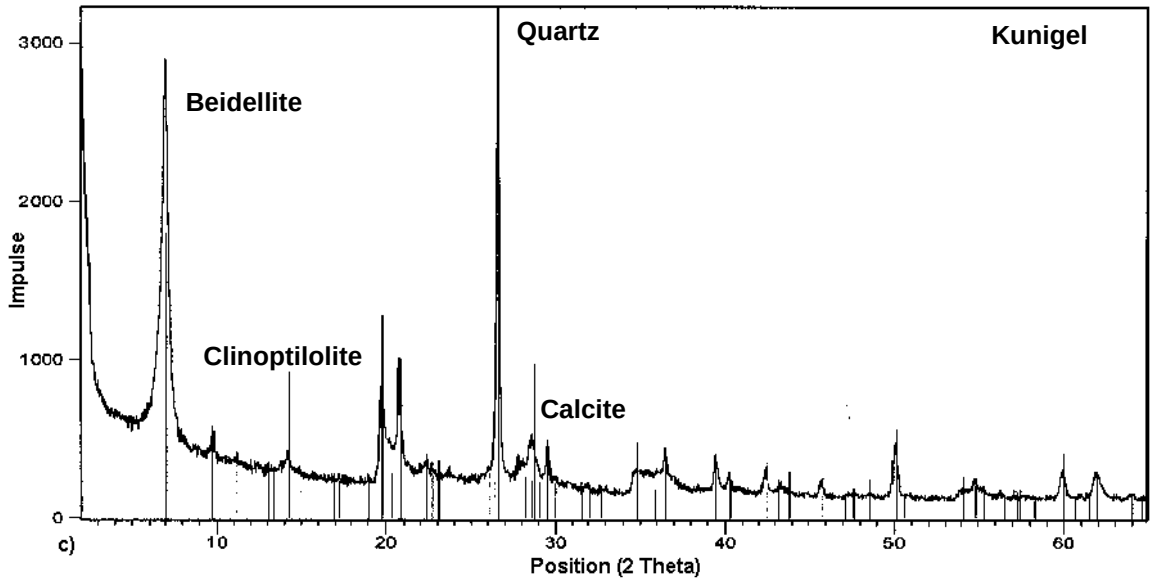


Figure 4.7 XRD results for a) Calcigel b) MX-80 and c) Kunigel bentonites

The chemical composition of bentonites studied was determined using emission spectroscopy method. The result is summarized in Table 4.2.

## 4.6 Summary of the material

Table 4.1 summarizes characteristics of clays used in this study and comparison with reported data from literature.

Table 4.1 Summary of properties of the clays studied

| Properties | Bentonites Calcigel | MX-80 | Kunigel |
|---|---|---|---|
| Specific gravity, G | 2.72 | 2.80 | 2.75 |
| Specific gravity from literature | 2.8* | 2.76[-] | 2.79[+] |
| Liquid limit, (%) | 110 | 490 | 405 |
| Liquid limit from literature | 180* | 411[-] | 473[+] |
| Plastic limit, (%) | 39 | 48 | 35 |
| Plastic limit from literature | 124* | 374[-] | 26.6[+] |
| Specific surface area, ($m^2/g$) | 525 | 711 | 430 |
| Specific surface area from literature | 526* | 562[-] | 388[+] |
| Basic exchangeable cation $Na^+$, $K^+$, $Ca^{2+}$, $Mg^{2+}$ (meq/100g) | 2,1,35,19 | 64,2,19,6 | 61,0,2,1 |
| BEC (meq/100g) from literature | 3,2,50,19* | 62,0.2,7,3[-] | - |
| Total cation exchange capacity (meq/100g) | 57 | 91 | 64 |
| Total CEC (meq/100g) from literature | 74* | 73[-] | 76[+] |
| Weighted average valency | 1.95 | 1.27 | 1.05 |
| Weighted average valency from literature | 1.93* | 1.14[-] | 1.50[+] |
| Hygroscopic water content (%) | 9.0 | 10.5 | 6.2 |
| Hygroscopic water content from literature | 9.2* | 10.8[-] | 6.5[+] |

* Date from Baille et al. (2010)
- Data from Müller-Vonmoos and Kahr (1982)
+ Data from Komine and Ogata (1996)

Table 4.2 Chemical composition of the clays studied (BGR Hannover)

| | Chemical | $SiO_2$ | $TiO_2$ | $Al_2O_3$ | $Fe_2O_3$ | MgO | CaO | $Na_2O$ | $K_2O$ | LOI |
|---|---|---|---|---|---|---|---|---|---|---|
| Present study | Calcigel | 53 | 0 | 17 | 5 | 3 | 2 | 0 | 2 | 17 |
| | MX-80 | 57 | 0 | 19 | 4 | 2 | 1 | 2 | 0 | 14 |
| | Kunigel | 66 | 0 | 13 | 2 | 2 | 2 | 2 | 0 | 11 |
| Agus (2005) | Calcigel | 53.2 | 0.32 | 18.4 | 5.4 | 3.8 | 3.6 | 0.74 | 1.7 | - |
| Pusch (2001) | MX-80 | 61 | - | 22 | 3 | 1 | 0.6 | 1 | 2 | - |

## 4.7 Experimental program

The experimental program consists of the determination of swelling pressure and saturated hydraulic conductivity of three types of bentonites (i .e., Calcigel, MX-80 and Kunigel bentonites). Both the tests were conducted in laboratory. The choice of these bentonites is based on the fact that they have been used extensively in many research programmes. The clays contain monovalent as well as divalent cations (Table 4.1). Calcigel bentonite contains predominantly divalent cations (see section 4.2). MX-80 bentonite contains primarily monovalent cations as well as divalent cations, whereas, Kunigel bentonite has monovalent cations.

Several placement conditions corresponding to different initial dry densities and initial water contents were chosen for each bentonite. The choice of the dry density and water content primarily based on the commonly adopted placement conditions dealt in many nuclear waste disposal repositories. The initial water content was varied to examine the effects on hydro-mechanical characteristic of the clays. Moreover, the high initial water content of the compacted specimens at each selected dry density was considered, so as to obtain near saturation conditions.

Swelling pressure tests followed by the hydraulic conductivity tests were carried out in the newly fabricated high pressure constant volume cells (see details in Chapter 5). Two types of permeant (i.e., distilled water having molal concentration of approximately ($10^{-4}$M) and high concentration solution ($10^{-2}$M)) are chosen for the swelling pressure and hydraulic conductivity tests. Only low initial water content specimens were tested on high concentration solution.

During the swelling pressure tests fluid were supplied to the compacted specimens without any additional injection pressure, whereas different constant heads (i.e., fluid injection pressure) were maintained during the hydraulic conductivity tests. Volume pressure controllers (VPC) were used for this purpose (see details in Chapter 5). The following Table 4.3 shows the initial condition and summary of the experimental program.

Table 4.3 Initial condition of specimens and summary of the experimental program

| Nr | Clay type | Test name | Dry density[a] ($Mg/m^3$) | Water content (%) | Void ratio[a] (e) | Permeant (M) | Injection pressure[b] (kPa) |
|---|---|---|---|---|---|---|---|
| 1 | Calcigel | Ca-B1 | 1.4 (1.37) | 9.0 | 0.94 (0.98) | $10^{-4}$ | 100 - 1000 |
| 2 | | Ca-B2 | 1.6 (1.56) | 9.0 | 0.70 (0.74) | $10^{-4}$ | 100 - 1000 |
| 3 | | Ca-B3 | 1.8 (1.75) | 9.0 | 0.51 (0.55) | $10^{-4}$ | 100 - 1000 |
| 4 | | Ca-B4 | 1.4 (1.37) | 34.5 | 0.94 (0.98) | $10^{-4}$ | 100 - 1000 |
| 5 | | Ca-B5 | 1.6 (1.56) | 25.7 | 0.70 (0.74) | $10^{-4}$ | 100 - 1000 |
| 6 | | Ca-B6 | 1.8 (1.75) | 18.8 | 0.51 (0.98) | $10^{-4}$ | 100 - 1000 |
| 7 | MX-80 | Mx-B7 | 1.4 (1.37) | 10.5 | 1.00 (1.04) | $10^{-4}$ | 100 - 1000 |
| 8 | | Mx-B8 | 1.6 (1.56) | 10.5 | 0.75 (0.79) | $10^{-4}$ | 100 - 1000 |
| 9 | | Mx-B9 | 1.8 (1.75) | 10.5 | 0.55 (0.60) | $10^{-4}$ | 100 - 1000 |
| 10 | | Mx-B10 | 1.4 (1.37) | 35.7 | 1.00 (1.04) | $10^{-4}$ | 100 - 1000 |
| 11 | | Mx-B11 | 1.6 (1.56) | 26.8 | 0.75 (0.79) | $10^{-4}$ | 100 - 1000 |
| 12 | | Mx-B12 | 1.8 (1.75) | 19.6 | 0.55 (0.60) | $10^{-4}$ | 100 - 1000 |
| 13 | Kunigel | Ku-B13 | 1.4 (1.39) | 6.2 | 0.96 (0.98) | $10^{-4}$ | 100 - 1000 |
| 14 | | Ku-B14 | 1.6 (1.57) | 6.2 | 0.72 (0.75) | $10^{-4}$ | 100 - 1000 |
| 15 | | Ku-B15 | 1.8 (1.75) | 6.2 | 0.53 (0.57) | $10^{-4}$ | 100 - 1000 |
| 16 | | Ku-B16 | 1.4 (1.39) | 34.9 | 0.96 (0.98) | $10^{-4}$ | 100 - 1000 |
| 17 | | Ku-B17 | 1.6 (1.57) | 26.1 | 0.72 (0.75) | $10^{-4}$ | 100 - 1000 |
| 18 | | Ku-B18 | 1.8 (1.75) | 19.3 | 0.53 (0.57) | $10^{-4}$ | 100 - 1000 |
| 19 | Calcigel | Ca-B19 | 1.4 (1.37) | 9.0 | 0.94 (0.98) | $10^{-2}$ | 100 - 1000 |
| 20 | | Ca-B20 | 1.6 (1.56) | 9.0 | 0.70 (0.74) | $10^{-2}$ | 100 - 1000 |
| 21 | | Ca-B21 | 1.8 (1.75) | 9.0 | 0.51 (0.55) | $10^{-2}$ | 100 - 1000 |
| 22 | MX-80 | Mx-B22 | 1.4 (1.37) | 10.5 | 1.00 (1.04) | $10^{-2}$ | 100 - 1000 |
| 23 | | Mx-B23 | 1.6 (1.56) | 10.5 | 0.75 (0.79) | $10^{-2}$ | 100 - 1000 |
| 24 | | Mx-B24 | 1.8 (1.75) | 10.5 | 0.55 (0.60) | $10^{-2}$ | 100 - 1000 |
| 25 | Kunigel | Ku-B25 | 1.4 (1.39) | 6.2 | 0.96 (0.98) | $10^{-2}$ | 100 - 1000 |
| 26 | | Ku-B26 | 1.6 (1.57) | 6.2 | 0.72 (0.75) | $10^{-2}$ | 100 - 1000 |
| 27 | | Ku-B27 | 1.8 (1.75) | 6.2 | 0.53 (0.57) | $10^{-2}$ | 100 - 1000 |

**Note:** Distilled water ($10^{-4}$M) and $10^{-2}$M (NaCl solution)

[a] Values shown in brackets correspond to corrected dry densities and void ratios after swelling pressure tests.

[b] The choice of the injection pressure depend upon the initial placement conditions of the specimens.

## 4.8 Summary

In this chapter three types of clays selected for the present research have been characterized successfully by determining their various properties including physical and chemical properties. A summary of physical and chemical properties of selected clays are presented in tables 4.1 and 4.2, respectively. The determination techniques of the properties of the clays used have also been detailed. The determined values are consistent with other reported observations of various researchers. The detailed experimental program with the initial placement conditions for the three types of clays are presented in Table 4.3.

# Chapter 5

# EXPERIMENTAL EQUIPMENTS, DESIGN AND METHODOLOGY

## 5.1 Introduction

This chapter describes the design and construction of the new devices to facilitate swelling and hydraulic conductivity tests which is the main objective of the present research work. Different devices available for measurement of hydraulic conductivity and their limitations are discussed. The chapter presents the necessity of new experimental devices to be built to carry out the tests mentioned in the experimental program in section 4.7. The design criteria to be met for the construction of new devices are discussed. Furthermore, the chapter gives description of new devices, and its various components. The calibration of the new devices and its working limits is covered. Experimental methodology developed to carry out the tests is discussed. It details the procedure and techniques employed for sample preparation and to determine swelling pressure and hydraulic conductivity.

## 5.2 Available devices and their limitation

Conductivity test devices range in forms as well as applied conditions during testing. During conductivity testing on an unsaturated swelling clay soil, changes in gravimetric water content, density, saturation, and suction are anticipated. This makes the choice of device extremely important as well as hydraulic conditions applied during tests. Type of devices include constant volume devices (Dixon et al. 1999) that allow no change in total volume, as well as oedometric type apparatuses that provide one-dimensional volume change in the direction of flow. Investigations into the anisotropy of hydraulic conductivity have also been performed in a rigid cell (Leroueil et al. 1990). In these devices all stress states are not explicitly measured and assumptions must be made. Devices which allow deformation include flexible membrane apparatuses as well as zero

stress devices (Rolland et al. 2005) which apply flow into specimens or monitor drainage out of specimens.

The devices and techniques described in the literature (Dixon 1995) can fall into the following four general categories:

i) rigid-walled, constant volume device with either, a constant hydraulic head (gradient), or a falling hydraulic head.

ii) rigid-walled, constant volume device with a fixed flow rate.

iii) flexible walled device, where the specimen volume is controlled by adjusting confining pressure and applying a predetermined hydraulic gradient.

iv) rigid-walled consolidation device, where consolidating specimens are tested using either a fixed or falling hydraulic gradients.

In rigid wall constant volume device, the specimen tested is rigidly confined to ensure volume change does not occur. Specimens are typically rigidly confined in a cylindrical sleeve with filters on the ends to ensure uniform wetting and drainage paths. The ends are also rigidly constrained and rigid filter stones are fitted to provide uniform wetting and drainage surfaces. In most relatively high hydraulic conductivity materials this technique provides a quick and consistent means of determining hydraulic conductivity. The ability to accurately monitor flow through specimens may be influenced by specimen size, and the influence of scale is typically associated with the possibility of higher flow rates along the soil permeameter wall interface i.e., preferential flow. There are also reports of potential volumetric straining as the result of applying back pressure to rigid wall systems (Pane et al. 1982, Edil and Erikson 1985). It should be noted that these observations were for low activity clay materials at intermediate densities. Swelling clays should not have these limitations, any channels opened as the result of wall irregularities or applied pore pressures would rapidly hydrate and swell to block such channels. Such clays are basically self-sealing. The ultimate flow rates measured for specimens originally having intentionally induced gaps, fissures or voids were found to be equivalent to those of initially intact specimens (Dixon et al. 1993b). The rigid wall constant volume device with either constant head or falling head method is shown in Figure 3.4, and the procedure is explained in section 3.4.2.

In rigid wall constant volume fixed flow rate device, a metering pump is used to inject water at a constant quantity per unit time. This flow rate (flux) is maintained, regardless of the pressure gradient developed across the specimen and can be measured using pore pressure transducers mounted at each end of the specimen. Alternatively, a differential pressure transducer can be used to measure the pressure difference across the specimen. This technique has a number of advantages to the other rigid walled testing techniques since it does not require any special displacement gauges or fluid reservoirs. Hence, the constant rate of flow device has fewer connections, less tubing and a lower number of potential sources of leakage. Dixon (1995) discussed the main limitation of this technique is development of hydraulic gradient during constant flow rate especially for low hydraulic conductivity clays (< $10^{-12}$ m/s). If the specimen cross section is to be increased, still the gradient attained would be well above the field conditions and limits the usefulness of this technique in studying the flow through materials of very low hydraulic conductivity. A schematic of this type of device is presented in Figure 5.1.

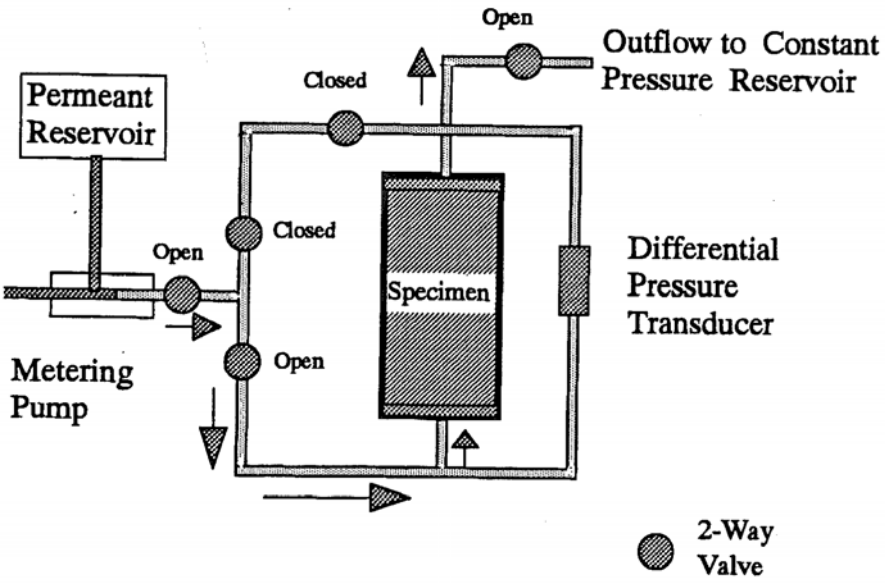


Figure 5.1 Rigid wall constant volume fixed flow rate design (from Dixon 1995)

Flexible walled device have been used for a number of years commonly in association with triaxial compression testing of materials. The equipment used is the same as that used in confined, drained triaxial tests, excepting that the top and bottom drainage reservoirs are

separate and held at different pressures. This induces a hydraulic gradient across the specimen and the flow rate across the specimen can be monitored using traditional displacement gauges. This technique has been used successfully in relatively short duration conductivity tests on materials of moderate to low hydraulic conductivity ($10^{-6}$ to $10^{-10}$ m/s) (Edil and Erickson 1985, Haug and Wong 1992, Haug and Sauer 1993).

Agus et al. (2003) described the development of a flexible wall permeameter device for measuring the coefficients of permeability of residual soils. Water and air coefficients of permeability were obtained for both the drying and wetting cycles for residual soils using the flexible wall permeameter. Volume changes of the soil specimens during unsaturated consolidation and during the water and air permeability measurements were monitored. The developed flexible wall permeameter was found to be capable of measuring water and air coefficients of permeability as low as $10^{-12}$ m/s. However, such devices have not been used for very long term testing of high swelling capacity specimens with very low hydraulic conductivity. The advantages, disadvantages and limitations of this type of device are discussed in considerable detail by a large number of researchers including, Olsen and Daniel (1981), Tavenas et al. (1983), Daniel et al. (1984, 1985), Olsen et al. (1985), Boynton and Daniel (1985), Bowders (1987) and Haug and Wong (1992). Most of these researchers prefer the use of a flexible walled device, but Daniel et al. (1985), Edil and Erikson (1985), Bowders (1987) and Peirce et al. (1987b) found that the results obtained using a flexible walled device are essentially the same as those obtained from a rigid walled device. At high hydraulic gradients the flexible walled device was preferred to the rigid walled since water channeling between the specimen and the cell wall was seen as a potential mechanism which could affect flow. The general setup for a flexible walled device is presented in Figure 5.2.

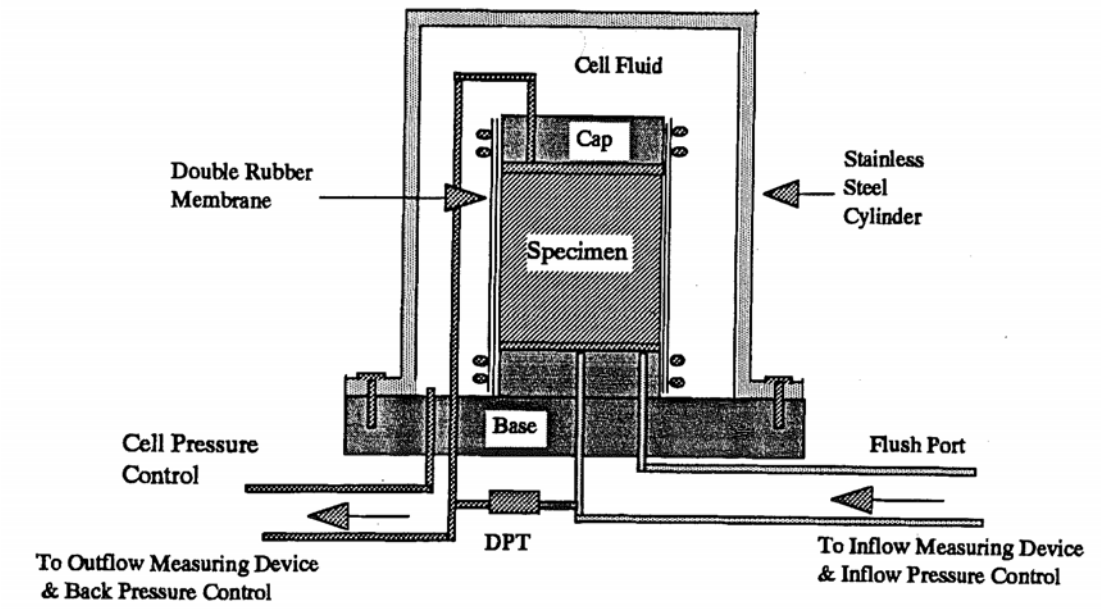


Figure 5.2 Basic design of Flexible walled device (from Dixon 1995)

The flexible walled device has some limitations in its application to testing very low conductivity materials, particularly in terms of potential sources of leakage (Tavenas et al. 1983). Membranes are not completely impermeable and so for long duration tests, diffusion into or out of the specimen can become significant. Membranes are also subject to chemical attack or mechanical failure if left for long time periods. There is an additional complication in using this technique for bentonite materials, the cell must be able to provide the 1 MPa to 2 MPa confining pressure needed to prevent specimen swelling (clay densities > 1.3 $Mg/m^3$ would require even higher confining pressures). This means that testing of bentonites would require special triaxial cells capable of providing high pressure confinement. The permeant reservoirs for these systems must also be pressurized and capable of maintaining a small pressure gradient across the specimen.

Rigid walled consolidation cell, in which consolidation testing is still widely used to obtain a measure of the hydraulic conductivity of a soil. This technique was presented by Terzaghi and Peck (1976) as one which could use the measured rate of clay compression, and hence the drainage rate, to calculate hydraulic conductivity. This procedure uses specimen strains to calculate flow, and so is not appropriate for use in determining the mass transport properties under low hydraulic gradients. Straining of the soil skeleton

during the consolidation process violates one of the basic requirements of Darcy's law that the soil fabric not change during the testing process. As a result, this technique is not appropriate for use in examining the performance of swelling clays under conditions of low applied hydraulic gradient.

## 5.3 Need for the new experimental device

The majority of literature dealing with measurement of hydraulic conductivity in clay soils focuses on materials of low swelling capacity and relatively high hydraulic conductivity. For these materials it is generally accepted that either rigid-walled or flexible-wall devices will produce comparable results (Daniel et al. 1985, Edil and Erikson 1985 and Pierce et al. 1987a). The final consideration in the process of selecting the most appropriate type of device for use in this project was the nature of the materials and range of dry density being investigated. The swelling clays examined in this research program contain a considerable fraction of montmorillonite. Additionally, the low hydraulic conductivity for these materials had already been established ($k < 10^{-12}$ m/s), and as a result the time required to complete each test was about 3 to 4 months. A flexible walled system therefore contained a larger number of potential sources of time dependent leakage or failure owing to the membranes used to confine the specimen.

A rigid walled system is simple to construct and contained a lower number of potential sources of mechanical failure. A newly designed rigid walled constant volume device was selected and constructed. A system of stainless steel cells, complete with stainless steel tubing was designed and built for use in present research program. Such systems provide the best combination of ability to resist the high swelling behaviour and aggressive nature of the high concentration pore fluid, while maintaining a nearly constant hydraulic gradient across the specimen. The description of devices used in this research program is outlined in section 5.5.

## 5.4 Design criteria of the devices

The experimental devices had to be designed to satisfy the following criteria so that the measurements of key parameters outlined in section 4.7 could be accomplished:

1- The clay sample can be compacted directly into the cell ring to avoid the air gap between the sample and the ring wall. The direct compaction of clay sample into the cell ring ensures the desire density and void ratio remains constant throughout the tests.

2- The cell has to be sufficiently strong to withstand any hydraulic or swelling pressures developed during a test.

3- The cell can be connected to data acquisition device to measure the swelling pressure throughout the tests.

4- The clay sample can be removed intact from the cell to allow sampling of water content, dry density and chemical concentration if needed.

5- The cell must be hydraulically sealed and no or minimum leakage for long tests duration.

6- The valves, fittings, and pressure lines should be high pressure resistant.

7- The cell must be both robust and easy to handle, assemble and dismantle.

8- The device needs to be compatible with existing auxiliary equipment required for this laboratory testing program.

9- The cell can be used for future research in hydraulic, mechanical and chemical studies of soils with minimal modifications.

10- The water injection device can measure very small volume of water induced by imposed hydraulic gradient and should maintain the pressure gradient.

11- The water injection device can apply a wide range of pressure gradient.

12- The device can apply no or high back pressures to the cell during saturation stage.

## 5.5 Description of the devices

To meet the testing requirements outlined in section 5.4, special high pressure constant volume cells, and a specialized volume pressure controller (VPC) that enables maintaining predetermined constant fluid injection pressure at the base of the specimens during hydraulic conductivity tests were fabricated and constructed. All the tubing and non-glass materials used in the system were stainless steel. This was to limit the effects of high concentration pore fluid, to limit tubing strain due to pressure and to prevent water diffusion through the walls of the tubing. The steel tubing allows very high back pressures or gradients to be applied to the specimens without concern for system leakage or failure. The following subsections give the description of the devices.

### 5.5.1 Constant volume high pressure cell

The constant volume high pressure cell is designed to calculate the swelling pressure and hydraulic conductivity of bentonites used in this research. The cell consisted of mainly two parts. Following section describe the material and components of the cell.

***Material***

An austenitic stainless steel of grade V2A (Stainless steel DIN 1.4541 AISI 321 specification) was used to make the main components of the high pressure cell. Type V2A stainless steel is low carbon molybdenum bearing steel. It is more resistant to corrosion and pitting especially in chloride rich environments than conventional nickel chromium austenitic stainless steels such as 302 - 304. It also has excellent machining, forming, cutting and welding characteristics with good rupture and tensile strength under high temperature.

***Top section***

The top section of the cell consists of a top cap, piston and load cell. The top cap carries a piston which is in turn attached with a load cell. The top part contains inlet and outlet lines. The top section has two primary functions, firstly, to measure the swelling pressure development during saturation of soil sample and secondly, the top inlet and outlet lines for measuring the outflow fluid volume during hydraulic conductivity tests. The top lines are also used for flushing and de airing during the test. The top lines are

connected with the porous plate and a water reservoir. The O-ring is used to avoid the leakage from the top part of the cell. The top and the bottom parts of the device are connected with the help of heavy screws.

***Bottom section***

The bottom section of the constant volume cell contains inlet and outlet lines for saturating the soil sample during swelling pressure tests and for applying constant fluid pressures during hydraulic conductivity tests. A thick stainless steel base at the bottom houses a stainless steel porous plate and a bottom water chamber. The bottom part also holds a thick walled ring of height 20 mm and diameter 50 mm that in turn accommodates a compacted soil sample. The wall of the ring has very low friction that helps easier sample extrusion at the end of the tests. Around the porous plate, steel base has a slot to take O-ring, which ensures the water tightness of the cell at bottom section. The O-ring was always slightly greased to seal the cell before start of the tests. The sketch of the new high pressure cell with detailed itemized components and a photograph view are shown in Figure 5.3.

***Summary of the cell specification and working limits***

| | |
|---|---|
| Cell construction: | Stainless steel V2A |
| Piston: | Stainless steel V2A |

***Ring size***

| | |
|---|---|
| Diameter: | 50 mm |
| Height: | 20 mm |
| Load cell: | 45 MPa |
| Max. Cell pressure: | 20 MPa |
| Total weight: | 9.5 kg |

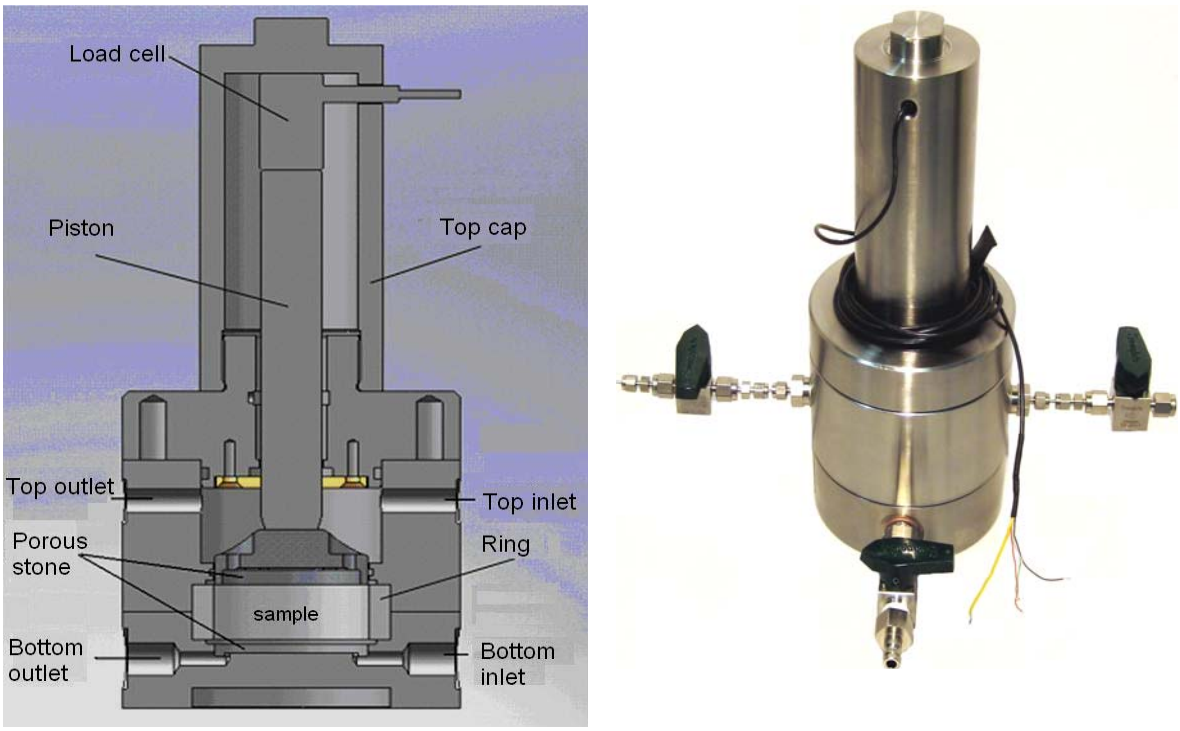


Figure 5.3 New constant volume high pressure device (sketch and photograph view)


Figure 5.4 Individual components of constant volume device

### 5.5.2 Volume pressure controller

The volume pressure controller (VPC) consists of a solid pressure cylinder with integrated spindle drive for the generation of water injection pressure up to 100 bar (10 MPa). An electronic pressure measuring sensor is integrated in the device for controlling the pressure and volume. The volume pressure controller works according to the electro-mechanic principle. The device consists of pressure cylinder which can be filled with the fluid of volume 250 ml. The pressure piston inside the cylinder moves by a precision stepping drive. Distilled water and low concentrated electrolytes can be pressurized using the device. During the hydraulic conductivity tests, the saturated bentonite specimens were subjected to constant fluid injection pressure that enabled the tests to be carried out under various hydraulic gradients. The volume pressure controller with labelled components is shown in Figure 5.5.

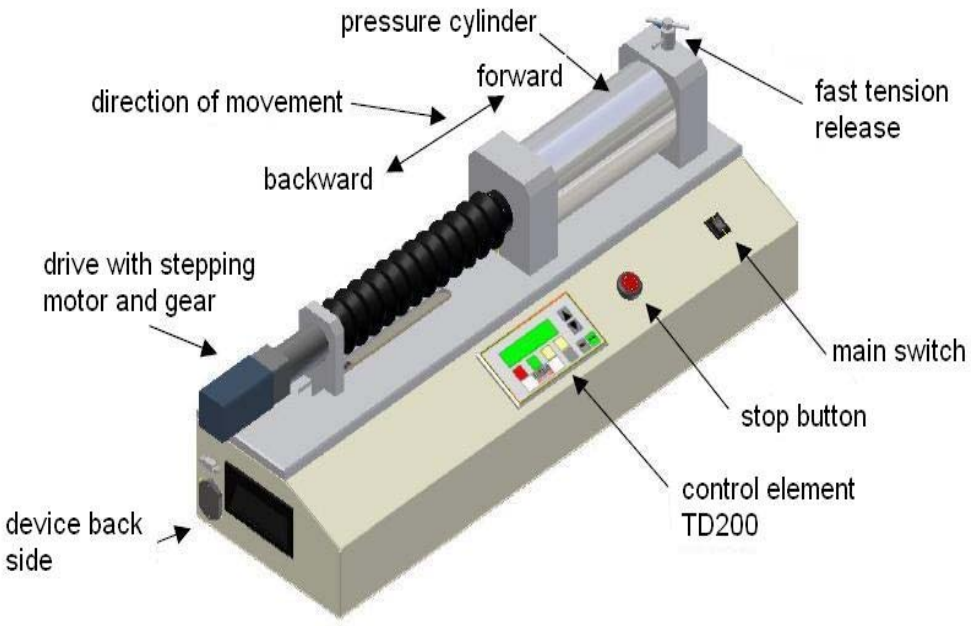


Figure 5.5 Volume Pressure Controller for fluid injection pressure

## 5.6 Calibration of the devices

Whenever a new device is designed and fabricated, the first step is to test its integrity and calibrate it. The following subsection outlines the calibration of the devices.

### 5.6.1 Constant volume high pressure cell

To enable the new device to be used accurately in testing, it was calibrated for the volume change due to the application of water pressure. The strength of cell was tested under fluid pressure of 10 MPa to ensure the safety of the operator and equipment. The procedure adopted for the calibration is given below:

Initially the cell was filled with distilled water in the presence of a dummy metal sample. The pressure-expansion characteristic of the cell was studied. Hydraulic pressure was applied step-wise up to a pressure of 10 MPa using the volume pressure controller (VPC) device and the corresponding immediate volume change was recorded. The expansion of the pipes of VPC was subtracted from the cell expansion. Based on the pressure-expansion characteristics of the cell, the dry density of the compacted specimens was corrected at the end of the each test. Figure 5.6 shows the calibration of the volume change of the cell.

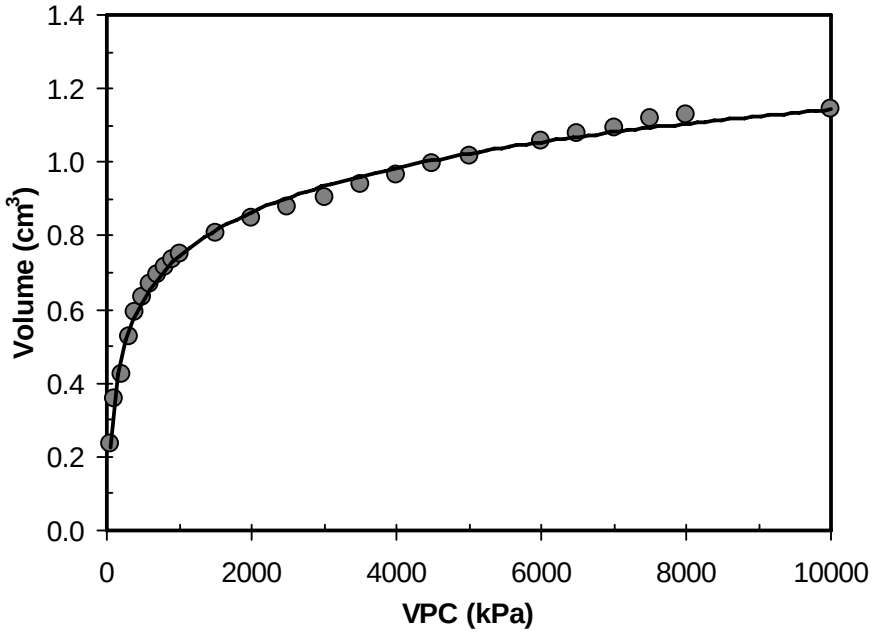


Figure 5.6 Calibration of the cell with volume pressure controller

***Load cell calibration***

Load cell calibration was done against two devices namely, volume pressure controller (VPC) and in high compression loading frame.

***Load cell versus VPC***

Calibration of load cell with VPC was achieved with same procedure as stated in section 5.6.1. The response of the load cell due to applied water pressure was determined by filling the cell with distilled water in the presence of a dummy metal sample. Hydraulic pressure was applied step wise using the VPC and the corresponding response of the load cell was recorded. The relationship between the load cell (kPa) and the volume pressure controller (kPa) is shown in Figure 5.7. The calibration best fitting line has the following equation:

$$Lc = 1.056 \times vpc - 13.21 \tag{5.1}$$

where: *Lc* represents the load cell reading (kPa) and *vpc* is applied hydraulic pressure from VPC (kPa).

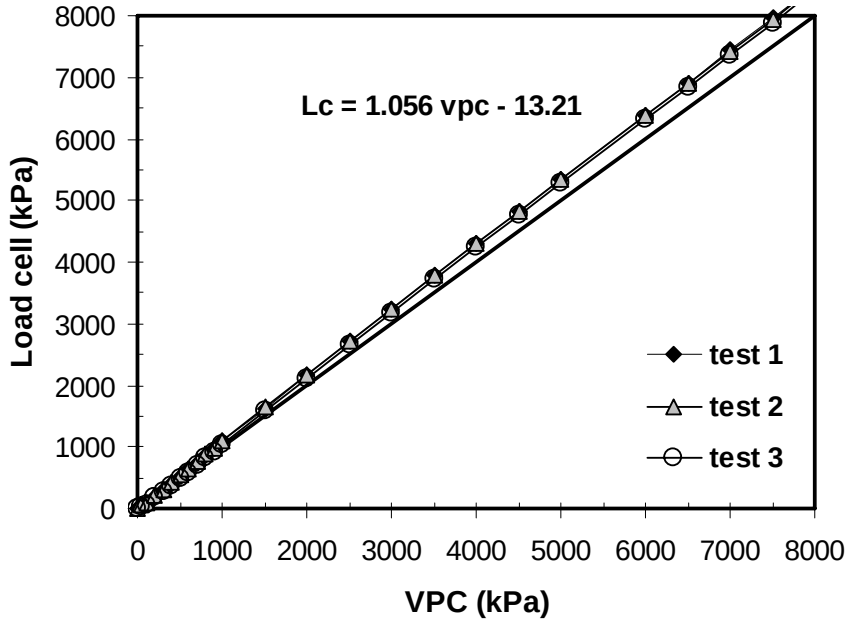


Figure 5.7 Calibration of the load cell with volume pressure controller

***Load cell versus high compression loading frame***

The load cell was verified by installing it in the loading compression machine. The vertical pressures were applied by the compression machine and check the response of the load cell. Figure 5.8 shows the calibration of the load cell with high pressure compression machine.

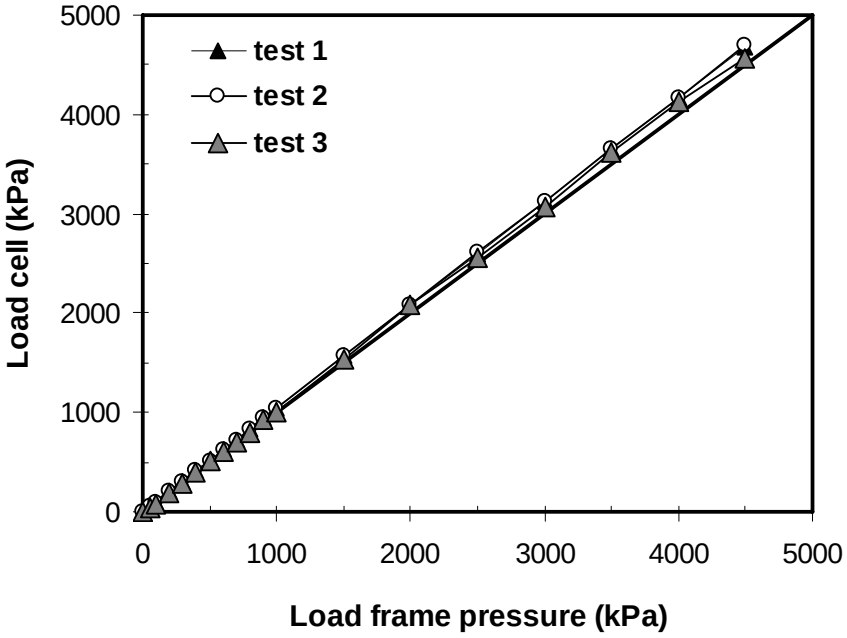


Figure 5.8 Calibration of load cell with high pressure loading machine

### 5.6.2 Volume pressure controller

Volume pressure controller (VPC) device which has been used for constant fluid injection pressure, before starting the tests, the device has been verified with the pressure meter i.e., manometer. The manometer device was connected with the VPC. The step wise increment of the fluid pressure in the VPC was applied and note down the readings of the manometer. The maximum fluid pressure applied could be 1000 kPa due to the limitation of the manometer. The relationship between the manometer (kPa) and VPC (kPa) is shown in Figure 5.9. Both the devices were in good agreement with the pressures applied by manometer and volume pressure controller.

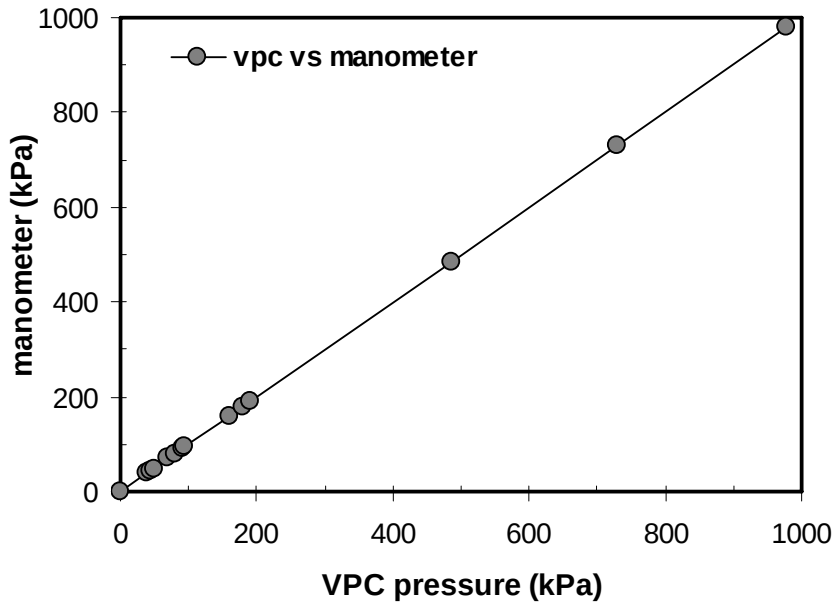


Figure 5.9 Calibration of load cell with manometer device

## 5.7 Methodology develop

An experimental methodology was developed to carry out experiments efficiently. The following sections discuss the important steps including sample preparation, swelling pressure and hydraulic conductivity determination.

### 5.7.1 Sample preparation

The total of 27 tests have been done as shown in Table 4.3 for three selected type of bentonite clays. All the clay specimens were composed of 100 % bentonite. In 27 sets of tests for swelling pressure and hydraulic conductivity, 9 tests were conducted on specimen with hygroscopic water content (low initial water content) and 9 tests were carried out on saturated water content (high water content) specimens. Distilled water was used for preparing the samples and for swelling pressure and hydraulic conductivity tests. The remaining 9 tests have been done with high concentration solution as permeant in swelling pressure and conductivity tests. Only low initial water content specimens were tested on high concentration solution.

Bentonite specimens were prepared at various predetermined dry densities and initial water content. Specimens of diameter 50 mm and height 20 mm were prepared by static compaction method by directly compacting bentonite-water mixtures in the specimen ring to overcome preferential flow along the soil-cell interface. The specimens in compaction machine were compacted in 4 layers into the cell ring, and each layer was compressed under static load. For high or saturated initial water content specimens, the predetermined amount of water (Table 4.3) depending upon the dry density was added to the specimens and mixed daily for about one week to ensure homogenous mixture and water distribution.

### 5.7.2 Method to achieve specimen saturation

Preparation of specimens for hydraulic conductivity testing will almost inevitably result in the presence of entrapped air. Unless the specimen is actually formed from slurry and then installed in a cell submerged under water, some degree of air entrainment is unavoidable. As slurry preparation and submerged construction is impractical or inappropriate for most situations, especially in clays having a high swelling capacity (Dixon 1995). The most commonly method to achieve saturation is to form the specimen as close to saturation as is practical and then use water under pressure referred to a back pressuring, to force the remaining air into solution (Mitchell et al. 1965). Immediately following this back pressuring, a substantial hydraulic gradient is typically applied in an effort to circulate the dissolved air - water solution out of the specimen and replace it with pore fluid. Black and Lee (1973) described this approach in detail, including a discussion on the time required to accomplish this saturation. They provided a good review of the technique and discuss their attempt to develop a time-based criterion for defining specimen saturation. They concluded that saturation was potentially a slow process and it might be appropriate to accept some degree of unsaturation in testing rather than wait for "full" saturation to be achieved. This type of saturation process can be undertaken on any specimen, provided the specimen volume is kept constant.

There are certain limitations to use back pressuring technique to achieve specimen saturation. The application of pressure to the pore spaces of a specimen can lead to straining of the soil fabric as the pore fluid forces its way through the specimen and into entrapped air pockets. This may cause the generation of macro or micro channels which can allow easier water conduction through the specimen (Dixon 1995). The applied back pressure must be maintained for the duration of the test. Any reduction in back pressure

can lead to dissolved gases coming out of solution, creating new voids and can obstruct the fluid movement. Depressuring the specimen can also induce specimen strain as the pore volume increases.

Skempton (1954) and Lee et al. (1969) described test for saturating the specimen in triaxial or flexible walled permeameter. This test involves increasing the confining pressure on the specimen and monitoring the pore pressure response through the closed end drains in the specimen. The change in the total stress of the specimen should be exactly equal to the change in the water pressure. By applying large confining pressure can result in macroscopic or micro strains within the soil. Such strains could change the soil fabric, and hence the hydraulic behaviour of the specimen. The time required to saturate a specimen will vary with the amount of pore air present, the pressure applied, and the rate at which the pore water can enter the specimen to dissolve and remove the entrapped air (Braden and Sides 1967, Lee et al. 1969).

A similar method mentioned above can be conducted on specimen rigidly confined. An increase in the pore water pressure is made at one end of an undrained specimen and pore pressure transfer is monitored at a pore pressure transducer mounted on the other end of the specimen. The time required for the pore pressure change to equal the change in applied pore pressure provides a measure of how close the specimen is to full saturation. A specimen with air voids present should exhibit a slower rate of pressure transfer than a saturated material with its very low compressibility. The methods have the same basic limitations, they are subjective and they have the potential to induce specimen strain.

In the present research, the saturation of the specimens was achieved by installing the burette level with 5 – 10 kPa pressure. The procedure for saturating the specimens is outlined in following section 5.7.3.

### 5.7.3 Swelling pressure measurement

Swelling pressures of compacted bentonite specimens used in this research were measured under isochoric condition using the high pressure constant volume cell (Figure 5.3). Filter papers were used at the top and bottom of the specimens to prevent direct contact of the specimens with the porous plate and to avoid chocking of the porous plate. The specimen rings were lubricated prior to the specimen preparation to minimize the side friction. During the swelling pressure tests, fluid was supplied initially via the bottom inlet

of the cell. After about 4-5 days of hydration period, a burette was connected to the top inlet of the cell to supply fluid from top. The procedure adopted enabled releasing air from the initially unsaturated bentonite specimens during the hydration process and also was found to reduce the swelling pressure equilibration time. The reason for the reduction in swelling pressure equilibration time was that the migration of water in the specimen from one end may take longer duration depending upon the type of clay.

The full saturation of any tested specimens was confirmed based on the time-swelling pressure response. The time needed for the full saturation was found to depend on the dry density of the specimen and generally varied between 3–5 weeks. The final water contents of several compacted specimens tested were measured by oven drying method. The calculated degree of saturation of the specimens based on the corrected volumes (i.e., based on expansion of the cell) and the measured water contents clearly indicated that the specimens were fully saturated after the tests. Furthermore, the saturation was also confirmed when the swelling pressure development was equilibrated upon the water uptake. The water uptake and swelling pressure versus time relationships for the bentonites used in this study are shown in chapter 6 in more detail.

### 5.7.4 Hydraulic conductivity measurement

Hydraulic conductivity tests were carried out in a constant volume cell after the swelling pressures of the specimens were equilibrated. A digital water volume pressure controller (Figure 5.5) was connected to the bottom inlet of the cell to apply predetermined hydraulic gradients. The hydraulic gradient was varied between 250 and 3500. To achieve these gradients, fluid injection pressures of 100 kPa to 700 kPa were required. Figure 5.10 shows the schematic of the test setup used for measuring hydraulic conductivities of compacted bentonite specimens. The increase of fluid injection pressure to the next level was done once the outflow rate become constant and the steady state conditions have been achieved. The time required to establish the steady state condition for each gradient was about two weeks. The system was then allowed to attain the pressure and flow equilibrium condition until the final pressure selected was reached. The cumulative outflow volumes were measured using a burette connected at the top of the cell. Step-wise hydraulic gradient was applied based on the constant outflow rate. Hydraulic conductivity tests were carried out in a temperature controlled room with a temperature of 20 ± 0.5°C. Evaporation

loss was considered by installing a dummy burette. The hydraulic conductivity ($k$) was calculated using Equation (5.2):

$$k = \frac{q}{A}\frac{H_0}{P_{in} - P_{out}} = \frac{q}{Ai} \tag{5.2}$$

where: $q$ is the average volume outflow at unit time ($m^3/s$), $A$ is the cross-sectional area, $P_{in}$ is the water-pressure at bottom of specimen, $P_{out}$ is the water pressure at the top of the specimen, $H_0$ is the specimen height, and $i$ is the head loss or hydraulic gradient.

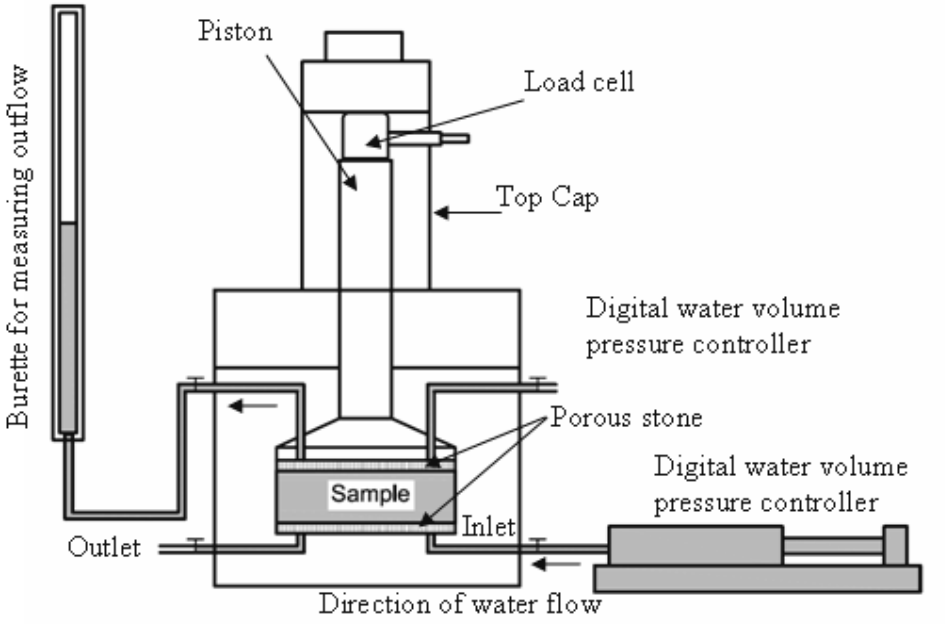


Figure 5.10 Schematic of the test setup for measuring hydraulic conductivity

To achieve the steady state flow, considerable effort has been expended in trying to define when saturation has been achieved (Section 5.7.2), and whether the flow through the specimen has achieved constant rate. Researchers such as Anderson (1982), Pierce and Witter (1986) have attempted to develop empirical techniques to define when steady state flow is reached. Pierce and Witter (1986) called for one to five pore volumes to be passed through the soil and constant hydraulic conductivity to be recorded before assuming specimen saturation is achieved. This type of criterion may be appropriate for the relatively high hydraulic conductivities they examined (approx. $10^{-6}$m/s). However, a material with

hydraulic conductivity of $10^{-13}$ m/s would require an unacceptably long time (4 - 5 months) to meet these requirements (Dixon 1995).

Techniques typically used to measure very low flow rates have been described by Dixon et al. (1987, 1992 a, b), Sri Ranjan and Karthigesu (1992), and Haug and Wong (1992). These techniques generally involve construction of nearly saturated specimens. The specimen was either percolated until enough fluid had been added to fill the air-filled pore spaces or, the specimen was back pressured to dissolve out any air. The specimens were then percolated until steady-state flow is achieved. There would also be an additional risk of inducing significant changes to the pore fluid chemistry as the result of such extensive flushing. Test conducted by (Dixon 1999) involved either monitoring of inflow only, or both inflow and outflow during hydraulic conductivity measurements. Monitoring continued until the flow into and out of the specimen was constant. If the inflow was the only displacement monitored, then percolation was continued until the flux was constant for an extended time period (more than 10 days).

## 5.8 Summary

This chapter has reported the successful design, fabrication and calibration of the new constant volume cells with each of the defined design criteria met. Furthermore, the volume pressure controller for water injection pressure in conjunction with the new cells. The new cell is capable of measuring the swelling pressure and hydraulic conductivity of highly plastic clays. It also facilitates the determination of moisture content, dry density at the end of the tests without damaging the soil sample. However, the working limits of the constant volume cells, for the load cell are 45 MPa and the maximum cell pressure sustained is 20 MPa.

The experimental methodology was developed and defined that includes the soil preparation, methods or techniques used to ensure the sample saturation and determination of hydro-mechanical behaviour of the compacted clays.

# Chapter 6

# EXPERIMENTAL RESULTS AND DISCUSSIONS

## 6.1 Introduction

This chapter presents the experimental results of the laboratory test program described in chapter 4. The aim of these tests is to investigate hydro-mechanical behaviour of three types of bentonite selected in this research. The aim of the test results to be used for a qualitative analysis of hydraulic behaviour of selected bentonites. The qualitative analysis to calculate the hydro-mechanical behaviour in clays will be undertaken in the chapter 7.

Results of water uptake and swelling pressure performed in newly designed constant volume device are presented. Effect of initial water content and high concentrated solution on swelling behaviour are shown and discussed. Similarly, after achieving the constant swelling pressure, the hydraulic conductivity tests results have been shown for distilled water (low and high initial water contents) as well as for high concentration solution. The results have been discussed in final section.

## 6.2 Swelling pressure results

In the following section, the results of swelling pressure are presented for the three types of bentonites described in section 4.2 and comparison with the swelling pressure results reported in literature. The series of tests were performed to obtain the swelling pressure of the bentonites. The method includes constant volume tests. The swelling pressure test results presented were analyzed by taking into account deformability of the swelling pressure measurement systems used. Other factors that might influence the results such as specimen-ring friction were not taken into account since the lubrication is assumed to be sufficient in minimizing the ring friction effects. Discussion on the experimental swelling pressure results have been carried out at section 6.3.

### 6.2.1 Calcigel bentonite

A series of constant volume swelling pressure tests was conducted on nine specimens of Calcigel bentonite (i.e., Ca-B1, Ca-B2, Ca-B3, Ca-B4, Ca-B5, Ca-B6, Ca-B19, Ca-B20, and Ca-B21). Among these specimens, three specimens (i.e., Ca-B1, Ca-B2, and Ca-B3) have low initial water content equal to 9.0 % and the other three specimens (i.e., Ca-B4, Ca-B5, and Ca-B6) have high initial water content equal to 34.6 %, 25.7 % and 18.8 %. The remaining three specimens (i.e., Ca-B19, Ca-B20, and Ca-B21) were tested against high concentration solution. The summary of the initial conditions of the specimens are tabulated in Table 4.3.

#### 6.2.1.1 Swelling pressure and water uptake with time

Figure 6.1 (a) and (b) shows, respectively, typical curves of swelling pressure and water uptake versus time plotted in semi-logarithmic scales. The increase in both the swelling pressure and amount of water uptake with time was rapid at the earlier stage of tests (i.e., up to around 2500 min). The rate of both swelling pressure development and amount of water uptake asymptotically decreases beyond a point which marks the end of primary swelling pressure development. However, the rate of swelling pressure development generally decreased with time after the maximum swelling pressure was attained.

As can be seen in Figure 6.1 (a), the swelling pressure development with elapsed time for specimens (Ca-B1, Ca-B2, Ca-B4 and Ca-B5) of Calcigel bentonite were found to be accompanied with two maxima. The first maxima during the saturation process occurred at about 2000 min followed by a decrease in the swelling pressure. Finally, the specimens attained equilibrium swelling pressures after about 35,000 min. For specimens (Ca-B3 and Ca-B6), the development of swelling pressure with elapsed time had single maxima until a maximum swelling pressure of about 10 MPa was reached in about 30,000 min. Discussion on the reason for the two maxima during swelling pressure development has been carried out in section 6.3.

The amount of water uptake is higher in specimen Ca-B1 than the specimen Ca-B2, whereas, specimen Ca-B2 takes more water than Ca-B3 (Figure 6.1b). The difference in the amount of water uptake is attributed to the difference in dry densities of specimens and initial degree of saturation at starting of the test.

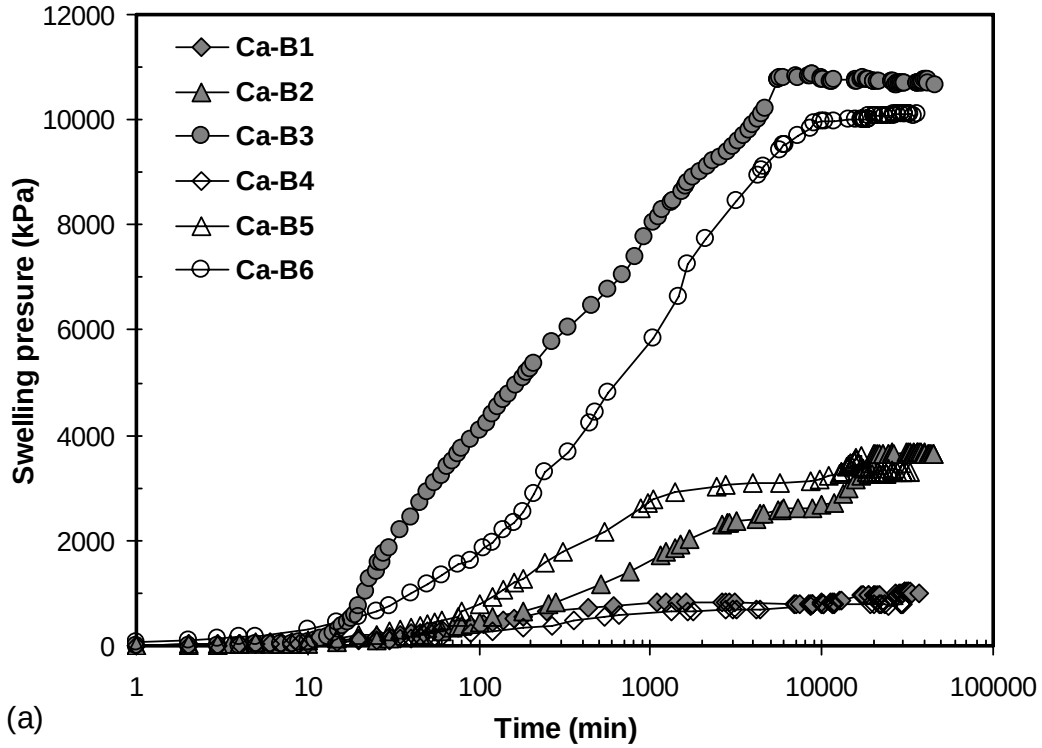


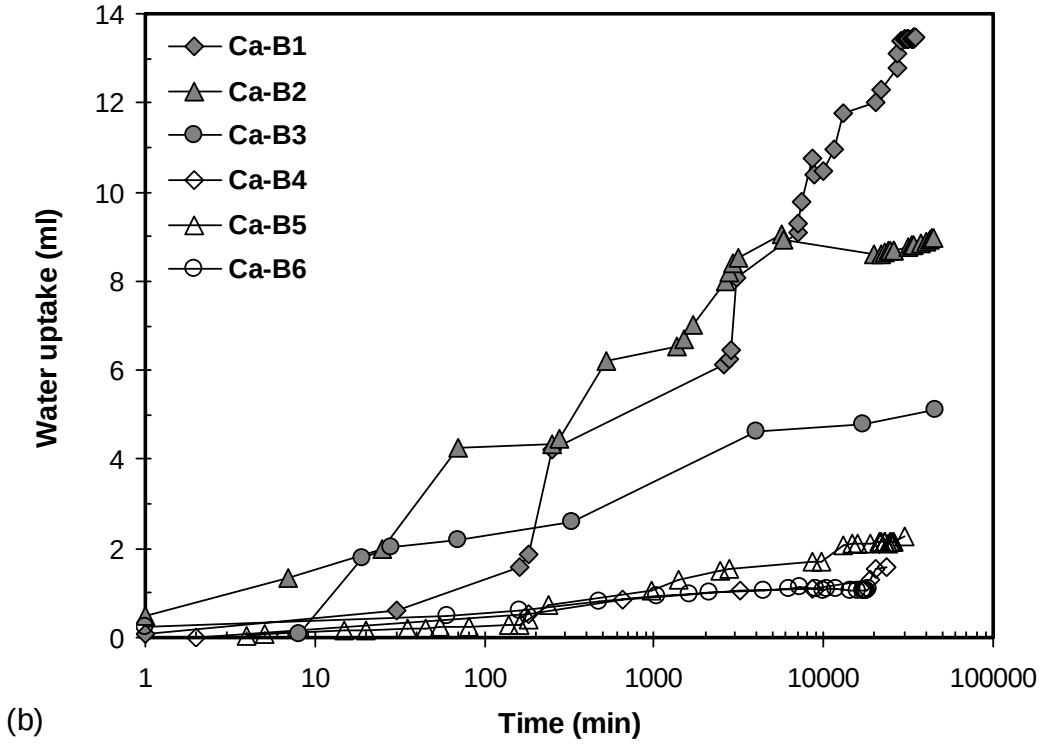


Figure 6.1 Development of constant volume swelling pressure of Calcigel bentonite (a) swelling pressure and (b) water uptake versus time

#### 6.2.1.2 Swelling pressure at low and high initial water content

Figure 6.2 shows the swelling pressure of the Calcigel bentonite plotted against the dry density. The dry density versus swelling pressure plot clearly shows that for specimens with the same initial water content, the swelling pressure increases with an increase in the dry density. As expected, the swelling pressure of the specimens show exponential function against dry density for both initial water content conditions. As depicted in the Figure 6.2, the curve of swelling pressures obtained for the specimens tested at high initial water content is located slightly below the curve of swelling pressure obtained for the specimens tested at low initial water content. Two distinct effects are noted when the initial water content is varied for Calcigel bentonite; at the same dry density, the swelling pressure decrease with an increase in the initial water content at low dry densities, whereas the initial water content practically has less influence on the swelling pressure of Calcigel bentonite. The experimental results of Calcigel bentonite for low initial water content and high initial water content indicates that the reduction ratio, *RR*, of swelling pressure in high initial water content is about 20 % for the dry density equal to 1.37 $Mg/m^3$ and the reduction ratio is about 2 % for the dry density equal to 1.56 $Mg/m^3$, whereas, the reduction ratio is about 7 % for the dry density equal to 1.75 $Mg/m^3$. Herein, the reduction ratio, *RR* (%), of swelling pressure in high initial water content to low initial water content is calculable using following equation:

$$RR = \frac{P_{LWC} - P_{HWC}}{P_{LWC}} \times 100 \tag{6.1}$$

where: $P_{LWC}$ is the maximum swelling pressure (kPa) at low initial water content and $P_{HWC}$ is maximum swelling pressure (kPa) in high initial water content.

Figure 6.3 shows the comparison of Calcigel bentonite from present study and swelling pressure results of other Calcigel bentonites from Schanz and Tripathy (2009) and Baille et al. (2010). The initial conditions of the reported Calcigel bentonite are shown in Table 7.1, and 7.2. As shown in Figure 6.3, the swelling pressure of Calcigel bentonites increases with increase of dry density and is in good agreement with the reported swelling pressure of Calcigel bentonites.

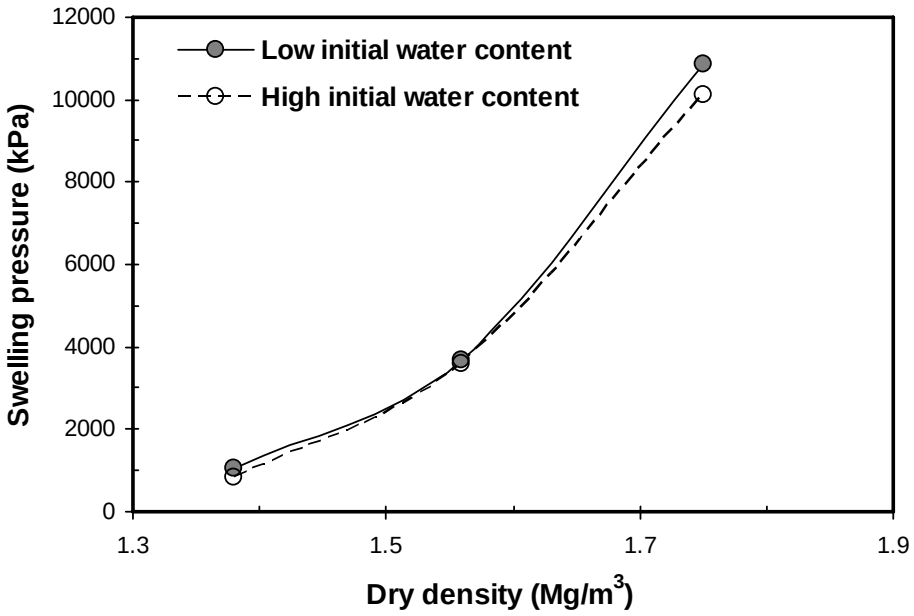


Figure 6.2 Swelling pressure as function of dry density for low and high initial water contents for Calcigel bentonite

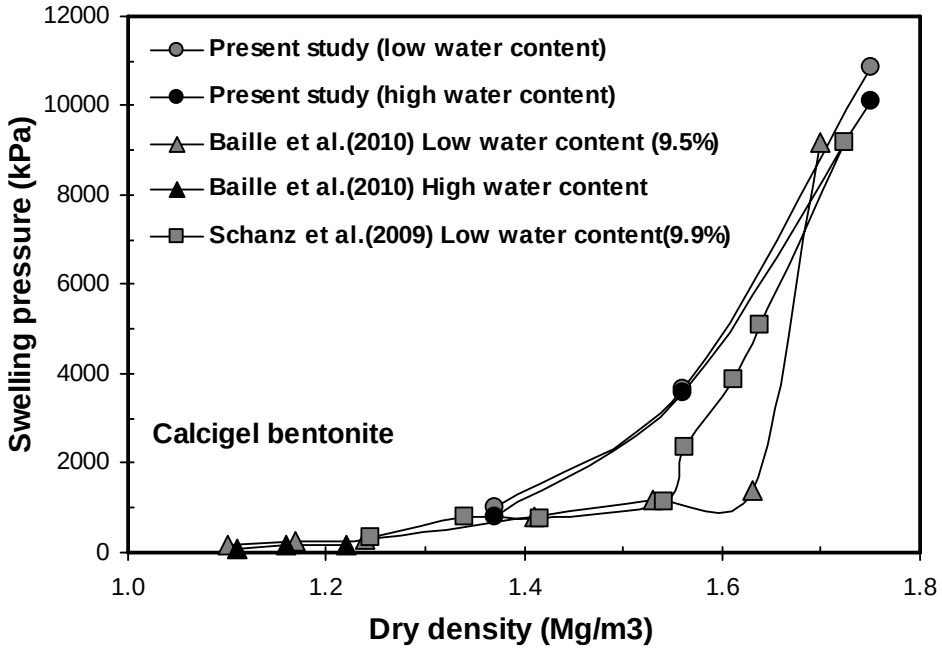


Figure 6.3 Comparison of swelling pressure versus dry density for Calcigel bentonites

### 6.2.1.3 Swelling pressure at distilled water and high concentration solution

Figure 6.4 shows the experimental results of the swelling pressure of the Calcigel bentonite specimens. The Figure shows the relationship between the swelling pressures which is exponentially increases against the dry density. The experimental results show that the swelling pressures obtained by permeating the specimen with distilled water ($10^{-4}$M) is slightly higher than the specimens permeated with high concentration ($10^{-2}$M) solution. Moreover, only a slight difference of swelling pressures is apparent between distilled water and high concentration conditions. The experimental results of Calcigel bentonite for distilled water ($10^{-4}$M) and high concentration solution ($10^{-2}$M) indicates that the reduction ratio, *RR*, of swelling pressure in high concentration solution is about 24 % for the dry density equal to 1.37 Mg/m$^3$ and the reduction ratio is about 7 % for the dry density equal to 1.56 Mg/m$^3$, whereas, the reduction ratio is about 18 % for the dry density equal to 1.75 Mg/m$^3$. Herein, the reduction ratio, *RR* (%), of swelling pressure in high concentration solution to distilled water is calculable using Equation 6.1.

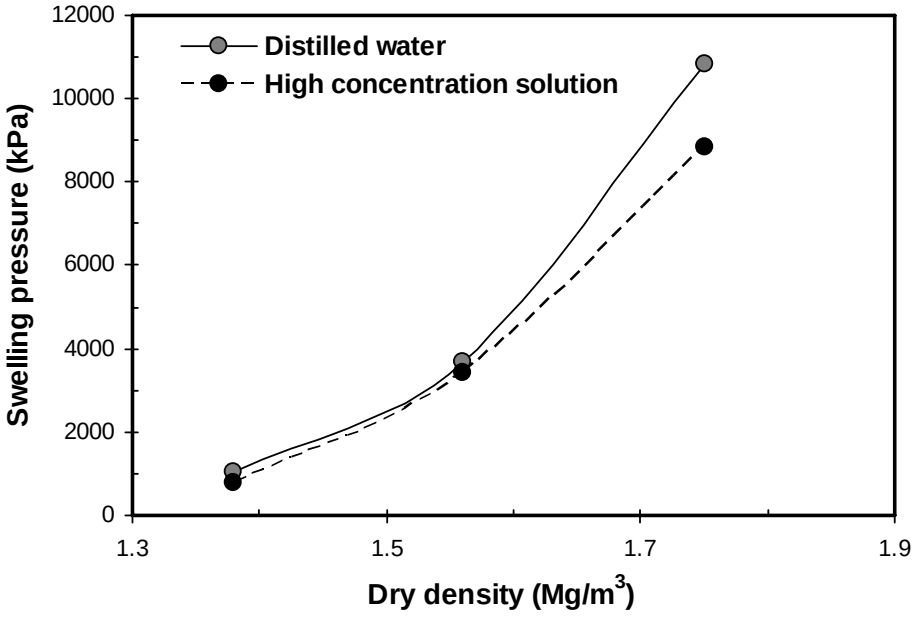


Figure 6.4 Swelling pressure as function of dry density for distilled water and high concentration solution for Calcigel bentonite

$$RR = \frac{P_{DW} - P_{HC}}{P_{DW}} \times 100 \quad (6.2)$$

where: $P_{DW}$ is the maximum swelling pressure (kPa) in distilled water and $P_{HC}$ is maximum swelling pressure (kPa) in high concentration solution.

### 6.2.2 MX-80 bentonite

Swelling pressure tests was conducted on nine specimens of MX-80 bentonite (i.e., Mx-B7, Mx-B8, Mx-B9, Mx-B10, Mx-B11, Mx-B12, Mx-B22, Mx-B23, and Mx-B24). Among these, three specimens (i.e., Mx-B7, Mx-B8, and Mx-B9) have low initial water content equal to 10.5 % and the other three specimens (i.e., Mx-B10, Mx-B11, and Mx-B12) have high initial water content equal to 35.7 %, 26.8 % and 19.6 %. The remaining three specimens (i.e., Mx-B10, Mx-B11, and Mx-B12) are tested against high concentration solution. The summary of the initial conditions of the specimens are tabulated in Table 4.3.

#### 6.2.2.1 Swelling pressure and water uptake with time

Typical curves of swelling pressure and water uptake versus time plotted in semi-logarithmic scales are shown in Figure 6.5 (a) and (b). The swelling pressure and water uptake is more at initial stage of the tests (i.e., up to around 3500 min in case of swelling pressure and water uptake around 6000 min). The swelling pressure development and amount of water uptake decreases beyond a point which marks the end of swelling pressure development.

Figure 6.5 (a) shows the swelling pressure development with elapsed time for specimens (Mx-B8, and Mx-B11) of MX-80 bentonite were found to be accompanied with two maxima. The first maxima during the saturation process occurred at about 6000 min followed by a slight decrease in the swelling pressure with specimen Mx-B8. The specimens Mx-B7 and Mx-B9 remain constant after 1st maxima. Finally, the specimens attained equilibrium swelling pressures after about 35,000 min. For specimens (Mx-B10, Mx-B11 and Mx-B12), the development of swelling pressure with elapsed time had single

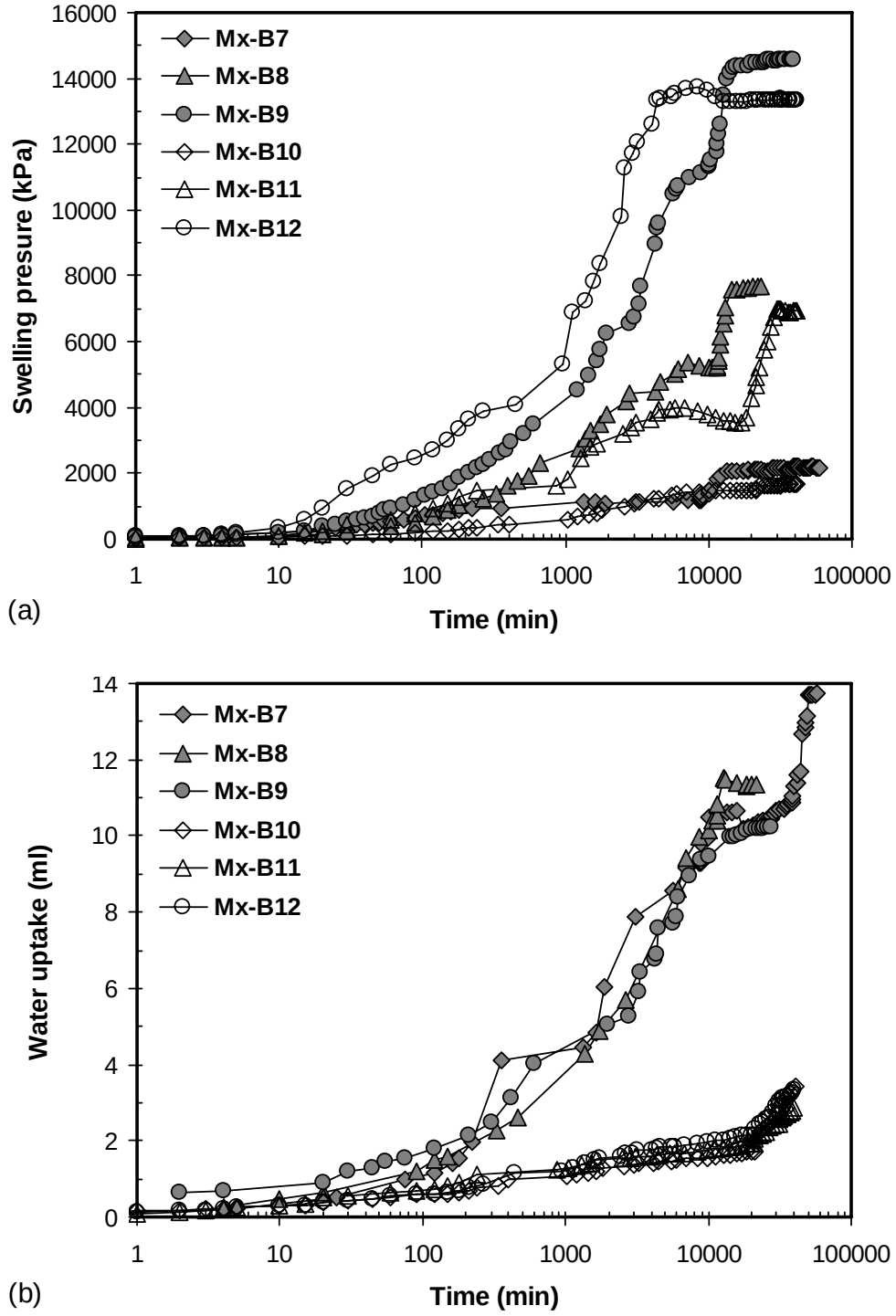


Figure 6.5 Development of constant volume swelling pressure of MX-80 bentonite (a) swelling pressure and (b) water uptake versus time

maxima until reached in about 6000 min, then there is little decrease in the swelling pressure. For specimen (Mx-B11), after 1st maxima, there is increase in swelling pressure till around 6990 kPa. For specimen (Mx-B12), slight decrease occurred in swelling pressure after attaining 1st maxima and then swelling pressure remain constant until 50,000 min. The phenomenon of two maxima during swelling pressure development has been carried out in section 6.3.

Figure 6.5 (b) shows the amount of water uptake of specimens (Mx-B7, Mx-B8, and Mx-B9) with more or less similar rate of water uptake till 10,000 min. After 10,000 min, the Mx-B7 specimen takes more amount of water due to low dry density or low degree of saturation. Similarly for specimens with higher degree of saturation i.e., Mx-B10, Mx-B11, and Mx-B12, the amount of water uptake is almost equal to 3ml.

#### 6.2.2.2 Swelling pressure at low and high initial water content

Figure 6.6 shows the swelling pressure of the MX-80 bentonite plotted against the dry density. The dry density versus swelling pressure plot clearly shows that for specimens with the same initial water content, the swelling pressure increases with an increase in the dry density. As expected, the swelling pressure of the specimens show exponential function against dry density for both initial water content conditions. As depicted in the figure, the curve of swelling pressures obtained for the specimens tested at high initial water content is located below the curve of swelling pressure obtained for the specimens tested at low initial water content. It was found that, at the same dry density, the swelling pressure decreased with an increase in the initial water content, whereas the initial water content practically had less influence on the swelling pressure of MX-80 bentonite. Such behaviour has been discussed in subsection 'influence of initial water content and dry density' under section 6.3. The experimental results of MX-80 bentonite for low initial water content and high initial water content indicates that the reduction ratio, *RR*, of swelling pressure in high initial water content is about 24 % for the dry density equal to 1.37 $Mg/m^3$ and the reduction ratio is about 9 % for the dry density equal to 1.56 $Mg/m^3$, whereas, the reduction ratio is about 6 % for the dry density equal to 1.75 $Mg/m^3$. Figure 6.7 shows the comparison between MX-80 bentonite of present study and swelling pressure results from Komine (2008, 2009). The initial conditions of the reported MX-80 bentonites are shown in Table 7.2. As shown in Figure 6.7, the swelling pressure of reported bentonites increases with increase of dry density and the swelling pressure of

MX-80 bentonite used in present study is higher than that of reported by Komine (2008, 2009).

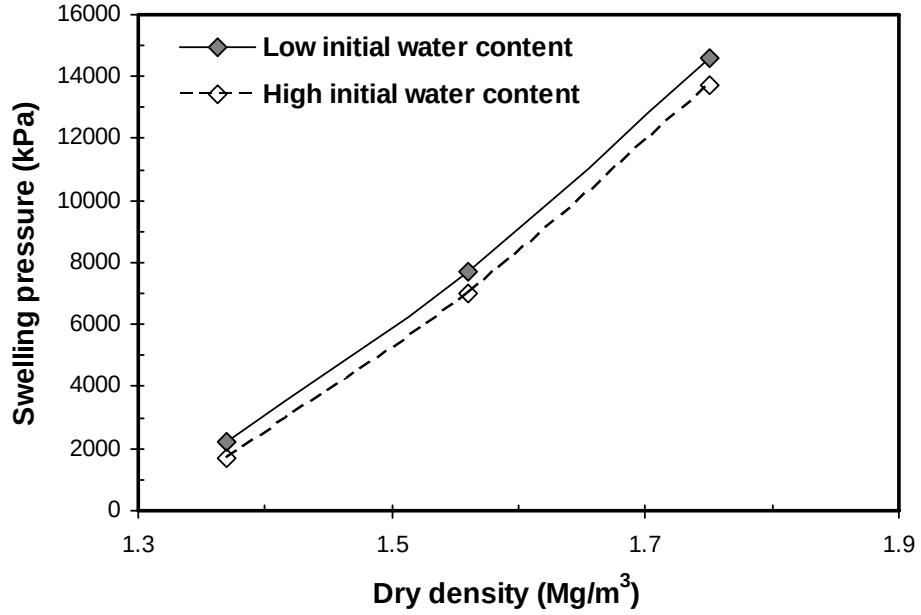


Figure 6.6 Swelling pressure as function of dry density for low and high initial water contents for MX-80 bentonite

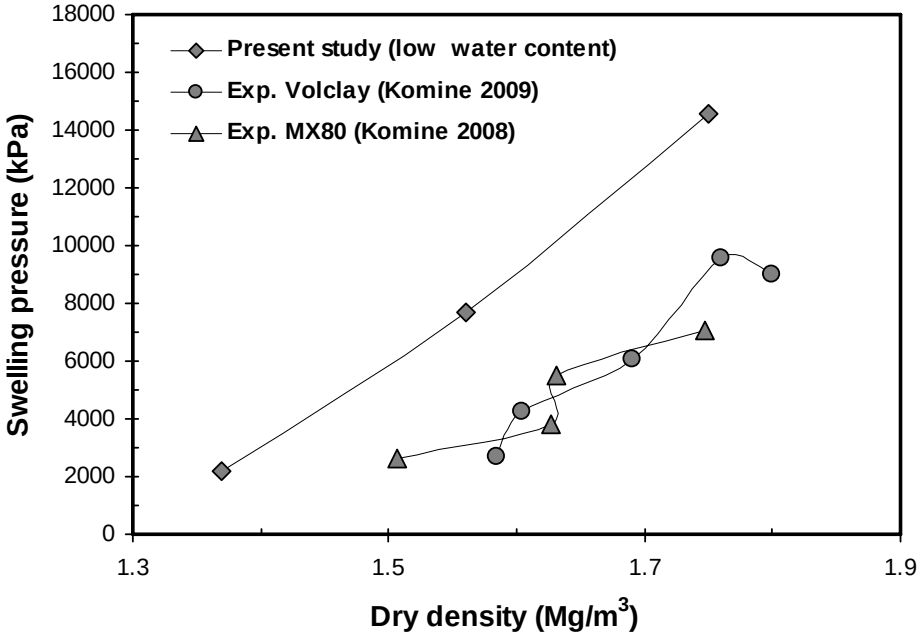


Figure 6.7 Comparison of swelling pressure versus dry density for MX-80 and Volclay bentonites

### 6.2.2.3 Swelling pressure at distilled water and high concentration solution

Figure 6.8 shows the experimental results of the swelling pressure of the MX-80 bentonite specimens against the dry density. The experimental results show that the swelling pressures obtained by permeating the specimen with distilled water ($10^{-4}$M) is slightly higher than the specimens permeated with high concentration ($10^{-2}$M) solution. Moreover, difference of swelling pressures is apparent between distilled water and high concentration conditions.

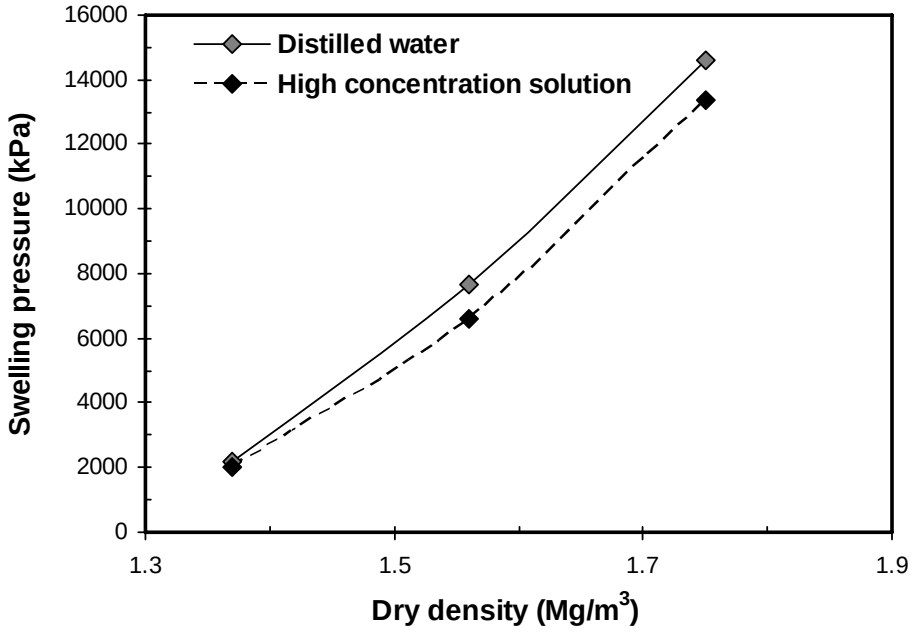


Figure 6.8 Swelling pressure as function of dry density for distilled water and high concentration solution for MX-80 bentonite

The experimental results of MX-80 bentonite for distilled water ($10^{-4}$M) and high concentration solution ($10^{-2}$M) indicate that the reduction ratio, *RR*, of swelling pressure in high concentration solution is about 8 % for the dry density equal to 1.37 Mg/m$^3$ and the reduction ratio is about 18 % for the dry density equal to 1.56 Mg/m$^3$, whereas, the reduction ratio is about 8 % for the dry density equal to 1.75 Mg/m$^3$. The reduction ratio, *RR* (%), of swelling pressure in high concentration solution to distilled water can be calculated using Equation 6.2. The decrease in swelling pressure due to increase in high concentration has been discussed in section 6.3 under subsection 'influence of pore fluid'.

### 6.2.3 Kunigel bentonite

Similarly in case of Kunigel bentonite, the constant volume swelling pressure tests was conducted on nine specimens (i.e., Ku-B13, Ku-B14, Ku-B15, Ku-B16, Ku-B17, Ku-B18, Ku-B25, Ku-B26, and Ku-B27). Three specimens (i.e., Ku-B13, Ku-B14, and Ku-B15) have low initial water content equal to 6.2 % and the other three specimens (i.e., Ku-B16, Ku-B17, and Ku-B18) have high initial water content equal to 34.9 %, 26.1 % and 19.3 % respectively. The remaining three specimens (i.e., Ku-B25, Ku-B26, and Ku-B27) are tested against high concentration solution. The summary of the initial conditions of Kunigel bentonites are tabulated in Table 4.3.

#### 6.2.3.1 Swelling pressure and water uptake with time

Typical curves of swelling pressure and water uptake versus time are plotted in semi-logarithmic scales are shown in Figure 6.9 (a) and (b). The increase in both the swelling pressure and amount of water uptake with time was rapid at the earlier stage of tests. The rate of both swelling pressure development and amount of water uptake decreases beyond a point which marks the end of primary swelling pressure development. The rate of swelling pressure development generally decreased with time after the maximum swelling pressure was attained.

For Kunigel bentonite specimens, the time swelling pressure plots invariably show two maxima as depicted in Figure 6.9 (a). In this case, the first maxima for all densities considered was reached in about 6000 min of saturation period followed by a decrease and further increase in swelling pressures. The swelling pressures of the specimens equilibrated after about 20,000 min in all cases. The phenomenon of two maxima during swelling pressure development has been outlined in section 6.3. Figure 6.9 (b) shows the amount of water uptake with time. It's clear from the Figure, that the Kunigel bentonite specimen Ku-B13 has taken around 18 ml of water and equilibrated around 20,000 min, while Ku-B14 has taken 13 ml of water during the saturation and the process last at around 30,000 min. On other hand, the specimen Ku-B15 has taken less amount of water (i.e., 11 ml) than the other two specimens (Ku-B13 and Ku-B14) due to high compacted dry density and high degree of saturation.

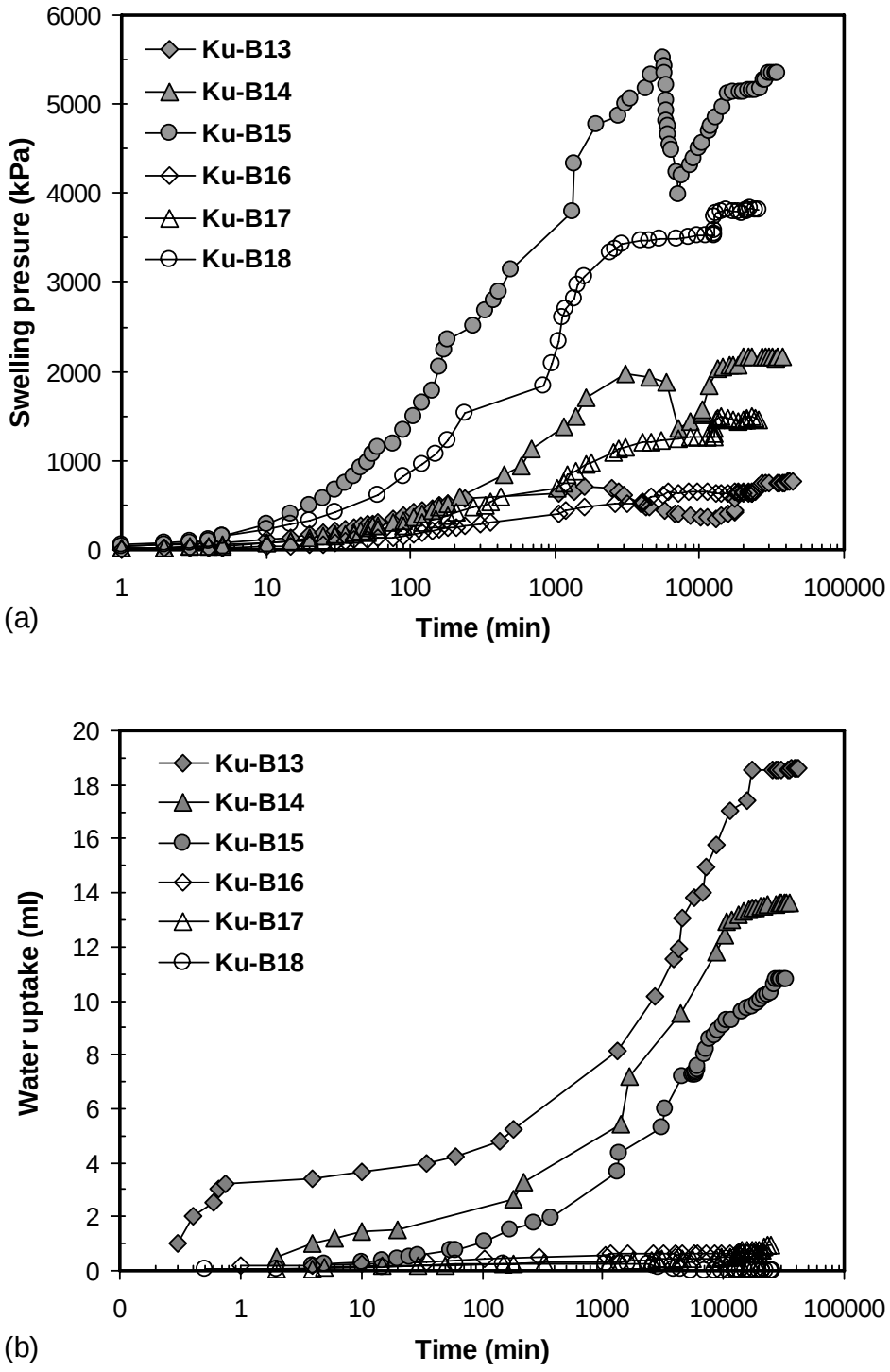


Figure 6.9 Development of constant volume swelling pressure of Kunigel bentonite (a) swelling pressure and (b) water uptake versus time

### 6.2.3.2 Swelling pressure at low and high initial water content

The effect of low and high initial water content on swelling pressure behaviour of Kunigel bentonite specimens are shown in Figure 6.10. The dry density versus swelling pressure plot clearly shows that for specimens with the same initial water content, the swelling pressure increases with an increase in the dry density. The swelling pressure of the Kunigel bentonite specimens show exponential function against dry density for both initial water content conditions. It is clear in the Figure 6.10; that the swelling pressures obtained for the specimens tested at high initial water content is less than the swelling pressure obtained for the specimens tested at low initial water content. It is noted when the initial water content is varied for Kunigel bentonite; at the same dry density, the swelling pressure decreased with an increase in the initial water content at low dry densities, whereas the initial water content practically had less influence on the swelling pressure at low dry density. The experimental results of Kunigel bentonite for low initial water content and high initial water content indicates that the reduction ratio, *RR*, of swelling pressure in high initial water content is about 14 % for the dry density equal to 1.39 $Mg/m^3$ and the reduction ratio is about 31 % for the dry density equal to 1.57 $Mg/m^3$, whereas, similar reduction ratio is noted about 31 % for the dry density equal to 1.75 $Mg/m^3$. The reduction ratio, *RR* (%), of swelling pressure in high initial water content to low initial water content can be calculated using Equation 6.1.

Figure 6.11 shows the comparison between Kunigel bentonite of present study and swelling pressure results reported by Komine and Ogata (1996) and Japan Nuclear Cycle Institute (1999). The initial conditions for the Kunigel and Kunigel VI can be found in Tripathy et al (2004). As shown in Figure 6.11, the swelling pressure of reported bentonites increases with increase of dry density and the swelling pressure of Kunigel bentonite used in present study is higher than that of reported bentonites.

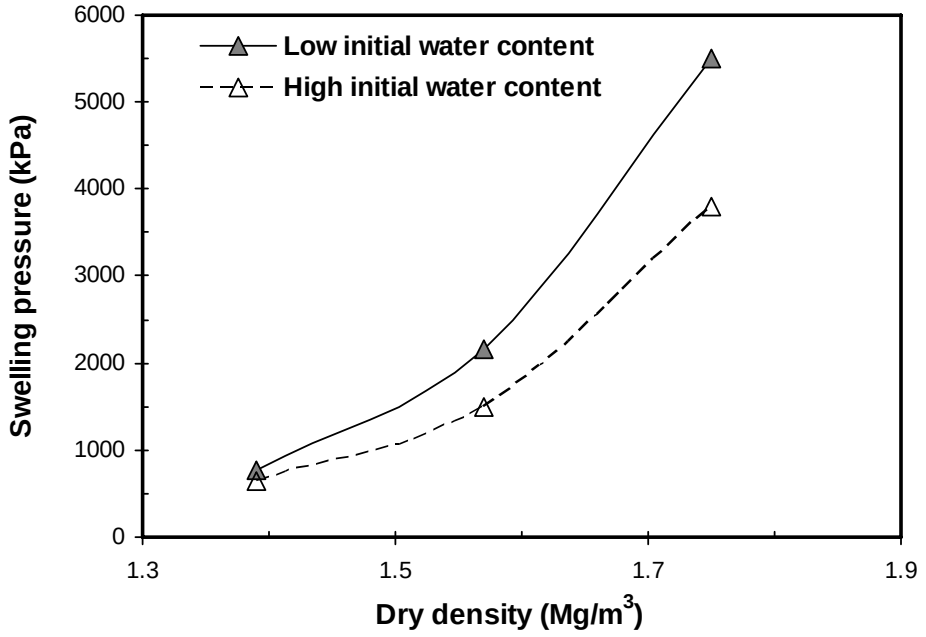


Figure 6.10 Swelling pressure as function of dry density for low and high initial water contents for Kunigel bentonite

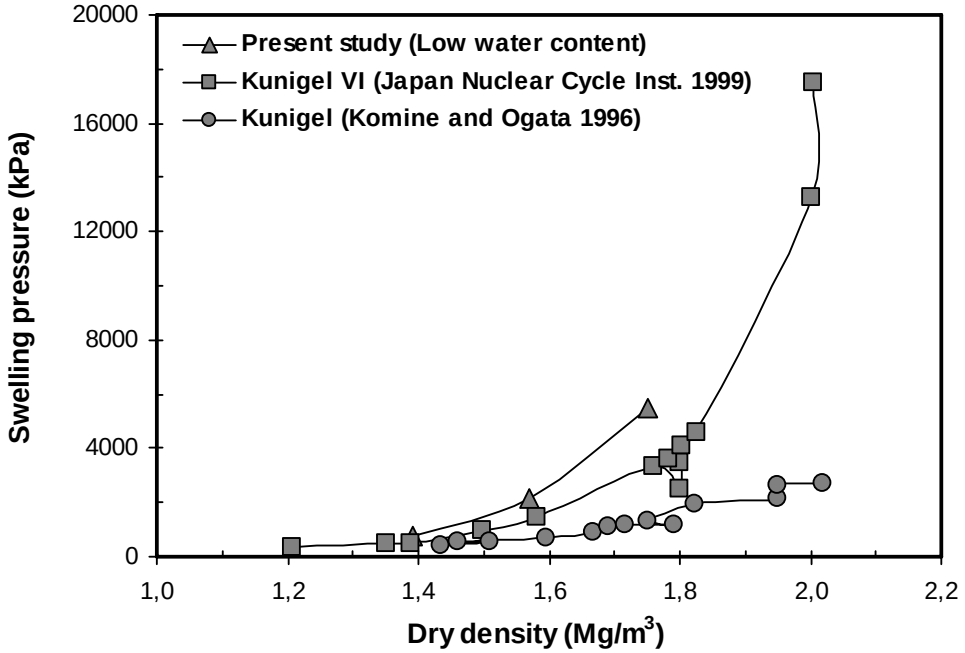


Figure 6.11 Comparison of swelling pressure versus dry density for Kunigel bentonites

### 6.2.3.3 Swelling pressure at distilled water and high concentration solution

Figure 6.12 indicates the relationship between swelling pressure and dry density for Kunigel bentonite specimen. The experimental swelling pressure results show that the swelling pressures obtained by permeating the specimen with distilled water ($10^{-4}$M) is higher than the specimens permeated with high concentration ($10^{-2}$M) solution. Moreover, only a slight difference of swelling pressures is apparent between distilled water and high concentration conditions at low dry density. The experimental results of Kunigel bentonite for distilled water ($10^{-4}$M) and high concentration solution ($10^{-2}$M) indicates that the reduction ratio, *RR*, of swelling pressure in high concentration solution is about 18 % for the dry density equal to 1.39 Mg/m$^3$ and the reduction ratio is about 26 % for the dry density equal to 1.57 Mg/m$^3$, whereas, the reduction ratio is about 23 % for the dry density equal to 1.75 Mg/m$^3$. The reduction ratio, *RR* (%), of swelling pressure in high concentration solution to distilled water can be calculated from Equation 6.2.

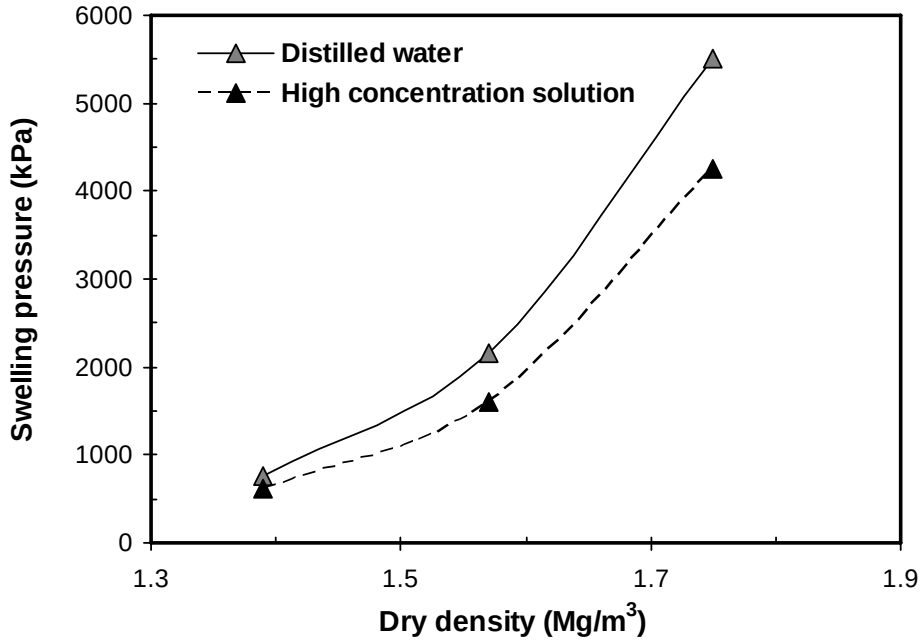


Figure 6.12 Swelling pressure as function of dry density for distilled water and high concentration solution for Kunigel bentonite

## 6.3 Overall discussion on swelling pressure results

In the earlier sections the results of swelling pressure and water uptake with time for three selected bentonites are presented. The effect of low and high initial water content on swelling pressure is shown. Furthermore, the results of swelling pressure with distilled water as permeant as well as the permeation with high concentration solution for three bentonite used in this study are presented. In this section the results are discussed in order to analyze the behaviour of specimens during water saturation at constant volume condition.

***Swelling pressure and water uptake with time***

Figures (6.1, 6.5, and 6.9) show the vertical swelling pressure and water uptake versus time curves for Calcigel, MX-80 and Kunigel bentonites. The increase in both the swelling pressure and amount of water with time was rapid at the earlier stage of tests. The rate of swelling pressure development decreases beyond a point which marks the end of primary swelling pressure development. The test results performed by Gattermann (1998) showed that swelling pressure was constant with time after the maximum value was reached.

Sridharan et al. (1986) showed that the swelling pressure versus time curve for several clays could also be approximated using the rectangular hyperbola equation. The hydration of smectites and the corresponding changes in microstructure at the level of clay layers and clay particles inside the aggregates have been described by clay mineralogists and soil scientists (e.g., Aylmore & Quirk 1962, Bird 1984, and Tessier 1990).

Saiyouri et al. (1998, 2000) provided a detailed description of the hydration of two heavily compacted smectites used for making engineered barriers (FoCa clay and MX-80). They confirmed that hydration was governed by the progressive placement of layers of water molecules along the surface of the elementary clay layer, inside the clay particles, starting from one layer in dry conditions and ending up with a maximum number of four layers. Alonso et al. (1999) showed that swelling pressure may also decrease as a result of collapse of the clay macro-structure. The rate of swelling of several expansive soils tested in oedometer was reported by Sridharan and Gurtug (2004), where the percent swell versus time curve was approximated using a rectangular hyperbola equation.

Agus (2005) stated that, in case of the swelling pressure development and the amount of water of the compacted Ca-bentonite (Calcigel) specimens used in his study, the rectangular hyperbola equation is found to be unable to give a satisfactory fit to the experimental data of either the swelling pressure development or the amount of water uptake with time. Agus (2005) showed that a linear relationship was obtained between the normalized swelling pressure ($P_s/P_{s\ max}$) and the square root of elapsed time at earlier stage of the swelling pressure development (i.e., mostly up to 60% of the maximum swelling pressure). Agus and Schanz (2005a) found that the rate of swelling pressure development is a function of the initial total suction of the compacted Calcigel bentonite specimen tested.

***Double peak phenomenon***

As shown in Figures (6.1, 6.5, and 6.9), the swelling pressure development with elapsed time for studied bentonite were found to be accompanied with two maxima. Interpretation of the two maxima (peaks) phenomenon in swelling pressure development with time was initially postulated as due to the loss of shear strength at aggregate level upon a decrease in suction that caused a collapse of macrostructure (Pusch 1982). A further increase in swelling pressure was attributed due to the redistribution of clay particles to a more homogenous and dispersed state. The evolution of swelling pressure with time during the saturation process has been shown to be influenced by the initial water content and dry density of clays (Schanz & Tripathy 2009, Baille et al. 2010).

Recently, studies on the microstructure of compacted bentonites by Saiyouri et al. (2004), Delage et al. (2006), and Delage (2007) showed that the initial saturation phase is accompanied by homogeneous swelling of clay aggregates in a granular assembly that results in an overall swelling with a temporary preservation of the interaggregates voids. Softening of the clay aggregates upon saturation tend to eliminate the aggregate structure that in turn results in a temporary collapse followed by further swelling of the bentonites.

Imbert & Villar (2006) reported the swelling pressure development for French FoCa bentonite compacted at different dry densities. Their results showed that irrespective of the initial dry density, the swelling pressure of the clay specimens increased and then decreased during the initial phase of water uptake process. Further, with an elapsed time, the swelling pressure increased and then stabilized. The decrease in swelling pressure was

attributed due to a collapse of the macrostructure on suction decrease, whereas a further increase in the swelling pressure interpreted as due to the redistribution of water towards the microstructure.

Schanz and Tripathy (2009) measured the swelling pressures of compacted divalent rich bentonite specimens employing constant volume for a range of dry density from 1.10 to 1.73 $Mg/m^3$. They stated that during the saturation process, the rates of expansion of the interlayer and interparticle pores, and the contraction of the larger voids, influence the overall swelling pressure development in compacted bentonites.

***Influence of initial water content and dry density***

Figures (6.2, 6.6 and 6.10) present the swelling pressures of Calcigel, MX-80 and Kunigel bentonite specimens plotted against the dry density for low and high initial water content. The swelling pressure of the specimens shows exponential function against dry density. This behaviour is due to increase in the dry density or a decrease in the void ratio causes a decrease in the interlayer spacing and an increase in the osmotic pressure between the clay platelets and thus the swelling pressure of the clay increases (Sridharan et al. 1986a). Such behaviour has been reported by many researchers such as Komine and Ogata (2003), Villar and Lloret (2004), Tripathy et al. (2004), Agus and Schanz (2005a), Schanz and Tripathy (2009) and Baille et al. (2010).

As depicted in the Figures (6.2, 6.6 and 6.10), the curves of swelling pressure obtained for the specimens tested at high initial water content is located below the curve of swelling pressure obtained for the specimens tested at low initial water content in case of all three type of bentonites used in this study. Gens and Alonso (1992) stated that at the same compaction dry density, clay specimens having very high initial water contents or very low initial suctions tend to exhibit lower swelling pressures than that of specimens with lower water contents or higher suctions.

Villar and Lloret (2008) checked the influence of initial water content of Febex bentonite with range of dry densities (1.4 – 1.6 $Mg/m^3$) on the swelling pressure behaviour. Figure 6.13 shows the influence of initial water content on swelling pressure. The results showed by Villar and Lloret (2008) indicated that there is not a big trend but slight reduction in the swelling pressure to change as a function of the initial water content.

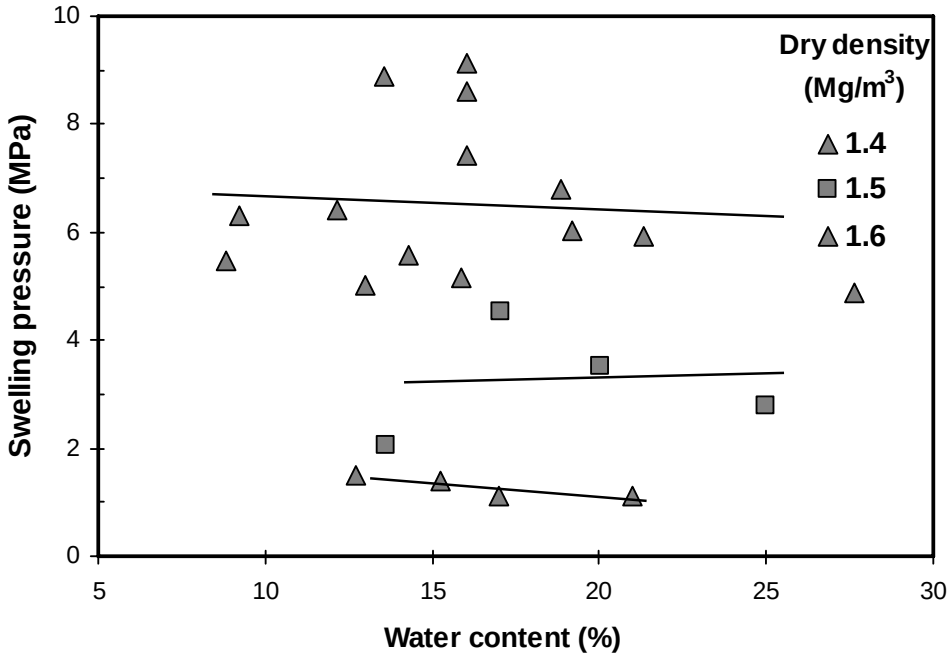


Figure 6.13 Influence of initial water content on the swelling pressure (modified from Villar and Lloret 2008).

Baille et al. (2010) studied the swelling behaviour and initial compaction condition of Calcigel bentonite. The initial water content used was in the range of 9.5 – 50 % and dry density considered from 1.11 – 1.73 Mg/m$^3$. They reported that both the initial water content and compaction dry density influence the swelling pressure of bentonite. At same water content, the swelling pressure increased with an increase in the dry density. Also, at the same dry density, the swelling pressure was found to decrease with an increase in the water content indicating that the influence of molding water on the fabric of the clay can be quite significant.

***Influence of Pore fluid***

Figures (6.4, 6.8 and 6.12) present the swelling pressures of Calcigel, MX-80 and Kunigel bentonite specimens plotted against the dry density for distilled water and high concentration solution. As shown in Figures, the swelling pressure obtained by permeating the specimen with distilled water ($10^{-4}$M) is higher than the specimens permeated with

high concentration ($10^{-2}$M) solution. Such behaviour is consistent with the results presented by Lloret and Villar (2007), Komine et al. (2009).

Lloret and Villar (2007) investigated the effect of high concentration solution of swelling behaviour of Febex bentonite. The bentonite was saturated under isochoric conditions using solutions of NaCl and $CaCl_2$ of different concentrations. Initially, the bentonite was compacted at a dry density of 1.65 $Mg/m^3$ at hygroscopic conditions. Their results show that an increase of concentration reduces the swelling pressure as can be seen in Figure 6.14. This reduction could be related to an increase of osmotic suction, however, it must be pointed out that the reduction in swelling pressure is slightly higher when NaCl is used as solute.

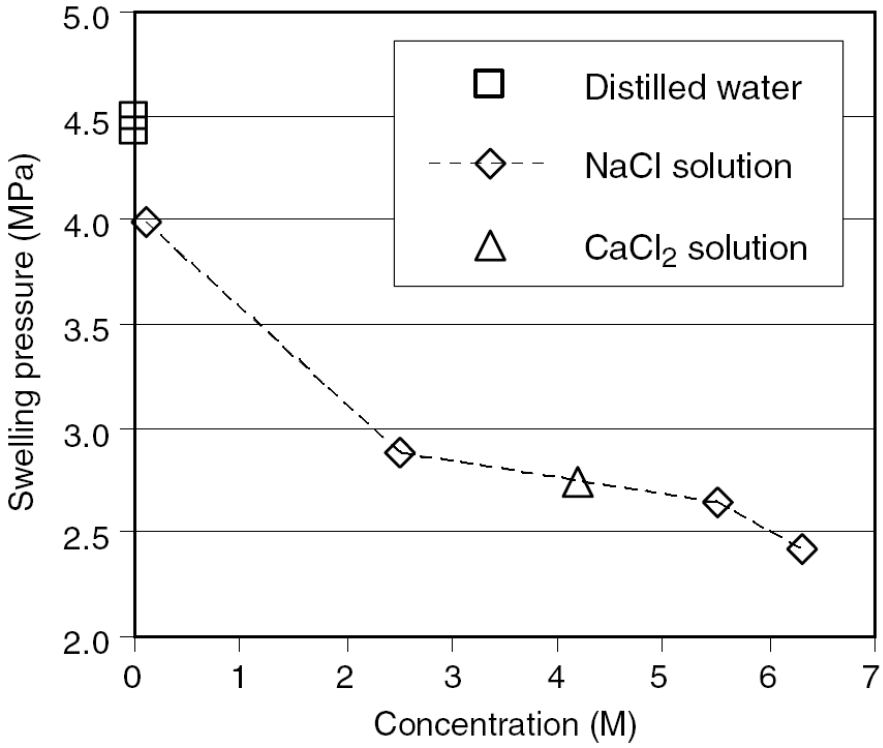


Figure 6.14 Swelling pressure values for different concentrations and solutions (Lloret et al. 2007)

Komine et al. (2009) examined the influence of sea water on swelling pressure of five kinds of bentonites. The bentonites tested contain sodium and calcium as predominant cations with different amounts of montmorillonite. The distilled water and artificial sea

water (higher concentration) was used in laboratory investigation as permeant. Figure 6.15 shows swelling pressure versus initial dry density result for MX-80 bentonite permeated with distilled and artificial seawater. Their results indicated that the influence of artificial seawater on the swelling characteristics of sodium-type and artificial sodium-type bentonites is low, provided that the dry density of compacted bentonite and the montmorillonite content of bentonite are high. Further, the influence of artificial seawater on the swelling characteristics of calcium-type bentonite is less than sodium-type and artificial sodium-type bentonites. The behaviour is attributed as: due to the high density or high montmorillonite content, the distances between montmorillonite mineral layers in the compacted bentonite remain small; the montmorillonite mineral layers in this condition can filter the cations in artificial seawater. The water chemistry inside the bentonite can retain low ion concentration through filtration of montmorillonite mineral layers. Moreover, almost no exchange reaction occurs between the exchangeable cations of montmorillonite minerals and cations in artificial seawater. Therefore, the influence of artificial seawater on swelling characteristics is slight in the case of high dry density, high montmorillonite content. Nevertheless, the cations in artificial seawater can infiltrate easily into bentonite and montmorillonite mineral layers in the case of low dry density, low montmorillonite content. Therefore, the influence of seawater in such cases is great.

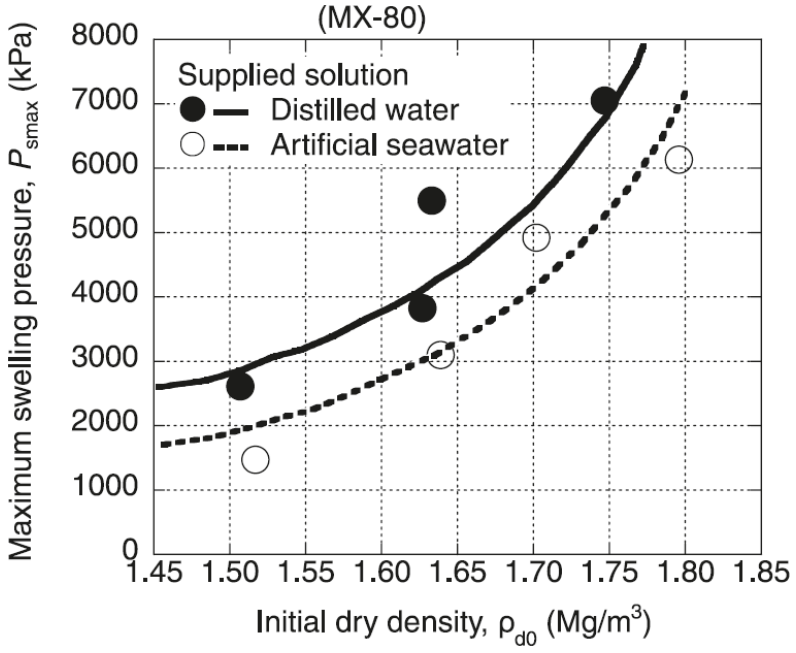


Figure 6.15 Swelling pressure as function of initial dry density for distilled water and artificial seawater (Komine et al. 2009)

## 6.4 Hydraulic conductivity results

In the following section, the results of hydraulic conductivity are presented for bentonites described in section (4.2). After getting maximum swelling pressure of the bentonites, the constant head hydraulic conductivity tests were performed to obtain the hydraulic conductivity of the bentonites. Discussion on the experimental hydraulic conductivity results are presented in section 6.5.

### 6.4.1 Calcigel bentonite

A series of tests was conducted to determine the influence of, (1) low and high initial water content, (2) pore fluid composition on the hydraulic performance of the bentonite specimens. These tests are important as they assist in identifying whether the parameters (initial water content, pore fluid) could have induced changes in the hydraulic performance of the bentonite specimens. Similar to section 6.2.1, nine specimens of Calcigel bentonite (i.e., Ca-B1, Ca-B2, Ca-B3, Ca-B4, Ca-B5, Ca-B6, Ca-B19, Ca-B20, and Ca-B21) were tested. Among these specimens, three specimens (i.e., Ca-B1, Ca-B2, and Ca-B3) have low initial water content equal to 9.0 % and the other three specimens (i.e., Ca-B4, Ca-B5, and Ca-B6) have high initial water content equal to 34.6 %, 25.7 % and 18.8 %. The remaining three specimens (i.e., Ca-B19, Ca-B20, and Ca-B21) were tested by infiltrating high concentration solution.

***Inflow and outflow or steady state condition***

Figure 6.16 shows the rate of inflow and outflow condition of Calcigel bentonite with dry density equal to 1.4 $Mg/m^3$. Different fluid injection pressures ranging from 25 kPa to 500 kPa were applied depending upon the density during the hydraulic conductivity tests. The stepwise pressure increment was increased and the outflow was monitored. The increase of fluid injection pressure to the next level was done once the outflow rate become constant or the steady state conditions have been achieved. The system was then allowed to attain the pressure and flow equilibrium condition until the final pressure selected was reached. Only one example of steady state condition (inflow and outflow) is shown in following section. Remaining results of inflow and outflow for three bentonites with different dry densities are presented in Appendix A1.

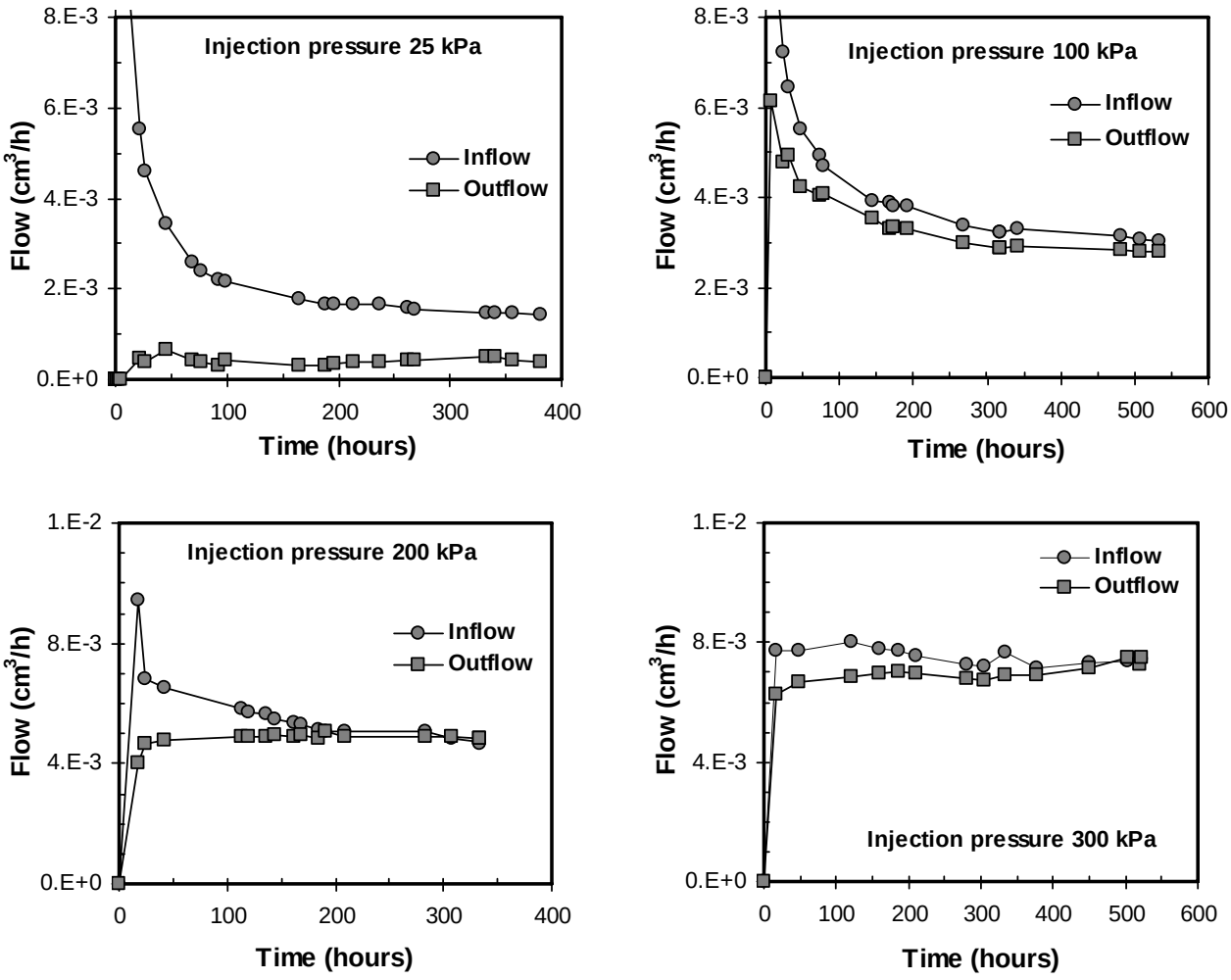


Figure 6.16 Inflow and outflow condition for Calcigel bentonite

#### 6.4.1.1 Hydraulic conductivity at low and high initial water content

The saturated hydraulic conductivities of compacted bentonite specimens were measured according to the experimental procedure discussed in section 5.7.4. The hydraulic conductivities were corresponding to the dry densities varying between 1.37 and 1.75 Mg/m$^3$. Figure 6.17 present the results of hydraulic conductivity measurement versus dry density. The test results shows that: (*i*) the hydraulic conductivity of the bentonites decreases with an increase in the dry density for specimens with the same initial water content and (*ii*) at the same initial dry density, the hydraulic conductivity slightly decrease

with an increase in the initial water content. The hydraulic conductivity for Calcigel bentonite specimens varied between $10^{-13}$ and $10^{-14}$ m/s. The test results clearly indicate that with an increase in the dry density, the swelling pressure increases which in turn reduce the effective porosity for the fluid flow and further a decrease in the hydraulic conductivity of compacted bentonites. The influence of initial water content on the hydraulic conductivity of Calcigel bentonite can be seen in Figure 6.17. For lower dry density (1.37 $Mg/m^3$), specimen with a low initial water content exhibited a higher hydraulic conductivity ($6.0 \times 10^{-13}$ m/s), whereas at the same dry density the high initial water content specimen showed a low hydraulic conductivity ($3.31 \times 10^{-13}$ m/s). For dry density (1.56 $Mg/m^3$), specimen with a low initial water content exhibited a hydraulic conductivity ($1.20 \times 10^{-13}$ m/s), whereas at the same dry density the high initial water content specimen show slightly low hydraulic conductivity ($8.83 \times 10^{-14}$ m/s). Similarly, for higher dry density (1.75 $Mg/m^3$), the effect of the initial water content was found to be negligible.

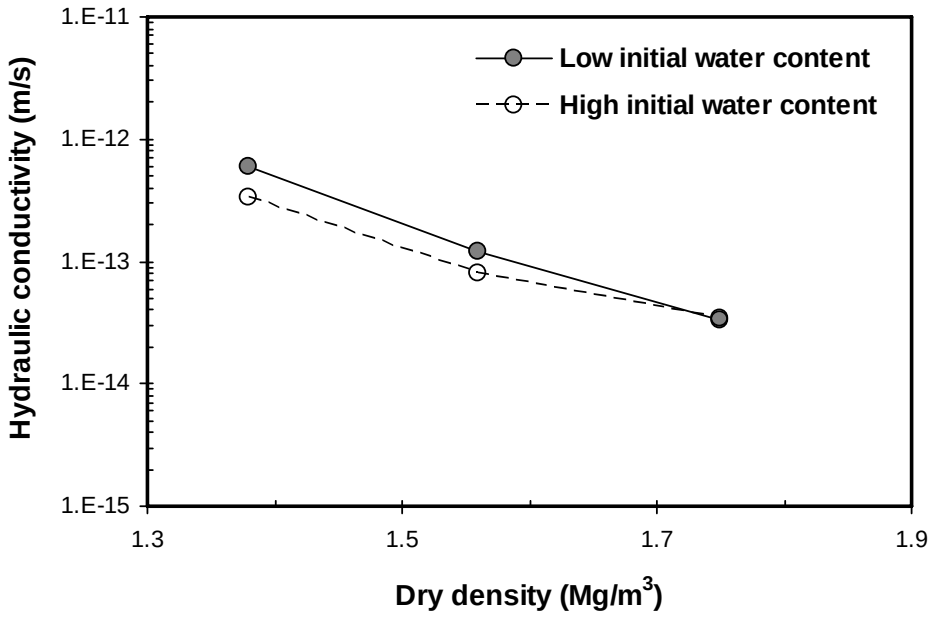


Figure 6.17 Hydraulic conductivity as function of dry density for low and high initial water content for Calcigel bentonite

### 6.4.1.2 Hydraulic conductivity at distilled water and high concentration solution

The influence of pore fluid chemistry on hydraulic conductivity was also examined on three specimens of Calcigel bentonite. Figure 6.18 show the relationship between hydraulic conductivity and dry density permeated with distilled water and high concentration solution. The test results show that the hydraulic conductivity of the bentonite decrease with an increase in the dry density for specimens permeated with distilled water and at the same initial dry density, the hydraulic conductivity slightly increase with an increase in the concentration of permeant. The influence of high concentration solution is more clear for the dry density (1.37 $Mg/m^3$). As the dry density increases, the difference in the hydraulic conductivity between distilled water and high concentration solution is found to be diminishing.

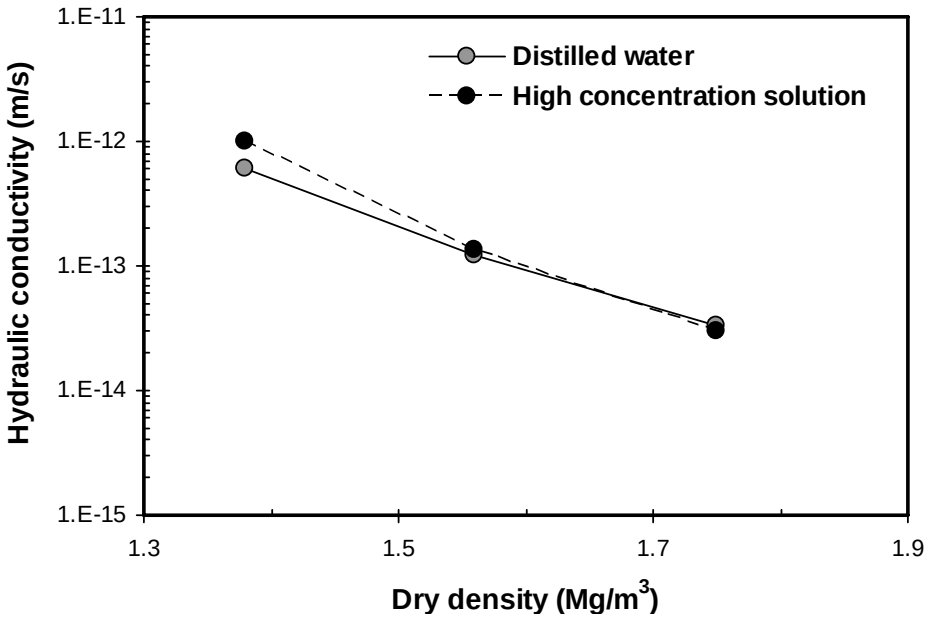


Figure 6.18 Hydraulic conductivity as function of dry density for distilled water and high concentration solution for Calcigel bentonite

### 6.4.2 MX-80 bentonite

A total of nine specimens of MX-80 clay were tested to determine the hydraulic conductivity (i.e., Mx-B7, Mx-B8, Mx-B9, Mx-B10, Mx-B11, Mx-B12, Mx-B22, Mx-B23, and Mx-B24). Three of these specimens (i.e., Mx-B7, Mx-B8, and Mx-B9) were

tested using low initial water content equal to 10.5 % and the other three specimens (i.e., Mx-B10, Mx-B11, and Mx-B12) were tested at high initial water content equal to 35.7 %, 26.8 % and 19.6 %. The remaining three specimens (i.e., Mx-B10, Mx-B11, and Mx-B12) are tested against high concentration solution. Table 4.3 outline the summary of the initial conditions of the bentonite.

#### 6.4.2.1 Hydraulic conductivity at low and high initial water content

The hydraulic conductivity tests for MX-80 bentonite with corresponding dry densities varying between 1.37 and 1.75 $Mg/m^3$ were conducted. Figure 6.19 present the results of hydraulic conductivity measurement versus dry density. As shown in the Figure, hydraulic conductivity of the bentonites decreases with an increase in the dry density. Similarly the effect of initial water content on hydraulic conductivity is also shown in Figure 6.19. At the same initial dry density, the hydraulic conductivity almost remains the same with an increase in the initial water content. The hydraulic conductivity of MX-80 bentonite specimens varied between $10^{-13}$ and $10^{-14}$ m/s. The negligible influence of initial water content on the hydraulic conductivity of MX-80 bentonite can be seen in Figure 6.19.

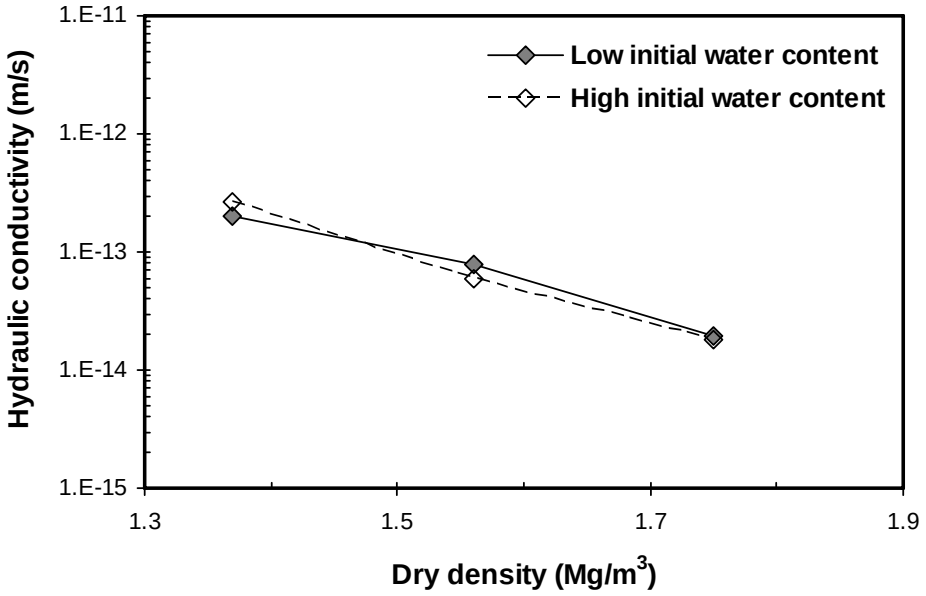


Figure 6.19 Hydraulic conductivity as function of dry density for low and high initial water content for MX-80 bentonite

For lower dry density (1.37 Mg/m$^3$), specimen with a high initial water content exhibited a higher hydraulic conductivity ($2.64 \times 10^{-13}$ m/s), whereas at the same dry density the low initial water content specimen showed a low hydraulic conductivity ($2.04 \times 10^{-13}$ m/s). For dry density (1.56 Mg/m$^3$), specimen with a low initial water content exhibited a hydraulic conductivity ($7.82 \times 10^{-14}$ m/s), whereas at the same dry density the high initial water content specimen show slightly low hydraulic conductivity ($6.00 \times 10^{-14}$ m/s). Similarly, for higher dry density (1.75 Mg/m$^3$), the effect of the initial water content was found to be negligible.

#### 6.4.2.2 Hydraulic conductivity at distilled water and high concentration solution

The influence of pore fluid chemistry on hydraulic conductivity was also examined in three specimens of MX-80 bentonite. Figure 6.20 show the relationship between hydraulic conductivity and dry density permeated with distilled water and high concentration solution. The test results show that the hydraulic conductivity of the bentonite decrease with an increase in the dry density for specimens permeated with distilled water and at the same initial dry density, the hydraulic conductivity slightly increase with an increase in the concentration of permeant.

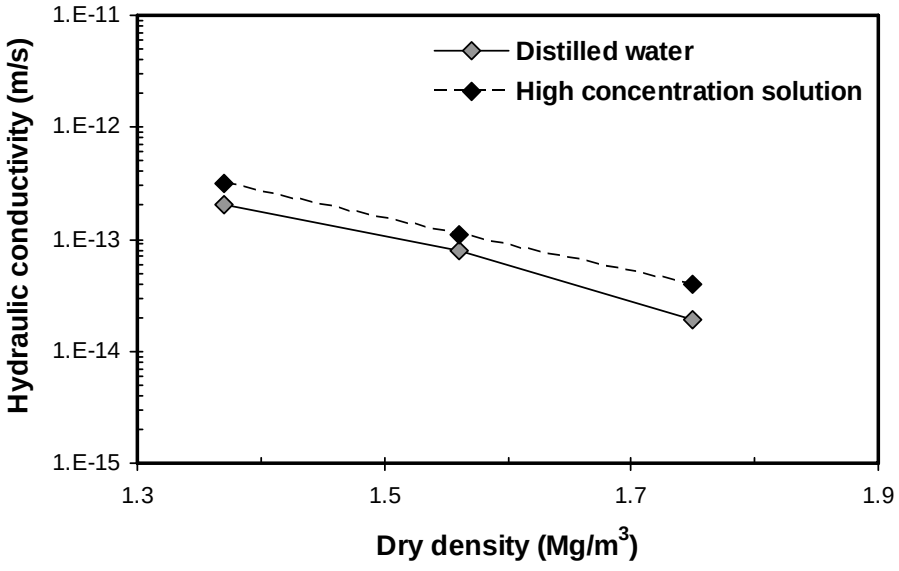


Figure 6.20 Hydraulic conductivity as function of dry density for distilled water and high concentration solution for MX-80 bentonite

The influence of high concentration solution seems to be consistent for entire range of dry densities (i.e., 1.37 – 1.75 Mg/m$^3$). In case of MX-80 bentonite, no reduction of hydraulic conductivity permeated with high concentration solution has been observed for high dry density range, as observed in case of Calcigel bentonite in Figure 6.18.

### 6.4.3 Kunigel bentonite

For Kunigel bentonite, hydraulic conductivity tests were conducted on nine specimens (i.e., Ku-B13, Ku-B14, Ku-B15, Ku-B16, Ku-B17, Ku-B18, Ku-B25, Ku-B26, and Ku-B27). Three specimens (i.e., Ku-B13, Ku-B14, and Ku-B15) have low initial water content equal to 6.2 % and the other three specimens (i.e., Ku-B16, Ku-B17, and Ku-B18) have high initial water content equal to 34.9 %, 26.1 % and 19.3 % respectively. The remaining three specimens (i.e., Ku-B25, Ku-B26, and Ku-B27) were tested against high concentration solution. The summary of the initial conditions, initial water content, dry density are tabulated in Table 4.3.

#### 6.4.3.1 Hydraulic conductivity at low and high initial water content

The hydraulic conductivity of Kunigel bentonite with range of dry densities varying between 1.37 and 1.75 Mg/m$^3$ are experimentally measured with the procedure described in section 5.7.4. Figure 6.21 present the results of hydraulic conductivity measurement versus dry density for low and high initial water content for Kunigel bentonite. The test results shows that, the hydraulic conductivity of the bentonites decreases with an increase in the dry density for specimens with the same initial water content and at the same initial dry density, the hydraulic conductivity slightly decrease with an increase in the initial water content. The hydraulic conductivity for Kunigel bentonite specimens for low and high initial water content varied between $10^{-13}$ and $10^{-14}$ m/s. The influence of initial water content on the hydraulic conductivity of Kunigel bentonite can be seen in Figure 6.21. For lower dry density (1.37 Mg/m$^3$), specimen with a low initial water content exhibited a higher hydraulic conductivity ($6.77 \times 10^{-13}$ m/s), whereas at the same dry density the high initial water content specimen showed a low hydraulic conductivity ($4.35 \times 10^{-13}$ m/s). For dry density (1.56 Mg/m$^3$), specimen with a low initial water content exhibited a hydraulic conductivity ($2.49 \times 10^{-13}$ m/s), whereas at the same dry density the high initial water content specimen show slightly low hydraulic conductivity ($1.58 \times 10^{-13}$ m/s). Similarly,

for higher dry density (1.75 Mg/m$^3$), the effect of the initial water content was found to be less influenced.

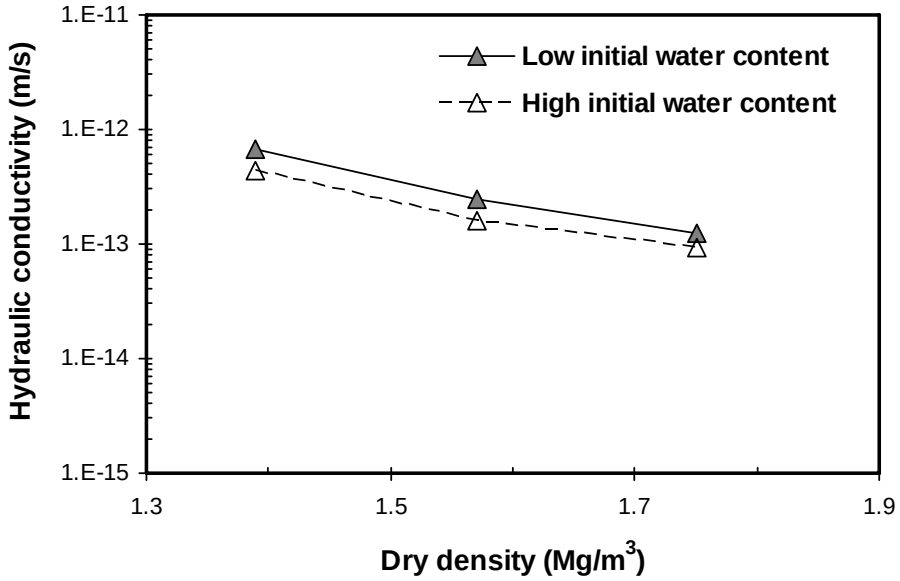


Figure 6.21 Hydraulic conductivity as function of dry density for low and high initial water content for Kunigel bentonite

### 6.4.3.2 Hydraulic conductivity at distilled water and high concentration solution

The influence of pore fluid chemistry on hydraulic conductivity was also examined in three specimens of Kunigel bentonite. Figure 6.22 show the relationship between hydraulic conductivity and dry density permeated with distilled water and high concentration solution. The test results show that the hydraulic conductivity of the bentonite decrease with an increase in the dry density for specimens permeated with distilled water and at the same initial dry density, the hydraulic conductivity slightly increase with an increase in the concentration of permeant. The influence of high concentration solution is clear for the dry density (1.37 Mg/m$^3$). As the dry density increases, the difference in the hydraulic conductivity between distilled water and high concentration solution is found to be diminishing.

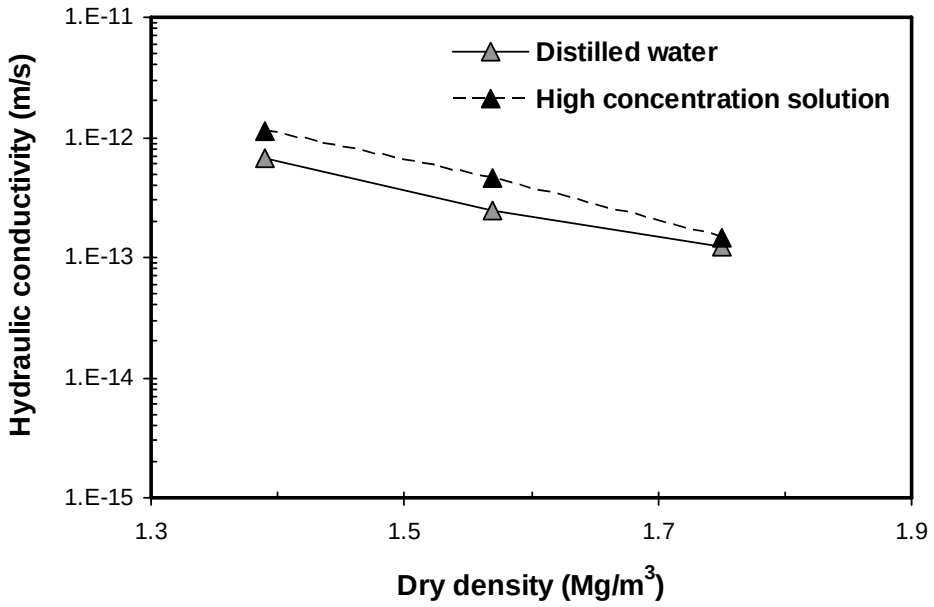


Figure 6.22 Hydraulic conductivity as function of dry density for distilled water and high concentration solution for Kunigel bentonite

## 6.5 Overall discussion on hydraulic conductivity results

In the earlier section 6.4, the results of hydraulic conductivity for three types of bentonites with low and high initial water content are presented. The effect of low and high initial water content on hydraulic conductivity is shown. Furthermore, the results of hydraulic conductivity with distilled water as permeant as well as the permeation with high concentration solution are presented. In this section the results are discussed in order to analyze the hydraulic behaviour of bentonites.

### *Influence of initial water content and dry density*

Figures (6.17, 6.19, and 6.21) show the results of hydraulic conductivity versus dry density of Calcigel, MX-80 and Kunigel bentonites for low and high initial water content. This was done to examine the effect of differing initial water content on hydraulic conductivity through bentonite. The test results indicated that compacting bentonites at higher initial water contents and lower dry densities or at lower initial water contents and higher dry densities, clay particles tend to attain a more oriented fabric that would offer more tortuous paths for the fluid flow that in turn reduces the hydraulic conductivity. As shown in

Figures (6.17, 6.19, and 6.21), the hydraulic conductivity at high initial water content is slightly lower than hydraulic conductivity at low initial water content and the difference is more clear at low dry densities. Moreover, the influence of initial compaction water content was found to be negligible at higher dry densities.

Pusch (1979) explained the low hydraulic conductivity of the bentonite compacted at high density in terms of the low water contents required to saturate the highly compacted clay, since under these conditions, the thickness of the adsorbed water is very small (3-5 Å) due to its high specific surface, meaning that the molecules of water are strongly adsorbed to the surfaces of the clay minerals, leaving only very tortuous interparticle channels for the transport of water.

Dixon (1999) investigated the effect of different water content having different initial degree of saturation varying from 0 – 90 % on hydraulic conductivity of Na-bentonites with range of dry densities from 0.50 $Mg/m^3$ to 1.5 $Mg/m^3$. He found that there is no clear relationship between initial degree of saturation and hydraulic conductivity for these materials. Figure 6.23 presents the results of the hydraulic conductivity measurement versus clay dry density, as can be seen in the figure, the hydraulic conductivity decreases with increasing clay density. Different symbols in Figure 6.23 indicate the initial degree of saturation or water content. The figure shows no clear relationship between initial degree of saturation and hydraulic conductivity for this material especially at high density. The lack of discernable differences in the hydraulic conductivity of specimens having low and high initial water content indicate there are no significant differences in the overall soil structure of these specimens at moderate to high densities. This is consistent with the study presented by Oliphant and Tice (1985), which assumes that fluid flow in clays, and in particular, bentonites, is largely controlled by conduction through a very limited number of channels through macro pores. Oliphant and Tice (1985) found that changes in density induced little change in the pathways taken to conduct the water through bentonites. The small number of macro pores through which water can flow was not much influenced by the initial compaction water content especially for high densities. This can be accounted by assuming that there is little in the way of true macro pores in any of these materials, the bulk of the porosity is taken up by discontinuous micro pores within individual peds, and spaces between the individual clay platelets.

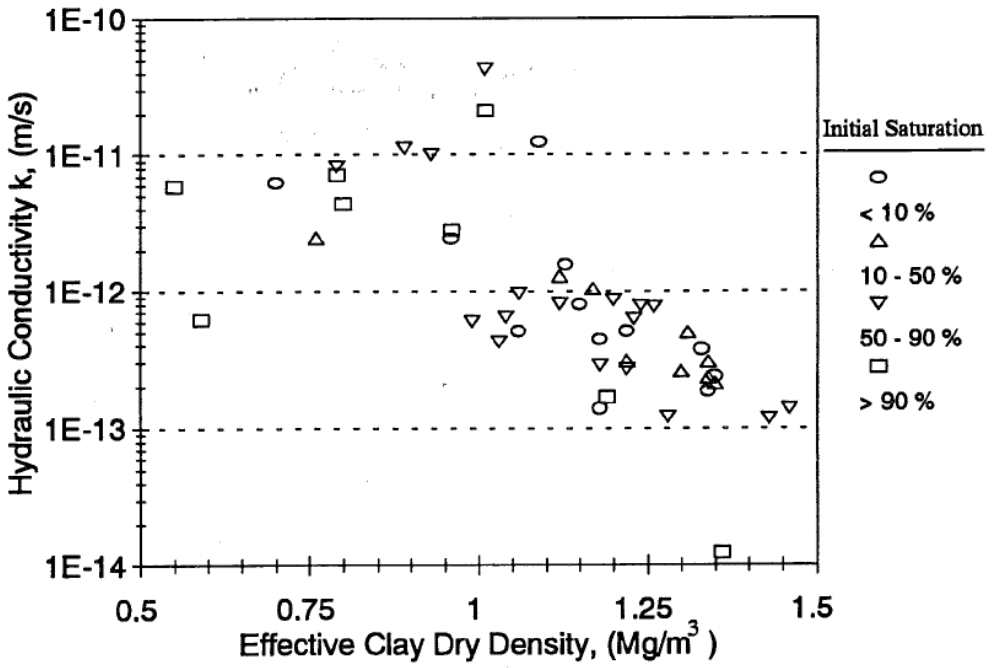


Figure 6.23 Influence of initial degree of saturation on the hydraulic conductivity bentonite specimens (Dixon 1999)

Baille et al. (2010) measured the hydraulic conductivity of Calcigel bentonite with density range 1.11 – 1.73 $Mg/m^3$ using a high pressure consolidation test apparatus for the two types of specimen i.e., initial saturated (Slurry) and compacted saturated. They found that the compacted saturated specimens having high initial water content showed slightly high hydraulic conductivity than the specimens having low initial water content.

***Influence of pore fluid***

Figures (6.18, 6.20, and 6.22) show the results of hydraulic conductivity versus dry density of Calcigel, MX-80 and Kunigel bentonites for distilled water and high concentration solution. The test results in present work show that the hydraulic conductivity of the bentonite slightly increases with an increase in the concentration of solution. Macey (1942) measured hydraulic conductivity of clays in water and non polar fluids. He reported that the hydraulic conductivity is higher when non polar fluid i.e., benzene is used as permeant than for water in the same clay. He considered that particle spacing, particle size as influence by aggregation or dispersion, particle rearrangement, adsorbed layers,

interlamellar swelling all influenced the hydraulic conductivity, but he considered the most important cause for the lower hydraulic conductivity in water to be the anomalous viscosity of the water near the clay surface.

The increase in hydraulic conductivity with the high concentration salinity of the permeating fluid has been underlined by Rolfe & Aylmore 1977 and attributed to: (1) alterations in pore dimension distribution as a result of variations in swelling pressure in the clay matrix, (2) variations in the mobility of the molecules of water associated with the exchangeable cations adsorbed on the surfaces or forming diffuse double layers (DDL), (3) alterations in the viscous behaviour of the structure of the water. As a result of these mechanisms, as the concentration of the electrolyte increases there is a reduction in the swelling pressure of the clay particles, the size of the flow channels increasing to the detriment of the number of small channels, this causing flow and therefore, hydraulic flow to increase. On the contrary, the increasing development of diffuse double layers on reduction of the concentration of the electrolyte causes a decrease in hydraulic conductivity. The reduction of effective porosity with the decreasing salinity of the permeating agent would be due to the fact that the pore space is occupied by the bound water (DDL), the viscosity of which is higher than that of free water. According to the diffuse double layer theories, the thickness of it decreases as the concentration of water in the pores increases, as a result of which, for a given porosity, the effective porosity of the clay would increase with increasing concentration of the solution, with the corresponding increase in hydraulic conductivity.

Dixon et al (1985) suggested that the effective porosity of clay is less than would be expected considering the total pore space per unit volume because some of the pore space is occupied by bound water which has a greater viscosity than free water. Diffuse double layer theory predicts that the diffuse double layer thickness decreases with increasing pore solution concentration. Therefore, at a given void ratio the effective porosity of the bentonite will increase as the solution strength increases (van Olphen 1977).

Ruhl and Daniel (1997) stated that hydraulic conductivity of bentonite decreases up to three orders when the PH of the solution changes from 2 to 14. This behaviour is attributed to the higher negative surface charge of the clay particle in contact with high PH solution. In this case, the double layer thickness is large and clay particles are dispersed due to electrostatic repulsion (Palomino and Santamarina 2005). Experimental evidence showed

that the presence of organic fluid increases the hydraulic conductivity of fine soils (Gnanapragasam et al. 1995).

Dixon (1999) examined the influence of pore fluid chemistry in the Na type bentonite, using fresh and saline water as permeant. Figure 6.24 shows data from the tests and data reported by Dixon et al. (1987). It separates the data from specimens tested using saline permeant from those tested using a distilled and deionised water. This figure also includes data from other researchers which is identified by Dixon (1995).

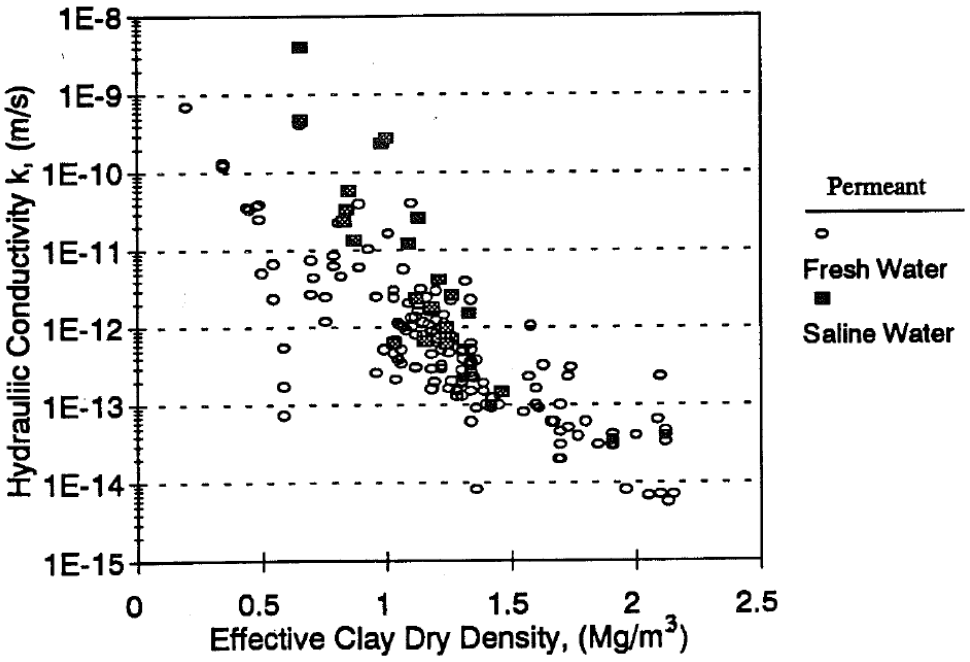


Figure 6.24 Influence of pore fluid on the hydraulic conductivity bentonite specimens (Dixon 1999)

Dixon (1999) concluded that this parameter is unlikely to significantly alter the performance of the material at clay densities greater than 1.0 $Mg/m^3$. At low clay densities (<1.0$Mg/m^3$), it is likely that pore fluid composition will influence the hydraulic performance of specimens. At these densities there is a well developed diffuse double layer surrounding the platelets and ionic concentration could become a factor in determining the porosity available for flow.

Studds et al. (1998) measured the hydraulic conductivity using distilled water and various chloride salt solutions of Wyoming Na-bentonite specimens that were initially prepared in an air-dry state, and then allowed to swell in the selected solution.

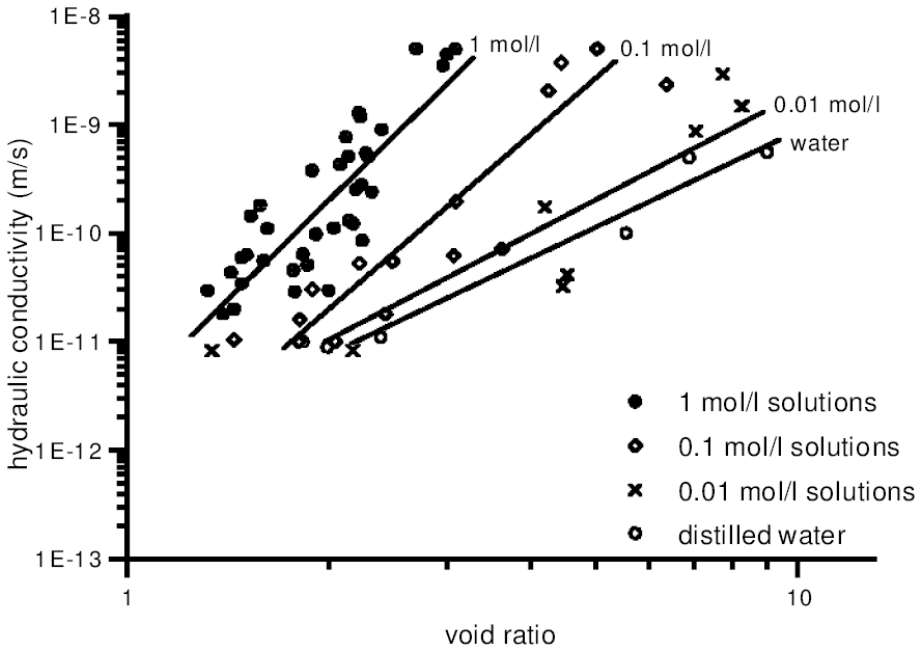


Figure 6.25 Hydraulic conductivity of bentonite with distilled water and different strength chloride salt solutions (Studds et al. 1998)

As shown in Figure 6.25, for each strength of the solution, there is a linear trend between the logarithm of hydraulic conductivity and the logarithm of void ratio. Also, at a given void ratio, the hydraulic conductivity of the bentonite increases as the solution strength increases. This later trend probably results from the influence of the permeant on the effective porosity.

Jo et al. (2001), Lee et al. (2005) mentioned that respect to the fluid properties, there is clear evidence that hydraulic conductivity of bentonitic clays increases when the ionic concentration or valence raises in the permeating fluid. The chemical properties of the fluid affect ion hydration and the formation of the diffuse double layer around soil particles.

Hence, fluid chemistry directly affects the soil fabric and the hydraulic properties of the porous media (Mitchell and Soga 2005).

Marcos et al. (2009) reported the influence of fluid chemistry, soil fabric on hydraulic conductivity of montmorillonite rich Na-bentonite by using organic (kerosene and paraffin) and inorganic (distilled water and different $CaCl_2$ solutions) fluids. They reported that the hydraulic conductivity of bentonite depends on the ion concentration in the permeating liquid. The increase of hydraulic conductivity is directly related to the rise of both $CaCI_2$ concentrations. In addition, the fluid chemical properties influence both hydraulic conductivity and intrinsic permeability which means that soil fabric changes during permeation. The effect of changing the ion concentration in the permeating fluid on double layer and soil conductivity is not fully reversible. Counterions can completely adsorb to the mineral surface when the $Ca^{2+}$ concentration rises; and this reaction is spontaneous according to the change of Gibbs free energy. However, when the $Ca^{2+}$ concentrations in the permeating fluid decreases, desorption reaction cannot take place without introducing additional energy to the system. Because of this, the increase of diffuse double layer thickness is lower than the expected thickness and the hydraulic conductivity increases when permeation with the $CaCl_2$ solution.

## 6.6 Summary

The experimental results of swelling pressure, water uptake and hydraulic conductivity are presented. The effect of varying the initial water content on swelling pressure and hydraulic conductivity are shown. The bulk fluid used is distilled water having concentration equal to ($10^{-4}$M) and high concentration NaCl permeant of salinity ($10^{-2}$M).

The increase in amount of water uptake with time was rapid at the earlier stage of tests and decreases beyond a point which marks the end of primary swelling pressure development. The swelling pressure results of the bentonites studied is a function of dry density. The decrease in the amount of swelling pressure at same dry density with varying initial water content is due to the molding compaction water content which influences the fabric and structure that may have some influence on the swelling pressure. Similarly, the amount of swelling pressure decreases when the high concentration solution is intruded to the clays.

The reduction is the swelling pressure is attributed to the contraction of the double layer, and this reduction could be also related to an increase of osmotic suction. Decrease in swelling pressure using high concentration solution is relatively occurs at low dry densities.

Furthermore, the effects of initial water content and high concentration solution on hydraulic conductivity are studied. The test results indicated that compacting bentonites at higher initial water contents and lower dry densities or at lower initial water contents and higher dry densities, yields clay particles to attain more oriented fabric that offer more tortuous paths for the fluid flow that may reduces the hydraulic conductivity.

The effect of high concentration on hydraulic properties showed that the hydraulic conductivity of the bentonite slightly increase with an increase in the concentration of pore fluid due to the contraction of the double layer at micro level leaving more spaces for the flow.

# Chapter 7

# ASSESSMENT OF HYDRAULIC CONDUCTIVITY AND SWELLING PRESSURE

## 7.1 Introduction

This chapter presents the experimental results of hydraulic conductivity and swelling pressures in each of the materials considered. The main aim of this chapter is to study the existing models for hydraulic conductivity and develop new approaches in the existing models to represent the hydraulic conductivity in clays. The experimental hydraulic conductivities of the bentonite in this study are compared with the existing models like: Kozeny-Carman model, Cluster model, and Laminar flow model. Different approaches have been considered in models to estimate the hydraulic conductivity such as (i) the Kozeny-Carman model by considering the effective porosity, (ii) the Kozeny-Carman model in conjunction with the diffuse double layer theory, and (iii) the laminar flow model with interlayer pore radii calculated using modified double layer equations, and Cluster model based on using the concept that clays exist as cluster having micro and macro voids. The limitations of each approach in the model have been discussed. Finally, each approach in the model is verified by applying it to conductivity data from literature.

Similarly, an approach to estimate the swelling pressure of compacted bentonite using Gouy-Chapman diffuse double layer theory is presented. A laboratory swelling pressure tests on compacted bentonites (MX-80 and Calcigel) are compared with the calculated swelling pressure using the theory. The study revealed that at low dry density the as prepared total void ratios, $e_T$ are less than theoretical void ratios using diffuse double layer theory, however, reverse behavior has been noticed for high compaction dry densities. New equations were derived on the basis of diffuse double layer theory and experimental swelling pressure data. The method categorizes the different bentonites into two groups depending upon the weighted average valency. Good agreement was observed in all the cases between experimental and estimated swelling pressure using derived equations.

## 7.2 Comparison of experimental results with existing models

The following section presents the comparison between experimental hydraulic conductivity results and the hydraulic conductivity models used in this study.

### 7.2.1 Kozeny-Carman model

Kozeny (1927) and Carman (1937) developed a theory for a series of capillary tubes of equal length for predicting the saturated hydraulic conductivity for soils. The derivation of Kozeny-Carman model is given in more detail in chapter 3. The Equation 3.26 is re-written for clarify as:

$$k_s = 1.99 \times 10^6 \left( \frac{1}{S_o^2} \right) \left( \frac{e^3}{1+e} \right) \qquad \text{(for } 20^{\circ}\text{C)} \qquad (7.1)$$

where: $k_s$ is in m/s.

The K-C model is based on uniform pore sizes and predicts a single value of hydraulic conductivity for a given void ratio. Carman (1937) verified the Kozeny model, and introduced the notion of hydraulic radius, and expressed the specific surface per unit mass of solid. Furthermore, Carman (1939) considered that water does not move in straight channels but around irregularly shaped solid particles. According to Carman (1939) a factor $C_{K\text{-}C} = 5$ gave the best fit with experimental results. The chosen for the coefficient included simultaneously the notions of equivalent capillary channel cross-section and tortuosity. The saturated hydraulic conductivities of compacted bentonite specimens were measured according to the experimental procedure discussed earlier. The hydraulic conductivities were corresponding to the dry densities varying between 1.37 and 1.75 $Mg/m^3$.

Figures 7.1, 7.2 and 7.3 present the relationship between hydraulic conductivity and dry density for distilled water and low initial water content for Calcigel, MX-80 and Kunigel bentonites. The predicted hydraulic conductivity values calculated using K-C model for those bentonites is also shown. The specific gravity and the specific surface area of the bentonites shown in Table 4.1 were considered for calculating the hydraulic conductivities.

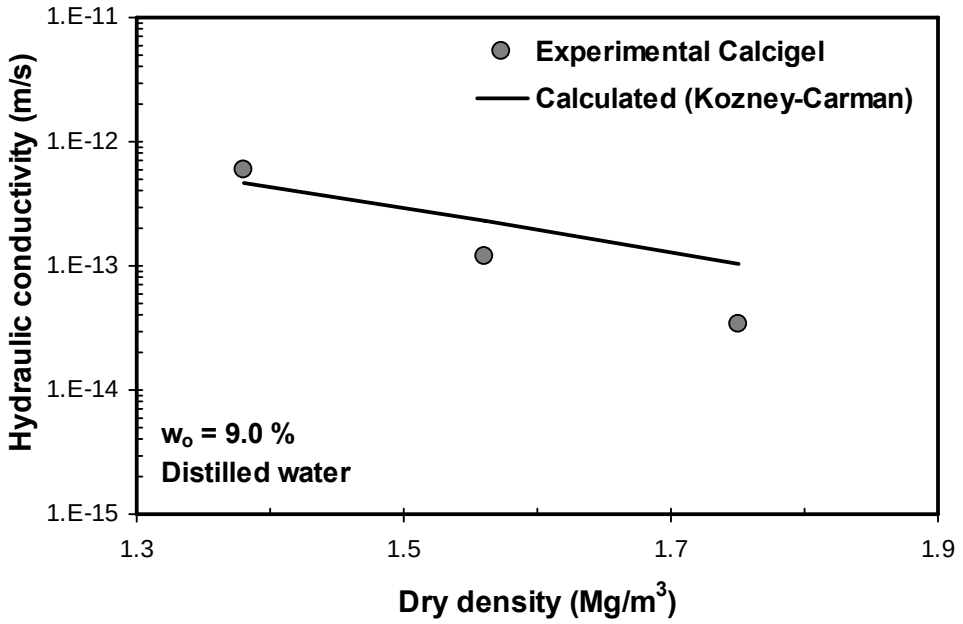


Figure 7.1 Measured and calculated hydraulic conductivity using Kozeny-Carman model for Calcigel bentonite

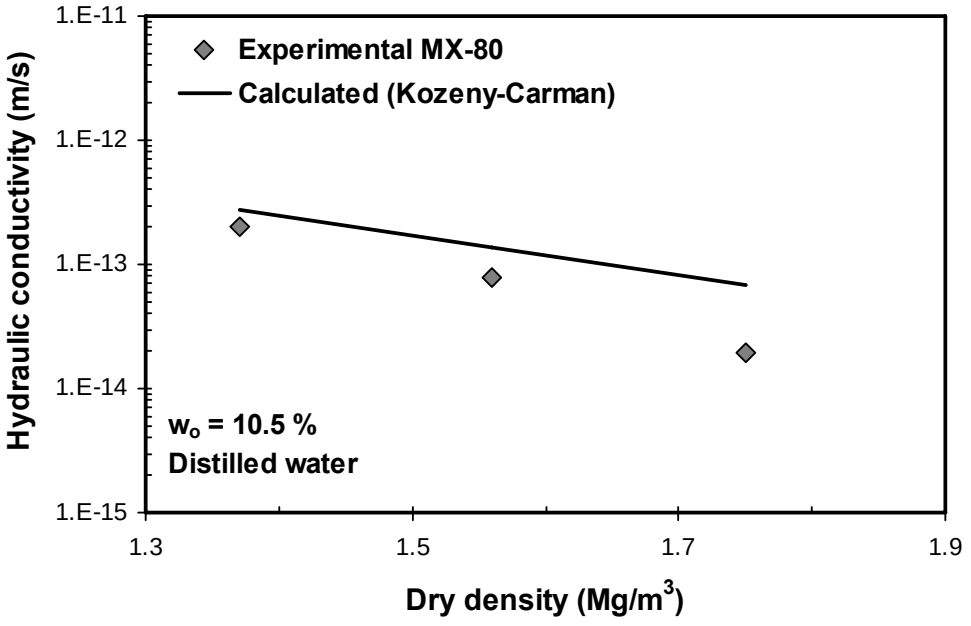


Figure 7.2 Measured and calculated hydraulic conductivity using Kozeny-Carman model for MX-80 bentonite

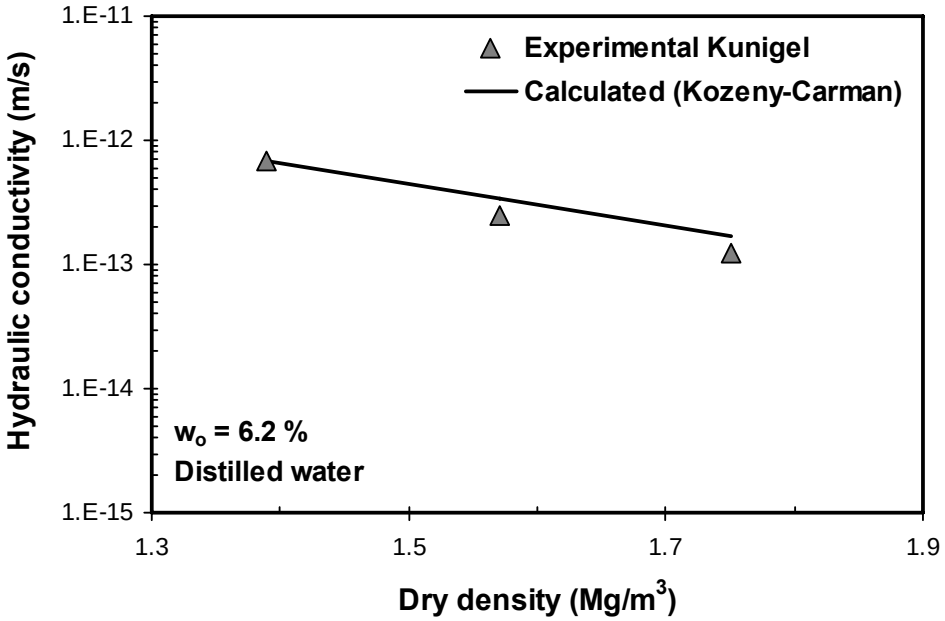


Figure 7.3 Measured and calculated hydraulic conductivity using Kozeny-Carman model for Kunigel bentonite

Figures 7.1 to 7.3 show that the theoretical results from K-C hydraulic model agree reasonably well with the measured hydraulic conductivities especially at low dry densities (i.e., < 1.56Mg/m$^3$). However, it is clear from Figures that as the density increases the prediction using K-C model becomes limited. The reason for the decrease in measured values more than the predicted values for higher dry density is that the porosity available for flow decreases. The amount of adsorbed water in the bentonite is small, some smaller passages or throats may close down as the water becomes locally structured. This small effect can produce reduction in measured hydraulic conductivity at high densities. Pusch (1979) explained the low hydraulic conductivity of the bentonite compacted at high density in terms of the low water contents required to saturate the highly compacted clay, since under these conditions, the thickness of the adsorbed water is very small (3-5 Å) due to its high specific surface, meaning that the molecules of water are strongly adsorbed to the surfaces of the clay minerals, leaving only very tortuous interparticle channels for the transport of water.

### 7.2.2 Cluster Model

Cluster model proposed by Olsen (1962) was used to derive the relationship between hydraulic conductivity and dry density for the selected bentonites. In the cluster model, information on cluster void ratio (i.e., intra-aggregate or micro void ratio) ($e_c$), total void ratio ($e_T$), and average number of clay particles per cluster ($N$) are required. Olsen (1962) assumed relationships between the total void ratio, $e_T$, micro void ratio, $e_c$ and macro void ratio, $e_p$ for which at high total void ratios the micro void ratio, $e_c$ value is constant upon compression and then begins to reduce when $e_p$ ratio is equal to 0.43 (Figure 3.6 in chapter 3).

Achari et al. (1999) used the modified diffuse double layer (DDL) theory in conjunction with the true effective stress concept proposed by Lambe and Whitman (1969) for computing the cluster void ratio. The repulsive force was computed from the basic DDL theory (Equation 2.6) whereas the attractive force is considered to be governed by the van der Waals attractive forces (Equation 3.30). The empirical relationship used to compute the $N$ value as a function of effective stress and concentration of permeant is given in Equation 3.31. The procedure adopted to calculate the micro void ratio, $e_c$, from diffuse double layer theory was as follows. For the given properties of the bentonites (i.e., $G$, $S$, $B$, $v$) and for known experimental swelling pressures, the $u$ values were calculated from Equation 2.6. The corresponding values of $z$ were calculated from Equation 2.7. Knowing $z$ and $u$ for any given swelling pressure, Equation 2.8 was used to calculate $Kd$ and $K$ from Equation 2.9. Knowing the values of $Kd$ and $K$, the distance between clay platelets, $d$ was calculated, after getting $d$ values, micro void ratios, $e_c$, was calculated using Equation 2.10. The number of particles per cluster, $N$, was calculated using Equation 3.31. Figure 7.4 shows the flow chart for the determination of hydraulic conductivity using cluster model.

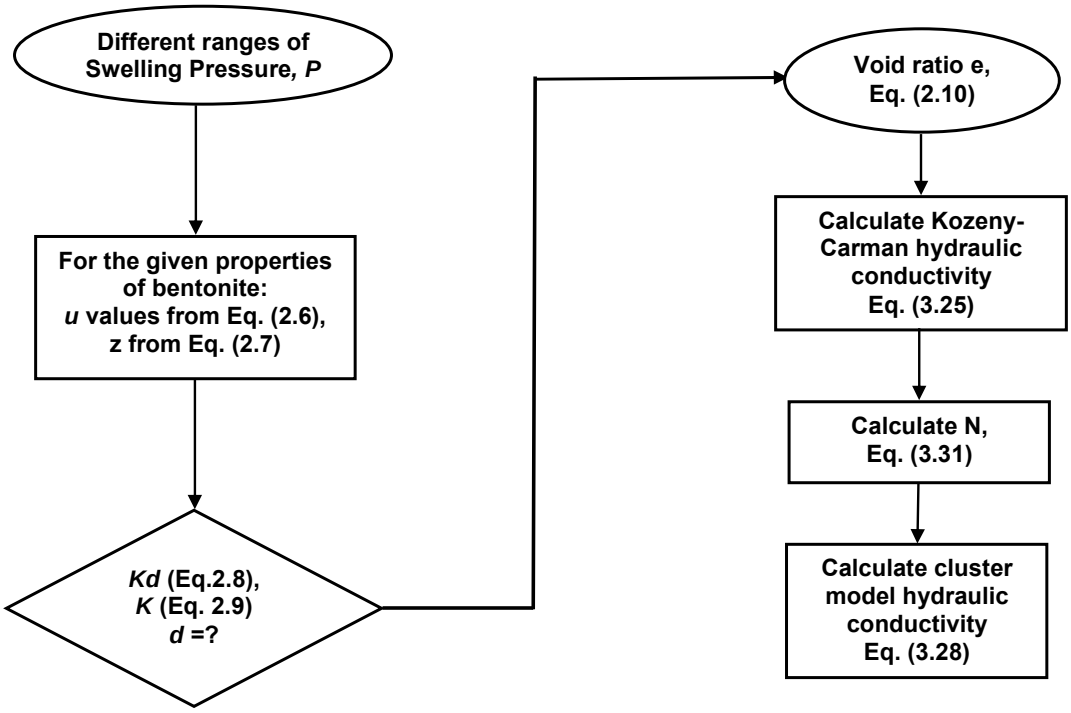


Figure 7.4 Flow chart showing the determination of hydraulic conductivity using cluster model

Figures 7.5 to 7.7 show the experimental and calculated hydraulic conductivities using cluster model with diffuse double layer micro void ratio, $e_c$, for Calcigel, MX-80 and Kunigel bentonites with increasing dry densities. Those Figures clearly indicate that there is not good agreement between the experimental and calculated hydraulic conductivity using micro void ratio, $e_c$, from diffuse double layer theory. The main discrepancies between the experimental and calculated values are due to the fact, that the use of micro void ratio, $e_c$, from diffuse double layer theory does not give appropriate void ratio value due to the limitation of the theory. Several factors may contribute to the discrepancies between the predicted void ratio using diffuse double layer and the experimental results such as: non parallel platelet concept, non uniform size of clay platelets and additional repulsive forces.

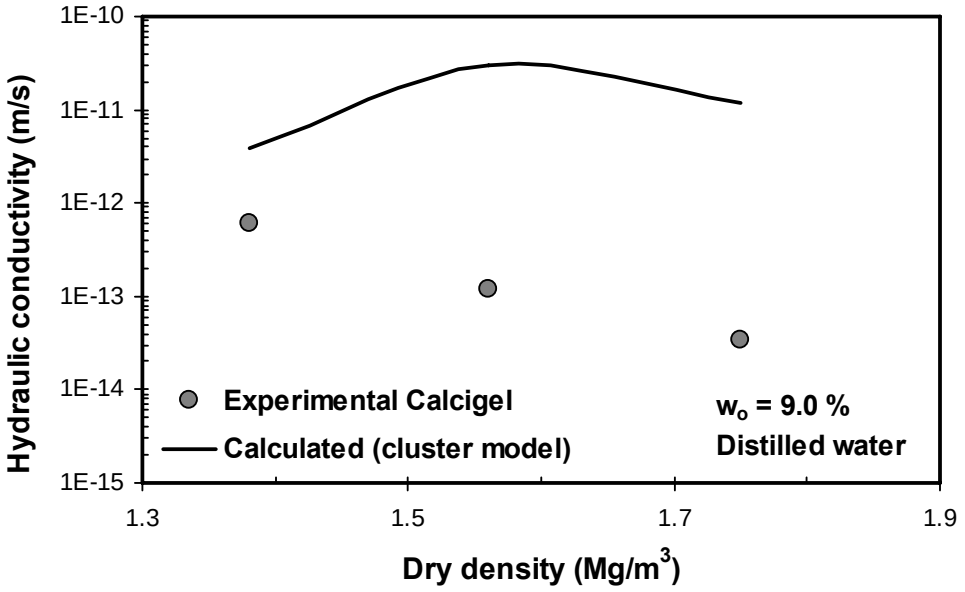


Figure 7.5 Measured and calculated hydraulic conductivity using cluster model for Calcigel bentonite

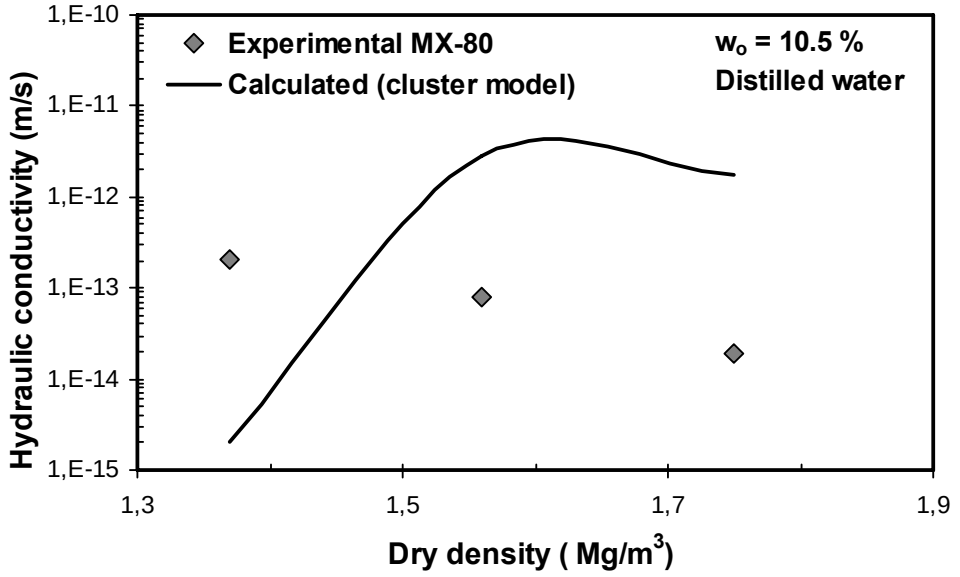


Figure 7.6 Measured and calculated hydraulic conductivity using cluster model for MX-80 bentonite

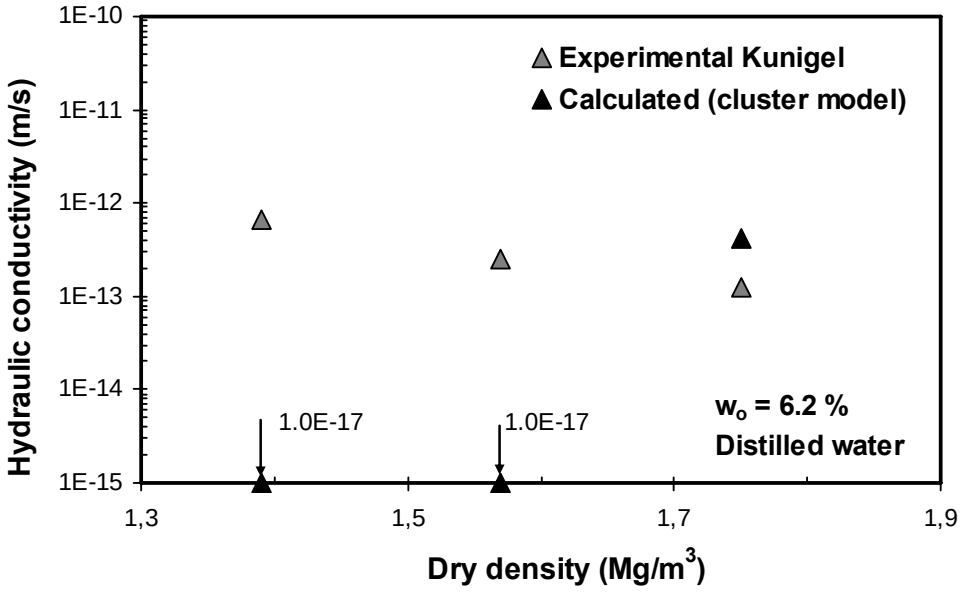


Figure 7.7 Measured and calculated hydraulic conductivity using cluster model for Kunigel bentonite

Diffuse double layer theory assumes an ideal fabric system i.e., the parallel platelets between the clays and uniform size of clay platelets (Nagaraj and Jayadeva 1981, Sridharan and Choudhury 2002, Schanz and Tripathy 2009). Additional repulsive forces can be contributed to the difference between the theory and experimental results, especially in case of high density state (Tripathy et al. 2004). Pashley (1981) and Israelachvili (1982) have also stated that additional repulsive forces could be present when the *d* spacing becomes less. Yong and Mohamed (1992) showed that the repulsive forces arising due to interaction of clay platelets at close particle spacing are primarily due to the hydration of ions. Pusch and Yong (2003) explained that the hydration forces reside in the inner Helmholtz plane where the ions are at their anhydrous state.

As shown in Figures 7.5 to 7.7, the experimental hydraulic conductivity values are less than that of calculated counterpart using cluster model for all ranges of dry densities considered. In case of Calcigel bentonite in Figure 7.5, the calculated values are higher as compared to measured values. Similarly, in case of MX-80 bentonite in Figure 7.6, at low density i.e., 1.38 Mg/m$^3$, the calculated hydraulic conductivity has negative value, which is due to the fact that at low dry density or high void ratio the computed micro void ratio, $e_c$,

from diffuse double layer theory has greater value than total void ratio, $e_T$, resulting in negative hydraulic conductivity, such behaviour can be seen in Figure 7.8 (in case of MX-80 bentonite at high void ratio). At low void ratio value, the total void ratio, $e_T$, is greater than void ratio calculated from diffuse double layer theory, whereas, at high void ratio value, the total void ratio, $e_T$, is less than that of micro void ratio, $e_c$, calculated from diffuse double layer theory.

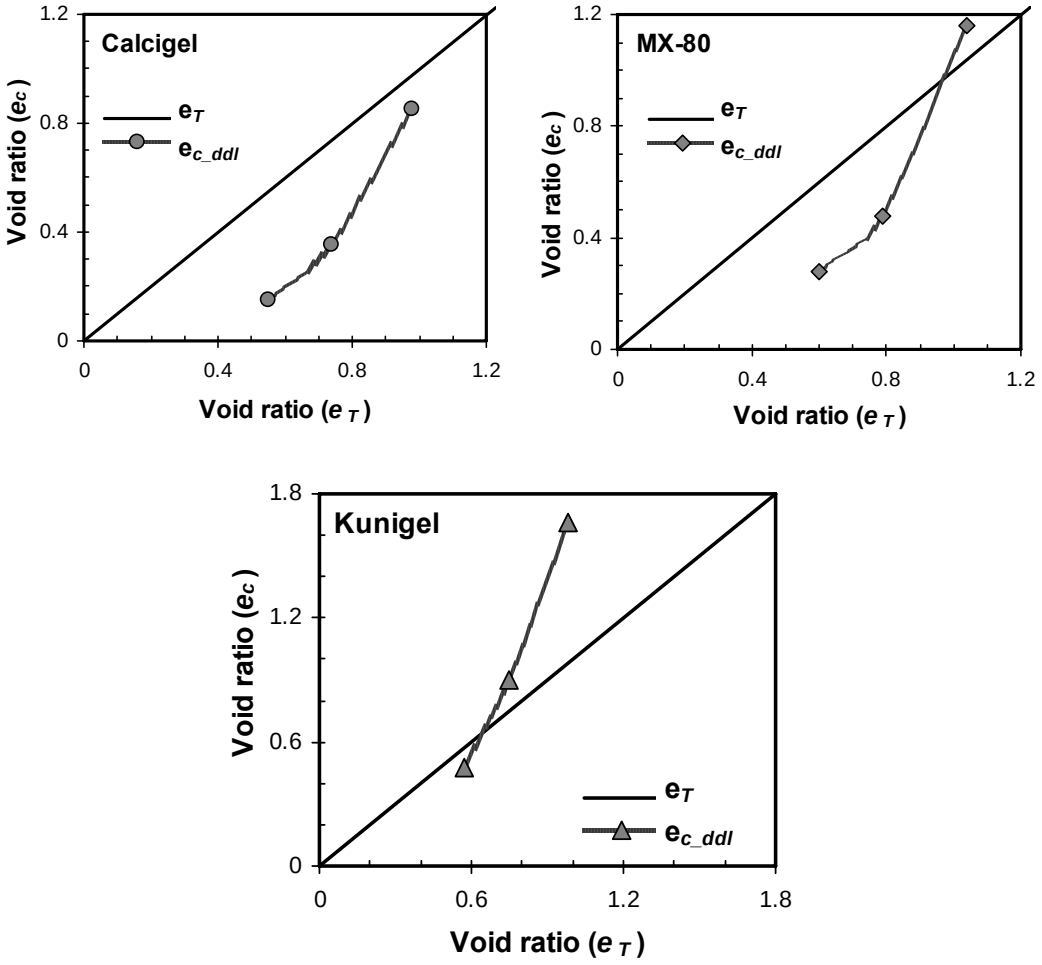


Figure 7.8 Relationship between the total $e_T$, and micro void ratio, $e_c$, from diffuse double layer (ddl) for Calcigel, MX-80 and Kunigel bentonites

### 7.2.3 Laminar flow model

The laminar flow model was developed to predict the average fluid flow through a tubular capillary with circular cross-section (Lambe & Whitman 1969, Mitchell 1993). Komine (2008) suggested that water mainly permeates between two swollen parallel clay platelets. The hydraulic conductivities of bentonite based materials can be predicted by calculating the flow velocity of water between two layers in the clay system. The equation for predicting the flow velocity used by Komine (2008) is given as:

$$k = \frac{\rho_{aw}}{12\mu_{aw}}(2d)^2 \tag{7.2}$$

where: $k$ is in (m/s)

Figures 7.9 to 7.11 depict the variation of hydraulic conductivity with dry density from experimental data in comparison with the Komine (2008) prediction for distilled water and initial water content.

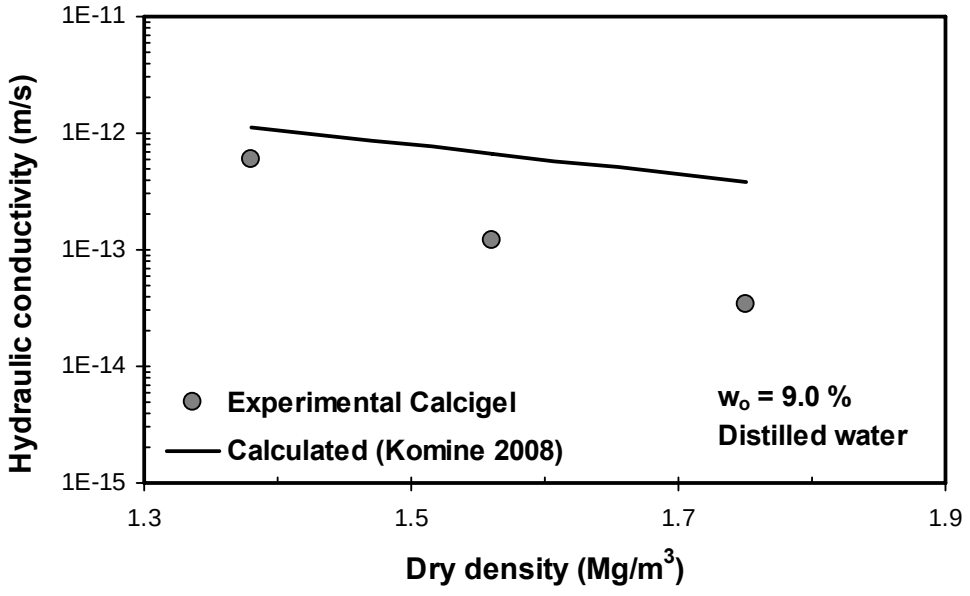


Figure 7.9 Measured and calculated hydraulic conductivity from laminar flow model for Calcigel bentonite

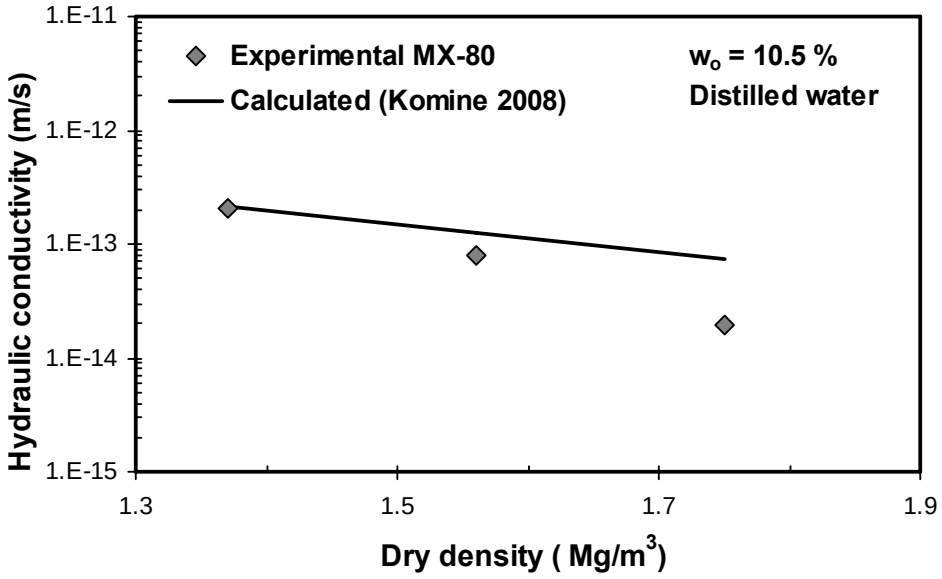


Figure 7.10 Measured and calculated hydraulic conductivity from laminar flow model for MX-80 bentonite

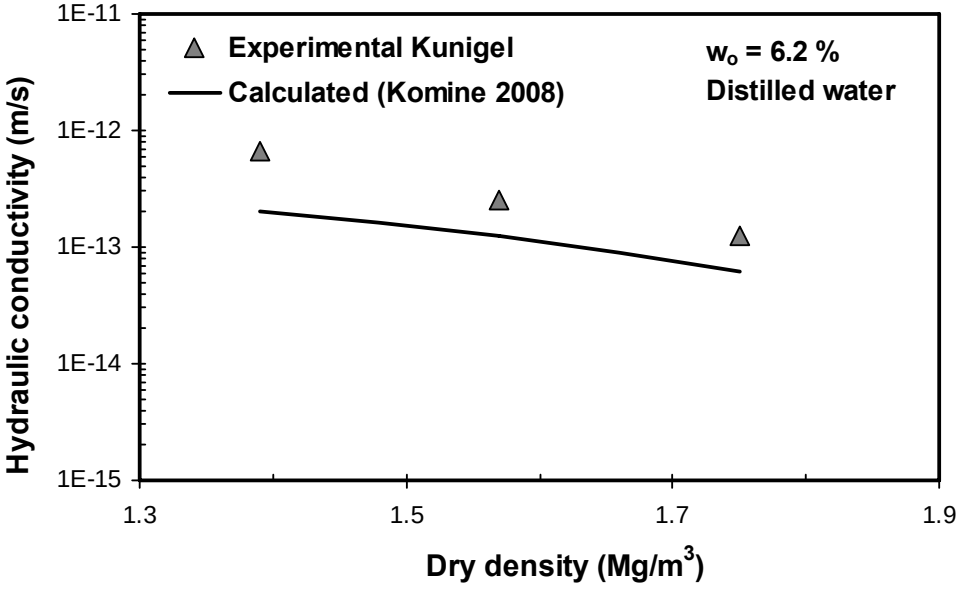


Figure 7.11 Measured and calculated hydraulic conductivity from laminar flow model for Kunigel bentonite

Figure 7.9 shows that the predicted hydraulic conductivity is less than that of measured for the case of Calcigel bentonite which is calcium rich bentonite. The difference between the predicted and experimental data reported by Komine (2008), as in proposed theoretical equations, it is assumed that water flows mainly through spaces between the montmorillonite parallel layers after absorbing water. For low dry density, the filling of voids by swelling of montmorillonite is inadequate, introducing the possibility of remaining voids that serve as water channels (Olsen 1962, Chapuis 1990, Achari et al. 1999, Abichou et al. 2004). However, the prediction of hydraulic conductivity in case of MX-80 bentonite (Figure 7.10) is fairly good at low dry density but as the density increases the agreement between measure and predicted values become limited. Figure 7.11 also indicates that the predicted hydraulic conductivity values are lower than that of experimental results in case of Kunigel bentonite. Komine (2008) reported that the method proposed by him is more accurate for sodium type bentonite and the applicability of the equations reduces for calcium type bentonites. The inaccuracy in the predicted results for calcium bentonite is due to the inaccuracy in applying the parameter on ratio of density and viscosity between interlayer water and free water to evaluate the hydraulic conductivity of for calcium type bentonite. Theoretical equations proposed by Komine (2008) for predicting hydraulic conductivities of bentonite-based buffer and backfill materials according to bentonite content and dry density. The proposed equations for hydraulic conductivity include some equations that are newly proposed for flow model between two parallel-plate layers. They were developed previously to describe swelling volumetric strain of montmorillonite.

## 7.3 New modifications in the existing models

It can be seen that the existing theories do not capture well enough the hydraulic conductivity in the clays considered. The new approaches were carried out in order to modify the existing models so that the new modified models can represent the hydraulic behaviour of the clays studied as well as other clays from the literature.

### 7.3.1 Kozeny-Carman model

As presented in the preceding section 7.2.1, the prediction of hydraulic conductivity using Kozeny-Carman model becomes limited for high ranges of dry density. Two new

approaches were developed in KC model to estimate the hydraulic conductivity of bentonite type materials i.e., (i) the Kozeny-Carman model by considering the effective porosity, (ii) the Kozeny-Carman model in conjunction with the diffuse double layer theory.

#### 7.3.1.1 Kozeny-Carman model (effective porosity approach)

Water in the soil pores is be said to be distributed between two phases, the phase containing free water, which is free to flow under a hydraulic gradient and second phase (adsorbed layer), which is made up of two or three layers of molecules and is directly affected by the particle surface forces (Fripiat et al. 1982, Zhu & Granick 2001). The thickness of the second phase is not fixed, but is a function of the electrochemical environment (Holtz & Kovacs 1981, Mitchell 1993) as well as interparticle stress (Lambe & Whitman 1969). In case of clay, particles interact with each other to form domain and aggregates. The particle association in the domain is characterized as either flocculated with edge to edge contact or dispersed with face to face (Holtz & Kovacs 1981). The most commonly used term that relates to the flow and transport processes of the medium is the porosity. In case of clay, fraction of pore volume does not conduct fluid and this volume has to be subtracted from total volume to give effective porosity. The fraction of the volume of water in the pore system that is not able to move under an induced gradient is held in "interconnected" pores, dead end pores, and adsorbed onto the mineral surface (Singh et al. 2008). The adsorbed water layer in clay affects the flow characteristics of the porous media in two ways. Firstly, the adsorbed water layer affects the effective porosity and secondly the tortuosity and the cross sectional characteristics of the flow conduit may change with changes in interparticle contact area and average inter-particle contact stress.

In the case of compacted bentonites, it is often difficult to precisely determine the effective porosity through which fluid flow takes place. In this study, for known hydraulic conductivities of the bentonites tested with distilled water and initial water content, the void ratios causing fluid flow at various dry densities were calculated from Equation. 7.1. Calcigel and MX-80 bentonites are selected to generate the equations. The tested bentonites are categorized into two groups according to their average weighted valencies of the cations present in the bentonites (Table 4.1), since the valency of the cations present has an influence on the soil behaviour.

Figure 7.12 shows the calculated effective void ratio versus the dry density of the Calcigel and MX-80 bentonites.

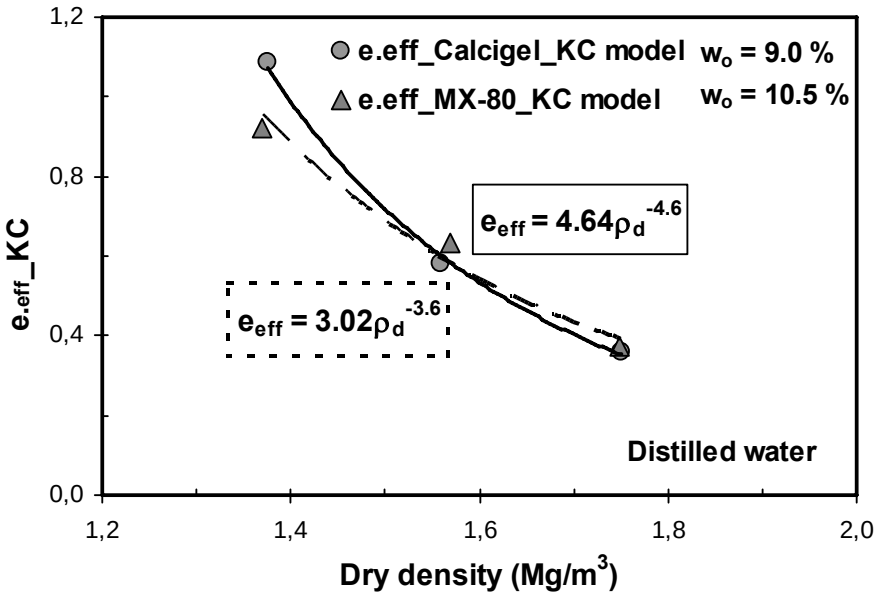


Figure 7.12 Effective void ratios versus dry density relationship for the Calcigel and MX-80 bentonites.

The relationship between the dry density and the effective void ratio (Figure 7.11) can be expressed as:

For MX-80 bentonite

$$e_{eff} = 3.02\rho_d^{-3.6} \qquad \text{valency (1.0 – 1.50)} \qquad (7.3)$$

For Calcigel bentonite

$$e_{eff} = 4.64\rho_d^{-4.6} \qquad \text{valency (1.51 – 1.97)} \qquad (7.4)$$

where: $e_{eff}$ is the effective void ratio and $\rho_d$ is the dry density.

For any compaction dry density, the effective void ratio causing fluid flow can be calculated using Equations 7.3 and 7.4. The effective void ratio can be used in Equation 7.1 instead of total void ratio to calculate hydraulic conductivity of bentonites.

#### 7.3.1.1.1 Verification and Application

The calculated hydraulic conductivities versus the experimentally measured hydraulic conductivities for the bentonites considered in this study are shown in Figure 7.13. Additionally, reported hydraulic conductivities of six other bentonites, such as Calcigel, Kunigel, Kunigel V1, MX-80, Febex, and Na-Kunigel (Pusch 1980, ENRESA 2000, Marcial et al. 2002, Komine 2008, Baille 2010) were considered to verify the applicability of Equations 7.3 and 7.4. The cation exchange capacities, the specific surface areas, weighted average valencies and other properties of the bentonites are shown in Table 7.1. Febex bentonite is a Spanish bentonite from Almeria, Spain. Kunigel VI bentonite is produced at Tsukinuno mine in Japan. Calcigel bentonite has been extracted from Bavaria, Germany. Comparing the physical properties of the bentonites in Table 7.1, Febex bentonite has a higher percentage of montmorillonite than Calcigel bentonite. Febex bentonite was found to contain about 59% of bivalent exchangeable cations ($Ca^{2+}$ and $Mg^{2+}$), whereas, for Calcigel bentonite, the bivalent cations were about 95%. The monovalent exchangeable cations ($Na^{+}$ and $K^{+}$) for Febex and Calcigel bentonite were about 22% and 5% respectively. The cation exchange capacity of Febex bentonite is higher than those of Calcigel bentonite, Kunigel and MX-80. The physical properties of MX-80 bentonite in present study are used for the MX-80 (Pusch 1980).

Knowing the dry densities of the bentonites, the effective void ratios were calculated from Equations 7.3 and 7.4. Further, the calculated effective void ratios were used to calculate the hydraulic conductivities of the bentonites and were compared with the experimental results (Figure 7.13).

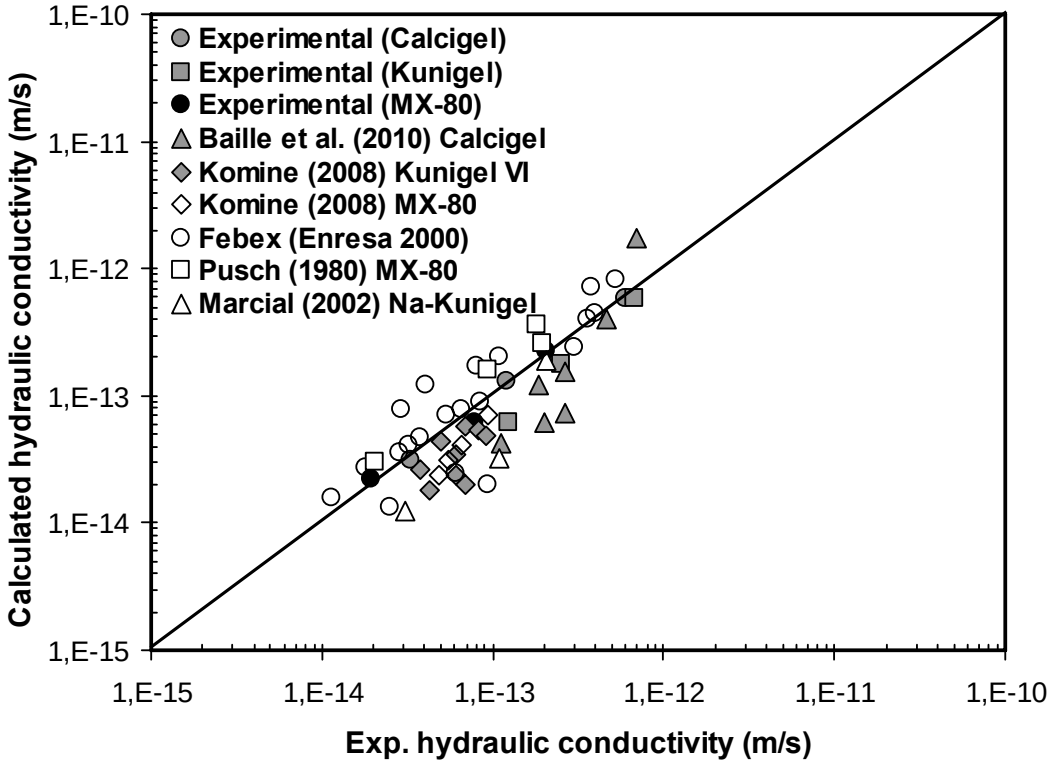


Figure 7.13 Calculated versus measured hydraulic conductivity for the bentonites using new approach

Figure 7.13 shows that the calculated hydraulic conductivity results generally agree well with the experimental results. The results also indicate that the effective void ratios of the bentonites are independent of the chemical properties; because no physico-chemical effect has been consider in this approach, however, the hydraulic conductivity is dependent upon the dry density and the specific surface area of the bentonites.

Table7.1. Properties of bentonites used for verification

| Bentonites | Specific gravity, G | Liquid limit, (%) | Cation exchange capacity (meq./100g) | Specific surface area ($m^2/g$) | Montmorillonite (%) | Weighted average valency, $v$ | Initial water content (%) |
|---|---|---|---|---|---|---|---|
| Calcigel | 2.80 | 178 | 74 | 525 | 60 | 1.93 | 9.2 |
| Febex | 2.70 | 102 | 111 | 725 | 92 | 1.73 | 13.7 |
| MX-80 | 2.80 | 495 | 91 | 711 | - | 1.27 | 10.2 |
| Kunigel VI | 2.79 | 473 | 76 | 388 | 48 | 1.50 | 5 - 6 |
| MX-80* | 2.77 | 520 | 110 | 616 | 80 | 1.41 | 8 - 9 |
| Na-Kunigel | 2.79 | 474 | 73 | 685 | 64 | 1.50 | 5 - 7 |

**Note:** Data from. Baille et al. (2010) for Calcigel, ENRESA (2000) for Febex, (Pusch 1980, values as present study) for MX-80, Komine (2008) for MX-80* and Kunigel VI, Marcial et al. (2002) for Na-Kunigel

Note that in Equation 7.1, the total specific surface areas of the bentonites were considered to calculate the hydraulic conductivities. If the total compaction void ratios are not responsible for the fluid flow, then the specific surface area contributing to the fluid flow should be determined alternatively, which has not been considered in this study.

#### 7.3.1.2 Kozeny-Carman model with diffuse double layer void ratio (reduce specific surface area approach)

The Gouy–Chapman diffuse double layer theory for parallel clay platelets has been widely used to understand the behaviour of clay-water system (Mitchell 1993). Based on the theory five important equations (Equations 2.6 to 2.10) are used to establish swelling pressure versus void ratio relationships for clays (Sridharan & Jayadeva 1982, Schanz and Tripathy 2009).

In this approach, the experimental swelling pressures of the bentonites were considered, the procedure to calculate the void ratio from DDL using the five equations is given section 7.2.2 in detail. Modified specific areas of the bentonites were considered and the hydraulic conductivities were calculated from Equation 7.1. The modified specific surface areas corresponding to various dry densities of the bentonites were determined from the ratio of the specific surface area and the dry density by dividing the specific surface area to the dry density values. In this context, Olsen (1962), Pusch (1980), and Tessier (1998) stated that with an increasing in the compaction effect, the size of the clusters reduce due to break down and rejoining of the particles. Barbour & Yang (1993) also stated that clay clusters are not solid spheres but soft agglomerates and are prone to modification and disintegration by increase in the applied stresses.

Figure 7.14 shows the experimental versus calculated hydraulic conductivities for the bentonites considered in this study. Additionally, the reported experimental hydraulic conductivities and the calculated hydraulic conductivities based on the swelling pressures of other bentonites are also shown in Figure 7.14. In general, a majority of the data points remained above the agreement line ($45^0$-line) indicating that the calculated hydraulic conductivities are less than their experimental counterparts.

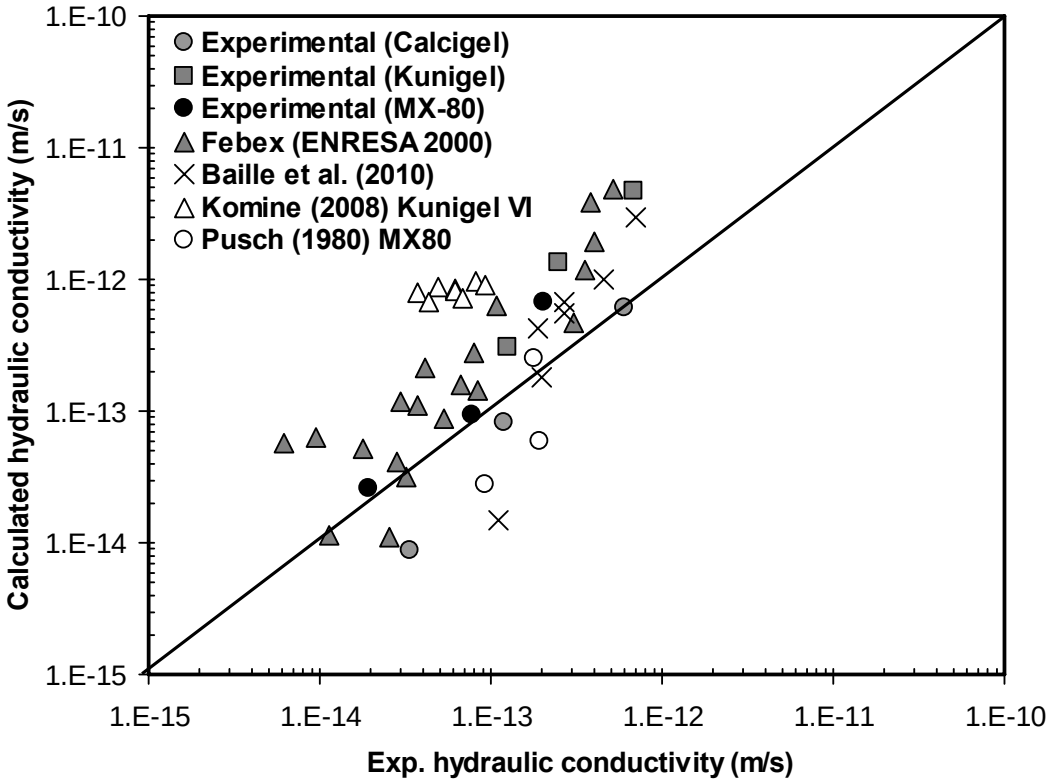


Figure 7.14 Calculated versus measured hydraulic conductivity for the bentonites using new approach

The main deficit in this approach is that although the specific areas of the bentonites were modified to calculate the void ratios causing the fluid flow, the half-spacing between the clay platelets (i.e., d) were calculated based on the diffuse double layer theory that considered the total specific surface areas of the bentonites. A lack of compatibility in the consideration of the specific surface areas caused the discrepancies between the calculated and experimental hydraulic conductivities of the bentonites.

### 7.3.2 Cluster model

It has been discussed in section 7.2.2 that hydraulic conductivity from cluster model using micro void ratio, $e_c$ from diffuse double layer theory do not give appropriate prediction.

An attempt was made to account for the micro void ratio, $e_c$, by back calculating from the cluster model using experimental hydraulic conductivity with increasing dry density of the bentonites. For the known experimental hydraulic conductivity, the micro void ratios, $e_{c\_bk}$, were back calculated using Equation 3.28. The relationship between the total void ratio, and micro void ratio was established. Figure 7.15 show the relationship between the back calculated micro void ratio, $e_{c\_bk}$, using Equation 3.28 for known hydraulic conductivity and total void ratio, $e_T$ for MX-80 and Calcigel bentonites. A linear relationship was found between $e_{c\_bk}$ and total void ratio, $e_T$. Recalling Figure 3.6 proposed by Olsen (1962), which assume relationships between the $e_T$, $e_c$ and $e_p$ for which at high total void ratios the micro void ratio, $e_c$ value is constant upon compression and then begins to reduce when *ep* ratio is equal to 0.43. As compression continues, the $e_c$ has linear relationship with $e_T$ until both values (void ratios) reaches to zero (Figure 3.6).

The assumption proposed by Olsen (1962) is in close agreement with the observed behaviour of back calculated micro void ratio, $e_{c\_bk}$ (Figure 7.15). However, there is no unique relationship between the total void ratios, $e_T$, and back calculated micro void ratio, $e_{c\_bk}$, for both bentonites (MX-80 and Calcigel) as can be seen in Figure 7.15. Therefore, in present study the bentonites were grouped depending upon their weighted average valency. The work presented by Tripathy et al. (2004) and Schanz and Tripathy (2009), the weighted average valency has been used to categorize the swelling behaviour of different bentonites.

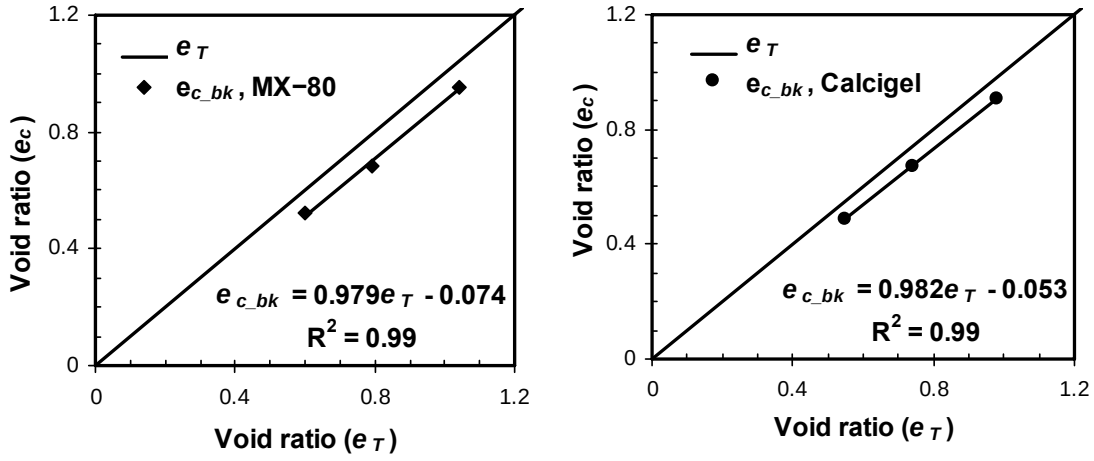


Figure 7.15 Relationship between the $e_T$, $e_c$, and $e_{c\_bk}$ from cluster model for MX-80 and Calcigel bentonites

In Equation 3.28, to compute the hydraulic conductivity, $k_{CM}$ of bentonite, the parameter, $k_{KC}$, can be predicted using Equation (3.26 or 7.1). Knowing the swelling pressure of the bentonites, the number of particles per cluster, $N$, can be calculated using Equation 3.31. By knowing all the parameters i.e., $k_{KC}$, $e_T$, $N$, Equations 7.5 and 7.6 can be used to calculate the hydraulic conductivity. Figure 7.16 shows the algorithm of the proposed method.

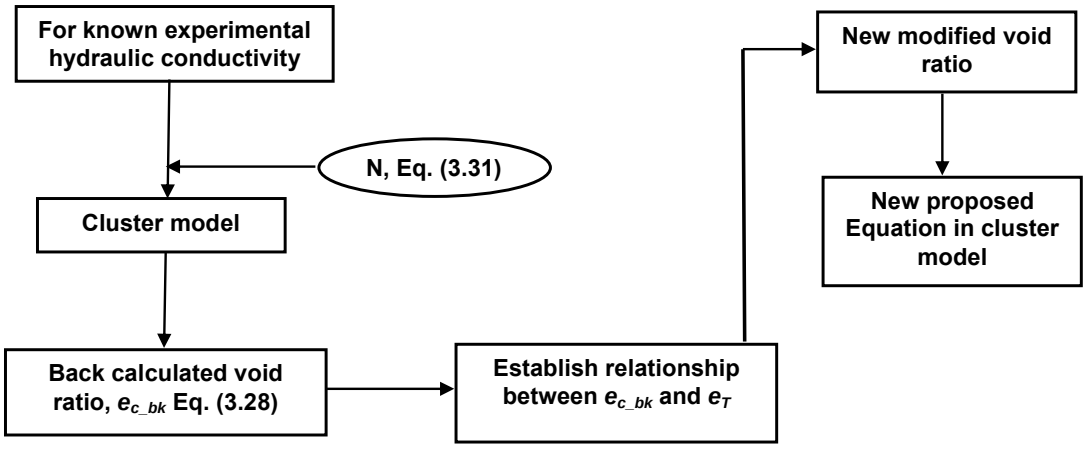


Figure 7.16 Algorithm of the proposed method

Actually Equations 7.5 and 7.6 are the modified forms of Equation 3.28. Micro void ratio, $e_c$, in the original equation was replaced by the best fit of $e_{c\_bk}$, of MX-80 bentonite (Equation 7.5). Similarly micro void ratio, $e_c$, in the original equation was replaced by the best fit of $e_{c\_bk}$, of Calcigel bentonite (Equation 7.6). The equations used to determine the hydraulic conductivity for each of the bentonites can be categorize as, Equation 7.5 can be used for bentonites having weighted average cation valency of up to 1.5, and Equation 7.6 for bentonites with a cation valency from 1.51 to 2.0.

The experimental hydraulic conductivity and those calculated from Equations 7.5 and 7.6 for MX-80 and Calcigel bentonites, respectively are shown in Figures 7.17 and 7.18. As expected, the dry density hydraulic conductivity relationships obtained from these two equations are in good agreement with the experimental data for the two bentonites.

$$\frac{k_{CM}}{k_{KC}} = N^{2/3}\frac{(1-(0.979e_T-0.074)/e_T)^3}{(1+(0.979e_T-0.074))^{4/3}} \qquad \text{valency } (1.01-1.50) \qquad (7.5)$$

$$\frac{k_{CM}}{k_{KC}} = N^{2/3}\frac{(1-(0.982e_T-0.053)/e_T)^3}{(1+(0.982e_T-0.053))^{4/3}} \qquad \text{valency } (1.51-2.0) \qquad (7.6)$$

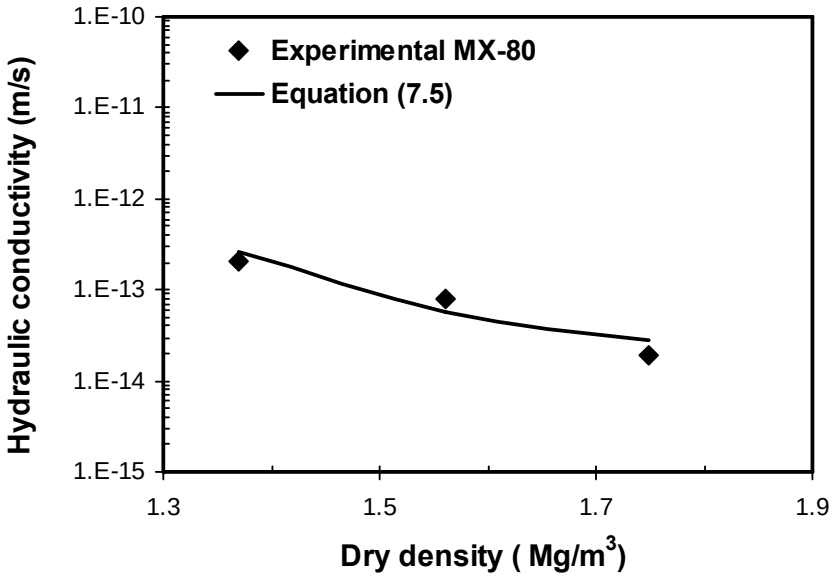


Figure 7.17 Experimental and calculated hydraulic conductivity from suggested equation for MX-80 bentonite

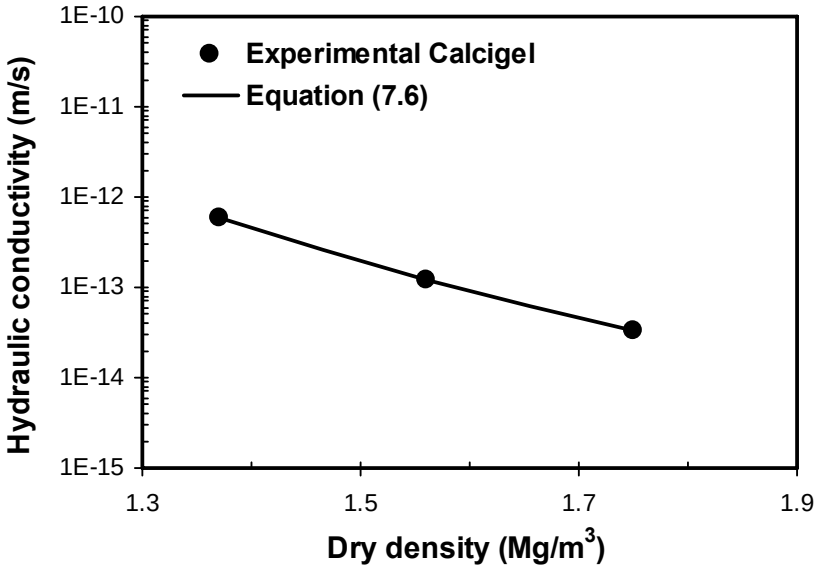


Figure 7.18 Experimental and calculated hydraulic conductivity from suggested equation for Calcigel bentonite

#### 7.3.2.1 Verification and Application

The new Equations (i.e., Eqs. 7.5 and 7.6) derived from the experimental data are for two different types of bentonites having different valencies of exchangeable cations and different mineralogical properties. The investigation was extended to use the equations for other bentonites that are also proposed for use as barrier materials. Experimental hydraulic conductivity results for MX-80 (Pusch 1980), Kunigel (present study), Calcigel bentonite (Baille et al. 2010), and Febex (ENRESA 2000) were chosen for the verification. Table 7.1 shows the properties of the bentonites.

The hydraulic conductivity for MX-80, Kunigel, Calcigel and Febex bentonites were calculated using Equations 7.5 and 7.6 for different dry densities. The calculated hydraulic conductivity from these Equations was matched with the reported experimental hydraulic conductivity of these bentonites. It was observed, however, that Equation 7.5 is applicable to MX-80 and Kunigel bentonites, whereas Equation 7.6 is suitable for Calcigel bentonite and Febex bentonites, which confirms the suggested grouping of average weighted valency of exchangeable cations. The experimental and calculated hydraulic conductivity of the bentonites are plotted in Figures 7.19 – 7.22. The agreement between the proposed equations and the experimental results is good in all cases.

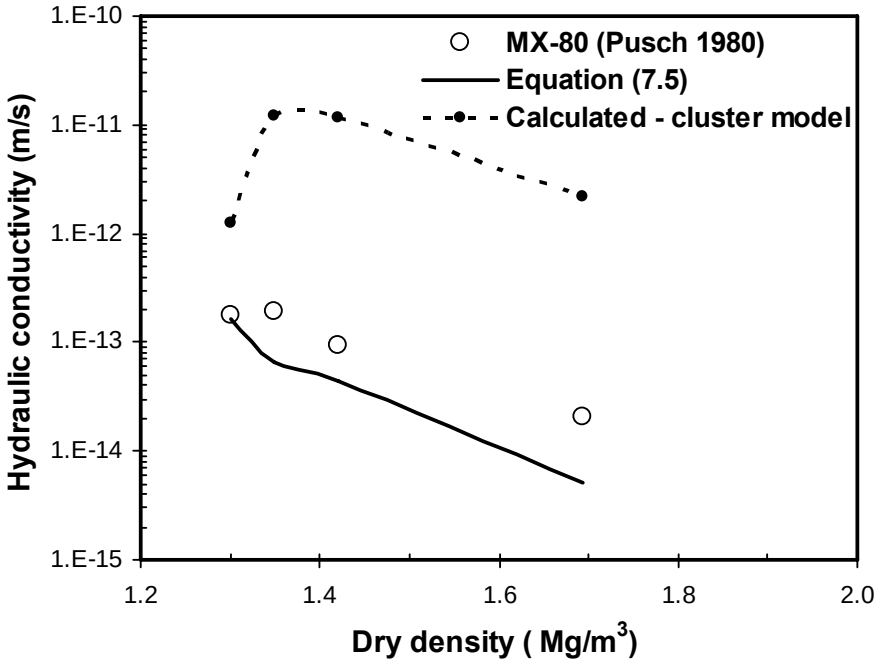


Figure 7.19 Experimental and calculated hydraulic conductivity from suggested equation for MX-80 bentonite (Data from Pusch 1980)

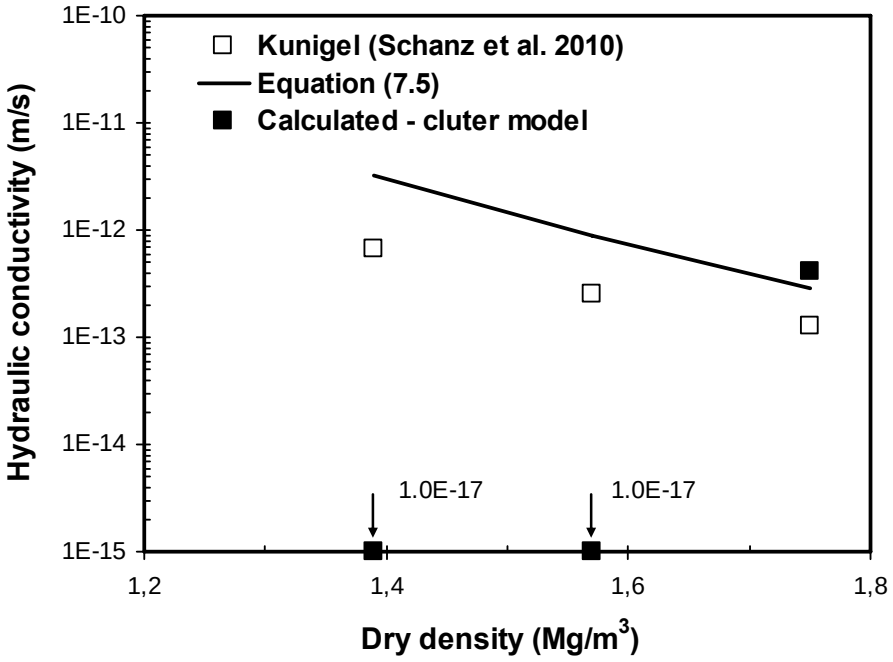


Figure 7.20 Experimental and calculated hydraulic conductivity from suggested equation for Kunigel bentonite (Data from Schanz et al. 2010)

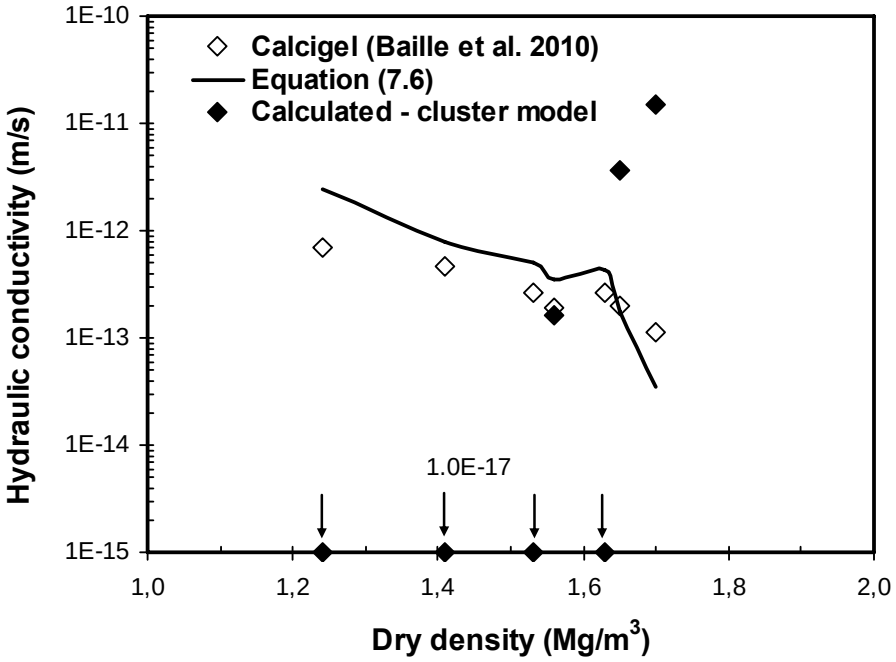


Figure 7.21 Experimental and calculated hydraulic conductivity from suggested equation for Calcigel bentonite (Data from Baille et al. 2010)

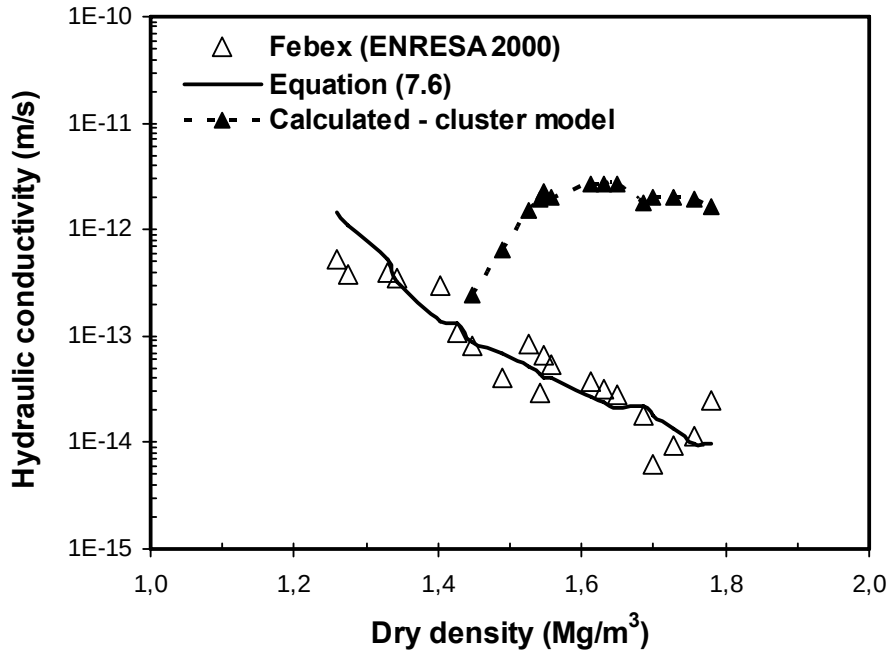


Figure 7.22 Experimental and calculated hydraulic conductivity from suggested equation for Febex bentonite (Data from ENRESA 2000)

Figures 7.19 – 7.22 also show the experimental and calculated hydraulic conductivity using cluster model with diffuse double layer theory micro void ratio. The results clearly indicate that the calculated hydraulic conductivity values are very high (some cases negative values) than the experimental counterpart. The reason for such behaviour is explained in section 7.2.2, which is due to the higher micro void ratio, $e_c$, using DDL than the total void ratio (Figure 7.8). Moreover, as it can be seen that, the calculated hydraulic conductivity using the proposed equations have unsmooth curves, except in case of Kunigel bentonite (Figure 7.20). This behaviour is related to the scattered results of the experimental swelling pressure values used to calculate the number of particles per cluster, $N$, using Equation 3.31.

Figure 7.23 shows the experimental and calculated hydraulic conductivity of the six bentonites considered in this study. The agreement between the experimental and calculated hydraulic conductivity using suggested equations (Eqs. 7.5 and 7.6) is very good for all the bentonites studied.

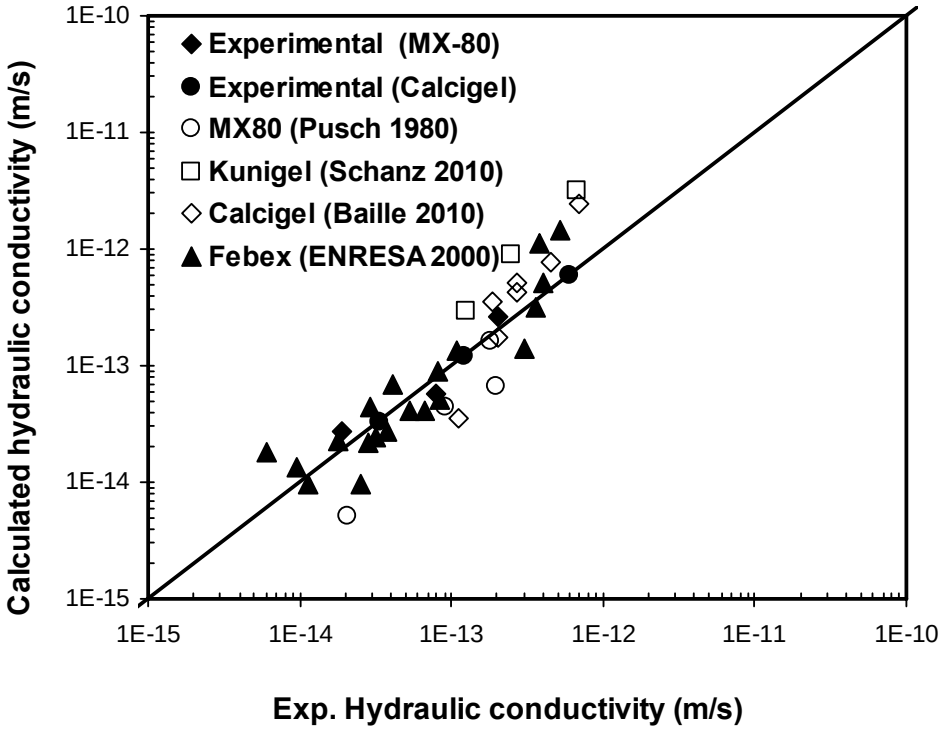


Figure 7.23 Experimental and calculated hydraulic conductivity of bentonites from the suggested equations

### 7.3.3 Laminar flow model

In Equation 7.2, the separation distance between the clay platelet (i.e., 2d) is required to calculate the hydraulic conductivity. Komine (2008) considered the actual hydrated radii of the exchangeable cations present in the bentonites to calculate the separation distance and the hydraulic conductivity. Tripathy et al. (2004) compared the experimental swelling pressure results for several mixed valent compacted bentonites with the swelling pressures determined from the diffuse double layer theory. It was noted that the relationships between the nondimensional midplane potential function (*u*) and nondimensional distance function (*Kd*) derived from the theory and that were back-calculated from the experimental results differed significantly leading to the disagreement between the theoretical predictions and experimental swelling pressure results. Based on the experimental swelling pressure results of several compacted bentonites, they proposed modified *u-Kd* relationships to be considered in Equation 2.6 for determining the swelling pressures of compacted bentonites. The following swelling pressure equations were proposed.

$$p = 2n_0kT(\cosh(-7.277\log 10Kd - 2.91) - 1) \qquad \text{valency (1.14 – 1.50)} \qquad (7.7)$$

$$p = 2n_0kT(\cosh(-10.427\log 10Kd - 7.72) - 1) \qquad \text{valency (1.66 – 1.73)} \qquad (7.8)$$

$$p = 2n_0kT(\cosh(-9.190\log 10Kd - 3.26) - 1) \qquad \text{valency (1.95 – 1.97)} \qquad (7.9)$$

Tripathy et al. (2004) noted that Equations 7.7 to 7.9 could be used for several bentonites based on the weighted average valency of exchangeable cations present in the clay. Equation 7.7 was found to be suitable for the bentonites containing greater percentage of $Na^+$ ions with the weighted average valency of exchangeable cations of 1.14 – 1.50. Equation 7.8 was found to be suitable for the bentonites with the values of the weighted average valency of exchangeable cations of 1.66 and 1.73. Similarly, Equation 7.9 is based on the test results for a divalent bentonite.

In the present study, for the known experimental swelling pressures of the bentonites, the half-distance between clay platelets (*d*) were calculated from Equation 7.7 for MX-80

bentonite and Equation 7.9 for Calcigel bentonite. Further, using Equation 7.2 the hydraulic conductivities of the bentonites were calculated. The specific surface areas and the weighted average valency of exchangeable cations of the bentonites shown in Table 4.1 were considered. Similarly, reported swelling pressures, specific surface areas, and the weighted average valencies for other bentonites (Table 7.1) were considered to calculate the hydraulic conductivities. Equations 7.7 to 7.9 were appropriately used to determine the distance between platelet (*d*) values. The hydraulic conductivities of the bentonites were calculated using Equation 7.2.

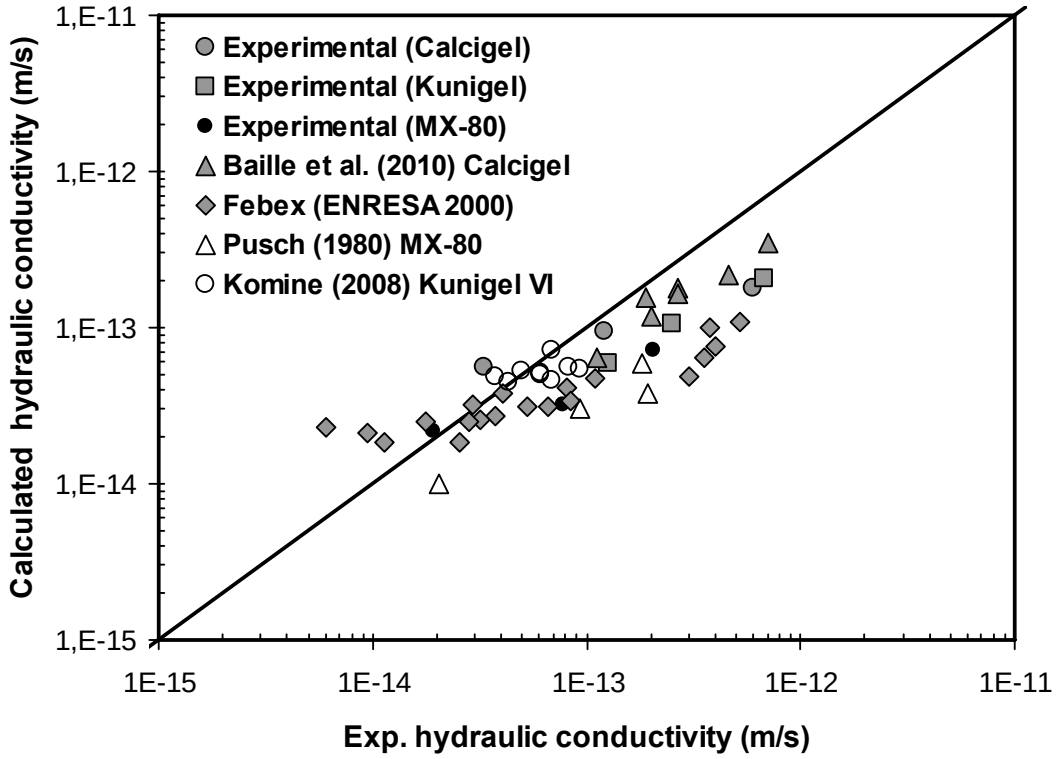


Figure 7.24 Calculated versus measured hydraulic conductivity for the bentonites using modified DDL equations

Figure 7.24 shows the experimental versus calculated hydraulic conductivities for all the bentonites considered in this study. A majority of the data points remaining below the agreement line ($45^0$-line) in Figure 7.24 clearly indicate that the calculated hydraulic conductivities of most bentonites are somewhat less than their experimental counterparts. The main limitation of this approach is that the separation distance between the clay platelets are calculated based on the modified equations that in turn are based on the

diffuse double layer theory. It was assumed in Equations 7.7 - 7.9 that the clay platelets in compacted clay-water ion systems are uniformly distributed which may not be completely true.

## 7.4 Estimation of swelling pressure

As discussed in section 2.5.2, two approaches have been adopted to use the diffuse double layer theory in describing the swelling behaviour of clays. The first approach given by Komine and Ogata (2003) and Xie et al. (2004) considers a single DDL without interaction between one DDL and another whereas the second approach proposed by Sridharan and Jayadeva (1982) and Tripathy et al. (2004) considers interacting DDL. The former approach may be applicable in the case of clay suspension while the later approach appears to be more applicable for compacted clays. Moreover, various approaches have been proposed in the past for determining the swelling pressure of clays.

Low and Margheim (1979) and Low (1980) suggested an empirical exponential relationship between dry density and swelling pressure for Na-montmorillonite clays. Madsen and Müller-Vonmoos (1985) reported a good agreement between the theoretical and experimental swelling pressures of an over consolidated Jurassic opalinum shale. Gens and Alonso (1992) stated that the advantage of using the diffuse double layer theory is that various parameters responsible for swelling of clays can be varied as and when required. Shang et al. (1994) discussed various applications of the theory in geotechnical and environmental practices. An attempt was made by Komine and Ogata (1996) to use the theory for determining the swelling strain and swelling pressure of a highly compacted bentonite. New equations were suggested based on the equations for single clay platelets. Sridharan and Choudhury (2002) proposed a swelling pressure equation for Na montmorillonite while analyzing the compression data of slurried samples of Na montmorillonite, reported by Bolt (1956), Mesri and Olson (1971), and Low (1980).

Tripathy et al. (2004) compared the experimental swelling pressure results for several mixed valent compacted bentonites with the swelling pressures determined from the diffuse double layer theory. Based on the experimental swelling pressure results of several compacted bentonites, they proposed modified *u-Kd* relationships to be considered for determining the swelling pressures of compacted bentonites.

### 7.4.1 Experimental and theoretical swelling pressure

Figures 7.25 – 7.26 show the *u–Kd* relationships for MX-80 and Calcigel bentonites respectively, the $n_0$ (ionic concentration of bulk fluid) value considered in this study is $10^{-4}$ M, which is equal to distilled water. To establish the theoretical *u–Kd* relationships for MX-80 and Calcigel bentonites, the following procedure was adopted: (*i*) for known swelling pressure values, *u* values were computed using Equation 2.6, (*ii*) actual *B* and *S* values were considered for computing $(dy/d\xi)_{x=0}$ values and then *z* values using Equation 2.7, and (*iii*) the corresponding *Kd* values were computed by numerical integration using Equation 2.8. To avoid interpolation for intermediate values of *Kd*, the *u* versus *Kd* values were plotted for each of the bentonites (Figures 7.25 – 7.26). From the plots, the best-fit equations were obtained for each of the bentonites using a least-squares method and the equations are also shown in the figures. These equations are then used to determine the *u* values for the computed *Kd* values and can be stated as:

$$u = 3.86 - 1.392\,In\left(Kd\right) \tag{7.10}$$

$$u = 3.56 - 1.434\,In\left(Kd\right) \tag{7.11}$$

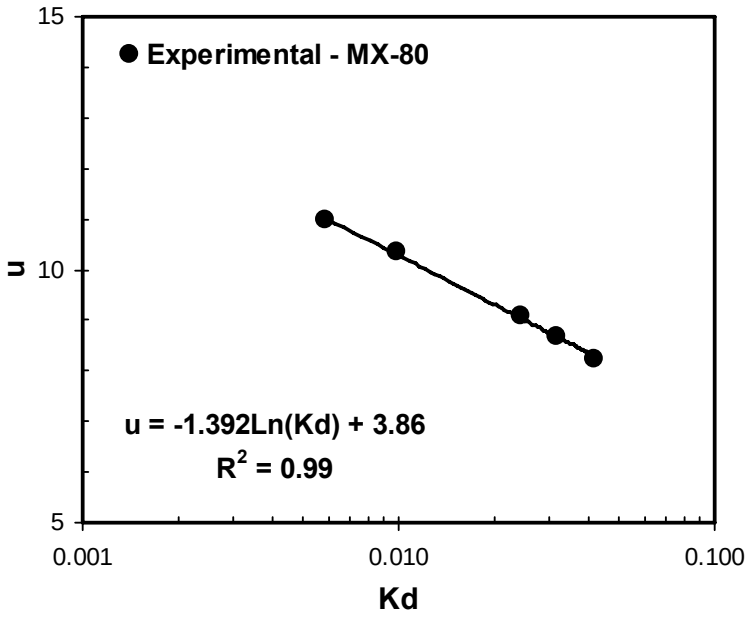


Figure 7.25 Theoretical *u-Kd* relationship of MX-80 bentonite ($v$ = 1.27)

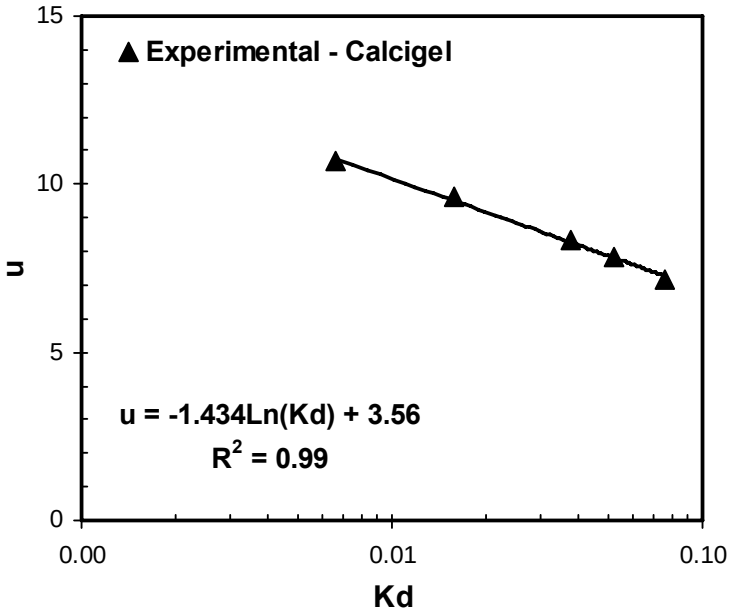


Figure 7.26 Theoretical *u-Kd* relationship of Calcigel bentonite ($v$ = 1.95)

Figures 7.27 - 7.28 show the experimental swelling pressure results for the corresponding dry densities of the MX-80 and Calcigel bentonites considered in the study. The equilibrium swelling pressure values were considered for comparing with the theoretical swelling pressure dry density relationship for the bentonite. The theoretical swelling pressure dry density relationship was determined using Equations 2.6 to 2.10. The parameters considered for determining the theoretical swelling pressure dry density relationship are shown in Table 4.1.

As can be seen in Figures 7.27 – 7.28 that there is good agreement between the experimental and theoretical swelling pressures at low dry densities (i.e., below 1.4 $Mg/m^3$), whereas at higher dry densities, the experimental swelling pressures are found to be greater than that predicted from the diffuse double layer theory. The disagreement between the theoretical and experimental swelling pressure results can be attributed due to the several factors that arise while applying the diffuse double layer theory to compacted bentonites systems (Schanz and Tripathy 2009) which includes non parallel platelet concept, non uniform size of clay platelets and additional repulsive forces. Diffuse double layer theory assumes an ideal fabric system i.e., the parallel platelets between the clays and

uniform size of clay platelets (Nagaraj and Jayadeva 1981). Additional repulsive forces can be contributed to the difference between the theory and experimental results, especially in case of high density state (Tripathy et al. 2004). Yong and Mohamed (1992) stated that the repulsive forces arising due to interaction of clay platelets at close particle spacing are primarily due to the hydration of ions. For dry densities of the clay greater than 1.4 $Mg/m^3$, the swelling pressures developed can be primarily attributed due to the hydration forces that are much greater than that predicted from the diffuse double layer theory. Pusch and Yong (2003) stated that the hydration forces reside in the inner Helmholtz plane where the ions are at their anhydrous state. Pashley (1981) and Israelachvili (1982) have also stated that additional repulsive forces could be present when the *d* spacing becomes less. Hence the theoretical prediction needs some modification which has been attempted in the following section.

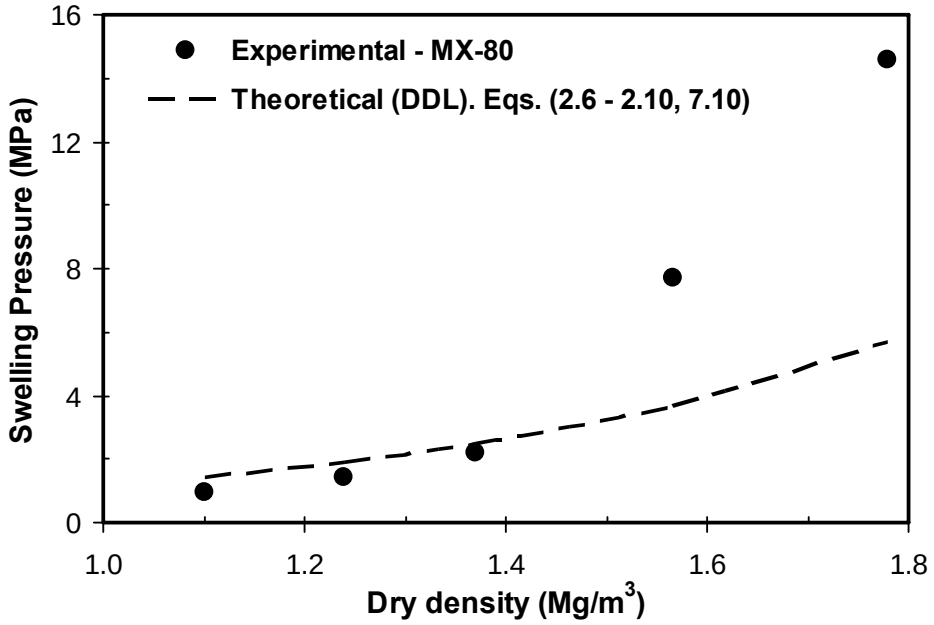


Figure 7.27 Experimental and theoretical swelling pressures of MX-80 bentonite

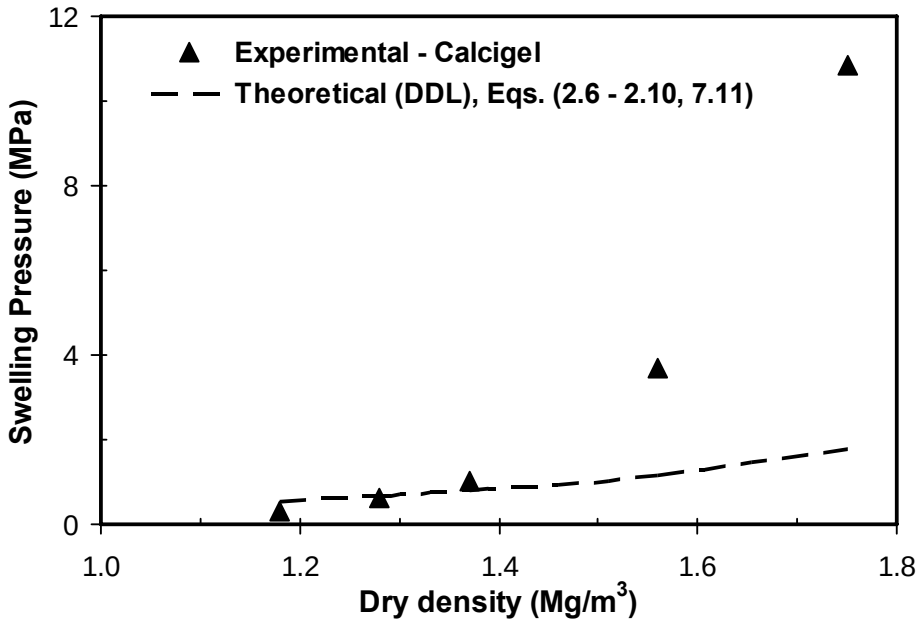


Figure 7.28 Experimental and theoretical swelling pressures of Calcigel bentonite

### 7.4.2 Proposed equations for void ratio

An attempt was made to account for the difference between the experimental and theoretical swelling pressures with increasing dry density of the bentonites. For the known experimental swelling pressures values, the void ratio, $e_d$ was calculated using diffuse double layer theory. The steps to calculate the void ratio, $e_d$ from diffuse double layer have been discussed in previous section. The relationship between the total void ratio, $e_T$ and void ratio, $e_d$ from diffuse double layer was established. Figures 7.29 and 7.30 shows the relationship between total void ratio, $e_T$ and void ratio calculated from diffuse double layer theory, $e_d$. As can be seen in the Figures, in case of MX-80 bentonite, for high total void ratio or for low dry density, the void ratio, $e_d$ calculated using diffuse double layer theory is greater than total void ratio, $e_T$. Similarly, in case of Calcigel bentonite, same trend has been observed. The resulting equations from the best fit line in Figures 7.29 and 7.30 relates total void ratio to the void ratio calculated from diffuse double layer. The new equations for the void ratios are also shown in Figures 7.29 and 7.30 and are given as follow:

$$e_d = 0.896 e_T^{2.09} \tag{7.12}$$

$$e_d = 0.832 e_T^{2.87} \tag{7.13}$$

For the known modified void ratios i.e., $e_d$ shown in Equation 7.12 and 7.13 for MX-80 and Calcigel bentonites respectively, the new $d$ spacing (i.e., half distance between parallel clay platelets) are calculated using Equation 2.10. Knowing $K$ values from Equation 2.9, the new $Kd$ values can be found.

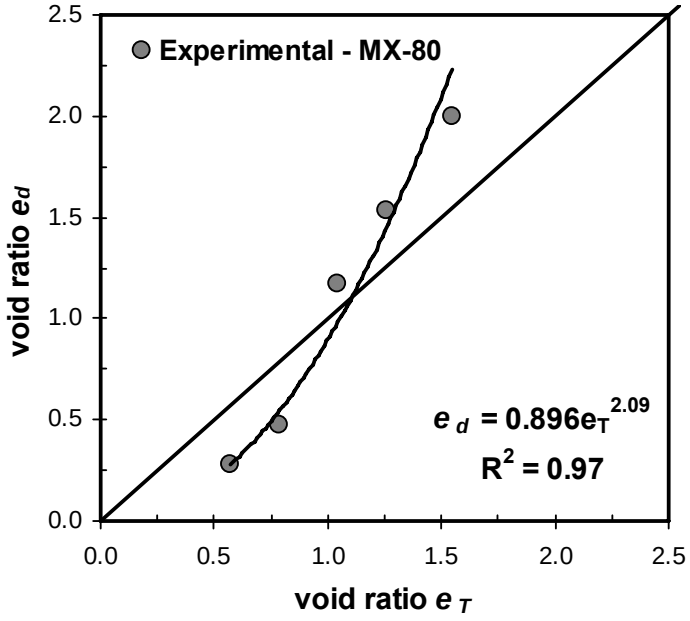


Figure 7.29 Relationship between the total void ratios, $e_T$ and void ratio from diffuse double layer, $e_d$ for MX-80 bentonite

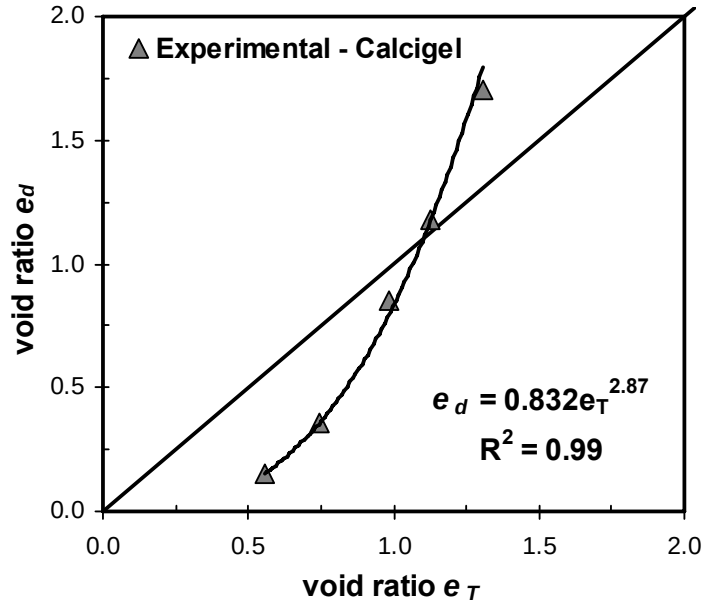


Figure 7.30 Relationship between the total void ratios, $e_T$ and void ratio from diffuse double layer, $e_d$ for Calcigel bentonite

As shown in Figures 7.25 and 7.26, the established *u–Kd* relationship were used to calculate the *u* values by knowing the new *Kd* values from the relationship between total void ratio, $e_T$ and void ratio from diffuse double layer, $e_d$ (Figures 7.29 and 7.30). Hence, Equations 7.10 and 7.11 can be directly used to calculate the *u* values. Substituting the *u* values of Equation 7.10 and 7.11 in Equation 2.6, the equations for swelling pressure are obtained as:

$$p = 2n_0kT(\cosh(3.86 - 1.392In(Kd)) - 1) \qquad \text{valency (1.01 – 1.50)} \qquad (7.14)$$

$$p = 2n_0kT(\cosh(3.56 - 1.434In(Kd)) - 1) \qquad \text{valency (1.51 – 2.00)} \qquad (7.15)$$

or, by using Equation 2.10 with new modified void ratio from Equations 7.12 and 7.13, *d* values can be obtained, and Equations 7.14 and 7.15 can be written as:

$$p = 2n_0 kT(\cosh\left(3.86 - 1.392In(\frac{K \times 0.896e_T^{2.09}}{G\rho_w S \times 10^6})\right) - 1) \qquad \text{v (1.01 – 1.51)} \qquad (7.14a)$$

$$p = 2n_0 kT(\cosh\left(3.56 - 1.434In(\frac{K \times 0.832e_T^{2.87}}{G\rho_w S \times 10^6})\right) - 1) \qquad \text{v (1.01 – 1.51)} \qquad (7.15a)$$

Equations 7.14a and 7.15a relate the swelling pressure to the void ratio for the know clay fluid system. The clay is represented by its specific surface, $S$ and its specific gravity, $G$. The pore fluid properties are given by $K$ (Equation 2.9) and the concentration of ions, $n_o$ in the bulk fluid.

The experimental swelling pressures and those calculated from Equations 7.14 and 7.15 for MX-80 and Calcigel bentonites, respectively are shown in Figures 7.31 and 7.32. As expected, the dry density – swelling pressure relationships obtained from these two equations are in good agreement with the experimental data for the two bentonites.

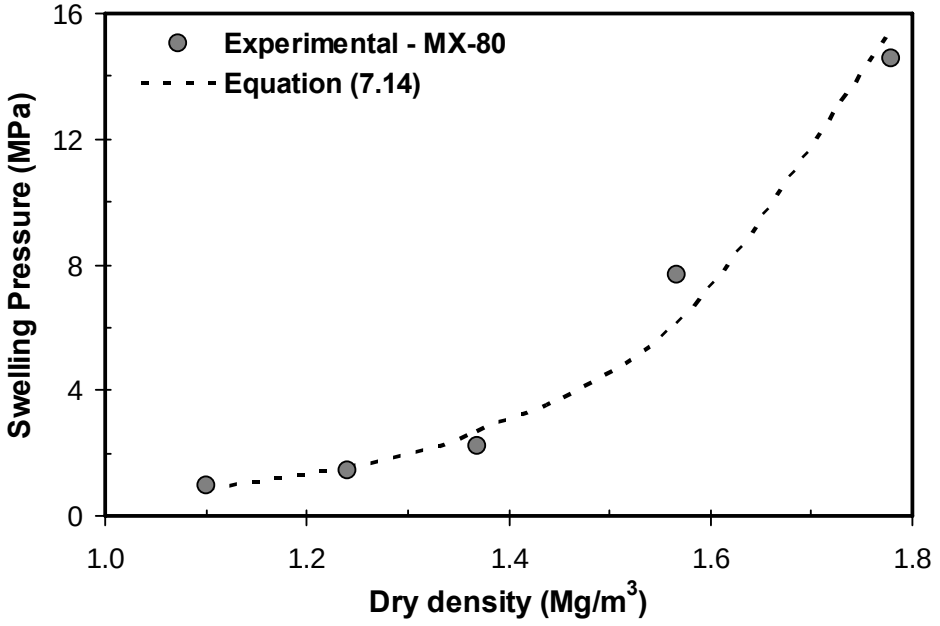


Figure 7.31 Experimental swelling pressure and swelling pressure from suggested equation for MX-80 bentonite

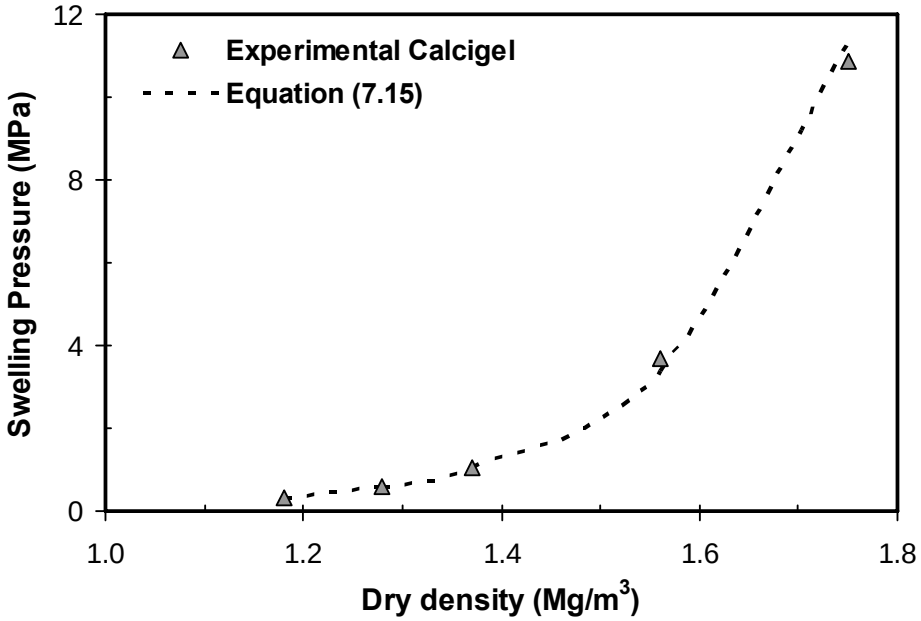


Figure 7.32 Experimental swelling pressure and swelling pressure from suggested equation for Calcigel bentonite

### 7.4.3 Verification of the new swelling pressure equations

The new swelling pressure equations (i.e., Eqs. 7.14 and 7.15) are for two different type of bentonites having different valencies of exchangeable cations and different mineralogical properties. The investigation was extended to use the equations for other bentonites that are also proposed for use as barrier materials. Experimental swelling pressure results for MX-80 (Bucher and Müller-Vonmoos 1989), Volclay (Komine et al. 2009), MX-80 (Komine et al. 2009), bentonite S-2 (ENRESA 2000), Calcigel bentonite (Schanz and Tripathy 2009) and Febex (ENRESA 2000) were chosen for the verification. Table 7.2 shows the properties of the bentonites.

MX-80 is produced in Wyoming in the United States. It contains more monovalent cations than divalent. This is sodium type bentonite. The amount of montmorillonite present in the MX-80 bentonite is about 75 %. Volclay is produced in Wyoming in the United States. This is also sodium type bentonite. The amount of montmorillonite present in the Volclay bentonite is about 69 %. MX-80 (Komine 2009) is also produced in Wyoming in United States. It contains amount of montmorillonite around 76 %. Bentonite S-2 is a Spanish bentonite from Almeria, Spain. The properties of the bentonite are different from those of

the Febex bentonite (ENRESA 2000). Calcigel bentonite has been extracted from Bavaria, Germany. Comparing the physical properties of the bentonites in Table 7.2, Febex bentonite has a higher percentage of montmorillonite than Calcigel bentonite. Febex bentonite was found to contain about 59% of bivalent exchangeable cations ($Ca^{2+}$ and $Mg^{2+}$), whereas, for Calcigel bentonite, the bivalent cations were about 95%. The monovalent exchangeable cations ($Na^{+}$ and $K^{+}$) for Febex and Calcigel bentonite were about 22% and 5% respectively. The cation exchange capacity of Febex bentonite is higher than those of Calcigel bentonite and bentonite S-2. The weighted average valencies for these bentonites (see Table 7.2) are 1.14, 1.43, and 1.49 for MX-80, Volclay and MX-80 (Komine 2009) respectively, whereas, 1.66, 1.90 and 1.73 for bentonite B-2, Calcigel and Febex bentonites respectively.

Table 7.2 Properties of bentonites used for verification of swelling pressure equations

| Bentonites | Specific gravity, G | Liquid limit, (%) | Cation exchange capacity (meq./100g) | Specific surface area ($m^2/g$) | Montmorillonite (%) | Weighted average valency, $v$ |
|---|---|---|---|---|---|---|
| MX-80 | 2.76 | 411 | 74 | 562 | 75 | 1.14 |
| Volclay | 2.84 | 565 | 105 | 560 | 69 | 1.43 |
| MX-80 | 2.88 | 437 | 135 | 615 | 76 | 1.49 |
| Bent. S-2 | 2.78 | 105 | 97 | 615 | 92 | 1.66 |
| Calcigel | 2.80 | 178 | 74 | 650 | 80 | 1.90 |
| Febex | 2.70 | 102 | 111 | 725 | 92 | 1.73 |

**Note:** Data from Bucher and Müller-Vonmoos (1989) for MX-80, Komine et al. (2009) for Volclay, Komine et al. (2009) for MX-80, ENRESA (2000) for bentonite S-2, Schanz and Tripathy (2009) for Calcigel, ENRESA (2000) for Febex.

The swelling for these bentonites were calculated using Equations (7.14 – 7.15) for different dry densities. The calculated swelling pressure from these equations was matched with the reported experimental swelling pressures of these bentonites. It was observed, however, that Equation 7.14 is applicable to MX-80, Volclay and MX-80 (Komine 2009) bentonites, whereas Equation 7.15 is suitable for Calcigel, bentonite S-2 and Febex bentonites, which confirms the suggested grouping of average weighted valency of exchangeable cations. Therefore, Equation 7.14 can be used for the bentonites having a cation valency from 1.01 to 1.50, and Equation 7.15 for bentonites with a cation valency from 1.51 up to 2.0. The experimental and calculated swelling pressures of the bentonites are plotted in Figures 7.33 – 7.38. The agreement between the proposed equations and the experimental results is good in all cases. Figure 7.39 shows the experimental and calculated swelling pressures of the eight bentonites considered in this study. The

agreement between the experimental and calculated swelling pressures using suggested equations (Eqs. 7.14 and 7.15) is very good for all the bentonites studied.

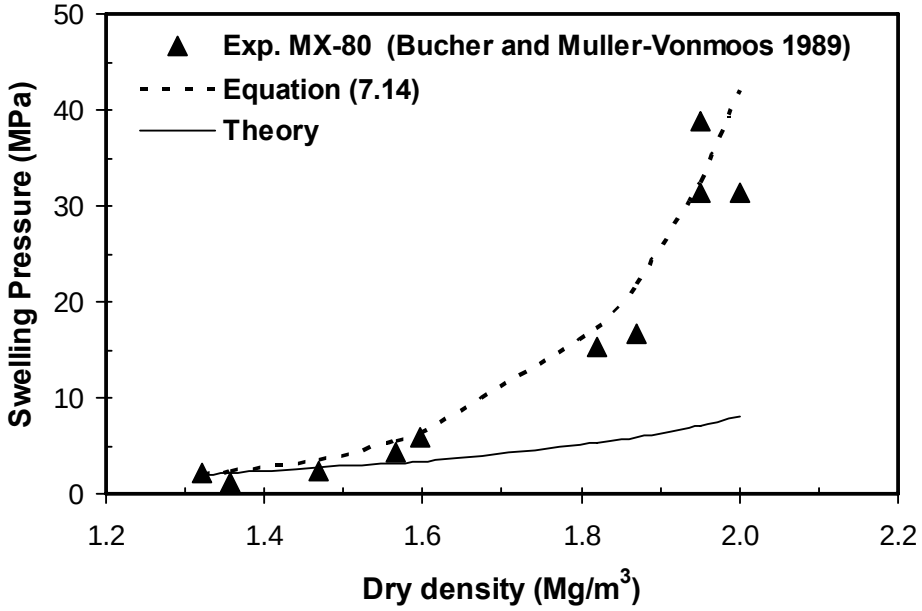


Figure 7.33 Experimental swelling pressure and swelling pressure from suggested equation for MX-80 bentonite (Data from Bucher and Muller-Vonmoos 1989)

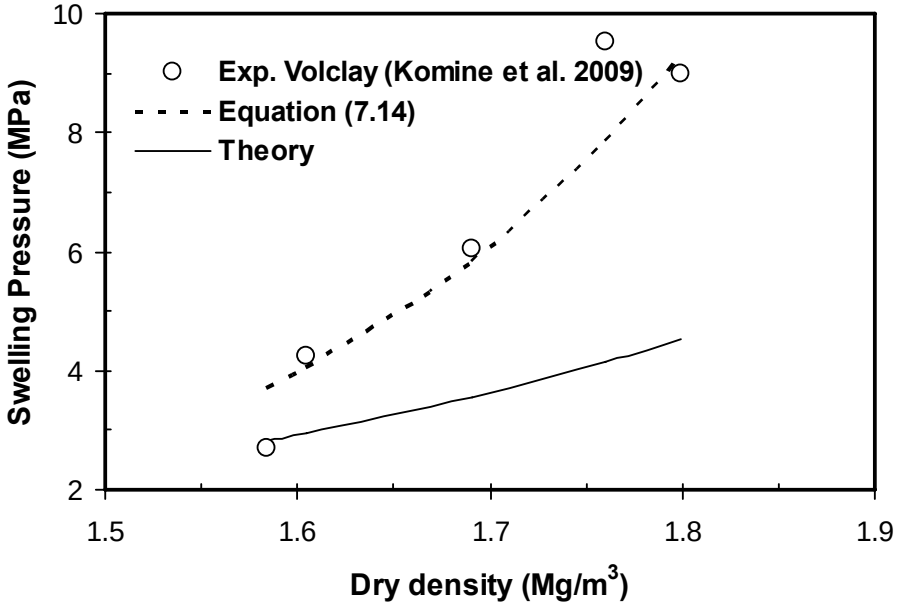


Figure 7.34 Experimental swelling pressure and swelling pressure from suggested equation for Volclay (Data from Komine et al. 2009)

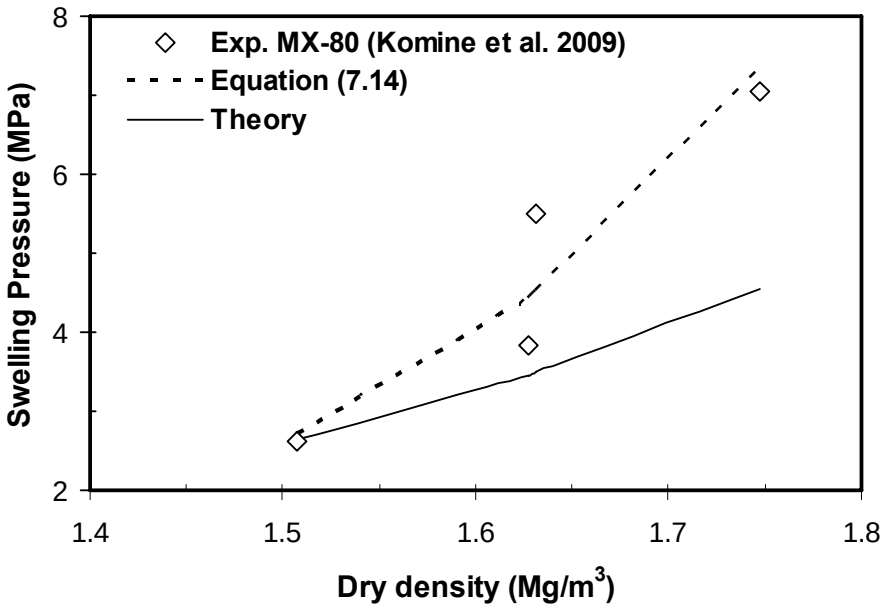


Figure 7.35 Experimental swelling pressure and swelling pressure from suggested equation for MX-80 bentonite (Data from Komine et al. 2009)

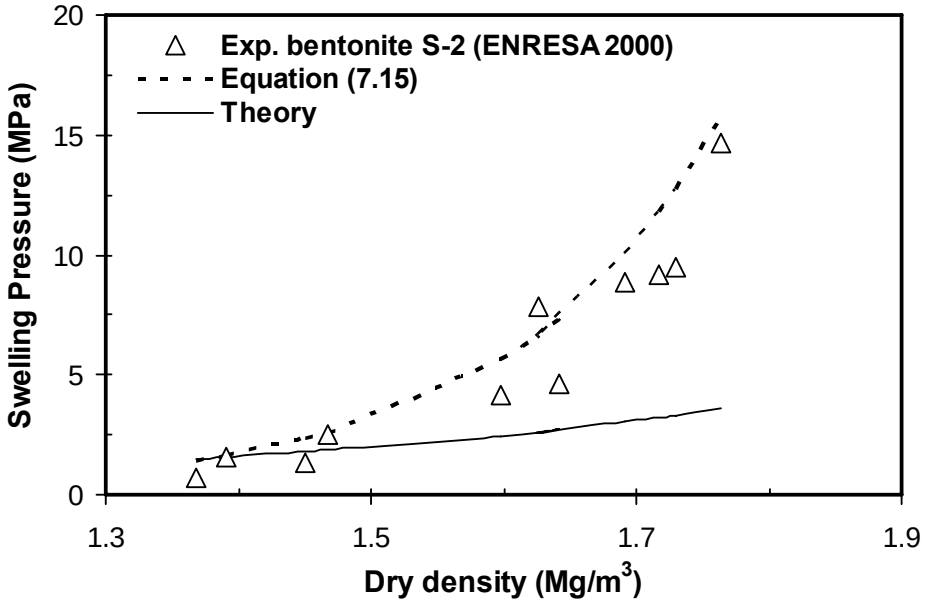


Figure 7.36 Experimental swelling pressure and swelling pressure from suggested equation for S-2 bentonite (Data from ENRESA 2000)

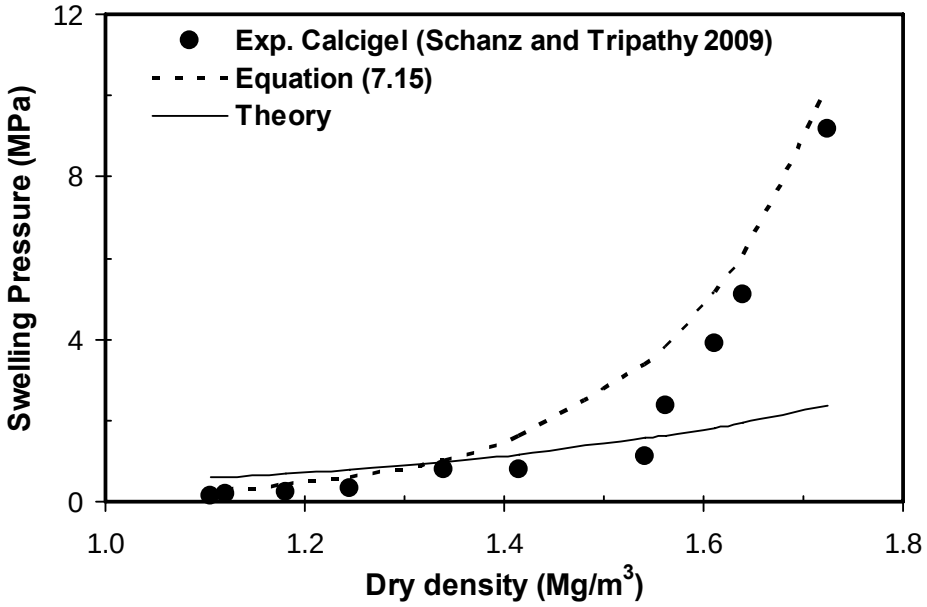


Figure 7.37 Experimental swelling pressure and swelling pressure from suggested equation for Calcigel bentonite (Data from Schanz and Tripathy 2009)

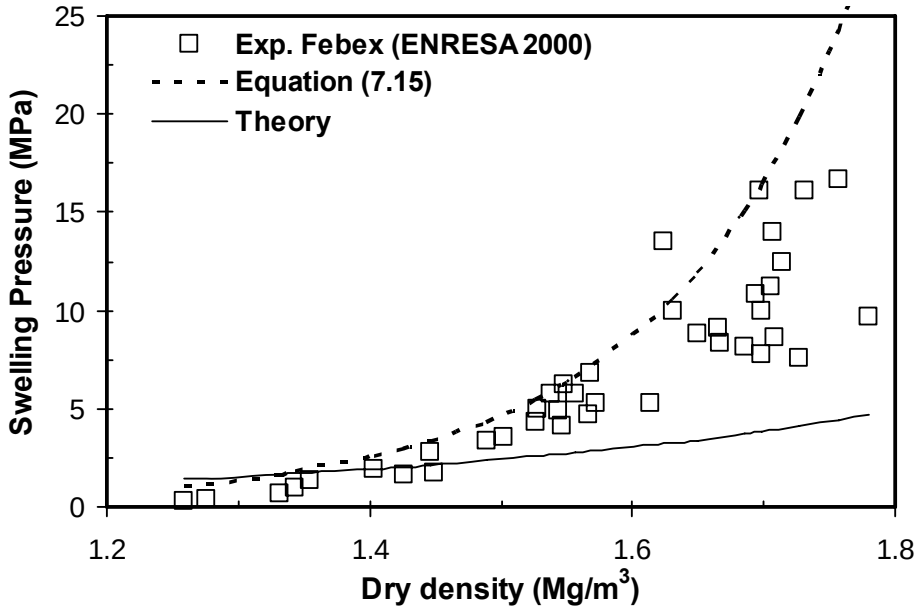


Figure 7.38 Experimental swelling pressure and swelling pressure from suggested equation for Febex bentonite (Data from ENRESA 2000)

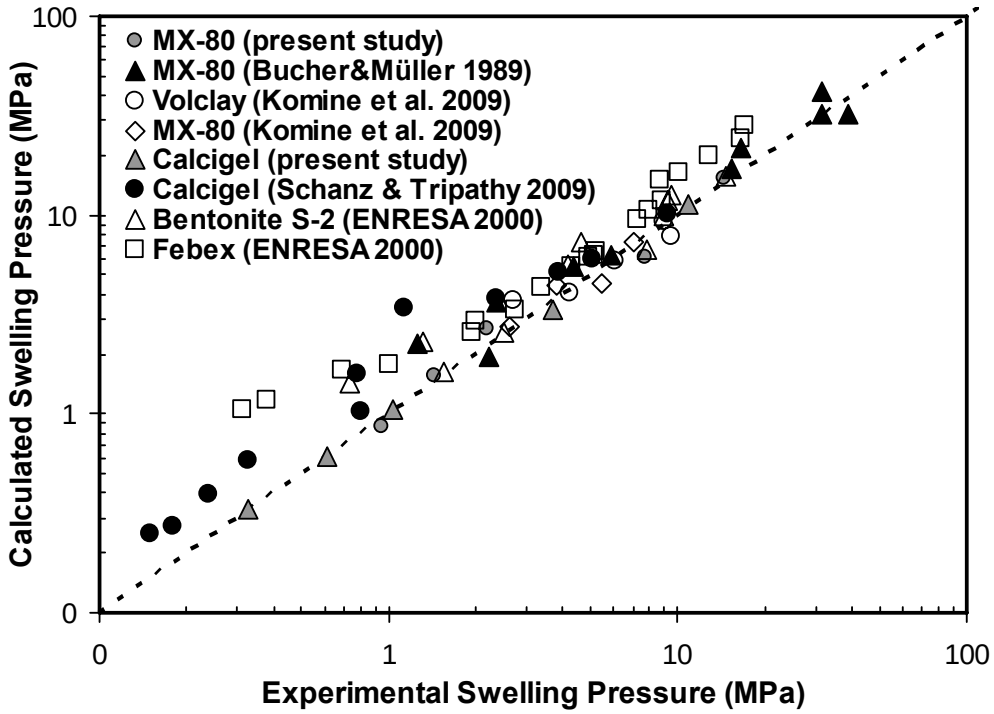


Figure 7.39 Experimental and calculated swelling pressures from suggested equations

## 7.5 Summary

This chapter summarized the hydraulic models used to calculate the saturated hydraulic conductivity. Three models namely, Kozeny-Carman model, Cluster model, and Laminar flow model were selected to evaluate the hydraulic behaviour of the selected bentonites. Kozeny-Carman showed better prediction with experimental hydraulic conductivity results at low dry density, but for high dry density the prediction is limited. Cluster model for predicting hydraulic conductivity using micro void ratio, $e_c$, from diffuse double layer gives unrealistic results. Similarly, laminar flow model, the calculated hydraulic conductivity was not in good agreement with the experimental conductivity results investigated in present study. Modifications in these hydraulic models were suggested and different approaches were employed in each model to give better estimation between calculated and experimental results. Limitations of each approach were shown and the reason for the discrepancies between measures and calculated results are discussed. At

the end it is concluded that each approach given some better estimation to calculate the hydraulic conductivity at moderate and high dense clays.

Swelling pressure of two bentonites with a range of dry density was experimentally determined and compared with the calculated swelling pressure using Gouy-Chapman diffuse double layer theory. The relationship between the theoretical void ratio from diffuse double layer theory and as prepared total void ratio was established and new modified void ratio were suggested. Two new equations based on average weighted valency were proposed for estimating swelling pressure that has theoretical support and the equations were verified with six other reported bentonites. The agreement between the calculated swelling pressure using the suggested equations and the reported experimental data was very good.

# Chapter 8

# CONCLUSIONS AND RECOMMENDATIONS

## 8.1 Introduction

The main aim of the work was to develop experimental and theoretical understanding of liquid movement in moderate and dense expansive clays. The main objectives of this study were defined in Chapter 1 as:

1. Provide a state-of-the-art review of theories and experimental work related to moisture movement in saturated clays from the beginning of 19$^{th}$ century to date. The literature review covers background on clay structure and mineralogy, clay-water interaction.

2. Design and build new test apparatus to facilitate a large number of various combinations of hydro-mechanical and hydraulic gradient experiments. Create new laboratory facilities to provide operational support for the new cells. Conduct a preliminary experimental programme to demonstrate the working capacity and functionality of the new apparatus.

3. Establish a basic experimental methodology for sample preparation to obtain uniform homogenous samples and subsequent testing. Determine basic geotechnical properties that include physical and chemical properties and flow parameters i.e. hydraulic and thermal material parameters of tested clays.

4. Perform hydro-mechanical tests to investigate the water uptake, swelling behaviour, moisture movement in clays with different initial water contents and dry density.

5. Develop different approaches in the existing hydraulic models to calculate the hydraulic conductivity of swelling clays. Verify and validate the new approaches against the results obtained from the experiments performed in this study as well as the hydraulic conductivity data from the literature.

The following sections detail the main conclusions drawn from this work, and suggestions are made for further research.

## 8.2 Conclusions

### 8.2.1 Summary of the experimental results and conclusions

Swelling pressures and the saturated hydraulic conductivity of bentonites were studied. Several compaction dry densities and water contents of the bentonites were considered. A newly developed high pressure constant volume cell and a volume pressure controller (VPC) device are presented, which enables performing the required experimental program. The following conclusions were drawn from the study.

1. Three types of bentonite were used in this study having different physico-chemical characterization. It was concluded that hydro-mechanical properties depends upon the type of bentonite as well as the initial conditions.

2. Initial compaction conditions affect the swelling pressure of the bentonites. At the same water content, swelling pressure increases with an increase in the dry density.

3. At the same dry density an increase in the initial water content yields a decrease in the swelling pressure particularly at smaller dry densities indicating that the influence of the molding water on the fabric of the bentonite can be quite significant at low dry densities.

4. Initial compaction conditions also affect the hydraulic conductivity. The increase in the dry density at same water content is found to reduce the hydraulic conductivity.

5. The influence of an increase in the compaction water content at same dry density is found to reduce the hydraulic conductivity of compacted saturated bentonites. A reduction in the hydraulic conductivity was attributed to the formation of oriented fabric of clay particles that reduced the effective porosity and produced more tortuous flow paths. The higher initial water content effect was found to be negligible at very high compaction dry densities.

6. Hydraulic conductivity of bentonites increases slightly when high concentrated solution (saline water) is used instead of distilled water as the permeating agent. The increase in hydraulic conductivity occur more, especially in the case of low densities. At high dry density the effect of the salinity of the permeant is found to be diminishing.

### 8.2.2 Summary of the theoretical results and conclusions

1. Despite of limitations of conventional flow equation, the Kozeny-Carman hydraulic model was found to predict reasonably well the hydraulic conductivities of bentonites at low compaction dry densities. However, differences were noted between the calculated and the measured hydraulic conductivities at higher dry densities of the bentonites.

2. Simplified approaches have been considered for estimating hydraulic conductivities of compacted bentonites based on flow models, such as the Kozeny-Carman model with modified flow void ratio, the Kozeny-Carman model in conjunction with the diffuse double layer theory and reduced specific surface area, and the laminar flow model with pore radii calculated based on reported semi-empirical equations.

3. In spite of some limitations in the approaches considered, particularly with regard to the consideration of the specific surface areas at two different stages of calculations, all the three approaches provided some useful estimation of the hydraulic conductivity of several compacted bentonites.

4. The calculated hydraulic conductivities of the bentonites based on the Kozeny-Carman model with effective void ratio approach is found to agree well with the experimental results of several reported compacted bentonites.

5. Kozeny-Carman model in conjunction with the diffuse double layer theory and reduced specific surface area also gives better results with little scattered in the data. The reason of scatter data is attributed due to the lack of compatibility in the consideration of the specific surface areas which cause the discrepancies between the calculated and experimental hydraulic conductivities of the bentonites.

6. Laminar flow model with separation distance between two platelets, $d$, calculated from the reported modified diffuse double layer equations (Tripathy et al. 2004) are found to

agree well with the experimental results of several compacted bentonites. The main limitation of this approach is that the separation distance between the clay platelets are calculated based on the modified equations that in turn are based on the diffuse double layer theory, which assume that the clay platelets in compacted clay-water ion systems are uniformly distributed which may not be completely true.

7. In the cluster model, based on the experimental hydraulic conductivity results of the bentonites, relationships between the total void ratio, $e_T$, and the micro void ratio, $e_c$, were established. New equations for the hydraulic conductivity were proposed. The use of the equations is based on weighted average valency of the cations in the bentonites. The agreement between the calculated hydraulic conductivity using the suggested equations and the reported experimental data is found to be good.

8. An approach to estimate the swelling pressure of compacted bentonite using Gouy-Chapman diffuse double layer theory was presented. Two new equations based on average weighted valency were proposed for estimating swelling pressure that has theoretical support and the equations were verified with six other reported bentonites. The agreement between the calculated swelling pressure using the suggested equations and the reported experimental data was very good.

## 8.3 Recommendations

In this research the issues associated with liquid transport through moderate and dense clays has been touched. As there has been little previous work done on fluid flow through such materials and at such density. Among the areas which warrant future investigation are the following.

1. A wide range of dry density from low to very high (i.e. 1.0 – 2.0 $Mg/m^3$) can be use to check the complete behaviour of hydraulic properties of bentonites.

2. Concentration of the solution as permeant can be increase to evaluate its effect of hydro-mechanical properties of such type of clays.

3. The size and number of interconnected macropores present in densely compacted bentonite based barriers remains to be determined. These pores control the ability of

fluid to move through and ultimately escape through clay barriers. A comprehensive study to establish the role of pore structure on flow would permit this issue to be resolved and lead to a better estimation of conductivity.

4. The growth of bacteria on the surface of a clay barrier has the potential to affect the flow process. Bacteria are capable of entering into pores and forming a biofilm on the surface of compacted clay. Such a film can result in a plugging of the pores and generation of a sealing layer of bacterial materials. This sort of testing could be conducted by introducing a species of bacteria which is not present in a specimen and monitoring the flow through the specimen.

# REFERENCES

Abichou T. Benson C.H. and Edil T.B. (2004) Network model for hydraulic conductivity of sand-bentonite mixtures. Canadian Geotechnical Journal, 41(4): 698-712.

Acar Y.B. and Olivieri I. (1989) Pore fluid effects on the fabric and hydraulic conductivity of laboratory compacted clay. Transportation Research Record. Transportation Research Board. National Research Council. Wasington D.C. 1219:144-159.

Achari G. Joshi R.C. Bentley L.R. and Chatterji S. (1999) Prediction of the hydraulic conductivity of clays using the electric double layer theory. Canadian Geotechnical Journal, 36:783-792.

Agus S.S. (2005) An experimental study on hydro-mechanical characteristics of compacted bentonite-sand mixtures. PhD dissertation. Bauhaus-Universität Weimar, Germany.

Agus S.S. and Schanz T. (2005a) Swelling pressure and total suction of compacted Bentonites and mixtures. Proceeding of International Conference on Problematic Soils. (Eds. Bilsel, H and Nalbantoglu, Z). North Cyprus. Vol.1, pp. 61-70.

Agus S.S. and Schanz T. (2005c) Effect of shrinking and swelling on microstructures and fabric of a compacted bentonite-sand mixture. Proceeding of International Conference on Problematic Soils (Eds. Bilsel, H and Nalbantoglu, Z). North Cyprus Vol.2, pp. 543-550.

Agus S.S. and Schanz T. (2008) Permeability of a heavily compacted bentonite-sand mixture as sealing and buffer element for nuclear waste repository. Unsaturated Soils: Advances in Geo-Engineering – Toll et al. (eds) © 2008 Taylor & Francis Group, London, ISBN 978-0-415-47692-8.

Agus S.S. Leong Eng-Choon and Rahardjo H. (2003) A flexible wall permeameter for measurements of water and air coefficient of permeability of residual soils. Canadian Geotechnical Journal, 40: 559-574.

Ahn H.S. and Jo H. Y. (2008) Influence of exchangeable cations on hydraulic conductivity of compacted bentonite. Applied Clay Science, doi: 10.1016 /j.clay.2008.12.018.

Al-Badran Y.M.H. (2011) Volumetric yielding behaviour of unsaturated fined-grained soils. PhD dissertation. Ruhr-Universität Bochum, Germany.

Alonso E.E. Vaunat J. and Gens A. (1999) Modelling the mechanical behaviour of expansive clays. Engineering Geology, 54, 173–183.

Al-Shamrani M.A. and Al-Mhaidib A.I. (2000) Swelling behaviour under oedometric and triaxial loading conditions. GeoDenver 2000: Advances in Unsaturated Geotechnics, ASCE, 344-360.

Alyamani M. S. and Sen Z. (1993) Determination of Hydraulic Conductivity from Grain-Size Distribution Curves. Ground Water, 31, 551-555.

Anderson D. (1982) Does landfill leachate make clay liners more permeable. Civil Engineering, ASCE, 52(9), 32-37.

Anderson D.M. and Low P.F. (1958) The density of water adsorbed by Lithium-, sodium-, and potassium-bentonite. S.S.S.A. Proceeding, 22, 99-1 03.

Arch J. Stephenson E. and Maltrnan A. (1993) Factors Affecting the Containment Properties of Natural Clays. Proceedings Coference of the Engineering Geology of Waste Disposal and Storage, Cardiff. pp 263-272.

Arifin Y.F. (2008) Thermo-Hydro-Mechanical behaviour of compacted bentonite sand mixture: An experimental study. PhD dissertation. Bauhaus-Universität Weimar, Germany.

Arora K.R. (1997) Soil mechanics and foundation engineering. 4th Ed. Standard Publishers Distributor, New Delhi.

ASTM (1997) Soil and Rock: dimension stone, geosynthetics. In 1997 Annual book of ASTM standards, Vol. 04.08 and Vol. 04.09. American Society for Testing and Materials, Philadelphia, PA.

Atomic Energy of Canada Limited. (1994) Environmental impact statement on the concept for disposal of Canada's nuclear fuel waste. Atomic Energy of Canada Limited, Ottawa, Ont. AECL-10711: COG-93–COG-1.

Aylmore L.A.G. and Quirk J.P. (1962) The structural status of clay systems. *In* Proceedings of the 9th National Conference on Clays and Clay Minerals, Lafayette, Ind., 5-8 Oct. 1960, Edited by A. Swineford, Pergamon Press, Oxford, pp. 104–130.

Baille W. Tripathy S. and Schanz T. (2010) Swelling pressure and one-dimensional compressibility behaviour of bentonite at large pressure. Applied Clay Science, doi:10.1016/j.clay.2010.01.002, 1-10.

Barbour S.L. and Yang N. (1993) A review of the influence of clay–brine interactions on the geotechnical properties of Ca-montmorillonitic clayey soils from western Canada. Canadian Geotechnical Journal, 30: 920–934.

Bear J. (1972) Dynamic of fluid in porous media. New York: Dover.764 pp.

Bennion D. W. and Goss M.J. (1971) A sinusoidal pressure response method for determining the properties of a porous medium and its in-situ fluid , Society Petrol Engineering, SPE 3541.

Benson C.H. and Boutwell G.P. (1992) Compaction control criteria and scale dependent hydraulic conductivity of clay liners. Proceeding of 15th Annual Madison Waste Conference. Madison: 62-83.

Benson C.H. and Daniel D.E. (1990) Influence of Clods on Hydraulic Conductivity of Compacted Clay. ASCE Journal of Geotechnical Engineering, 111(8), 123 1-1248.

Benson C.H. Gunter A.G. Boutwell G.P. Trautwein S.J. and Berzanski P.H. (1997) Comparison of four methods to assess hydraulic conductivity. Journal Geotechnical and Geoenvironmental Engineering, ASCE, V123, 10: 929-937.

Benson C.H. Hardianto F.S. and Motan E.S. (1993) Representative sample size for hydraulic conductivity assessment of compacted soil liners. Hydraulic Conductivity and Waste Contaminant Transport in Soils. ASTM. Philadelphia. ASTM STP 1142: 3-29.

Bernabé Y. (2006) A note on the oscillating flow method for measuring rock permeability. International Journal Rock Mechanics Min. Science and Geomech. Abstr. 43: (2),311-316.

Bird P. (1984) Hydration phase diagrams and friction of montmorillonite under laboratory and geologic conditions with implications for shale compaction, slope stability and strength of fault gauge. Tectonophysics 107, Nos 3–4, 235–260.

Black D.K. and Lee K.L. (1973) Saturating laboratory samples by back pressure, Journal Soil Mech. Found. Div. ASCE, Vol. 99, No. SM1, pp. 75-93.

Blatz J.A. and Graham J. (2000) A system for controlled suction in triaxial tests. Géotechnique, 50(4): 465-469.

Bolt G.H. (1956) Physico-chemical analysis of the compressibility of pure clays. Géotechnique, 6(2), 86–93.

Bowders J.J. (1987) Hydraulic conductivity of compacted clay to dilute organic chemicals. Journal of Geotechnical Engineering, ASCE, 1 13(12), 1432-1 448.

Boynton S.S. and Daniel D.E. (1985) Hydraulic conductivity tests on compacted clay, Journal Geotechnical Engineering, ASCE, 109(4), 465-478.

Bradbury M.H. and Baeyens B. (2002) Pore water chemistry in compacted re-saturated MX-80 bentonite: Physico-chemical characterization and geochemical modeling. PSI Bericht Nr Switzerland.

Bradbury M.H. and Baeyens B. (2003) Porewater chemistry in compacted re-saturated MX-80 bentonite. Journal of Contaminant Hydrology, Elsevier. 61, 329-338.

Braden L. and Sides G.R. (1967) The diffusion of air through the pore water in soils, Proceeding of 3rd Asian Conference on Soil Mech. and Found. Engineering, Haifa, Isreal, pp 135-1 38.

Brookins D. (1984) Geochemical aspects of radioactive waste disposal, Springer-Verlag, pp.267- 278.

Bucher F. and Müller-Vonmoos M. (1989) Bentonite as a containment barrier for the disposal of highly radioactive waste. Applied Clay Science, 4(2): 157–177.

Bucher F. Jedelhauser P. and Mayor P.A. (1986) Quell-Durchlassigkeits und Schrumpfersuchin an quartsand bentonit-gemischen, Inst. Fur Grundbau und Bodenmechanik, ETH, Zurich, National Co-operative for the storage of radioactive materials (NAGRA), Technical Report 86-1 3.

Carlsson T. (1986) Interaction in MX-80 bentonite/water/electrolyte systems. PhD Thesis, University of Luleá, Sweden.

Carman P.C. (1956) Flow of Gases through Porous Media. Butterworths Scientific Publications, London.

Carman P.C. (1937) Fluid flow through granular beds, Transactions, Inst. of Chemical Engineers, London. 15,150-166.

Carman P.C. (1939) Permeability of saturated sands, soils and clays. Journal of Agriculture Science, 29: 263–273.

Carrier III W.D. (2003) Goodbye, Hazen; Hello, Kozeny-Carman. Journal of Geotechnical and Geoenvironmental Engineering, 129(11): 1054-1056.

Carter D.L. Mortland M.M. and Kemper W.D. (1986) Specific surface. Methods of soil analysis. Part 1, 2nd Ed. A. Klute (Ed.), American Society of Agronomy, Madison, Wis., 413-423.

Cerato A. B. and A. J. Lutenegger (2002) Determination of surface area of fine grained soils by the ethylene glycol monoethyl ether (EGME) method, ASTM Geotechnical Testing Journal, 25 (3), 315-321.

Chapman D.L. (1913) A contribution to the theory of electro-capillarity. Philosophical Magazine, 25(6), 475-481.

Chapman D.L. (1913) A contribution to the theory of electro-capillarity. Philosophical Magazine, 25(6), 475-481.

Chapuis P. (1981) Permeability testing of soil-bentonite mixtures. Proceedings, 10th International Conference on Soil Mechanics and Foundation Engineering, Stockholm, vol. 4, pp. 744- 745.

Chapuis P. Baass K. and Davennne L. (1989) Granular soils in rigid-wall permeameters: method for determining the degree of saturation. Canadian Geotechnical Journal, 26: 71-79.

Chapuis R.P. (1990) Sand–bentonite liners: predicting permeability from laboratory tests. Canadian Geotechnical Journal, 27: 47–57.

Chapuis R.P. (1990*a*) Sand–bentonite liners: field control methods. Canadian Geotechnical Journal, 27: 216–223.

Chapuis R.P. (1990b) Sand–bentonite liners: predicting permeability from laboratory tests. Canadian Geotechnical Journal, 27: 47–57.

Chapuis R.P. and Pouliot G. (1996) Determination of bentonite content in soil–bentonite liners by X-ray diffraction. Canadian Geotechnical Journal, 33: 760–769.

Chapuis R.P. (2002) The 2000 R.M. Hardy Lecture: Full-scale hydraulic performance of soil–bentonite and compacted clay liners. Canadian Geotechnical Journal, 39: 417–439.

Cheng C. and Chen X. (2007) Evaluation of Methods for Determination of Hydraulic Properties in an Aquifer- Aquitard System Hydrologically Connected to River. Hydrogeology Journal. 15: 669-678.

Cho W.J. Lee J.O. and Chun K.S. (1999) The temperature effects on hydraulic conductivity of compacted bentonite. Applied Clay Science 14: 47-58.

Cho W.J. Lee J.O. and Kang C.H. (2000) Influence of temperature elevation on the sealing performance of the potential buffer material for a high-level radioactive waste repository. Annals of Nuclear Energy, 27**:** 1271-1284.

Cho W. J. Lee O. and Kang C.H. (2002) Influence of salinity on the hydraulic conductivity of compacted bentonite. Material research society Symposium, proceeding, vol. 713, p-50.1 – 50.7.

Collins K. and McGown A. (1974) The form and function of micro-fabric features in a variety of natural soils, Géotechnique, Vol. 24, No. 2, pp. 223–254.

Cui Y. J. Loiseau C. and Delage P. (2002) Microstructure changes of a confined swelling soil due to suction controlled hydration. Proc. 3rd Int. Conf. on Unsaturated Soils, Recife 2, 593–598.

Daniel D.E. Trautwein S.J. Boynton S.S. and Foreman D.E. (1984) Permeability testing with flexible-wall permeameters. Geotechnical Testing Journal, 7(3), 113-122.

Daniel D.E. Anderson D.C. and Boynton S.S. (1985) Fixed-wall vs. flexible-wall permeameters. ASTM STP 874, 107-126. A.I.Johnson, R.K.Frobel, N.J.Cavalli, and C.B.Pettersson eds., Am. Soc. for Testing and Materials, Philadelphia.

Daniel D.E. and Trautwein S.J. (1986) Filed permeability test for earthen liner. Proceeding Insitu 86, ASCE Specialty Conference on Use of In-situ Tests in Geotechnical Engineering. Virginia Poly. Inst. and State Univ. Blacksburg. New York: 146-160.

Daniel D.E. and Benson C.M. (1990) Water content-density criteria for compacted soil liners. Journal of Geotechnical Engineering, ASCE 116, 1811-1930.

Darcy H. (1856) Determination of the laws of the flow of water through sand (translated from the french), in Physical Hydrogeology, ed by R.A.Freeze and W.Back, pp.14-19, Huchinson Ross, Stroudsburg, Pa.

Day S.R. and Daniel D.E. (1985) Hydraulic conductivity of two prototype clay liners. Journal of Geotechnical Engineering. ASCE, 111(8): 957–970.

De Magistris F.S. Silvestri F. Vinale F. (1998) Physical and mechanical properties of compacted silty sand with low bentonite fraction. Canadian Geotechnical Journal 35: 909– 925.

Delage P. Howat M. and Cui Y.J. (1998) The relationship between suction and swelling properties in a heavily compacted unsaturated clay. Engineering Geology, 50 (1-2): 31-48.

Delage P. Marcial D. Cui Y.J. and Ruiz X. (2006) Ageing effects in the compacted bentonite: a microstructure approach. Géotechnique, 56 (4): 291-304.

Delage P. (2007) Microstructure features in the behaviour of engineered barriers for nuclear waste disposal, Proceeding 2nd International Conference: Mechanics of

Unsaturated Soils (Ed. Tom Schanz), Weimar, Germany. Springer proceedings in physics. Vol.1, pp. 11- 32.

Dergaguin B.V. Karasev V.V. and Khromov E.N. (1986) Thermal expansion of water in fine pores. Journal of Colloid and lnterface Science. 106(2), 586-587.

DIN (1987) Deutsche Institut für Normung (DIN 4022-1). Deutsche Institut für Normung e.V. Beuth Verlag GmbH, Berlin.

Dixon D.A. Gray M.N. Thomas A.W. (1985) A study of the compaction properties of potential clay-sand buffer mixtures for use in nuclear fuel waste disposal. Engineering Geology, 21: 247-255.

Dixon D.A. and Woodcock D.R. (1986) Physical and engineering properties of candidate buffer materials, Atomic Energy of Canada Limited Technical Record, TR-352.

Dixon D.A. Cheung S.C.H. Gray M.N. and Davidson B. (1987) The hydraulic conductivity of dense clay soils. In, Proceedings of 40th Canadian Geotechnical Conference, Regina, Saskatchewan, 389-396.

Dixon D.A. Gray M.N. and Hnatiw D.S.J. (1992a) Critical gradients and pressures in dense swelling clays. Canadian Geotechnical Journal, 29(6),1113-1119.

Dixon D.A. Sri Ranjan R. and Graham J. (1992b) Applicability of Darcy's law in laboratory measurement of water flow through low permeability clays. 45th Canadian Geotech. Conference, Toronto.

Dixon D.A. Gray M.N. Lingnau B. Graham J. and Campbell S.L. (1993a) Thermal expansion testing to determine the influence of pore water structure on water flow through dense clays. 46th Canadian Geotechnical Conference, Saskatoon, Sk., Sept. 1993.

Dixon D.A. Wan A.W-L. Graham J. and Campbell S.L. (1993b) Assessment of self sealing and self-healing abilities of dense, high-bentonite-content sealing materials, Proceeding 1993 Joint CSCE-ASCE Natl. Conf. on Environmental Engineering, Montreal, PQ, 1993.

Dixon D.A. (1995) Towards an understanding of water structure and water movement through dense clays. Ph.D. Thesis, University of Manitoba.

Dixon D.A. Gray M.N. and Graham J. (1996) Swelling and hydraulic properties of bentonites from Japan, Canada and USA. Proceedings of the second International Congress on Environmental Geotechnics, Osaka, Japan, 5-8 November 1996, 43-48.

Dixon D.A. Graham J. and Gray M.N. (1999) Hydraulic conductivity of clays in confined tests under low hydraulic gradients. Canadian Geotechnical Journal, 36: 815-825.

Dixon D. Chandler, N. Graham J. Gray M.N. (2002) Two largescale sealing tests conducted at Atomic Energy of Canada's underground research laboratory: the buffer-container experiment and the isothermal test. Canadian Geotechnical Journal, 39: 503– 518.

Edil T.B. and Erickson A.E. (1985) Procedure and equipment factors affecting permeability testing of a bentonite-sand liner material, in, Hydraulic Barriers in Soil and Rock, ASTM STP 874, pp. 155-1 70.

Elsbury B.R. Straders G.A. Anderson D.C. Rehage J.A. Sai J.O. and Daniel D.E. (1988) Field and laboratory testing of a compacted soil liner. PB-89- 125942, U.S. Environmental and Protection Agency. Washington D.C.

Eltantawy I.N. and Arnold P.W. (1973) Reappraisal of ethylene glycol mono-ethyl ether (EGME) method for surface area estimation of clays. Soil Science, 24, 232-238.

ENRESA (2000) FEBEX Project - Full Scale Engineered Barriers Experiments for a Deep Geological Respiratory for High Level Radioactive Waste in Crystalline Host Rock: Final report, (ENRESA), Madrid, Spain.

Ferber V Auriol J.C. Cui Y.J and Magnan J.P (2008) Wetting induce volume changes in compacted silty clays and high plasticity clays. Canadian Geotechnical Journal, 45: 252-265.

Fernandez F. and Quigley R.M. (1985) Hydraulic Conductivity of Natural Clays Permeated with Simple Liquid Hydrocarbons. Canadian Geotechnical Journal, 22, pp. 205-214.

Fernandez F. and Quigley R.M. (1988) Viscosity and Dielectric Constant Controls on the Hydraulic Conductivity of Clayey Soils Permeated with Water-Soluble Organics. Canadian Geotechnical Journal, 25, pp. 582-589.

Fernuik N. and Haug M. (1990) Evaluation of in situ permeability testing methods. Journal of Geotechnical Engineering, ASCE, 116(2): 297–311.

Fisher G. J. (1992) The determination of permeability and storage capacity: Pore pressure oscillation method in Fault Mechanics and Transport properties of Rocks, edited by B. Evans and T. F Wong, pp 187-211, Academic Press, San Diego.

Frank H.S. (1972) Structural models in Water, a comprehensive treatise, F.Franks (ed,), Vol. 1, pp. 51 5-543, Plenum Press.

Fredlund D.G. and Rahardjo H. (1993) Soil mechanics for unsaturated soils, J. Wiley and Sons Publishers, New York.

Fripiat J. Cases J. Francois M. and Letellier M. (1982) Thermodynamic and microdynamic behavior of water in clay suspensions and gels, Journal Colloid. Interf. 89: 378–400.

Gattermann J.H. (1998) Theorie und Modellversuch für ein Abdichtungsbauwerk aus hochverdichteten Bentonit-formsteinen, Verlag Glückauf, Essen, Germany.

Gens A. and Alonso E.E. (1992) A framework for the behaviour of unsaturated expansive clays. Canadian Geotechnical Journal, 29: 1013-1032.

Gnanapragasam N. Lewis B.C. Finno R. (1995) Microstructural changes sand-bentonite soils when exposed to aniline. Journal of Geotechnical Engineering 121(2): 119-125. doi:10.1061/(ASCE)0733- 9410(1995) l21:2 (119).

Gouy G. (1910) Sur la constitution de la charge electrique a la surface d'un electrolyte. Anniue Physique (Paris). 4(9): 457-468.

Grace H. P. (1953) Resistance and compressibility of filter cakes: Chemical Engineering Prog. 49, 303-318, 367-377.

Graham J. Oswell J.M. and Gray M.N. (1992) The effective stress concept in saturated sand–clay buffer. Canadian Geotechnical Journal, 29: 1033–1043.

Grant C.D. and Groenevelt P.H. (1993) Air permeability. In M.R. Carter (ed). Soil Sampling and Methods of Analysis. Canadian Society of Soil Science. Lewis: 645-650.

Gray M.N. Cheung S.C.H. and Dixon D.A. (1984) The influence of sand content on swelling pressures and structure developed in statically compacted Na-bentonite. Report 7825, Atomic Energy of Canada Limited, Mississauga, Ont. pp. 1–24.

Grim R. E. (1968) Clay Mineralogy. McGraw-Hill, Inc., New York.

Grjotheim K. and Krogh-Moe J. (1954) Correlation between structure and some properties of water, Acta Chemica Scandinavica, 8, 1193-1202.

Guven N. (1992a) Molecular aspects of clay-water interactions, in, CMS Workshop Lectures, Vol. 4, Clay-Water Interface and its Rheological Implications, eds. N.Guven, and R.M.Pollastro, Clay Minerals Society Publishing.

Hansbo S. (1960) Consolidation of clay, with special reference to influence of vertical drains. A study made in connection with full-scale investigations at SkaEdeby. Doctoral thesis. Swedish Geotechnical Institute. Proceedings. No. 18, 216-236.

Hashm A.A. (1999) A study of the transport of a selection of heavy metals in unsaturated soil. Ph.D. Thesis, School of Engineering, University of Wales, Cardiff.

Haug M.D. and Sauer E.K. (1993) Hydraulic conductivity of heavily over consolidated reconstituted cretaceous clay shale, 4th Annual Canadian Geotechnical Conference, Saskatoon, Saskatchewan, Sept. 1993.

Haug M.D. and Wong L.C. (1992) Impact of molding water content on hydraulic conductivity of compacted sand-bentonite, Canadian Geotechnical Journal, 29(2), 253-262.

Hazen A. (1892) Some physical properties of sands and gravels, with special reference to their use in filtration. 24th Annual Report. Massachusetts State Board of Health. Publication Document No. 34: 539-556.

Herbert H.-J. and Moog H.C. (2002) Untersuchungen zur Quellung von Bentonit in hochsalinaren Lösungen. Report GRS-179, Gesellschaft für Anlagen und Reaktorsicherheit (GRS) mbH, Berlin.

Hesse P.R. (1971) A text book of soil chemical analysis. Chemical Publishing Co. Inc., New York.

Hillel D. 1980. Fundamentals of soil physics. London: Academic Press.

Holtz and Gibbs (1956) Engineering properties of expansive soils. Transaction ASCE, 121.

Holtz R. D. and Kovacs W. D. (1981) An introduction to geotechnical engineering, Prentice-Hall, Englewood Cliffs, N.J.

Hossain D. (1992) Prediction of Permeability of Fissured Tills, QJEG, Vol. 25 No.4 pp 331-342.

Ingles O. G. (1962) Bonding forces in soils, Part 3: A theory of tensile strength for stabilized and naturally coherent soils, Proceedings of the First Conference of the Australian Road Research Board, Vol. I, pp. 1025–1047.

Israelachvili J.M. (1982) Forces between surfaces in liquids. Advances in Colloid and Interface Science, 16, 31–47.

Ito H. (2006) Compaction properties of granular bentonites. Applied Clay Science 31, 47-55.

Iwata S. Tabuchi T. and Warkentin B.P. (1995) Soil-water interactions: mechanisms and applications. Marcial Dekker, NY.

Japan Nuclear Cycle Development Institute. (1999) H12: project to establish the scientific and technical basis for HLW disposal in Japan: supporting report 2 (respiratory design and engineering Technology). Japan Nuclear Cycle Development Institute, Tokyo.

Jo HY. Katsumi T. Benson CH. Edil TB. (2001) Hydraulic conductivity and swelling of nonprehydrated GCLs permeated with single-species salt solutions. Journal of Geotechnical and Geoenvironmental Engineering 127(7): 557-567.

Johnson G.J. Crumley W.S. and Boutwell G.P. (1990) Field verification of clay liner hydraulic conductivity. Waste Contaminant Systems. ASCE: 226-245.

Jones D.E. Jr. and Holtz W.G. (1973) Expansive soils-the hidden disaster: Civil Engineering, 43(8): 49-51.

Kanno T. and Wakamatsu H. (1992) Water uptake and swelling properties of unsaturated bentonite buffer materials. Canadian Geotechnical Journal, 29: 1102–1107.

Karnland O. Pusch R. Sanden T. (1992) The importance of electrolyte on the physical properties ofMX-80 bentonite. SKB Report AR 92-35. Stockholm (in Swedish).

Karthigesu T. (1994) Validity of Darcy's law for low-gradient saturated flow through bentonite and sand mixtures, Master of Science Thesis, Dept. of Agricultural Engineering, University of Manitoba, Winnipeg, Canada.

Katti D.R. and Shanmugasundaram V. (2001) Influence of swelling on the microstructure of expansive clays. Canadian Geotechnical Journal, 38: 175-182.

Kell G.S. (1972) Water and aqueous solutions, ed R.A. Horne, Wiley Interscience, New York

Kenney T. C. van Veen W. A. Swallow M. A. and Sungaila M. A. (1992) Hydraulic conductivity of compacted bentonite-sand mixture. Canadian Geotechnical Journal, 29, 364-374.

Kharaka Y.K. Smalley W.C. (1976) Flow of water and solutes through compacted clays. AAPG Bull. 60 (6), 973– 980.

Khemissa M. (1998) Mesure de la permeabilite des argiles sous contrainte et tempe´rature. Rev. Fr. Geotech. 82 (1), 11 –22 (in French).

King F.H. (1898) Principles and conditions of the movement of groundwater, U.S. Geol. Survey 19th Annual Rept., Part 2, 59-294.

Komine H. and Ogata N. (1994) Experimental study on swelling characteristics of compacted bentonite. Canadian Geotechnical Journal, 31: 478-490.

Komine H. Ogata N. (1996) Prediction for swelling characteristics of compacted bentonite, Canadian Geotechnical Journal, 33, 11–22.

Komine H. and Ogata N. (1999) Experimental study on swelling characteristics of sand-bentonite mixture for nuclear waste disposal. Soils Foundation, 39(2), 83–97.

Komine H. (2001) Evaluation of swelling characteristics of buffer and backfill materials considering the exchangeable-cations compositions of bentonite and its applicability. Proceedings of the 15th International Conference on Soil Mechanics and Geotechnical Engineering. Vol. 3, pp. 1981– 1984.

Komine H. and Ogata N. (2003) New equations for swelling characteristics of bentonite-based buffer materials. Canadian Geotechnical Journal, 40(2): 460–475.

Komine H. (2004) Simplified evaluation on hydraulic conductivities of sand-bentonite mixture backfill. Applied Clay Science, 26: 13-19.

Komine H. (2008) Theoretical equations on hydraulic conductivities of bentonite-based buffer and backfill for underground disposal of radioactive wastes. Journal of Geotechnical and Geoenvironmental Engineering, 134(4): 497-508.

Komine H. Yasuhara K. and Murakami S. (2009) Swelling characteristics of bentonites in artificial seawater. Canadian Geotechnical Journal, 46, 177–189. doi:10.1139/T08-120.

Komornik A. Livneh M. and Smucha. (1980) Shear strength and swelling of clays under suction. Proceedings of the 4th International Conference on Expansive Soils Denver, Colorado, 206-226.

Kozeny J. (1927) Ueber kapillare Leitung des Wassers im Boden. Sitzungsberichte Wiener Akademie, 136(2a): 271–306.

Kranz R. L. (1990) Hydraulic diffusivity measurements on laboratory rock samples using an oscillating pore pressure method. International Journal Rock Mechanics Min. Science and Geomech. Abstr. 27: (5),345-352.

Lagarde B. and Tessier D. (1988) Etude structurale de I' argile de Fourge-Cahaignes soumises a une humectation. Note Technique SESD/88.13, DRDD/ANDRA, 77pp.

Lahti L.R. King K.S. Reades D.W. and Bacopoulos A. (1987) Quality assurance monitoring of a large clay liner. Geotechnical Practise for Waste Disposal 87:640-654. ASCE. New York.

Laird D.A. (2006) Influence of layer charge on swelling of smectites, Applied Clay Science, Elsevier. 34: 74-87.

Lamb T. W. (1954) The Permeability of Fine-Grained Soils. Permeability of soils, ASTM, STP, 163, 55-67.

Lambe T. W. (1958a) The Structure of Compacted Clay, Journal of the Soil Mechanics and Foundations Division, ASCE, Vol. 84, No. SM2, 1654–1 to 1654–35.

Lambe T.W. (1962). Soil Stabilization, Foundation Engineering, Ed. G.A. Leonards, McGraw-Hill, pp 351- 437.

Lambe T.W. and Whitman R.V. (1969) Soil mechanics, John Wiley & Sons, New York.

Lambe T.W. and Whitman R.V. (1979) Soil Mechanics, SI Version, J. Wley and Sons, Toronto, 553 p.

Lavkulich L. (1981) Soil analysis manual. Pedology Laboratory, Department of Soil Science, University of British Columbia, Vancouver.

Law K.T. and Lee C.F. (1981) Initial gradient in a dense glacial till, in, Proc. 10$^{th}$ Intl.Conf. Soil Mech. Foundn. Engrg., Stockholm, Sweden, 441 -446.

Lee J. Shackelford C.D. (2005) Impact of bentonite quality on hydraulic conductivity of geosynthetic clay liners. Journal of Geotechnical and Geoenvironmental Engineering, 131(1), 64–77.

Lee K.L. Morreson R.A. and Haley S.C. (1969) A note on the pore pressure parameter B, Proceeding.

Leroueil S. Bouclin G. Tavenas F. Bergeron L. and Rochelle P.LA. (1990) Permeability anisotropy of natural clays as a function of strain. Canadian Geotechnical Journal, 27: 568-579.

Leroueil S. Le Bihan J.P. and Bouchard R. (1992) Remarks on the design of clay liners used in lagoons as hydraulic barriers. Canadian Geotechnical Journal, 29: 512–515.

Lian G. Thornton C. and Adams M. J. (1993) A theoretical study of the liquid bridge forces between two rigid spherical bodies. Journal of Colloid Interface Science, Vol. 161, pp. 138–148.

Likos W.J. (2004) Measurement of crystalline swelling in expansive clay. Geotechnical Testing Journal, 27(6): 1-7.

Little J.A. Muir Wood D. Paul M.A. and Bouazza A. (1992). Some Laboratory Measurements of Permeability of Bothkennar Clay in Relation to Soil Fabric, Géotechnique 42, No. 2, pp 355-361.

Lloret A. Villar M.V. (2007) Advances on the knowledge of the thermo-hydro-mechanical behaviour of heavily compacted ‘‘FEBEX’’ bentonite, Physics and Chemistry of the Earth, 32, 701–715.

Lloret A. Romero E. Villar M.V. (2004) FEBEX II Project Final report on thermo-hydro-mechanical laboratory tests. Publicacion Tecnica ENRESA 10/04, Madrid, 180 pp.

Low P.F. and Margheim J.F. (1979) The swelling of clay. I. Basic concepts and empirical equations. Journal of the Soil Science Society of America, 43: 473–481.

Low P.F. (1980) The swelling of clay. II. Montmorillonites. Journal of the Soil Science Society of America, 44(4): 667–676.

Lundgren T. A. (1981) Some bentonite sealants in soil mixed blankets. Proceedings, 10th International Conference on Soil Mechanics and Foundation Engineering, Stockholm, 2, 349-354.

Lutz J.F. and Kemper W.D. (1959) Intrinsic permeability of clay as affected by clay-water interaction, Soil Science. 88, 83-90.

Macey H.H (1942) Clay-Water Relationship and the Internal Mechanisms of Drying. Transactions Ceramic Society, 41, pp 73-141.

Madsen F.T. and Müller-Vonmoos M. (1985) Swelling pressure calculated from mineralogical properties of a Jurassic opalinum shale, Switzerland. Clays and Clay Minerals, 33: 501–509.

Madsen F.T. and Müller-Vonmoos M. (1989) The swelling behaviour of clays. Applied Clay Science, Elsevier. 4: 143-156.

Marcial D. Delage P. and Yu Jun Cui. (2002) On the high stress compression of bentonites. Canadian Geotechnical Journal, 39: 812-820. doi:10.1139/T02-019.

Marcos A. and Francisca F.M. (2010) Soil permeability controlled by particle-fluid interaction. Geotechnical Geology Engineering, 28: 851-864. doi:10.1007/s10706-010-9348-y.

Martin M. Cuevas J. Leguey S. (2000) Diffusion of soluble salts under a temperature gradient after the hydration of compacted bentonite. Applied Clay Science 17, 55-70.

Mason B. and Berry L.G. (1968) Elements of Mineralogy, W.H. Freeman and Co., San Francisco, California.

Mata C. Romero E. and Ledesmana A. (2002) Hydro-chemical effects on water retention in bentonite-sand mixtures. Proc. 3rd Int. Conf. on Unsaturated Soils, UNSAT 2002 (Eds.Jucá, J.F.T., de Campos, T.M.P. and Marinho, F.A.M.), Recife, Brazil. Swets& Zeitlinger Vol. 1, pp. 283-288.

Mata C. Ledesma A. (2003) Hydro-mechanical behaviour of bentonite based mixtures in engineered barriers. In: Proceedings of the International Workshop Large Scale Field Tests in Granite. Advances in Understanding and Research Needs. Universitat Politecnica de Catalunya-ENRESA. Sitges, November 12–14, 2003.

McKeen R.G. (1992) A model for predicting expansive soil behaviour. Proceeding in 7th International Conference on Expansive soils. Dallas, 1-6.

Mesri G. and Olson R.E. (1970) Mechanisms controlling the permeability of clays. Clays and Clay Minerals. 19(3), 151 -1 58.

Michaels A.S. and Lin C.S. (1954) The Permeability of Kaolinite. Industrial and Engineering Chemistry, Vol. 46, pp. 1239-1246.

Mingarro E. Rivas P. del Villar L.P. de la Cruz B. Gómez P. Hernández A.I. Turrero M.J. Villar M.V. Campos R. Cózar J.S.(1991) Characterization of clay (bentonite)/crushed granite mixtures to build barriers against the migration of radionuclides: diffusion studies and physical properties. Task 3-Characterization of radioactive waste forms. A series of final reports (1985-1989)-No.35. Nuclear Science and Technology Series. Commission of the European Communities, Luxembourg. 136 pp.

Mitchell J. K. Hooper D. R. and Campanella R. (1965) Permeability of Compacted Clay. Journal of the Soil Mechanics and Foundations Division, ASCE, 21, SM4, 41-65.

Mitchell J. K. (1993) Fundamentals of soil behavior, 2nd Ed., Wiley, New York, 236–271.

Mitchell J.K. (1976) Fundamentals of Soil Behaviour, J. Wiley and Sons, Toronto.

Mitchell J.K. Soga K. (2005) Fundamentals of soil behavior. Wiley, New York.

Müller-Vonmoos M. and Kahr G. (1982) Bereitstellung von Bentonit für Laboruntersuchungen. Nagra Technischer Bericht 82-04.

Mundell J.A. and Boos T.A. (1990) Interpretation of field permeability test results on full-scale liner system. Environmental Aspects of Geotechnical Engineering. Proceeding of Ohio River Valley Soils Seminar XXI. ASCE. Cincinnati: 1-6.

Murray E.J. Rix D.W. and Humphrey R.D. (1992) Clay Linings to Landfill Sites. QJEG, 25, pp 371-376.

Murray E.J. Jones R.H. and Rix D.W. (1997) Relative importance of factor influencing the Permeability of clay soils. Geoenvironmental Engineering, Thomas Telford, London, pp 229-239.

Nagaraj T.S. and Jayadeva M.S. (1981) Re-examination of one-point methods of liquid limit determination. Géotechnique. 31 (3), 413-425.

National Cooperative for the Storage of Radioactive Waste. (1985) Nuclear waste management in Switzerland: feasibility studies and safe analyses. Nagra Project Report NGB 85-09, Nagra, Wettingen, Switzerland.

Oliphant and Tice (1985) An experimental measurement of channeling of flow in porous media. Soil Science, 139(5): 394-399.

Olsen H.W. (1962) Hydraulic flow through saturated clays. In Proceedings of the 9th National Conference on Clays and Clay Minerals, pp. 131–160.

Olsen H.W. (1965) Deviations from Darcy's Law in saturated clays. S.S.S.A. Proceeding, 29(2), 135-1 40.

Olsen H.W. Nichols R.W. and Rice T.L. (1985) Low gradient permeability measurements in a triaxial system. Geotechnique, 35(2), 145-1 57.

Olson R.E. and Daniel D.E. (1981) Measurement of the hydraulic conductivity of fine-grained soils. Permeability and Groundwater Contaminant Transport. ASTM STP 746:18-64.

Oscarson D.W and Dixon D.A. (1989) Elemental mineralogical and pore solution composition of selected Canadian Clays. Atomic Energy of Canada Report AECL-9891.

Palomino A. Santamarina J.C. (2005) Fabric map for kaolinite: effects of pH and ionic concentration on behavior. Clays and Clay Minerals 53(3):211-223. doi:10.l346/CCMN.2005.0530302.

Pane V. Croce P. Znidarcic D. Ko H.-Y. Olsen H. W. and Schiffman R.L. (1982) Effects of consolidation on permeability measurements for soft clays. Geotechnique, 32, 67-72.

Pashley R.M. (1981) DLVO and hydration forces between mica surfaces in L+, Na+, K+, and Cs+ electrolyte solutions: a correlation of double layer and hydration forces with surface cation exchange properties. Journal of Colloid and Interface Science, 83, 531–546.

Pashley R.M. and Isrealachvili J.N. (1984a) DLVO and hydration forces between mica surfaces in Mg2', Ca2', Si2' and Ba2' chloride solutions, Journal Colloid and interface Science, 97, 446-455.

Pashley R.M. and Isrealachvili J.N. (1984b) Molecular layering of water in their-films between mica surfaces and its relation to hydration forces. Journal Colloid interface Science, 101, 501-523.

Pierce J.J. Sallfors G. and Ford K. (1987a) Differential flow patterns through compacted clays, Geotechnical Testing Journal, ASTM, 10(4): 21 8-222.

Pleysier J.L. Juo A.S.R. (1980) A single-extraction method using silver-thiourea for measuring exchangeable cations and effective CEC in soils with variable charges. Journal of Soil Science 129, 205–211.

Pusch R. (1979) Unfrozen water as a function of clay microstructure. H.L. Jessberger ed. Ground Freezing, development in Geotechnical. Engineering Vol. (26) Elsevier Science Publ. Co., Amsterdam.

Pusch R. (1980) Permeability of highly compacted bentonite, Swedish Nuclear Fuel and Waste Management Company. Technical Report 80-16, Stockholm, Sweden.

Pusch R. (1982) Mineral–water interactions and their influence on the physical behaviour of highly compacted Na bentonite, Canadian Geotechnical Journal, 19, 381–387.

Pusch R. (1983) Use of clays as buffers in radioactive repositories, Swedish Nuclear Fuel and Waste Management Company, SKBF-KBS Technical Report 3-46, Stockholm, Sweden.

Pusch R. Karlnland O. and Hokmark H. (1990) GMM-a general microstructural model for qualitative and quantitative studies of smectite clays. SKB Technical Report 90-43, Stockholm, Sweden.

Pusch R. (2001) The microstructure of MX-80 clay with respect to its bulk physical properties under different environmental conditions. SKB Technical Report, TR-01-08. The Swedish Nuclear Fuel and Waste Management Company (SKB), Stockholm, Sweden.

Pusch R and Yong R.N. (2003) Water saturation and retention of hydrophilic clay buffer – microstructure aspects. Applied Clay Science 23: 61–68.

Pusch R. and Yong R.N. (2006) Microstructure of smectite clays and engineering performance. Taylor & Francis, London. pp. 94–97.

Rao N.S. and Mathew P.K. (1995) Effect of exchangeable cations on hydraulic conductivity of marine clay. Clays and Clay minerals. Vol. 43, No.4, 433 – 437.

Razouki S.S Haik M. Spyridon G. Mosa S. Wazir H. Majead G. and Ibrahim E. (1980) On the compaction and CBR behaviour of Basrah soil. Bulletin of the college of engineering, University of Basrah, 4, No1: 107-133.

Razouki S.S Kuttah D. Al-Damluji O. and Nashat I. (2008) Using gypsiferous soil for embankments in hot desert areas. ICE, Construction materials, 6, CM2, 63-71.

Renner J. (2000) Rock mechanical characterization of an argillaceous host rock of a potential radioactive waste repository. Rock Mech. Rock Eng, 33, 153-178.

Rolfe PF & Aylmore LAG (1977) Water and salt flow through compacted clays: I. Permeability of compacted illite and montmorillonite. Soil Science Society. Am. J. 41: 489-495.

Rolland S. Stemmelen D. and Moyne C. (2005) Experimental hydraulic measurements in an unsaturated swelling soil using the dual-energy gamma ray technique. International Symposium Advanced Experimental Unsaturated Soil Mechanics, Trento, Italy. 27-29 June 2005, 305-310.

Romero E. Gens A. and Lloret A. (2000) Temperature effects on water retention and water permeability of unsaturated clay. Proceeding of Unsaturated Soils for Asia (Eds. Rahardjo, Toll and Leong), Balkema, Rotterdam, pp. 433-438.

Romero E. Gens A. and Lloret A. (2001) Temperature effects on the hydraulic behaviour of an unsaturated clay. Geotechnical and Geological Engineering 19: 311-332.

Romero E. Gens A. and Lloret A. (2003) Suction effects on compacted clay under nonisothermal conditions. Géotechnique, 53(1): 65-81.

Ruhl J.L. Daniel D.E. (1997) Geosynthetic clay liners permeated with chemical solutions and leachate. Journal of Geotechnical and Geoenvironmental Engineering, 123(4): 369-381.

Saiyouri N. Hicher P. Y. and Tessier D. (1998) Microstructural analysis of highly compacted clay swelling. Proc. 2nd Int. Conference on Unsaturated Soils, Beijing, 1, 119–124.

Saiyouri N. Hicher P. Y. and Tessier D. (2000) Microstructural approach and transfer water modelling in highly compacted unsaturated swelling clays. Mech. Cohesive Frict. Materials 5, 41–60.

Saiyouri N Tessier D. Hicher P.Y. (2004) Experimental study of swelling in unsaturated compacted clays. Clay Minerals, 39: 469-479.

Sällfors G. and Öberg-Högsta (2002) Determination of hydraulic conductivity of sand bentonite mixtures for engineering purposes. Geotechnical and Geological Engineering. 20:65 - 80.

Sato H. Suzuki S. (2003) Fundametal study on the effect of an orientation of clay particles on diffusion pathway in compacted bentonite. Applied Clay Science 23, 51-60.

Schanz T. Tripathy S. (2009) Swelling pressure of a divalent-rich bentonite: diffuse double-layer theory revisited. Water Resources Research 45 (2), W00C12 CiteID.

Schanz T. Khan M.I. Tripathy S. (2010) Swelling pressure and hydraulic conductivity of compacted bentonites. International Conference on Geotechnical Engineering, Lahore, Pakistan. pp. 111-118.

Schmid W.E. (1957) The Permeability of Soils and the Concept of a Stationary Boundary Layer. Proceedings of the American Society for Testing of Materials, 57, 1195.

Schofield R.K. (1946) Ionic forces in thick films of liquid between charged surface. Transaction of Faraday Society, 42B: 219.

Seed H.B. and Chan C.K. (1959) Structure and strength characteristics of compacted clays. Journal of the Soil Mechanics and Foundations Division, ASCE, 85(SM5): 87–128.

Shakelford C.D. (1993) Contaminant Transport, Geotechnical Practice for Waste Disposal, Ed. D.E.Daniel, Chapman and Hall, pp 33-65.

Shang J.Q. Lo K.Y. and Quigley R.M. (1994) Quantitative determination of potential distribution in Stern–Gouy double-layer model. Canadian Geotechnical Journal, 31, 624–636.

Sharma R.S. (1998) Mechanical behaviour of unsaturated highly expansive clays. PhD thesis, Keble College, University of Oxford.

Singh P. N. and Wallender W. W. (2008) Effects of Adsorbed Water Layer in Predicting Saturated Hydraulic Conductivity for Clays with Kozeny–Carman Equation, Journal of Geotechnical and Geoenvironmental. Engineering, ASCE, doi:10.1061(ASCE)1090-0241(2008) 134:6 (829).

Sivapullaiah P. V. Sridharan A. and Stalin V. K. (2000) Hydraulic conductivity of bentonite-sand mixtures. Canadian Geotechnical Journal, 37, 406–413.

Skempton A. W. **(**1954) The pore pressure coefficients A and B, Géotechnique, 4, 143-1 47.

Slade P.G. and Quirk J.P. (1991) The limited crystalline swelling of smectite in $CaCl_2$, $MgCl_2$, and $LaCl_3$ solutions. Journal of Colloid Interface Science, 144: 18-26.

Song I. Renner J. (2007) Analysis of oscillatory fluid flow through rock samples. Geophysics Journal International, 170, 195-204.

Sposito G. and Prost R. (1982) Structure of water adsorbed on smectites. Chemical Reviews, 82(6), 553-573.

Sposito G. (1992) The diffuse-ions swarm near smectite particles suspended in 1:1 electrolyte solutions: Modified Gouy-chapman theory and quasicrystal formation, in, CMS Workshop Lectures, Vol. 4, Clay-Water Interface 'and its rheological implications, N.Guven and R.M.Pollastro eds., Clay Min. Soc. Publ.

Sri Ranjan R. and Gillham R. W. (1991) Non-Linear electro-osmotic and hydraulic flow phenomena in saturated clays, Can. Society Agricultural Engineering, Agric. Instit. Canada Annual Mtg., Fredrecton N.B, July 1991, Paper 91 -1 05.

Sri Ranjan R. and Karthigesu T. (1992) Validity of conventional hydraulic conductivity measurement methods for clayey soils, Proceeding 35th Annual Mtg. Manitoba Society of Soil Science, Winnipeg, Jan. 6-7, 104-1 08.

Sridharan A. and Jayadeva M.S. (1982) Double layer theory and compressibility of clays. Géotechnique. 32(2), 133–144.

Sridharan A. Sreepada Rao A. Sivapullaiah P.V. (1986a) Swelling pressure of clays. Geotechnical Testing Journal 9 (1), 24–33.

Sridharan A. Choudhury D. (2002) Swelling pressure of sodium montmorillonites. Géotechnique. 52 (6), 459–462.

Sridharan, A. and Gurtug, Y. (2004) Swelling behaviour of compacted fine-grained soils. Engineering Geology, 72: 9-18.

Stewart C.R. (1961) The use of alternating flow to characterize porous media having storage porous, Trans. AIME, 222, 383-389.

Stewart D.I. Studds P.G. Cousens T.W. (2003) The factors controlling the engineering properties of bentonite-enhanced sand. Applied Clay Science 23, 97-110.

Studds P.G. Steward D.I. Cousens T.W. (1998) The effects of salt solutions on the properties of bentonite-sand mixtures. Clay Miner. 33, 641-660.

Sun D.A. Sheng D. and Xu Y.F (2007) Collapse behaviour of unsaturated compacted soil with difference initial densities. Canadian Geotechnical Journal, 44(2), 673–686.

Swedish Nuclear Fuel and Waste Management Company. (1983) Final storage of spent nuclear fuel-KBS-3, III barriers. Swedish Nuclear Fuel Supply Company, Division KBS Technical Report, pp. 9:1–16:12.

Swedish Nuclear Fuel and Waste Management (1992) SKB91 final disposal of spent nuclear fuel. Importance of the bedrock for safety, SKB Tech. Report, 92-20.

Tavenas F. Leblond P. Jean P. and Leroueil S. (1983) The permeability of natural soft clays. Part I: Methods of laboratory measurement, Canadian Geotechnical Journal, 20(4), 629-644.

Terzaghi C. (1925) Determination of the Permeability of Clay, Engineering News Record, 95, pp 832-836.

Terzaghi K. (1922) Soil failure at barrages and its prevention. Die Wasserkraft, Special Forchheimer Issue, pp. 445. (In German).

Terzaghi K. and Pack R.B. (1967) Soil mechanics in engineering practice, Second edition, J.Wiley and Sons Publishers, Toronto.

Tessier D. (1990) Organisation des matériaux argileux en relation avec leur comportement hydrique. *In* Matériaux argileux, structure, propriétés et applications. Edited by A. Decarreau, Société Française de Minéralogie et de Cristallographie, Paris. pp. 387–445.

Tessier D. Dardaine M. Beaumont A. and Jaunet A.M (1998) Swelling pressure and microstructure of activated swelling clay with temperature. Clay minerals, 33(2), 255-267.

Thakur V.K.S. and Singh D.N. (2005) Rapid determination of swelling pressure of clay minerals. Journal of Testing and Evaluation. 33(4): 239-245.

Towhata I. Kuntiwattanakul P. Seko I. Ohishi K. (1993) Volume change of clays induced by heating as observed in consolidation tests. Soils Foundation, 33 (4), 170–183.

Trautwein S.J. and Boutwell G.P. (1994) In-situ hydraulic conductivity tests for compacted soil liners and caps. ASTM STP 1142:184-223.

Trautwein S.J. and Williams C.E. (1990) Performance evaluation of earthen liners. Waste Contaminant Systems. Geotechnical Special Pub. ASCE. 26:30-49.

Tripathy S. Sridharan A. and Schanz T. (2004) Swelling pressures of compacted bentonites from diffuse double layer theory, Canadian Geotechnical Journal, 41, 437-450.

Tripathy S. and Schanz T. (2007) Compressibility behaviour of clays at large pressures. Canadian Geotechnical Journal, 44: 355 – 362.

Turner G.A. (1958) The flow structure in packed beds. Chem. Engineering Science, 7, 156-165.

Turner G.A. (1959) The frequency response of some illustrative models of porous media. Chem. Engineering Science, 10, 14-21.

van Olpen, H. (1963) An introduction to clay colloid chemistry. New York and London: Interscience.

van Olphen H. (1991) Clay colloid chemistry. Krieger Publishing Company, Malabar, Fla.

Vanapalli S.K. Fredlund D.G. and Pufahl D.E. (1997) Comparison of saturated–unsaturated shear strength and hydraulic conductivity behavior of a compacted sandy-clay till. In Proceedings of the 50th Canadian Geotechnical Conference, Ottawa, 20–22 Oct., The Canadian Geotechnical Society. Vol. 2, pp. 625–632.

Villar M.V. Lloret A. Romero E. (2003) Thermo-mechanical and geochemical effects on the permeability of high-density clays. In: Proceedings of the International Workshop Large Scale Field Tests in Granite. Advances in Understanding and Research Needs. Universitat Politecnica de Catalunya-ENRESA. Sitges, November 12–14.

Villar M.V., Lloret A. (2004) Influence of temperature on the hydro-mechanical behaviour of a compacted bentonite. Applied Clay Science, Elsevier. 26: 337-350.

Villar M. Garcia-Sineriz J. Barcena I. Lloret A. (2005) State of the bentonite barrier after five years operation of an in situ test simulating a high level radioactive waste repository. Engineering Geology, 81, 317-328.

Villar M.V. Garcıa-Sineriz J.L. Barcena I. and Lloret A. (2005) State of the bentonite barrier after five years operation of an in situ test simulating a high level radioactive waste repository. Engineering Geology, 80: 175-198.

Villar M.V. Lloret A. (2008) Influence of dry density and water content on the swelling of a compacted bentonite. Applied Clay Science, Elsevier. 39: 38-49.

Vukovic M. and Soro A. (1992) Determination of hydraulic conductivity of porous media from grain-size composition. Water Resource Pub. 69 pp.

Wan A.W.L. Gray M.N. and Graham J. (1995) On the relations of suction, moisture content and soil structure in compacted clays. In Proceedings of the 1st International Conference on Unsaturated Soils, Paris, France, September 1995. Edited by E.E. Alonso and P. Delage. A.A. Balkema, Rotterdam, The Netherlands, Vol. 1, pp. 215–222.

Wan A. W. L. (1996) The use of thermocouple psychrometers to measure insitu suctions and water contents in compacted clays. A thesis submitted to the faculty of graduate studies in the partial fulfillment. Department of civil and Geological engineering, university of Manitoba, Winnipeg, Canada.

Watabe Y. Leroueil S. and Le Bihan J.P. (2000) Influence of compaction conditions on pore-size distribution and saturated hydraulic conductivity of a glacial till. Canadian Geotechnical Journal, 37: 1184–1194.

Woessner D.E. (1980) An NMR investigation onto the ranges of the surface effect on the rotation of water molecules, Journal of Magnetic Resonance. 39: 297-308.

Wright S.P. Walden P.J. Sangha C.M. and Langdon N.J. (1996) Observations on Soil Permeability, Moulding Moisture Content and Dry Density Relationships, QJEG, 29, pp. 249-255.

Wright S.P. Walden P.J. Sangha C.M. and Langdon N.J. (1997) Observations of soil permeability, moulding moisture content and dry density relationships. Quarterly Journal of Engineering Geology, 29: 249–255.

Xie M. Agus S.S. Schanz T. and Kolditz, O. (2004) An upscaling method and a numerical analysis of swelling/shrinking processes in a compacted bentonite/sand mixture. International Journal for Numerical and Analytical Methods in Geomechanics, 28(15): 1479-1502.

Yahia-Aisse M. (1999) Comportement hydromechnique d' une argile gonflante fortement compactee. These de doctorat. Ecole Nationale de Ponts et Chaussees, Paris, 241 pp.

Yong R. N. and Sheeran D. E. (1973) Fabric unit interaction and soil behavior, Proceedings of the International Symposium on Soil Structure, Gothenburg, Sweden, pp. 176–183.

Yong R.N. and Warkentin, B.P. (1975) Introduction to soil behaviour. The Macmillan Company, New York.

Yong R.N. Sadana M.L. and Gohl W.B. (1984) A particle interaction model for assessment of swelling of an expansive soil. *In* Proceedings of the 5th International Conference on Expansive Soils, Adelaide, Australia, May 1984. pp. 4–12.

Yong R.N. and Mohamed A.M.O. (1992) A study of particle interaction energies in wetting of unsaturated expansive clays. Canadian Geotechnical Journal, 29, 1060–1070.

Yong R.N. (1999) Soil suction and soil-water potentials in swelling clays in engineered clay barriers. Engineering Geology, Elsevier. 54: 3-13.

Yong R.N. Yaacob W.Z.W. Bentley S.P. Harris, C. and Tan, B.K. (2001) Partitioning of heavy metals on soil samples from column tests. Engineering Geology, 60, 307- 322.

Yukselen Y. and Kaya A. (2006) Prediction of cation exchange capacity from soil index properties. Clay Minerals, Vol. 41, No. 4, 827-837.

Zaradny H. (1993) Groundwater flow in saturated and unsaturated soil. Rotterdam: Balkema, 279 pp.

Zhu Y. and Granick S. (2001) Viscosity of interfacial water, Phys. Rev. Lett. 87, 096104.

# APPENDIX-A1

## Inflow and outflow condition
## Steady state condition

# Distilled water

## A.1 Calcigel

Dry density = 1.4 $Mg/m^3$
Low initial water content = 9.0 %
Permeant = Distilled water ($10^{-4}$M)

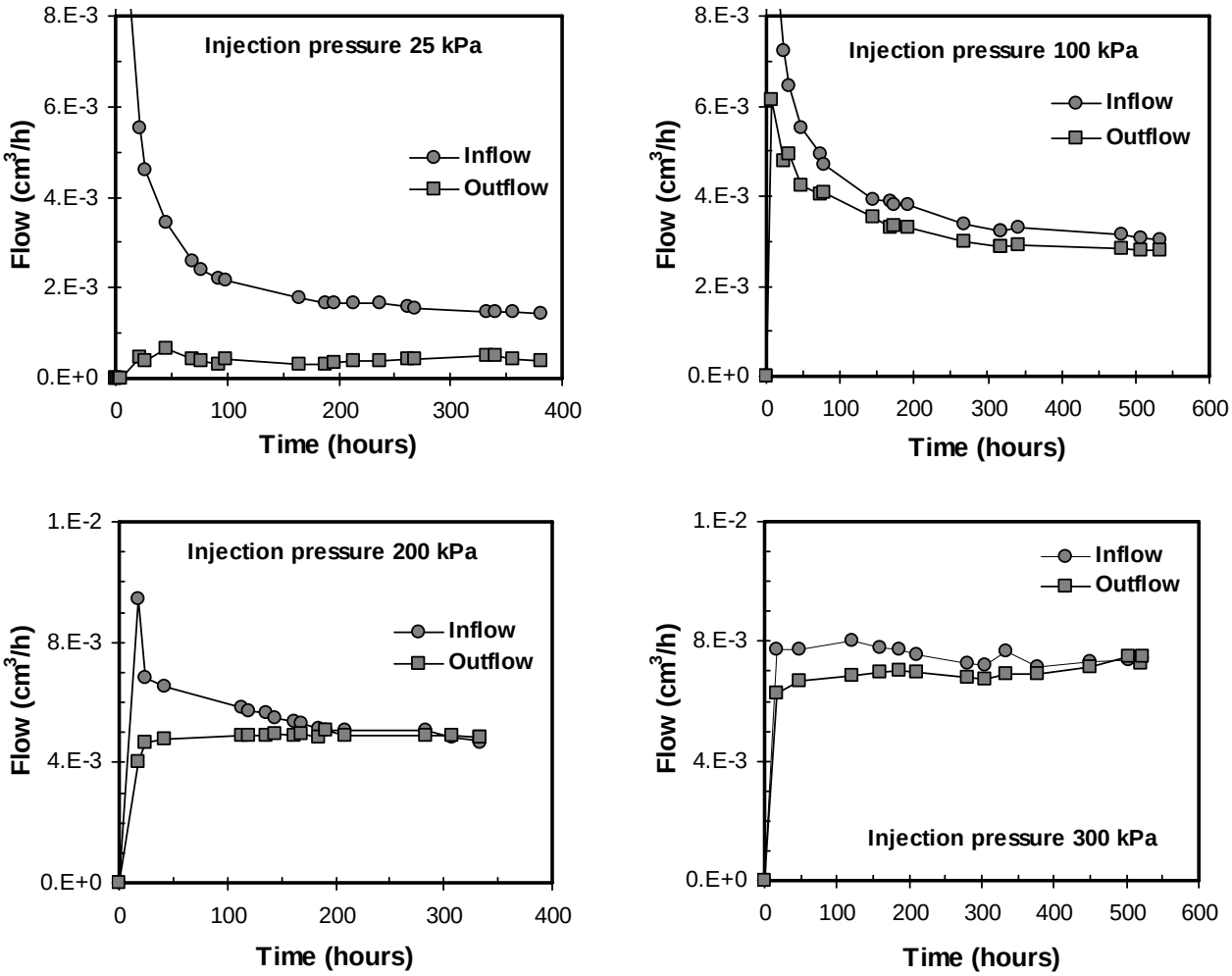


Figure A.1 Inflow and outflow condition for Calcigel bentonite

## A.1 Calcigel

Dry density = 1.6 Mg/m$^3$
Low initial water content = 9.0 %
Permeant = Distilled water ($10^{-4}$M)

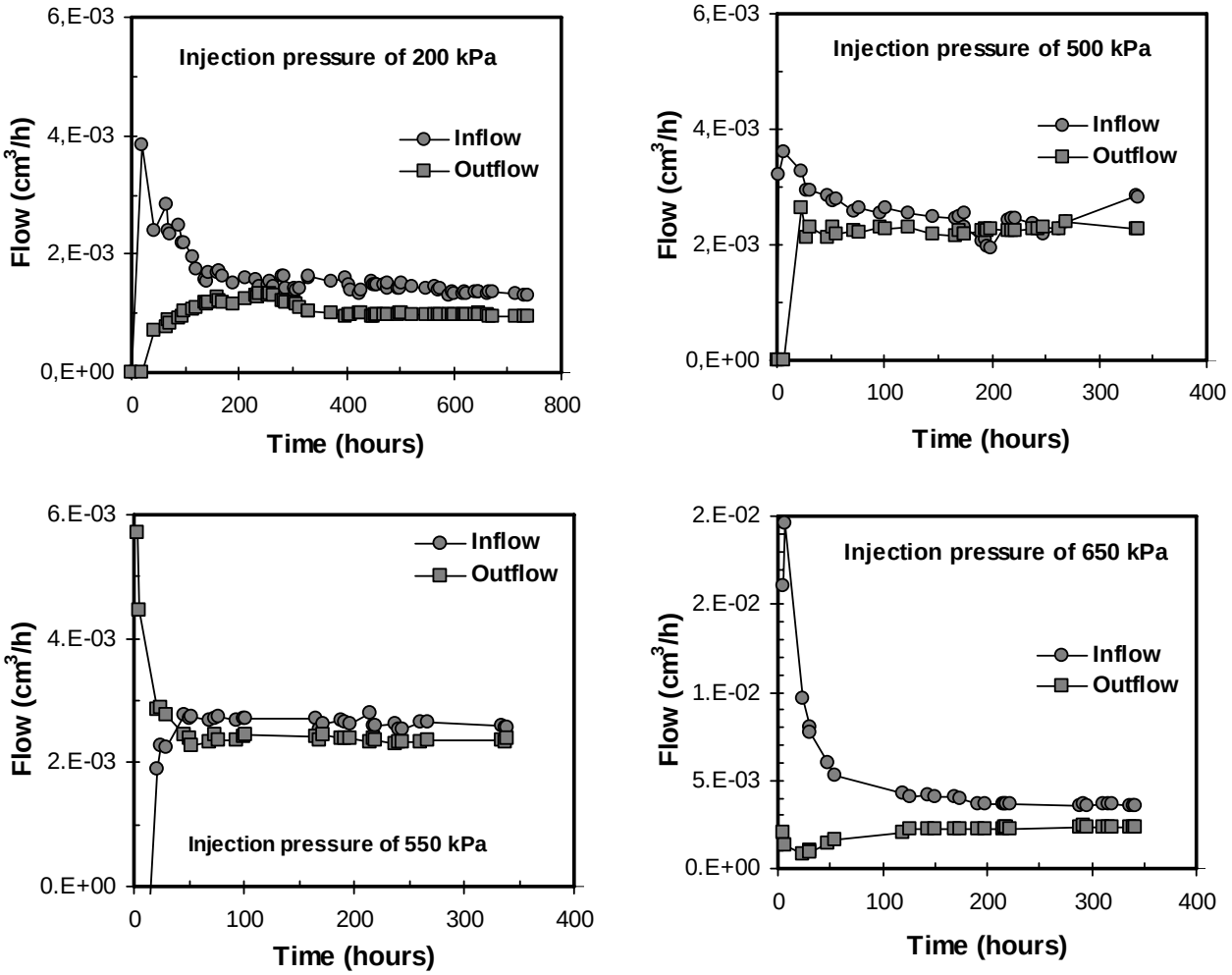


Figure A.2 Inflow and outflow condition for Calcigel bentonite

## A.1 Calcigel

Dry density = 1.8 $Mg/m^3$
Initial water content = 9.0 %
Permeant = Distilled water ($10^{-4}$M)

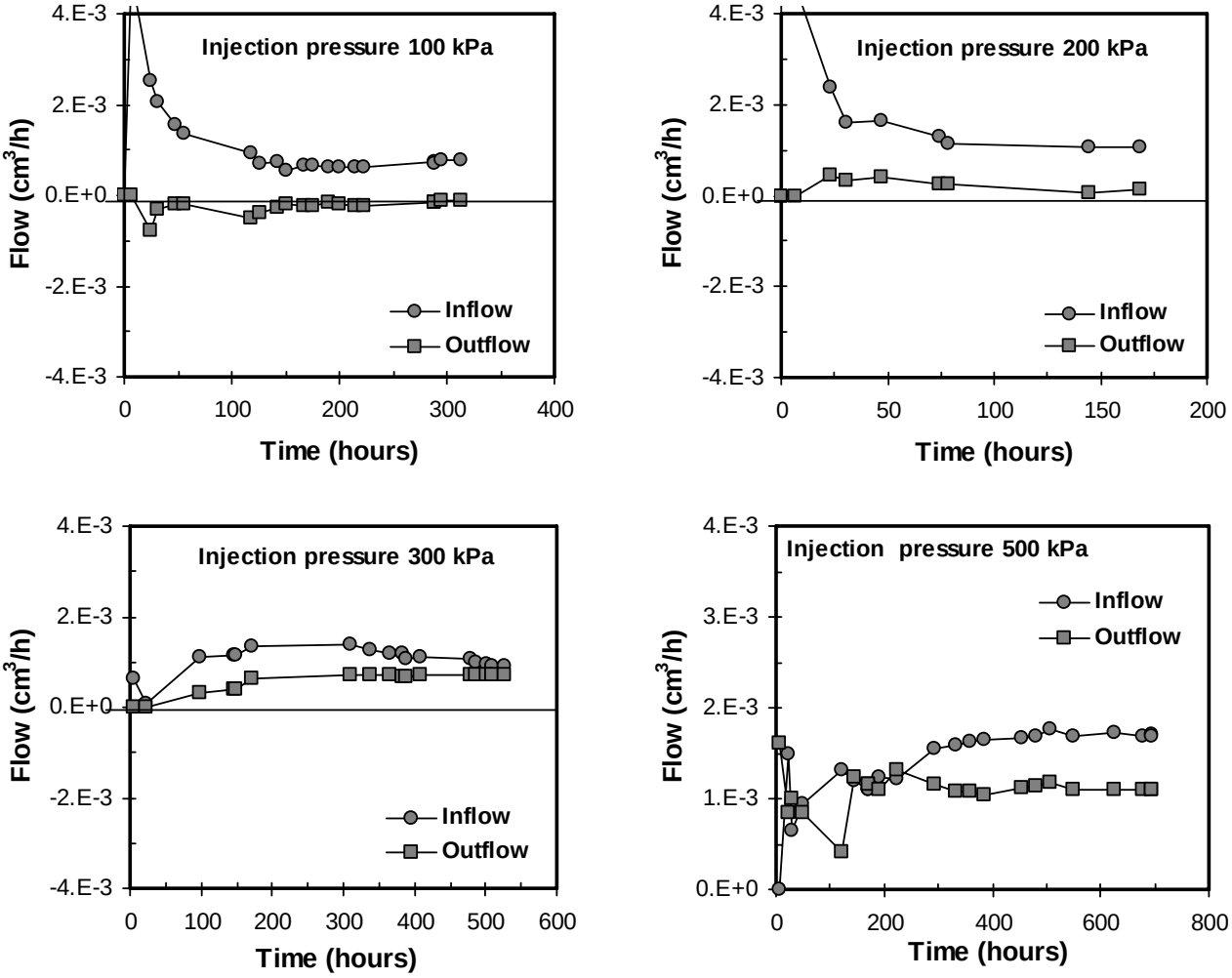


Figure A.3 Inflow and outflow condition for Calcigel bentonite

## A.1 Calcigel

Dry density = 1.4 $Mg/m^3$
High initial water content = 34.5 %
Permeant = Distilled water ($10^{-4}$M)

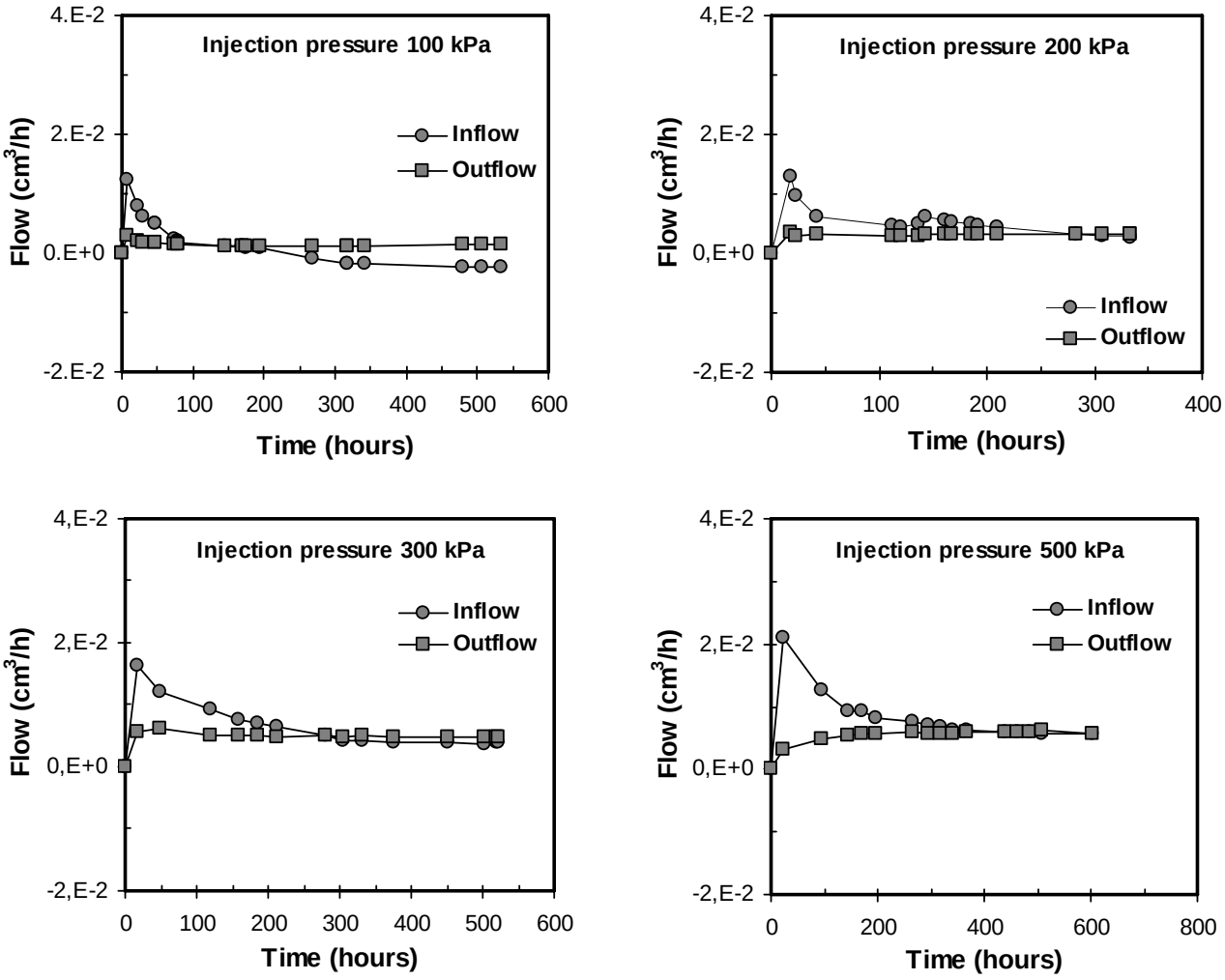


Figure A.4 Inflow and outflow condition for Calcigel bentonite

## A.1 Calcigel

Dry density = 1.6 $Mg/m^3$
High initial water content = 25.7 %
Permeant = Distilled water ($10^{-4}$M)

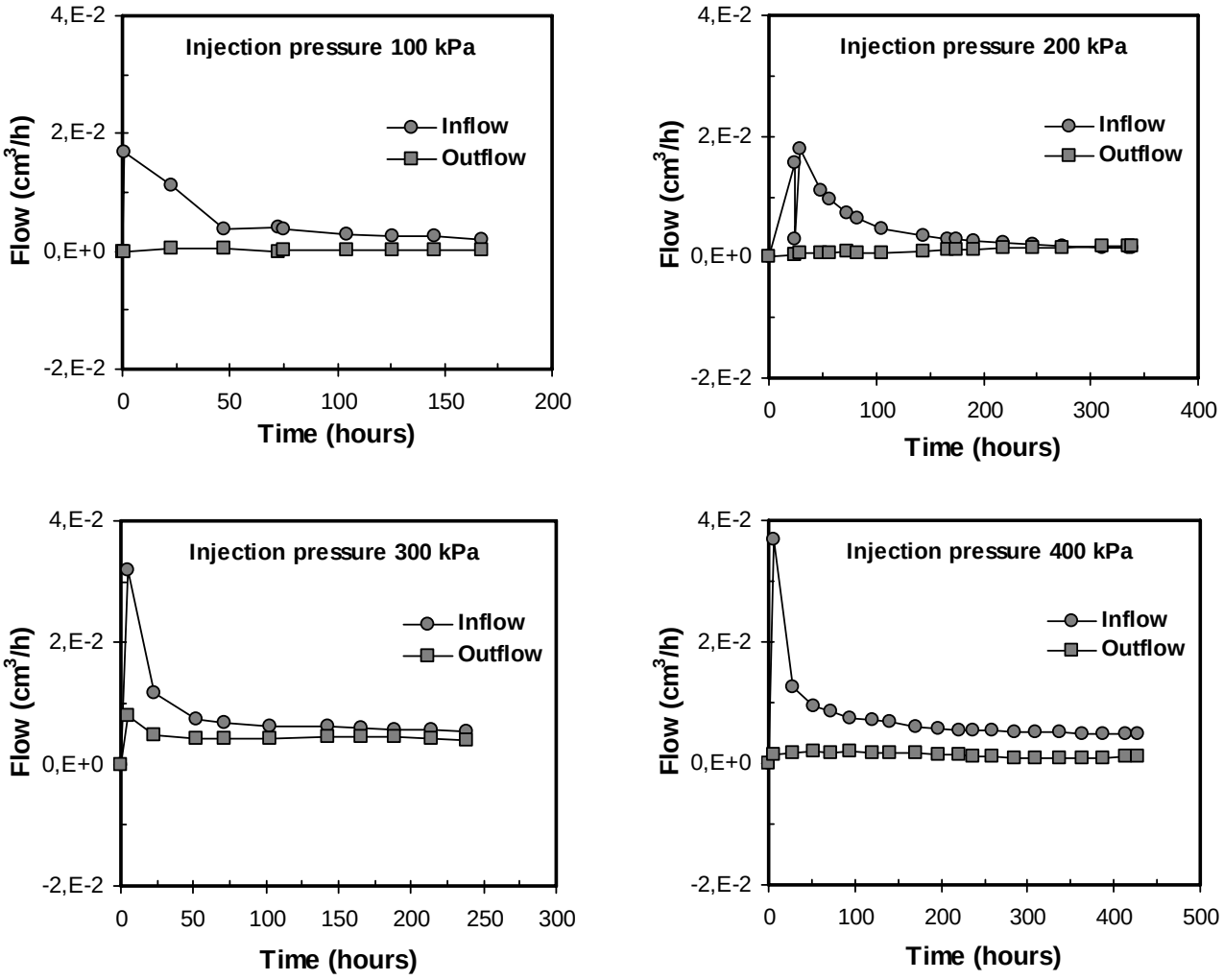


Figure A.5 Inflow and outflow condition for Calcigel bentonite

## A.1 Calcigel

Dry density = 1.8 Mg/m$^3$
High initial water content = 18.8 %
Permeant = Distilled water ($10^{-4}$M)

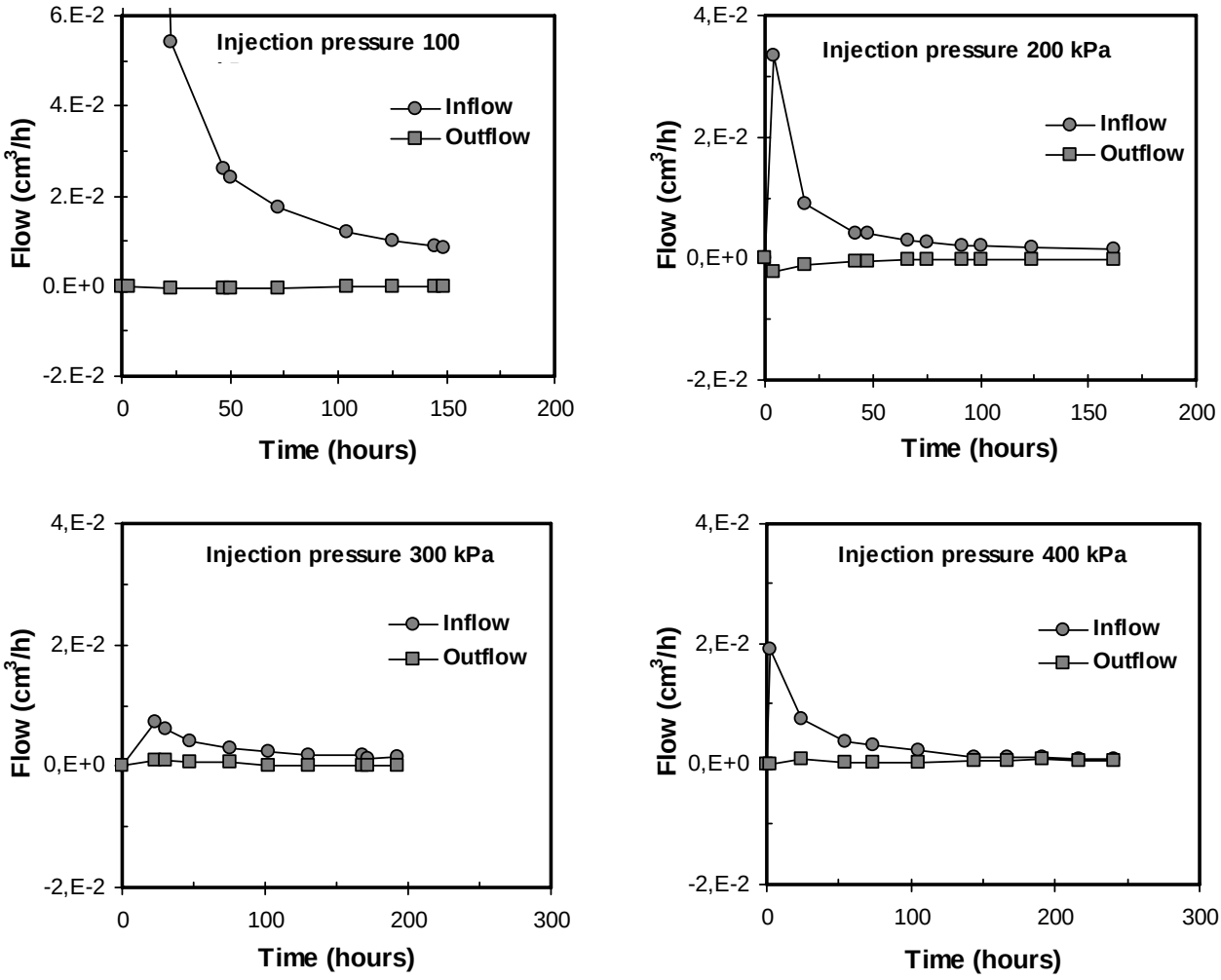


Figure A.6 Inflow and outflow condition for Calcigel bentonite

## A.2 MX-80

Dry density = 1.4 $Mg/m^3$
Low initial water content = 10.5 %
Permeant = Distilled water ($10^{-4}$M)

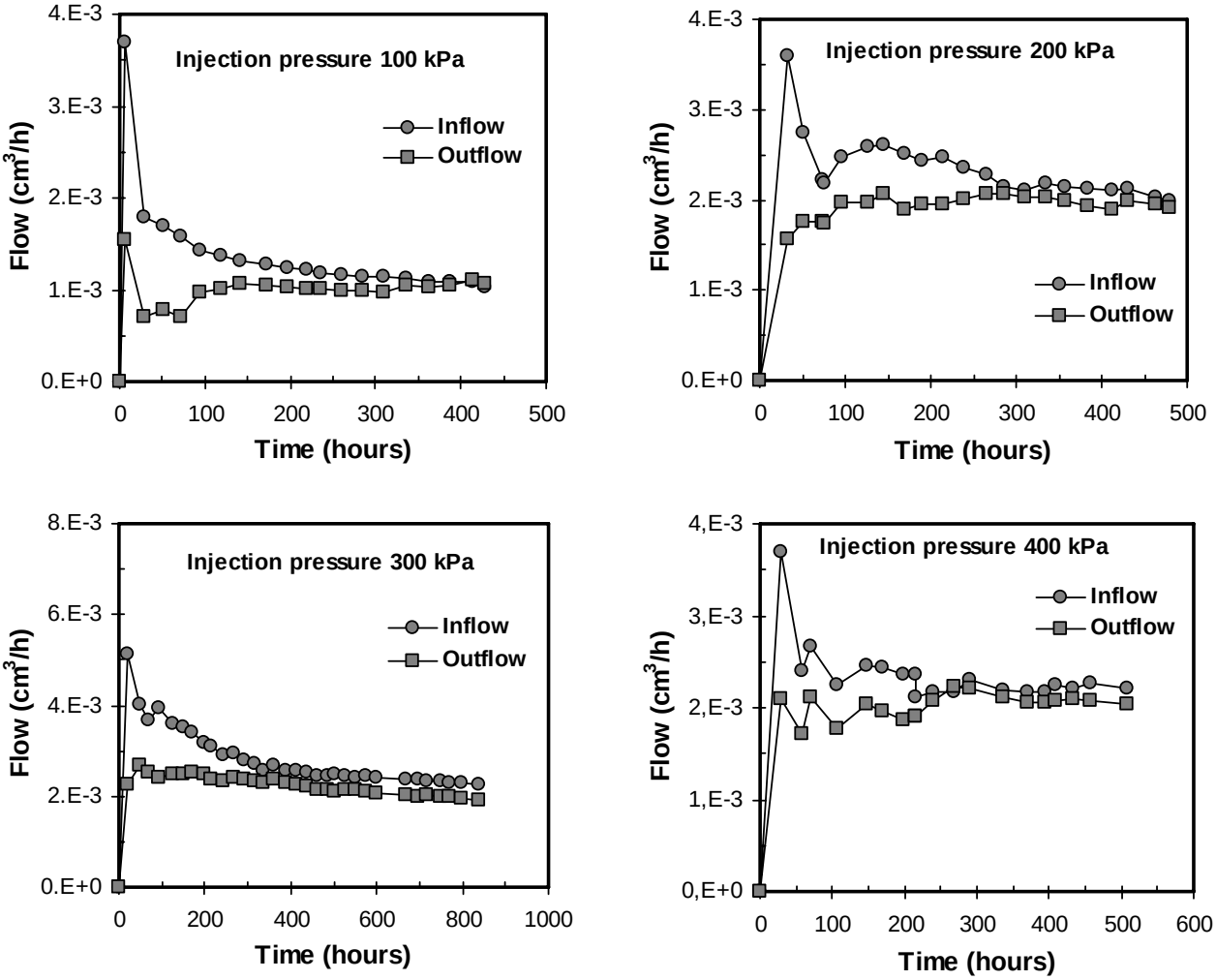


Figure A.7 Inflow and outflow condition for MX-80 bentonite

## A.2 MX-80

Dry density = 1.6 Mg/m$^3$
Low initial water content = 10.5 %
Permeant = Distilled water ($10^{-4}$M)

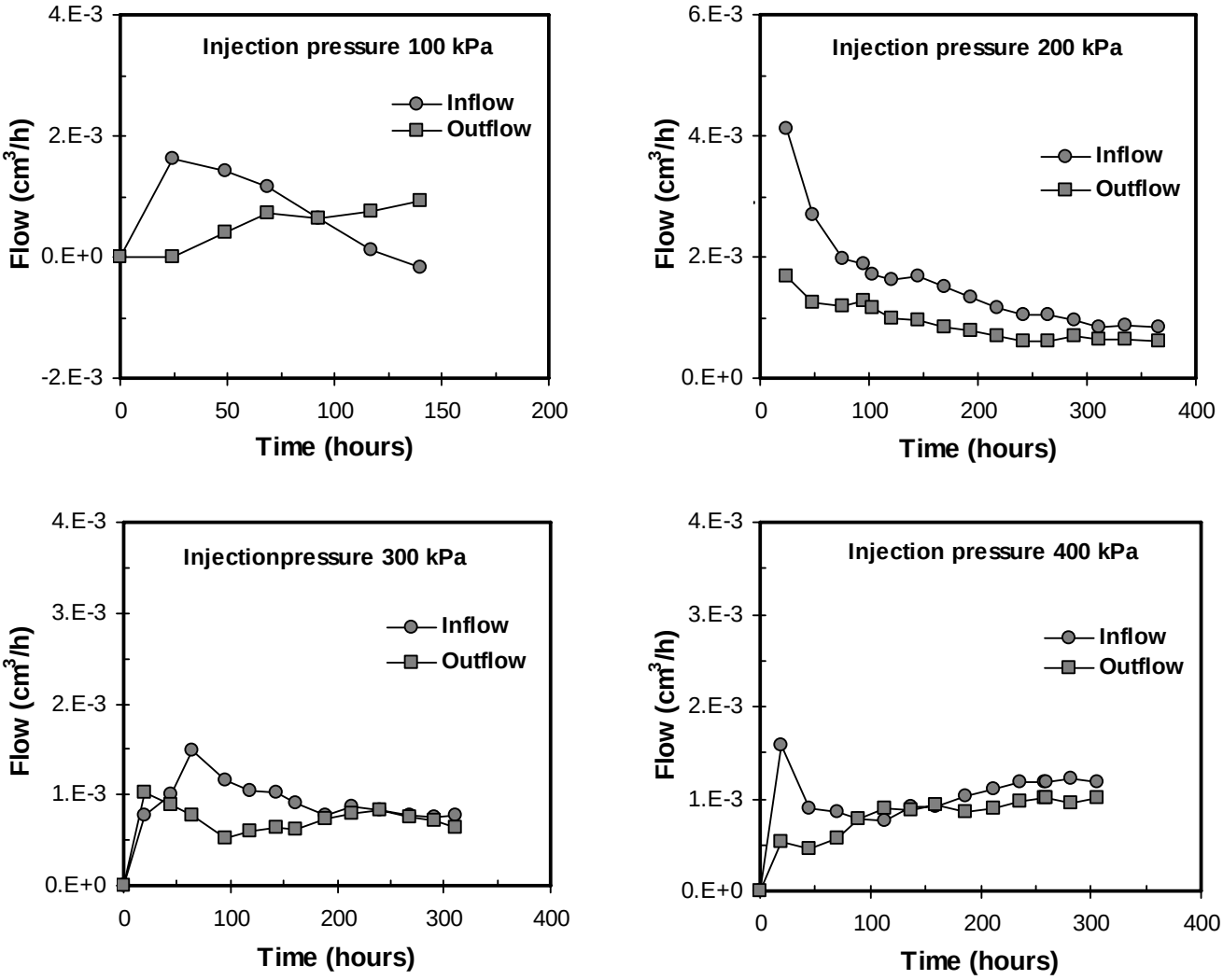


Figure A.8 Inflow and outflow condition for MX-80 bentonite

## A.2 MX-80

Dry density = 1.8 $Mg/m^3$
Low initial water content = 10.5 %
Permeant = Distilled water ($10^{-4}$M)

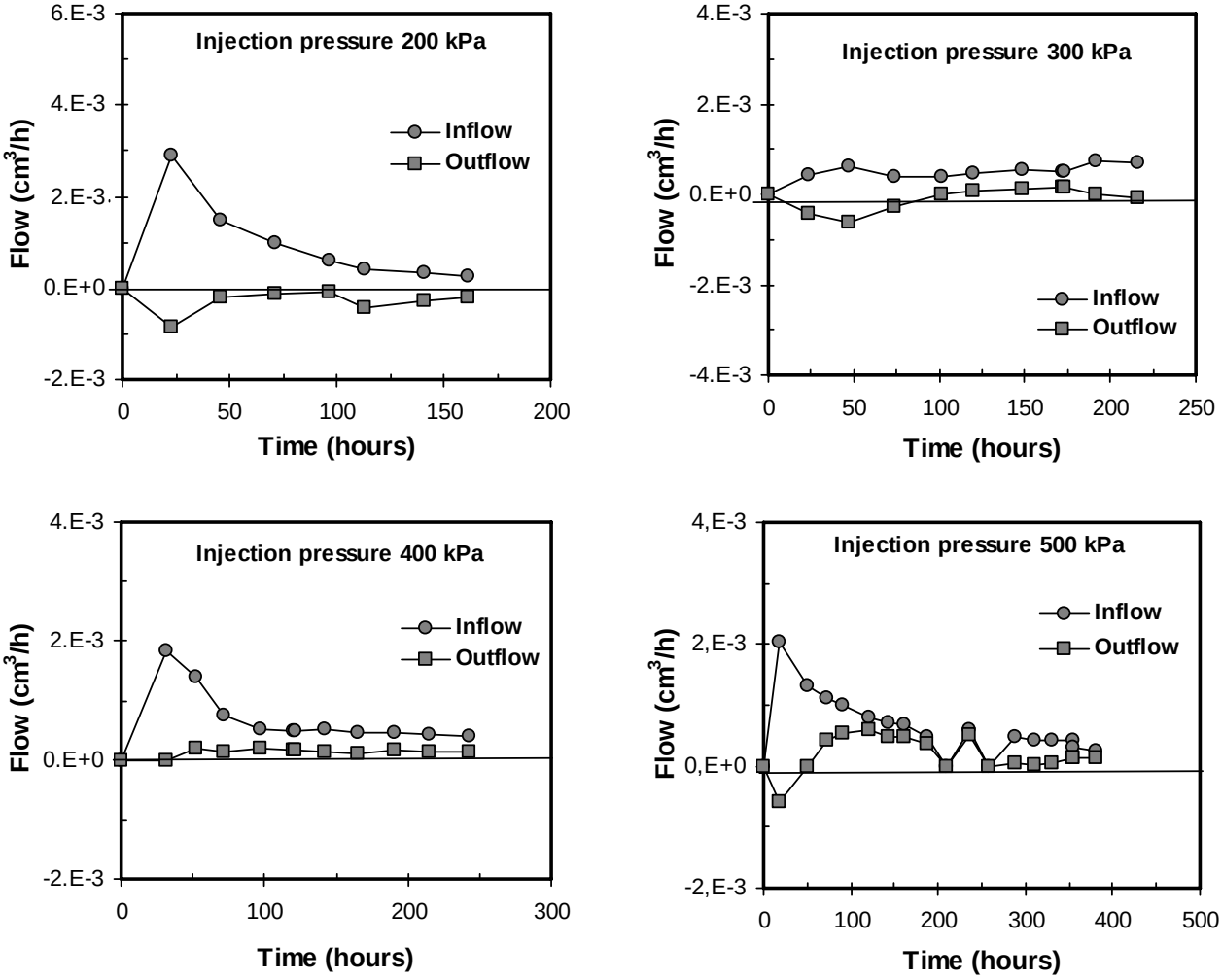


Figure A.9 Inflow and outflow condition for MX-80 bentonite

## A.2 MX-80

Dry density = 1.4 Mg/m$^3$
High initial water content = 35.7 %
Permeant = Distilled water ($10^{-4}$M)

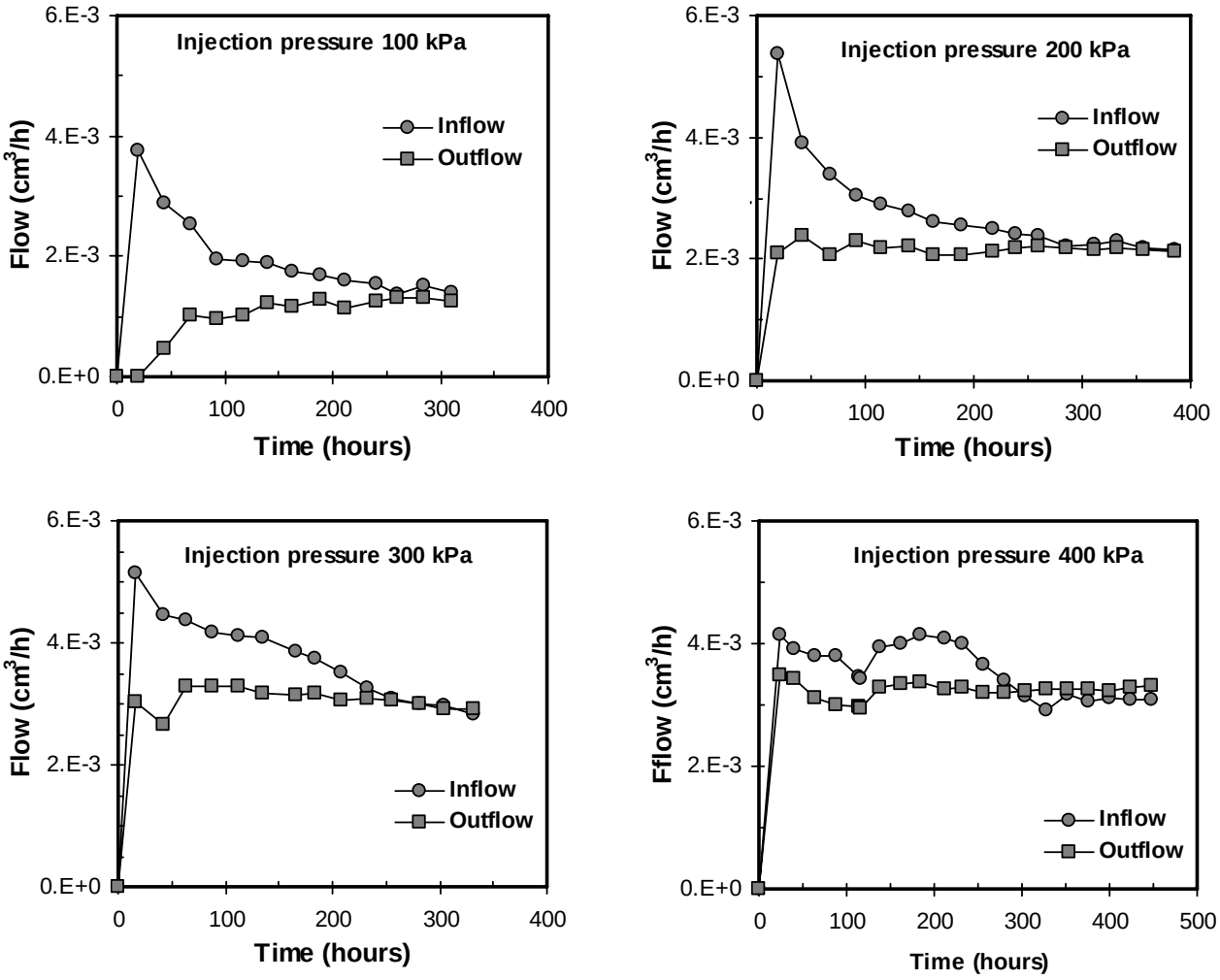


Figure A.10 Inflow and outflow condition for MX-80 bentonite

## A.2 MX-80

Dry density = 1.6 $Mg/m^3$
High initial water content = 26.8 %
Permeant = Distilled water ($10^{-4}$M)

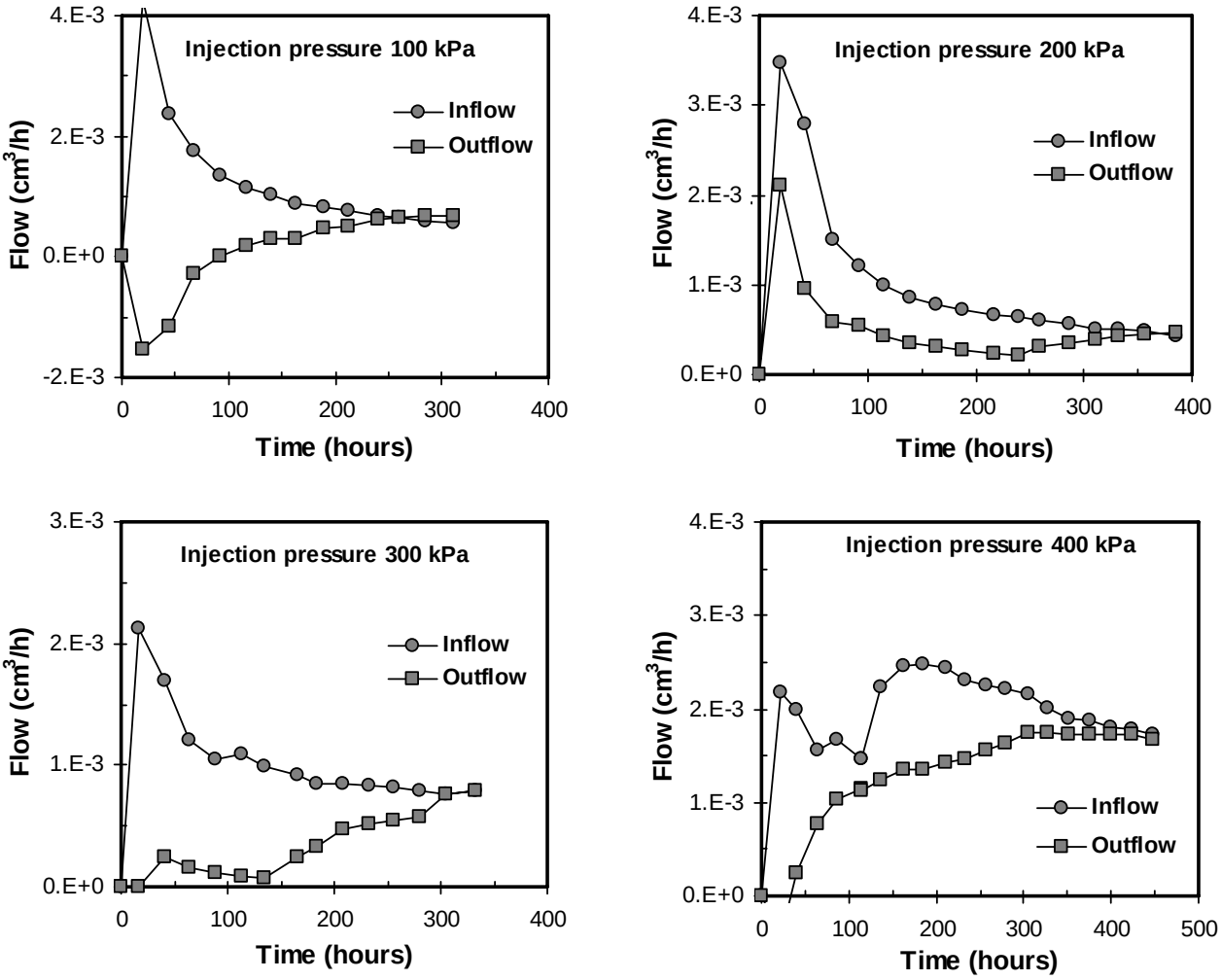


Figure A.11 Inflow and outflow condition for MX-80 bentonite

## A.2 MX-80

Dry density = 1.8 Mg/m$^3$
High initial water content = 19.6 %
Permeant = Distilled water ($10^{-4}$M)

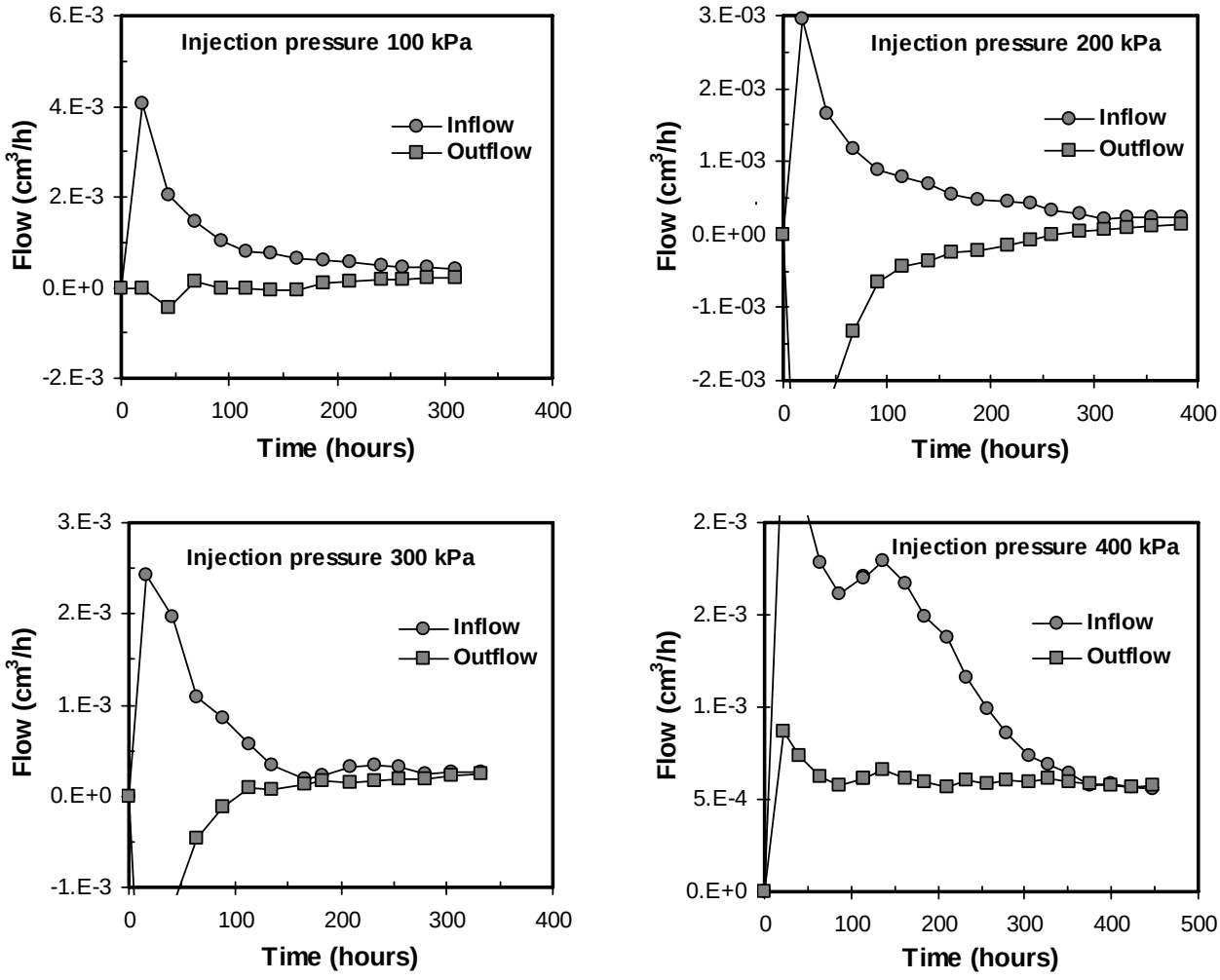


Figure A.12 Inflow and outflow condition for MX-80 bentonite

## A.3 Kunigel

Dry density = 1.4 $Mg/m^3$
Low initial water content = 6.2 %
Permeant = Distilled water ($10^{-4}$M)

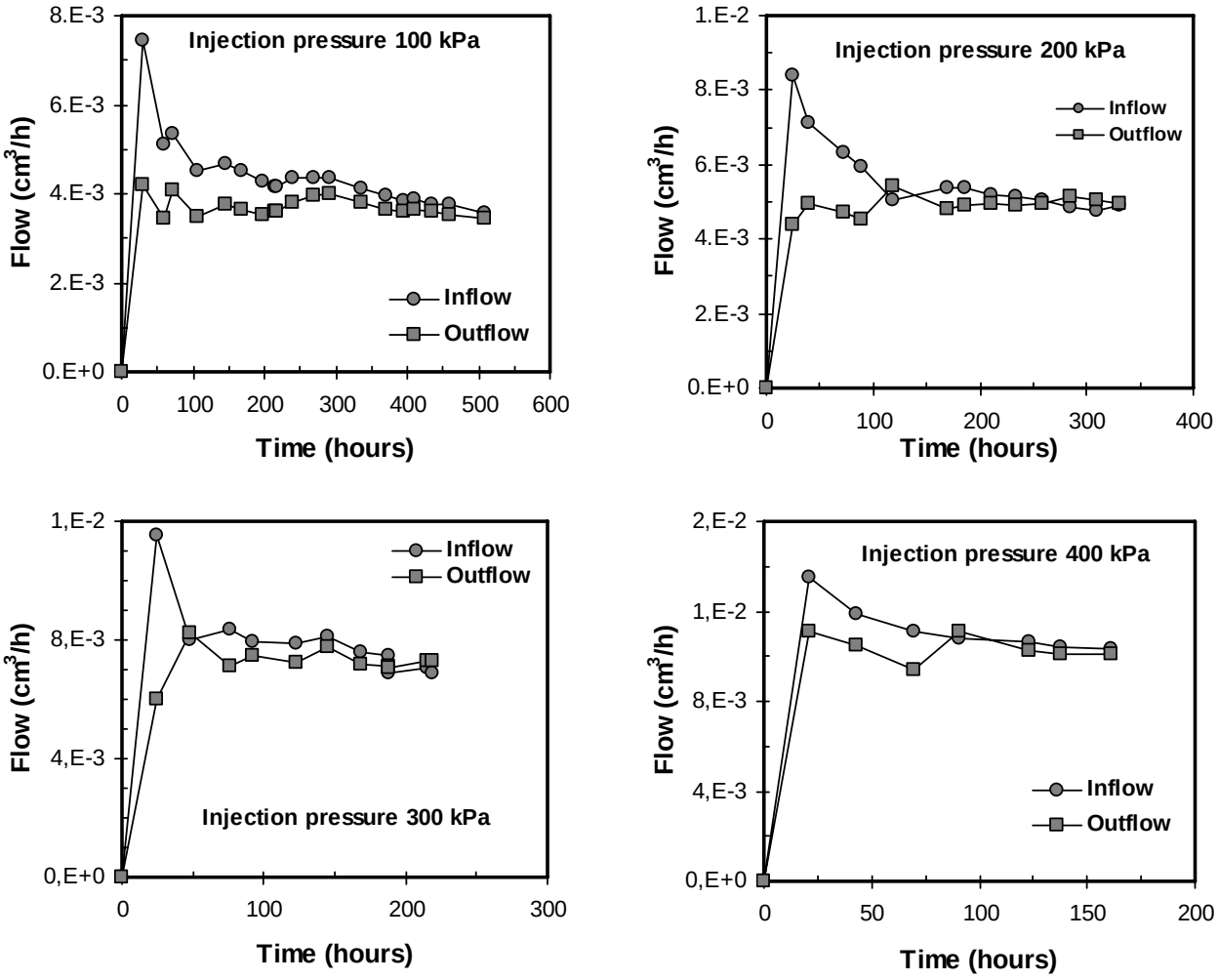


Figure A.13 Inflow and outflow condition for Kunigel bentonite

## A.3 Kunigel

Dry density = 1.6 Mg/m$^3$
Low initial water content = 6.2 %
Permeant = Distilled water ($10^{-4}$M)

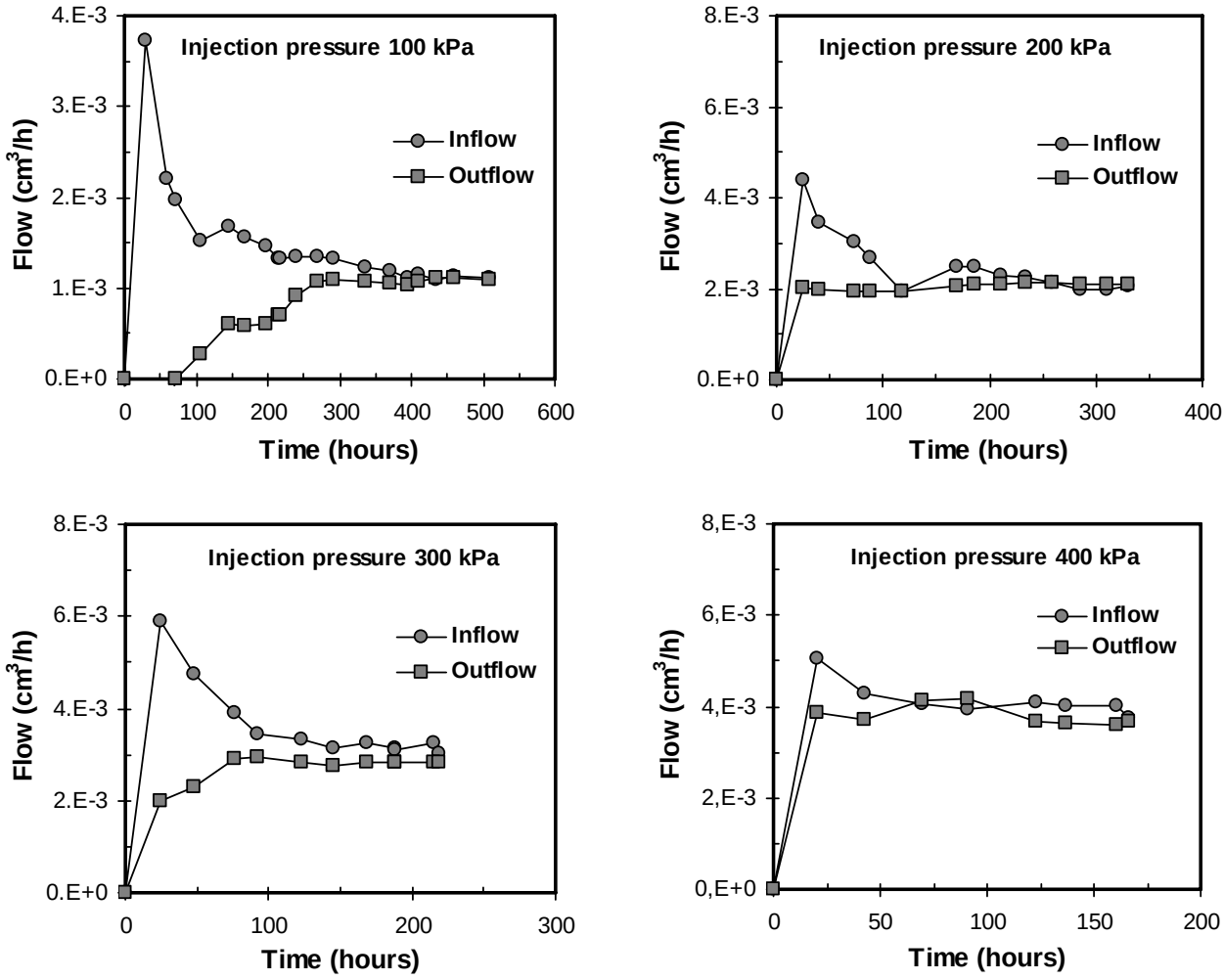


Figure A.14 Inflow and outflow condition for Kunigel bentonite

## A.3 Kunigel

Dry density = 1.8 $Mg/m^3$
Low initial water content = 6.2 %
Permeant = Distilled water ($10^{-4}$M)

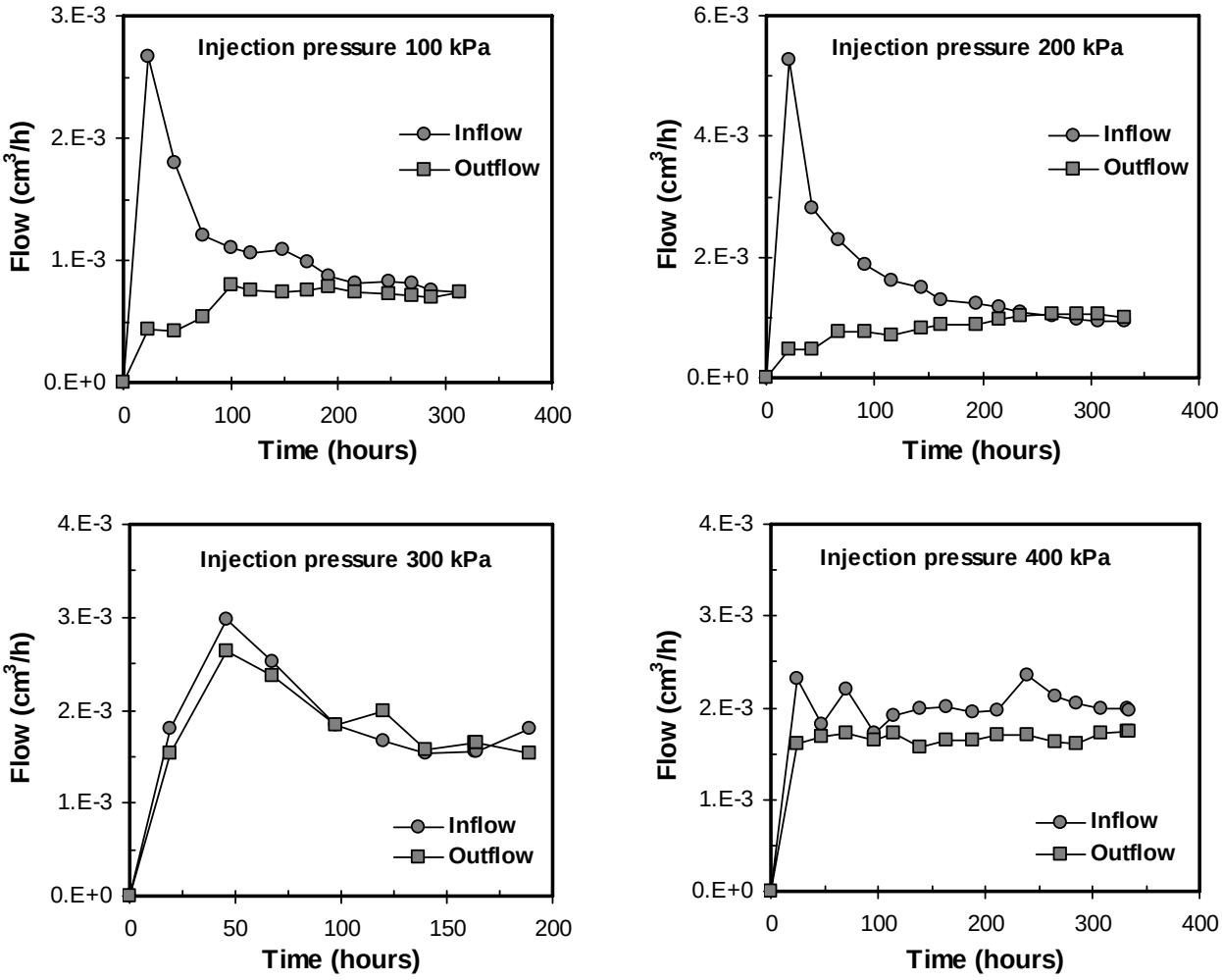


Figure A.15 Inflow and outflow condition for Kunigel bentonite

## A.3 Kunigel

Dry density = 1.4 Mg/m$^3$
High initial water content = 34.9 %
Permeant = Distilled water ($10^{-4}$M)

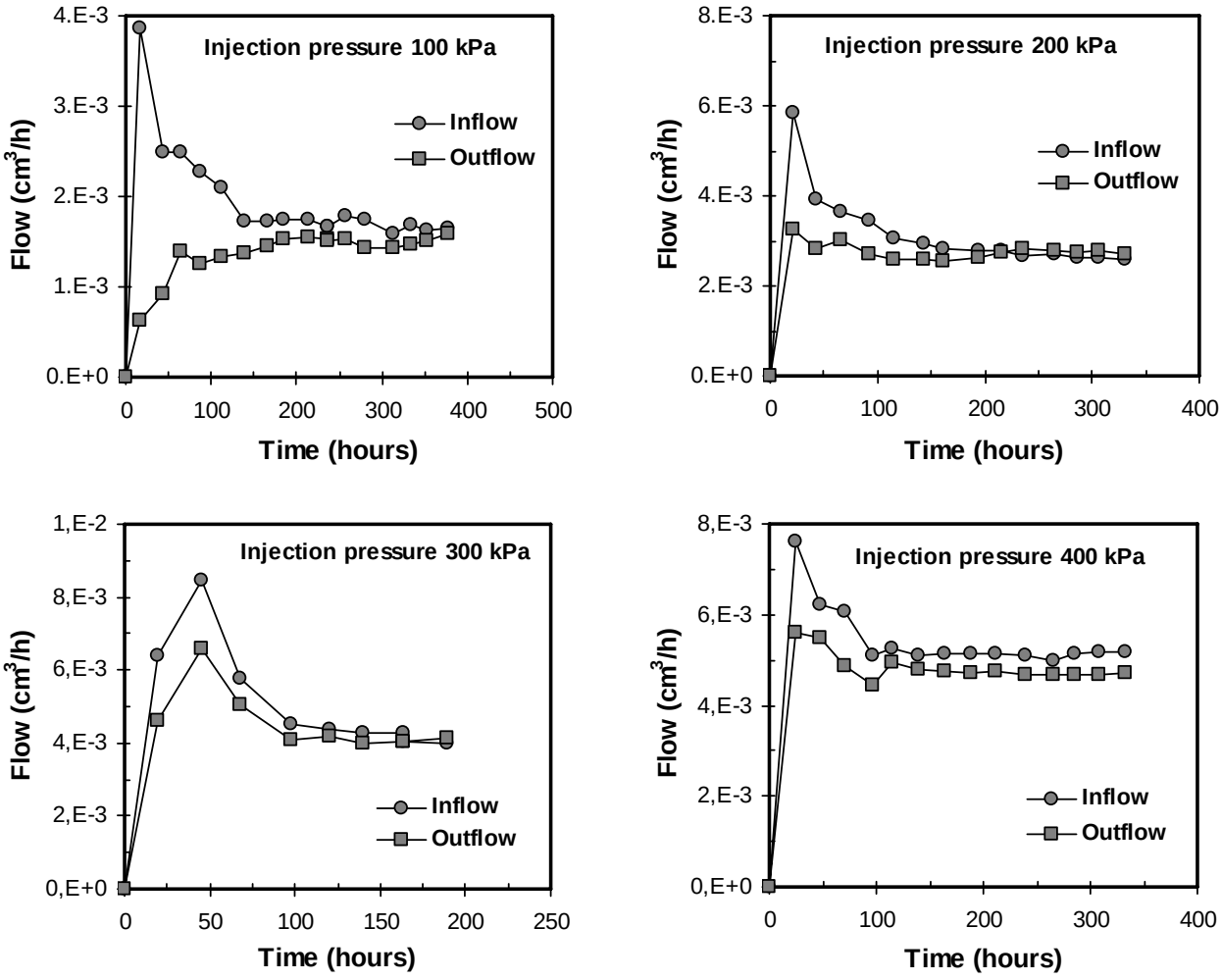


Figure A.16 Inflow and outflow condition for Kunigel bentonite

## A.3 Kunigel

Dry density = 1.6 $Mg/m^3$
High initial water content = 26.1 %
Permeant = Distilled water ($10^{-4}$M)

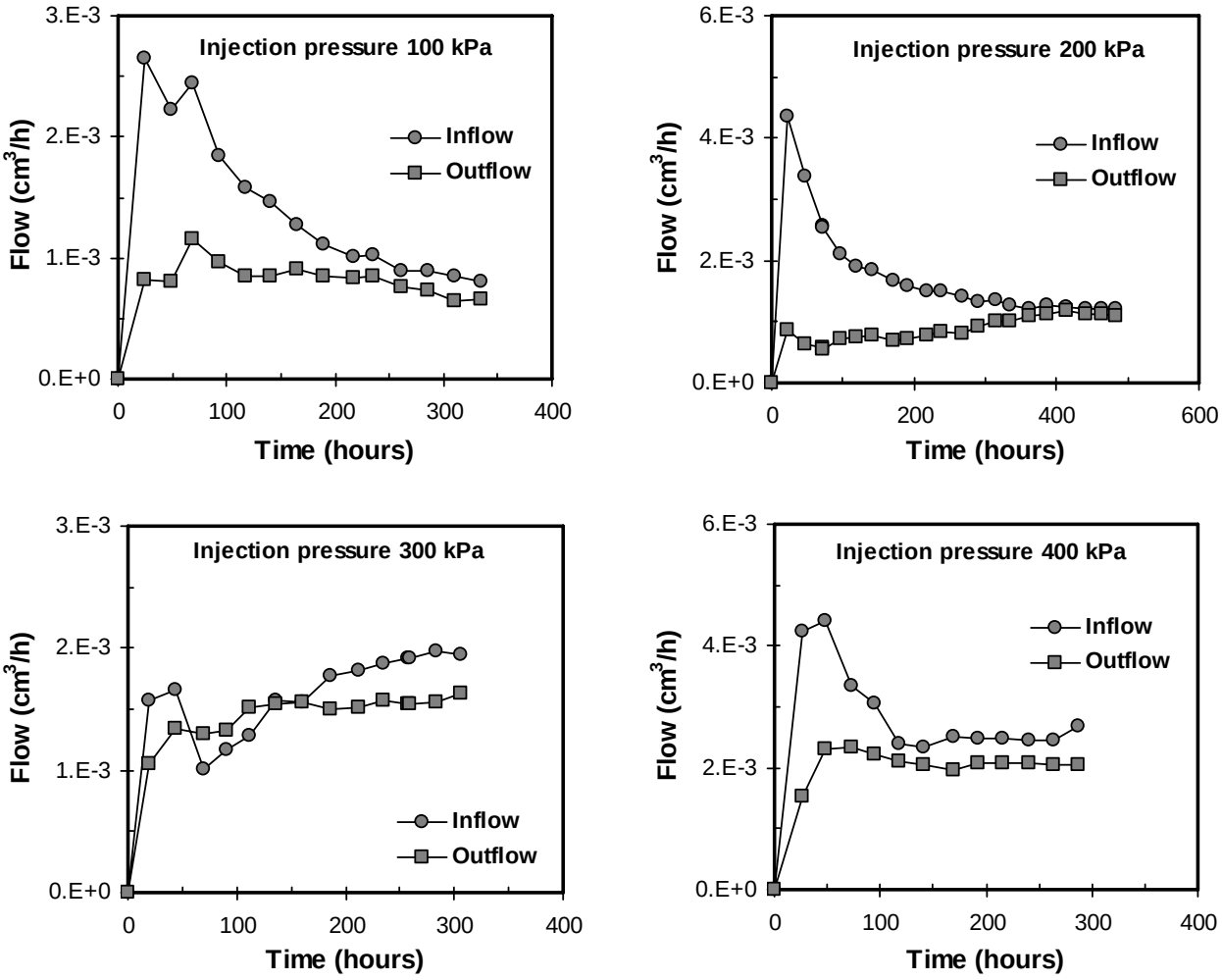


Figure A.17 Inflow and outflow condition for Kunigel bentonite

## A.3 Kunigel

Dry density = 1.8 Mg/m$^3$
High initial water content = 19.3 %
Permeant = Distilled water ($10^{-4}$M)

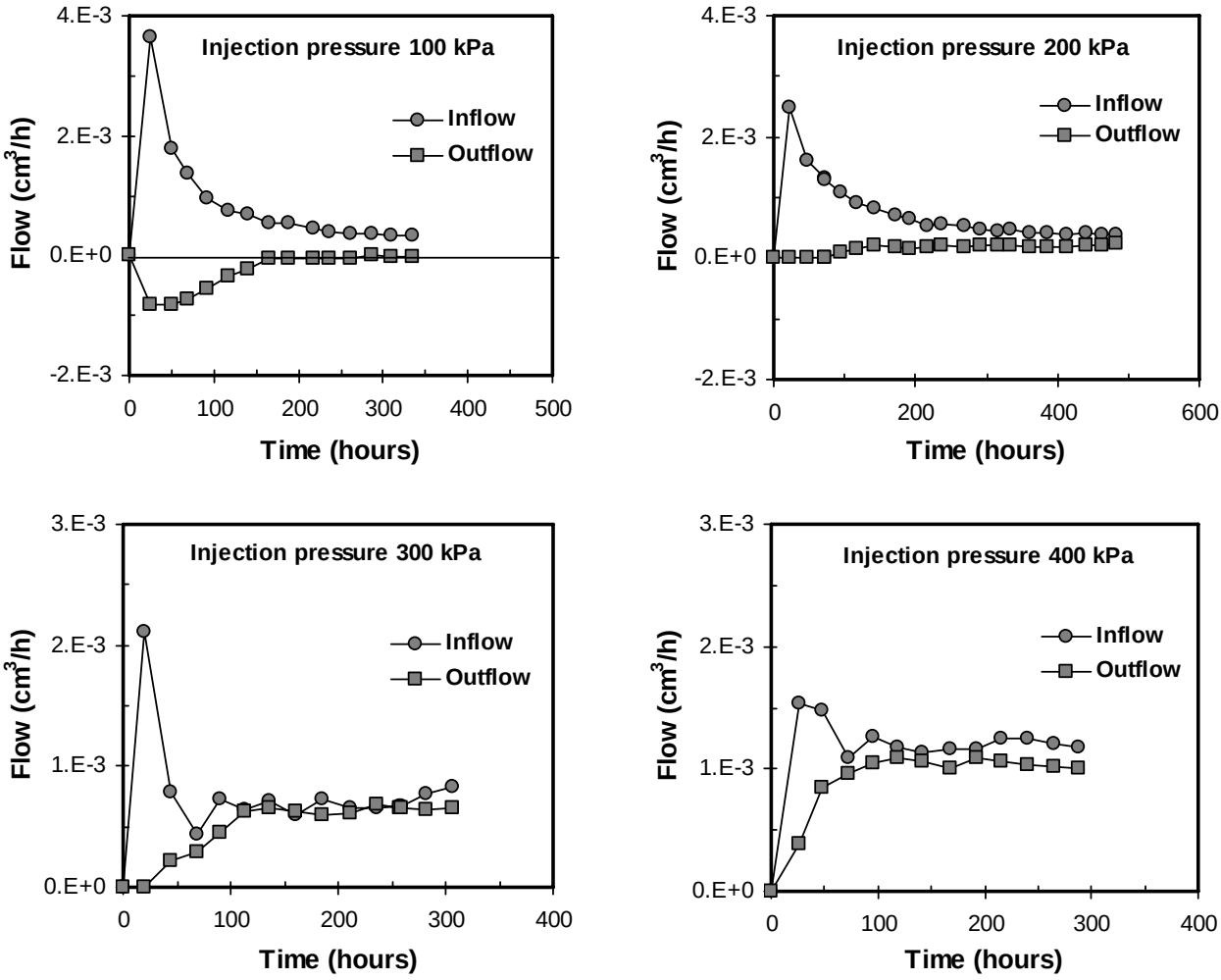


Figure A.18 Inflow and outflow condition for Kunigel bentonite

# High concentration solution

## A.1 Calcigel

Dry density = 1.4 $Mg/m^3$
Low initial water content = 9.0 %
Permeant = High concentration solution ($10^{-2}$M)

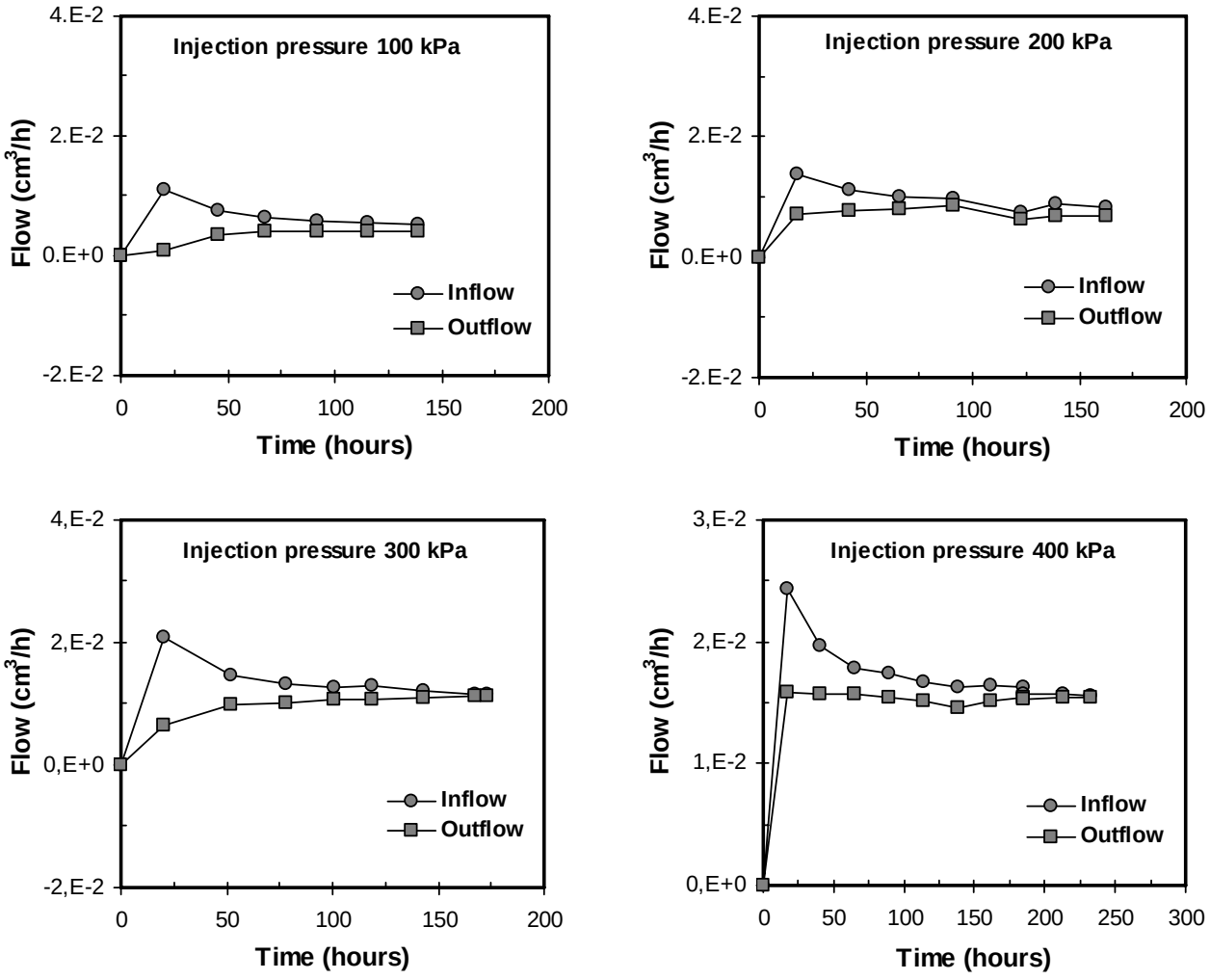


Figure A.19 Inflow and outflow condition for Calcigel bentonite

## A.1 Calcigel

Dry density = 1.6 $Mg/m^3$
Low initial water content = 9.0 %
Permeant = High concentration solution ($10^{-2}$M)

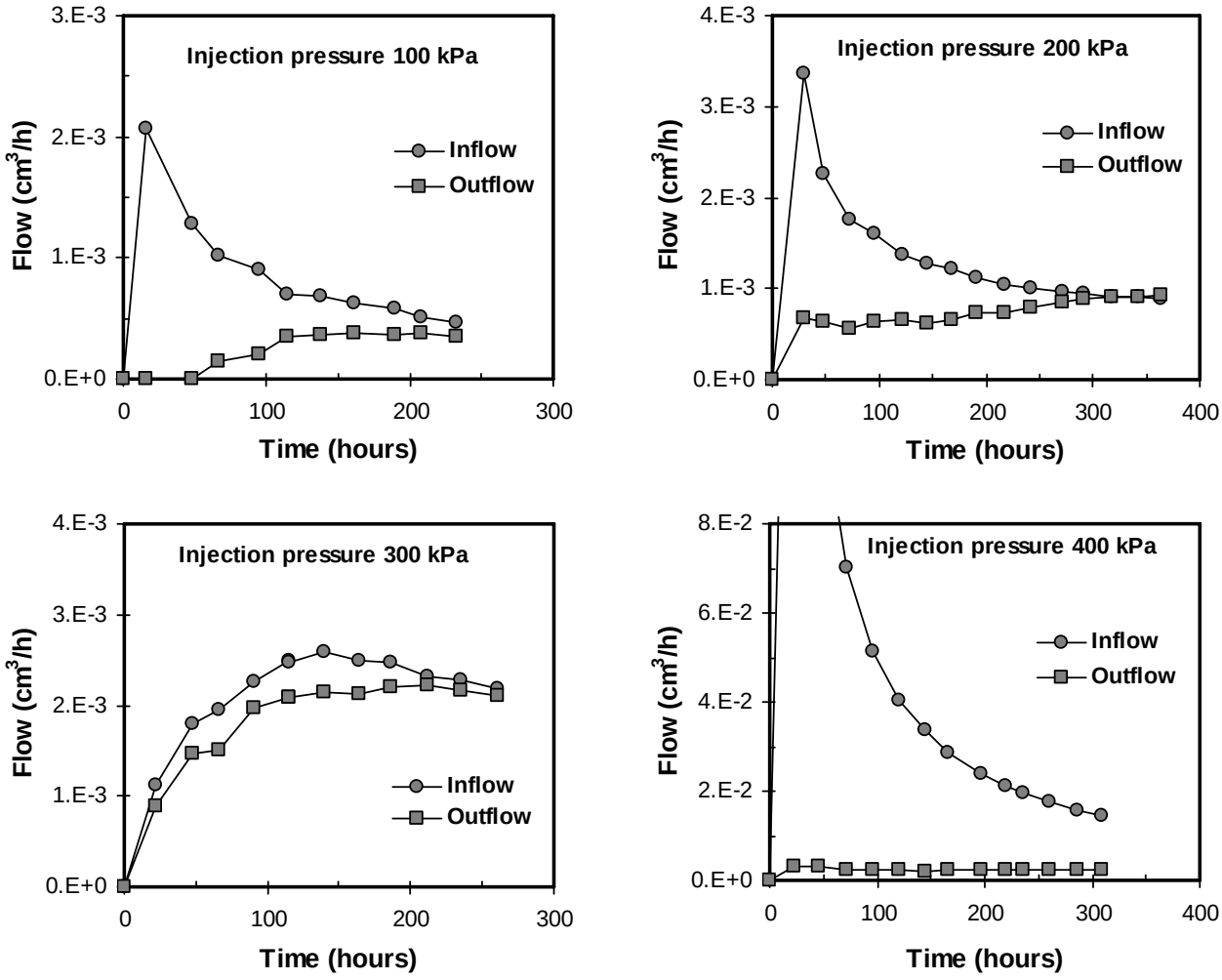


Figure A.20 Inflow and outflow condition for Calcigel bentonite

## A.1 Calcigel

Dry density = 1.8 $Mg/m^3$
Low initial water content = 9.0 %
Permeant = High concentration solution ($10^{-2}$M)

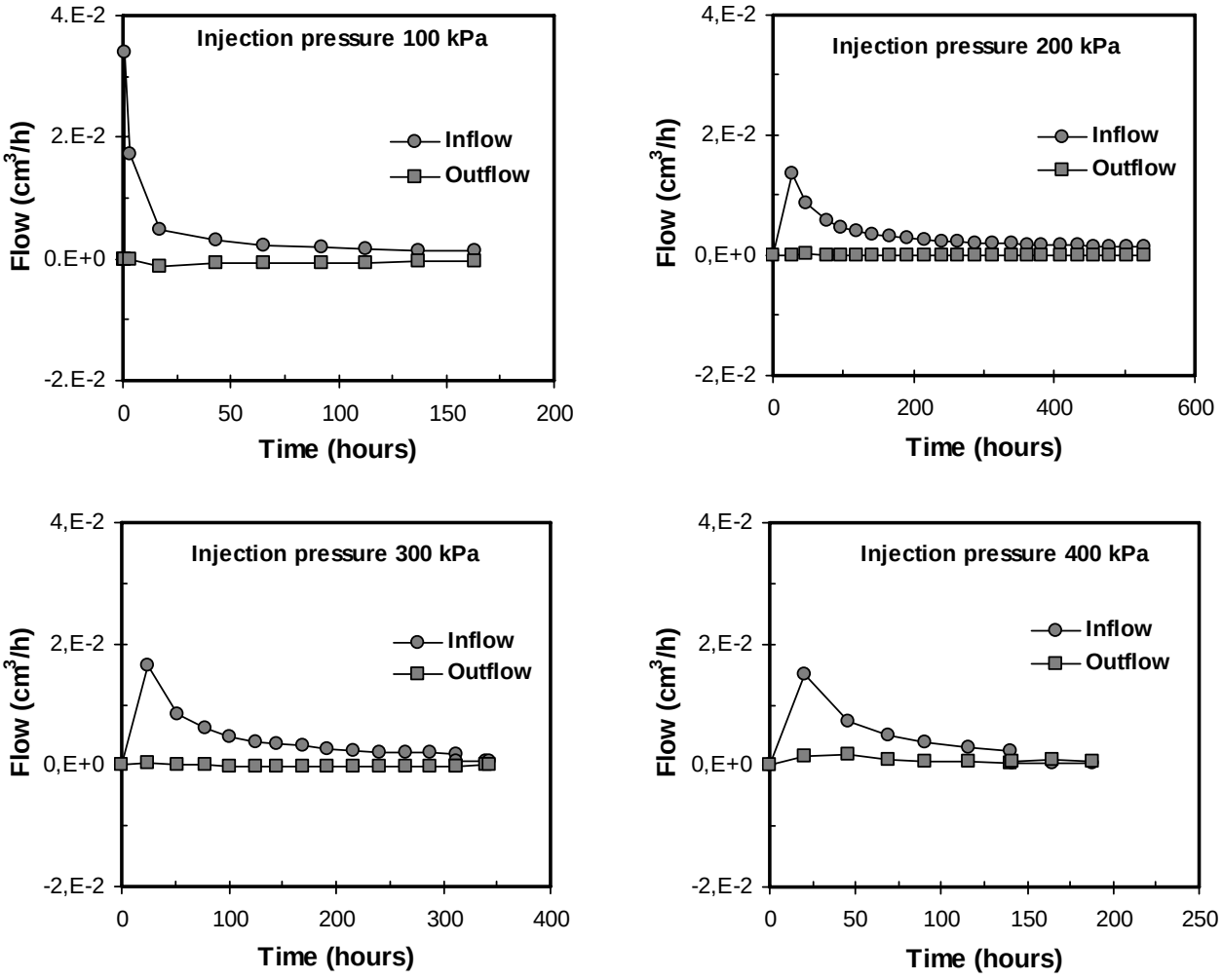


Figure A.21 Inflow and outflow condition for Calcigel bentonite

## A.2 MX-80

Dry density = 1.4 $Mg/m^3$
Low initial water content = 10.5 %
Permeant = High concentration solution ($10^{-2}$M)

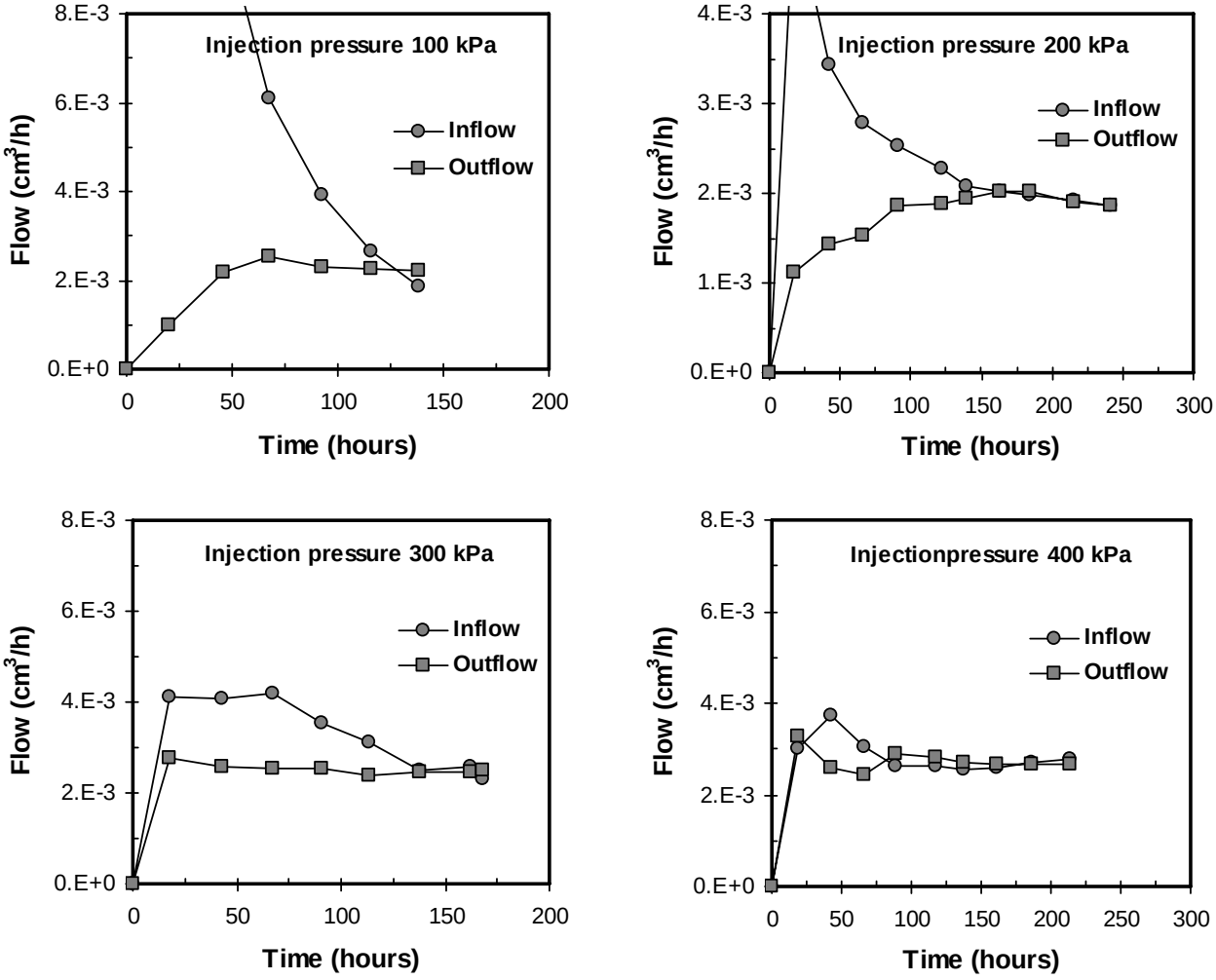


Figure A.22 Inflow and outflow condition for MX-80 bentonite

## A.2 MX-80

Dry density = 1.6 $Mg/m^3$
Low initial water content = 10.5 %
Permeant = High concentration solution ($10^{-2}$M)

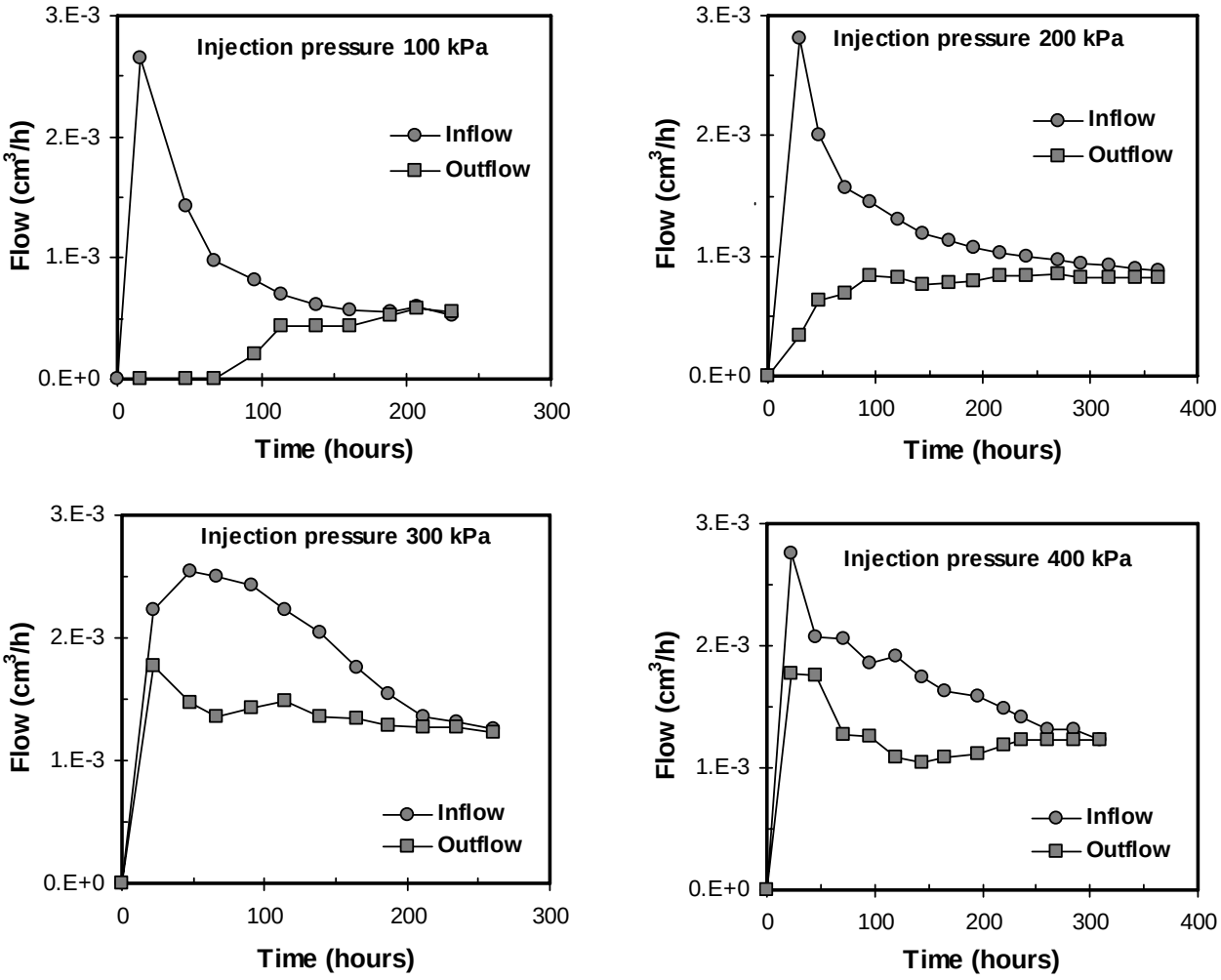


Figure A.23 Inflow and outflow condition for MX-80 bentonite

## A.2 MX-80

Dry density = 1.8 Mg/m$^3$
Low initial water content = 10.5 %
Permeant = High concentration solution ($10^{-2}$M)

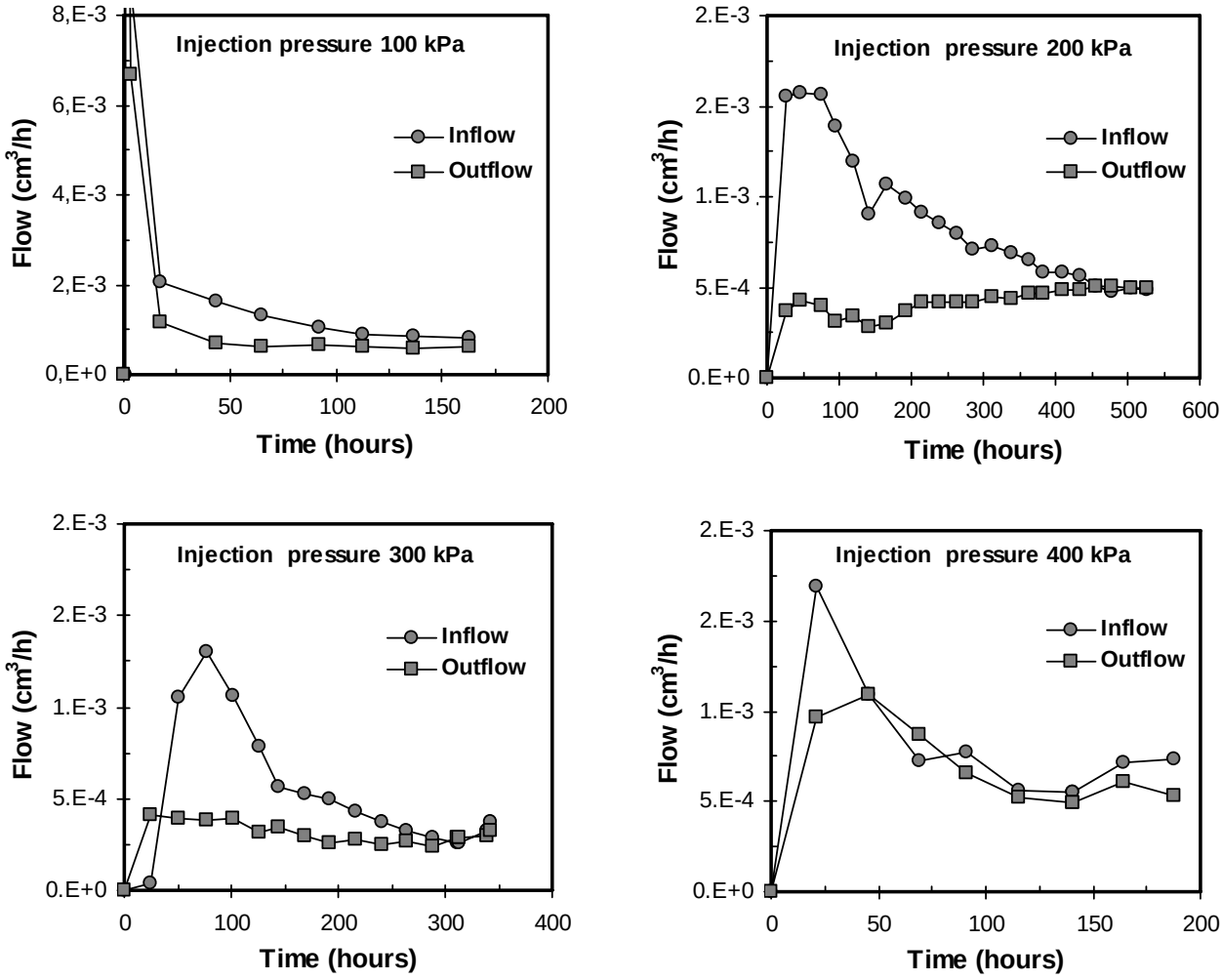


Figure A.24 Inflow and outflow condition for MX-80 bentonite

## A.3 Kunigel

Dry density = 1.4 $Mg/m^3$
Low initial water content = 6.2 %
Permeant = High concentration solution ($10^{-2}$M)

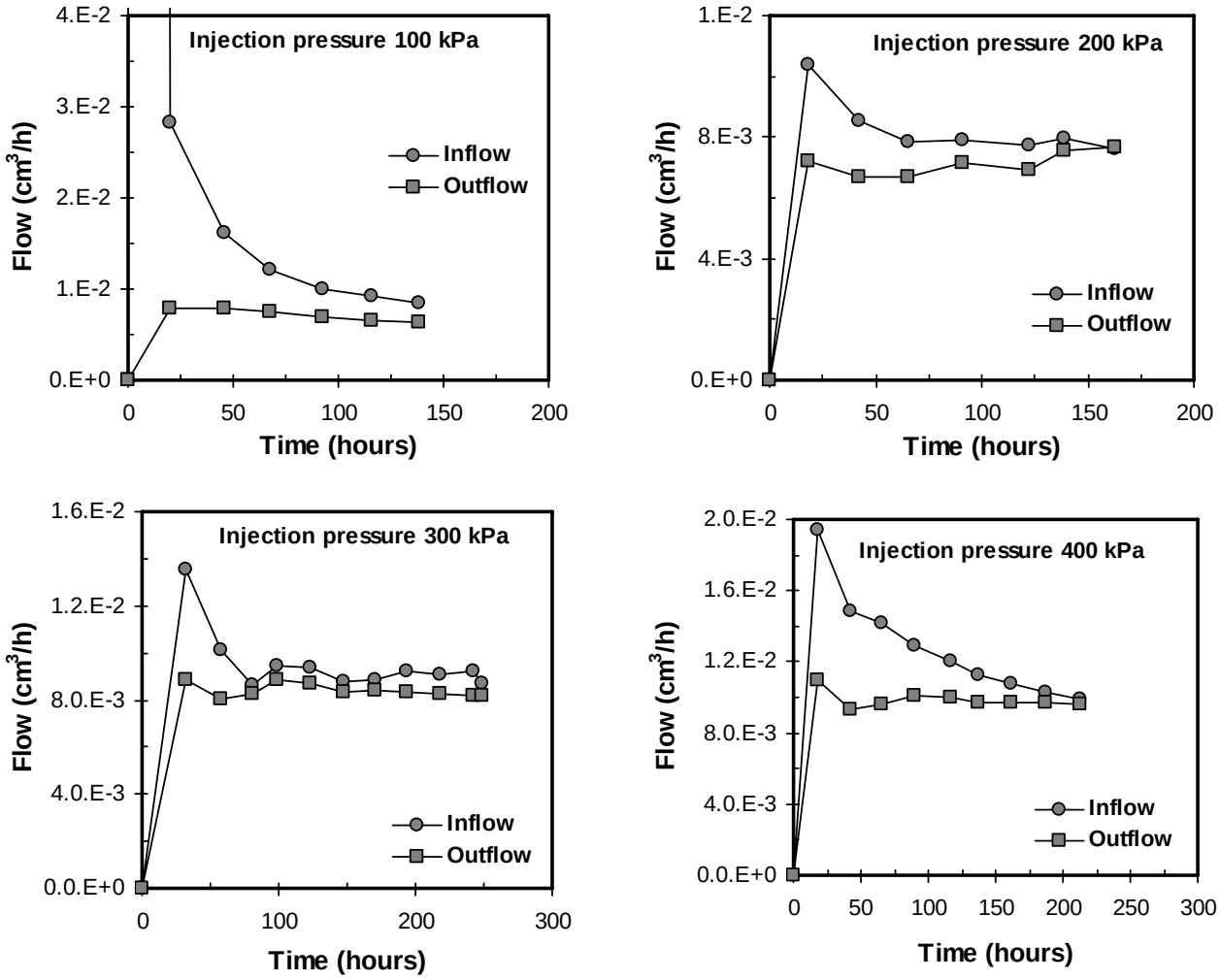


Figure A.25 Inflow and outflow condition for Kunigel bentonite

## A.3 Kunigel

Dry density = 1.6 $Mg/m^3$
Low initial water content = 6.2 %
Permeant = High concentration solution ($10^{-2}$M)

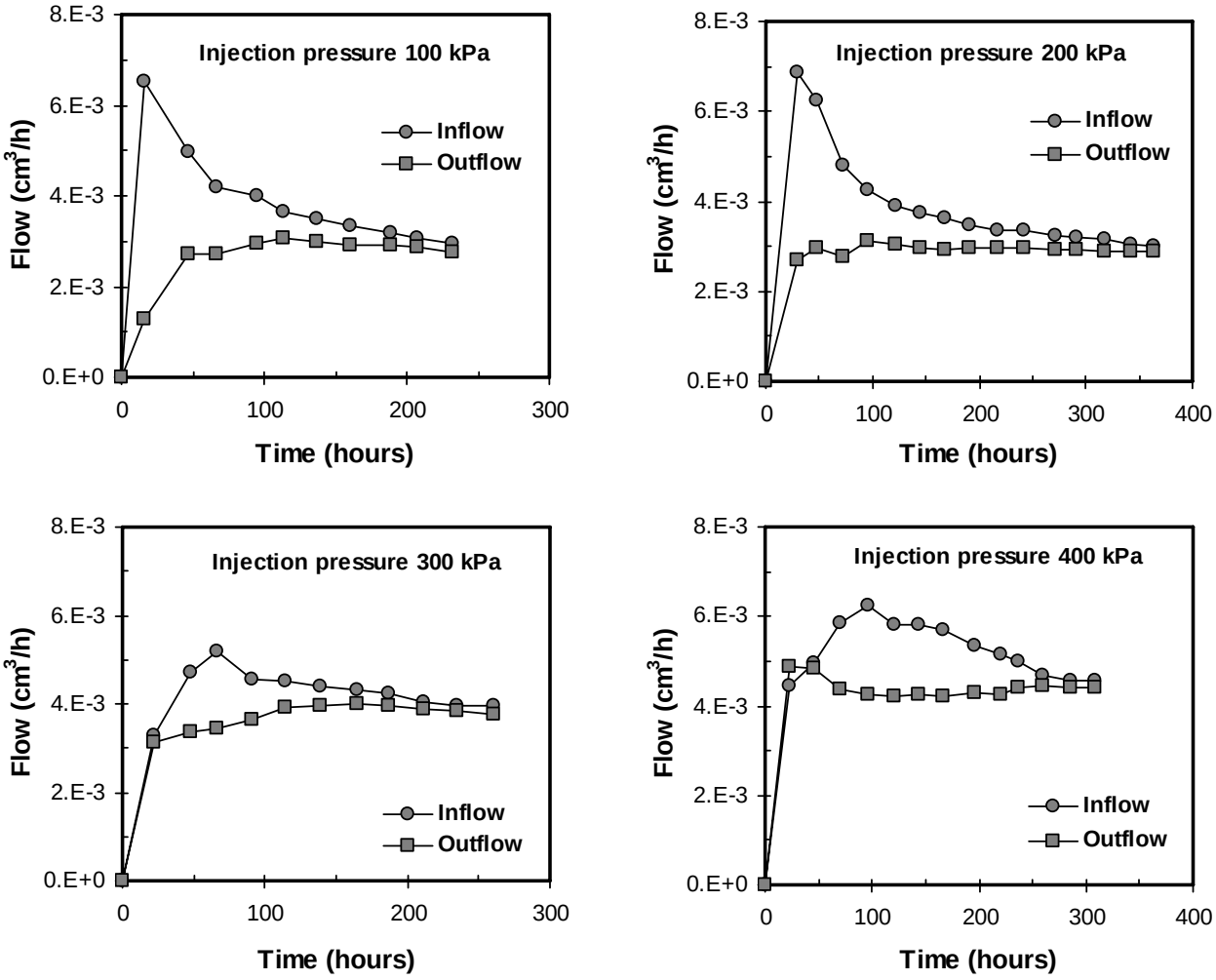


Figure A.26 Inflow and outflow condition for Kunigel bentonite

## A.3 Kunigel

Dry density = 1.8 $Mg/m^3$
Low initial water content = 6.2 %
Permeant = High concentration solution ($10^{-2}$M)

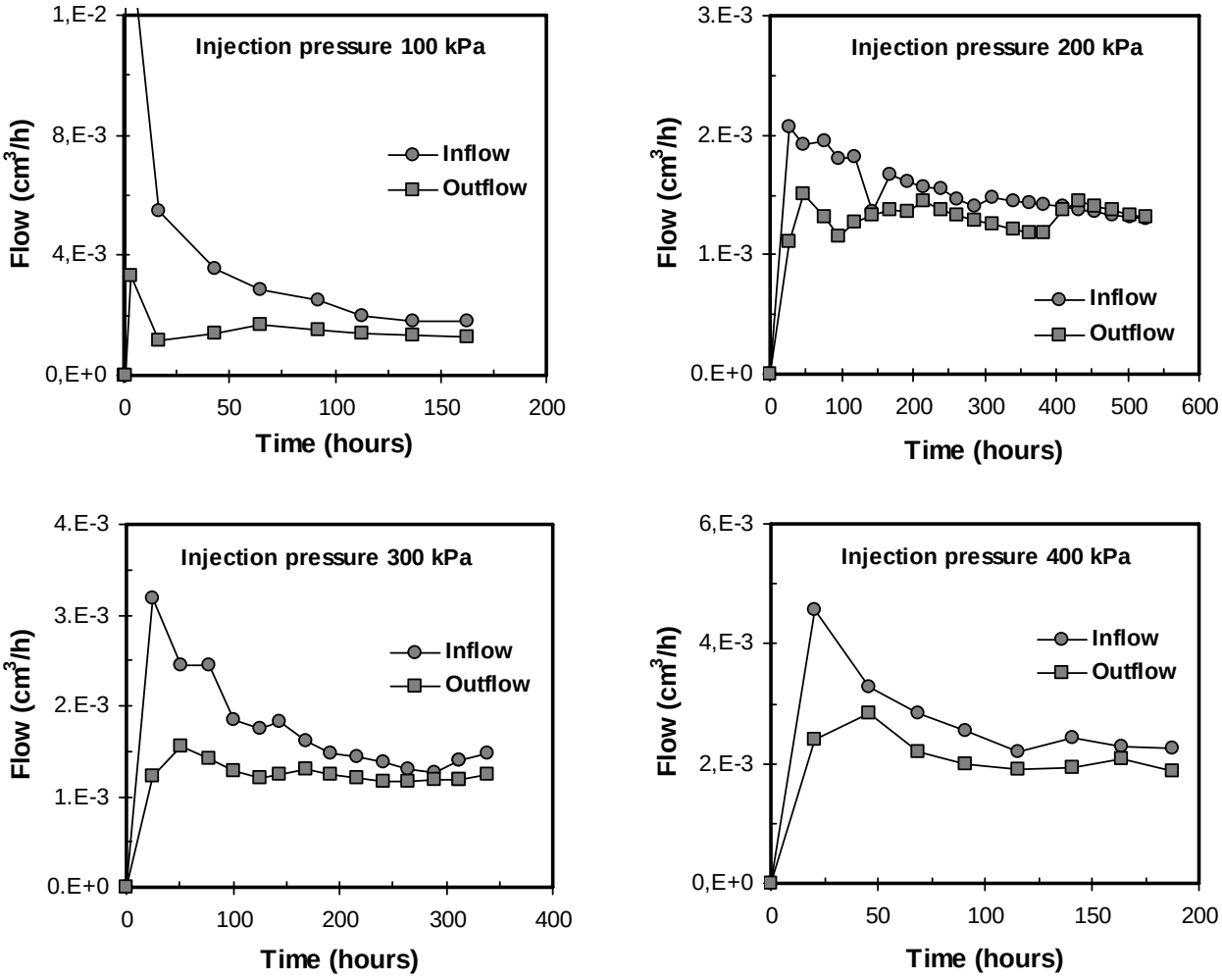


Figure A.27 Inflow and outflow condition for Kunigel bentonite

**Schriftenreihe des Lehrstuhls für Grundbau, Boden- und Felsmechanik der Ruhr-Universität Bochum**

*Herausgeber: H.L. Jessberger*

***Heft Nr.***

| | | |
|---|---|---|
| 1 | (1979) | **Hans Ludwig Jessberger**<br>Grundbau und Bodenmechanik an der Ruhr-Universität Bochum |
| 2 | (1978) | **Joachim Klein**<br>Nichtlineares Kriechen von künstlich gefrorenem Emschermergel |
| 3 | (1979) | **Heinz-Joachim Gödecke**<br>Die Dynamische Intensivverdichtung wenig wasserdurchlässiger Böden |
| 4 | (1979) | **Poul V. Lade**<br>Three Dimensional Stress-Strain Behaviour and Modelling of Soils |
| 5 | (1979) | **Roland Pusch**<br>Creep of soils |
| 6 | (1983) | **Norbert Diekmann**<br>Zeitabhängiges, nichtlineares Spannungs-Verformungsverhalten von Gefrorenem Schluff unter triaxialer Belastung |
| 7 | (1984) | **Rudolf Dörr**<br>Zeitabhängiges Setzungsverhalten von Gründungen in Schnee, Firn und Eis der Antarktis am Beispiel der deutschen Georg-von-Neumayer- und Filchner-Station |
| 8 | (1984) | **Ulrich Güttler**<br>Beurteilung des Steifigkeits- und Nachverdichtungsverhaltens von ungebundenen Mineralstoffen |
| 9 | (1986) | **Peter Jordan**<br>Einfluss der Belastungsfrequenz und der partiellen Entwässerung möglichkeiten auf die Verflüssigung von Feinsand |
| 10 | (1986) | **Eugen Makowski**<br>Modellierung der künstlichen Bodenvereisung im Grundwasser durchströmten Untergrund mit der Methode der finiten Elemente |
| 11 | (1986) | **Reinhard A. Beine**<br>Verdichtungswirkung der Fallmasse auf Lastausbreitung in nichtbindigem Boden bei der Dynamischen Intensivverdichtung |

12 (1986) **Wolfgang Ebel**
Einfluss des Spannungspfades auf das Spannung-verformungsverhalt von gefrorenem Schluff im Hinblick auf die Berechnung von gefrierschächten

13 (1987) **Uwe Stoffers**
Berechnungen und Zentrifugen-Modellversuche zur Verformungsabhängigkeit der Ausbaubeanspruchung von Tunnelausbauten In Lockergestein

14 (1988) **Gerhard Thiel**
Steifigkeit und Dämpfung von wassergesättigtem Feinsand unter Erdbebenbelastung

15 (1991) **Mahmud Thaher**
Tragverhalten von Pfahl-Platten-Gründungen im bindigen Baugrund, Berechnungsmodelle und Zentrifugen-Modellversuche

16 (1992) **Rainer Scherbeck**
Geotechnisches Verhalten mineralischer Deponieabdichtungsschichten bei ungleichf¨ormiger Verformungswirkung

17 (1992) **Martin M. Bizialiele**
Torsional Cyclic Loading Response of a Single Pile in Sand

18 (1992) **Michael Kotthaus**
Zum Tragverhalten von horizontal belasteten Pfahlreihen aus langen Pfählen In Sand

19 (1993) **Ulrich Mann**
Stofftransport durch mineralische Deponieabdichtungen: Versuchsmethodik und Berechnungsverfahren

20 (1992) **Festschrift anlässlich des 60. Geburtstages von Prof. Dr.-Ing. H. L. Jessberger**
20 Jahre Grundbau und Bodenmechanik an der Ruhr-Universität Bochum

21 (1993) **Stephan Demmert**
Analyse des Emissionsverhaltens einer Kombinationsabdichtung im Rahmen Der Risikobetrachtung von Abfalldeponien

22 (1994) **Diethard König**
Beanspruchung von Tunnel- und Schachtausbauten in kohäsionslosem Lockergestein unter Berücksichtigung der Verformung im Boden

23 (1995) **Thomas Neteler**
Bewertungsmodell für die nutzungsbezogene Auswahl von Verfahren zur Altlastensanierung

24 (1995) **Ralph Kockel**
Scherfestigkeit von Mischabfall im Hinblick auf die Standsicherheit von Deponien

25 (1996) **Jan Laue**
Zur Setzung von Flachfundamenten auf Sand unter wiederholten Lastereignissen

26 (1996) **Gunnar Heibrock**
Zur Rissbildung durch Austrocknung in mineralischen Abdichtungsschichten an der Basis von Deponien und Baugrund infolge stoßartiger Belastung

27 (1996) **Thomas Siemer**
Zentrifugen-Modellversuche zur dynamischen Wechselwirkung zwischen Bauwerken

28 (1996) **Viswanadham V. S. Bhamidipati**
Geosynthetic Reinforced Mineral Sealing Layers of Landfills

29 (1997) **Frank Trappmann**
Abschätzung von technischem Risiko und Energiebedarf bei Sanierungsmaßnahmen für Altlasten

30 (1997) **André Schürmann**
Zum Erddruck auf unverankerte flexible Verbauwände

31 (1997) **Jessberger, H. L. (Herausgeber)**
Environment Geotechnics, Report of ISSMGE Technical Committee TC 5 on Environmental Geotechnics

*Herausgeber: Th. Triantafyllidis*

32 (2000) **Triantafyllidis, Th. (Herausgeber)**
Boden unter fast zyklischer Belastung: Erfahrung und Forschungsergebnisse (Workshop)

33 (2002) **Christof Gehle**
Bruch- und Scherverhalten von Gesteinstrennflächen mit dazwischenliegenden Materialbrücken

34 (2003) **Andrzej Niemunis**
Extended hypoplastic models for soils

35 (2004) **Christiane Hof**
Über das Verpressankertragverhalten unter kalklösendem Kohlensäureangriff

36 (2004) **René Schäfer**
Einfluss der Herstellungsmethode auf das Verformungsverhalten von Schlitzwänden in weichen bindigen Böden

37 (2005) **Henning Wolf**
Zur Scherfugenbänderung granularer Materialien unter Extensionsbeanspruchung

38 (2005) **Torsten Wichtmann**
Explicit accumulation model for non-cohesive soils under cyclic loading

39 (2008) **Christoph M. Loreck**
Die Entwicklung des Frischbetondruckes bei der Herstellung von Schlitzwänden

40 (2008) **Igor Arsic**
Über die Bettung von Rohrleitungen in Flüssigböden

41 (2009) **Anna Arwanitaki**
Über das Kontaktverhalten zwischen einer Zweiphasenschlitzwand und nichtbindigen Böden

*Herausgeber: T. Schanz*

42 (2009) **Yvonne Lins**
Hydro-Mechanical Properties of Partially Saturated Sand

43 (2010) **Tom Schanz (Herausgeber)**
Geotechnische Herausforderungen beim Umbau des Emscher-Systems
Beiträge zum RuhrGeo Tag 2010

44 (2010) **Jamal Alabdullah**
Testing Unsaturated Soil for Plane Strain Conditions: A New Double-wall Biaxial Device

45 (2011) **Lars Röchter**
Systeme paralleler Scherbänder unter Extension im ebenen Verformungszustand

46 (2011) **Yasir Al-Badran**
Volumetric Yielding Behavior of Unsaturated Fine-Grained Soils

47 (2011) **Usque ad finem**
Selected research papers

48 (2012) **Muhammad Ibrar Khan**
Hydraulic Conductivity of Moderate and Highly Dense Expansive Clays

ISSN 2190-3255